

UNCLASSIFIED

AD NUMBER	
AD376293	
CLASSIFICATION CHANGES	
TO:	unclassified
FROM:	confidential
LIMITATION CHANGES	
TO:	Approved for public release, distribution unlimited
FROM:	Distribution authorized to U.S. Gov't. agencies and their contractors; Critical Technology; SEP 1966. Other requests shall be referred to Air Force Rocket Propulsion Laboratory, Attn: RPPR/STINFO, Edwards AFB, CA 93523.
AUTHORITY	
AFRPL ltr 7 May 1973; AFRPL ltr 7 May 1973	

THIS PAGE IS UNCLASSIFIED

CONFIDENTIAL

AFRPL-TR-66-242

376293

(Unclassified Title)

**QUARTERLY PROGRESS REPORT
ADVANCED CRYOGENIC ROCKET ENGINE PROGRAM,
AEROSPIKE NOZZLE CONCEPT**

**F. B. Lary
Rocketdyne, A Division of
North American Aviation, Inc.
6633 Canoga Ave.
Canoga Park, California**

Technical Report AFRPL-TR-66-242

September 1966

**Group 4
Downgraded at 3-Year Intervals
Declassified After 12 Years**

**D D C
OCT 17 1968
RECEIVED
A**

THIS MATERIAL CONTAINS INFORMATION AFFECTING THE NATIONAL DEFENSE OF THE UNITED STATES WITHIN THE MEANING OF THE ESPIONAGE LAWS, TITLE 18 U.S.C., SECTIONS 793 AND 794, THE TRANSMISSION OR REVELATION OF WHICH IN ANY MANNER TO AN UNAUTHORIZED PERSON IS PROHIBITED BY LAW.

"In addition to security requirements which must be met, this document is subject to special export controls and each transmittal to foreign governments or foreign nationals may be made only with prior approval of AFRPL (RPPR/STINFO), Edwards, California, 93523."

**Air Force Rocket Propulsion Laboratory
Research and Technology Division
Edwards Air Force Base, California
Air Force Systems Command
United States Air Force**

CONFIDENTIAL

"When U. S. Government drawings, specifications, or other data are used for any purpose other than a definitely related Government procurement operation whatsoever, and the fact that the Government may have formulated, furnished, or in any way supplied the said drawings, specifications, or other data, is not to be regarded by implication or otherwise, or in any manner licensing the holder or any other person or corporation, or conveying any rights or permission to manufacture, use, or sell any patented invention that may in any way be related thereto."

CONFIDENTIAL

AFRPL-TR-66-242

(Unclassified Title)
Quarterly Progress Report
Advanced Cryogenic Rocket Engine Program,
Acrospike Nozzle Concept

F. B. Lary
Rocketdyne, A Division of
North American Aviation, Inc.
6633 Canoga Ave.
Canoga Park, California

September 1966

Group 4
Downgraded at 3-Year Intervals
Declassified After 12 Years

THIS MATERIAL CONTAINS INFORMATION AFFECTING THE NATIONAL DEFENSE OF THE UNITED STATES WITHIN THE MEANING OF THE ESPIONAGE LAWS, TITLE 18 U.S.C., SECTIONS 793 AND 794, THE TRANSMISSION OR REVELATION OF WHICH IN ANY MANNER TO AN UNAUTHORIZED PERSON IS PROHIBITED BY LAW.

"In addition to security requirements which must be met, this document is subject to special export controls and each transmittal to foreign governments or foreign nationals may be made only with prior approval of AFRPL (RPPR/STINFO), Edwards, California, 93523."

Air Force Rocket Propulsion Laboratory
Research and Technology Division
Edwards Air Force Base, California
Air Force Systems Command
United States Air Force

CONFIDENTIAL

CONFIDENTIAL

FOREWORD

(U) This report presents the work accomplished during the second report period of the Aerospike Advanced Development Program under Air Force Contract AF04(611)-11399. The report covers the period 1 June 1966 through 31 August 1966. A portion of the design and tooling effort in Task II represents a joint effort with the Advanced Engineering Program, Systems and Dynamics Investigation (aerospike) Contract NAS 8-19. This report has been assigned Rocketdyne report No. R-6537-2.

(U) Publication of this report does not constitute Air Force approval of the reports' findings or conclusions. It is published only for the exchange and stimulation of new ideas.

Vernon L. Mahugh
1/Lt, USAF
Project Engineer

ABSTRACT

(U) Program status and technical results obtained at the end of the report period are described for the Advanced Development Program, Aerospike. This program includes analysis and preliminary design of an advanced rocket engine using an aerospike nozzle. It further includes analysis, test hardware design, and test evaluation of thrust chamber performance and thrust chamber durability.

CONFIDENTIAL

This page is intentionally left blank

CONFIDENTIAL

CONFIDENTIAL

CONTENTS

SECTION		PAGE
	ILLUSTRATIONS	vi
	TABLES	vi
	LIST OF ABBREVIATIONS AND SYMBOLS	
I	INTRODUCTION	1
II	SUMMARY	3
III	PROGRAM STATUS	5
	A. Task 1, Design and Analysis	5
	1. Module Design	5
	2. Applications Study	85
	B. Task 2, Fabrication and Test	103
	1. 2.5K Segment Injector Performance Investigation	103
	2. Thrust Chamber Cooling Investigations	139
	3. Thrust Chamber Nozzle Demonstration	177
	4. Segment Structural Evaluation	208
IV	CONCLUSIONS AND RECOMMENDATIONS	211
	REFERENCES	213
	APPENDIX A - Determination and Value of Influence Coefficients Used in Thrust Chamber Data Reduction	215
	APPENDIX B - Heat Transfer Data Reductions for Water-Cooled Segments	223
	APPENDIX C - Hot Gas Tapoff Calculations	227
	APPENDIX D - Instrumentation Box Identification System	231

CONFIDENTIAL

ILLUSTRATIONS

FIGURE		PAGE
1	Demonstrator Module System Schematic	7
2	Constant Thrust Criteria	11
3	Maximum Speed Criteria	11
4	Control Point Schematic	15
5	Closed-Loop Mixture Ratio Control Systems	21
6	Open Loop Mixture Ratio Controller	23
7	Effect of Pump and Turbine Curves on Open Loop Mixture Ratio Control System	24
8	Cycle Schematics	30
9	Transient Performance, Pressure and Pump Speed vs Time	33
10	Transient Performance, Hot-Gas and Pump Flowrate vs Time	34
11	Valve Sequencing for ADP Start	35
12	Preliminary Layout Demonstrator Module	37
13	Igniter Hot-Gas and Isolation Valve/Manifold Assembly	41
14	Proposed Adjustable Pump Mounting Concept	43
15	Thrust Subsystem Designs	45
16	Thrust Structure Candidates	46
17	Titanium Thrust Structure Weight vs Depth of Truss Structure	47
18	Gimbal Height and Thrust Structure Space Limitation Diagram	48

CONFIDENTIAL

ILLUSTRATIONS

FIGURE		PAGE
19	Increase in Dynamic Envelope Requirement with Gimbal Center Elevation Above Position where $R_{static} = R_{dynamic}$	48
20	Preliminary Layout 350K Flight Module	49
21	Chamber Pressure vs Mixture Ratio	52
22	Mark 30 H-Q and Efficiency Curves	56
23	One and One-Half-Stage Hydrogen Impeller Backplate Allowable Tip Speeds	58
24	Two-Stage Hydrogen Impeller Backplate Allowable Tip Speeds	59
25	Deflections of Hydrogen Volute due to Internal Static Pressure	61
26	Structural Concept, 250K Aerospike Thrust Chamber Demonstrator Module	66
27	Proposed 250K Aerospike Thrust Chamber, Two Bolt Integral Baffle-Injector Configuration (40 Pieces)	67
28	ADP Demonstration Chamber Study (Honeycomb Structure)	69
29	ADP Demonstration Chamber, Pressure Diffusion-Bonded Titanium	71
30	250K Flow Circuits	73
31	Structural Tie Concepts	74
32	Proposed 250K Aerospike Thrust Chamber, 80-Subsonic Strut Configuration	75
33	Full-Length Shroud Pressure Profile	79
34	Candidate Engine Arrangements: Case 1, Expendable First Stage; Case 3 Expendable Single Stage to Orbit	87

CONFIDENTIAL

ILLUSTRATIONS

FIGURE		PAGE
35	Case 1, Relative Performance Index Decrease Module Diameter	88
36	Case 3, Relative Performance Index Decrease Module Diameter	89
37	Five Module Thrust Structure	90
38	Case 2, Relative Performance Index Decrease vs Mount Height	92
39	Case 6, 250K Relative Performance Index vs Mount Height	93
40	Candidate Engine Arrangements: Case 4, Removable First Stage (VFOH-L)	94
41	Case 4, 250K Modules Relative Performance Index Decrease vs Module Diameter	96
42	Candidate Engine Arrangements: Case 5, Recoverable Second-Stage Pickaback	97
43	Tubular Design With Cross-Members	98
44	Sheet-Stringer Design With Cross-Members	99
45	60-Degree LOX Impinging Triplet With Fuel Post Extended and Both Chamfered and Nonchamfered LOX Strips	108
46	LOX Fan Injector Pattern (with Fuel Post)	109
47	Reversed Pattern, 60-Degree Fuel on LOX Fan	110
48	Primary 250K Injector Patterns Candidates	111
49	Performance Comparison, 250K Candidate Injector	120
50	2.5K Hot-Gas Tapoff Configuration	121
51	Measured Hot-Gas Tapoff Characteristics (2.5K Chamber)	122

CONFIDENTIAL

ILLUSTRATIONS

FIGURE		PAGE
52	Simulated 250K Hot-Gas Tapoff Ports in 250K Thrust Chamber.	123
53	Gas Tapoff Configuration for Tests 088 Through 092	125
54	Gas Tapoff Configuration for Tests 093 Through 099	126
55	Correlation of LOX Flow Data for the No. 1 Selected 250K Injector Configuration	127
56	Correlation of GH ₂ Flow Data for the No. 1 Selected 250K Injector Configuration	130
57	2.5K Film-Cooled, Solid-Wall Segment Coolant Passage Location.	132
58	Variation in Heat Transfer Rates into Passage Immediately Upstream of Throat	133
59	Variation in Local Heat Fluxes During ADP 2.5K Water-Cooled Segment Firings (Tests No. 79 and 80)	135
60	Comparison of Q/A for Triplet and Fan Injectors . . .	137
61	250K Injector Chamber Pressure Tap Configuration. .	138
62	2.5K Segment End Plate Prior to Assembly	141
63	Nickel Segment Brazed Assembly	142
64	2.5K Tube-Wall Segment	144
65	Cooling Limit Results for OFHC Copper	145
66	Cooling Limits for Nickel 200	146
67	Material Selection Program	148
68	Plastic Strain Analysis	151

CONFIDENTIAL

FIGURE		PAGE
69	Comparison of OFHC Copper Tube Grain Size in the Annealed Condition and After Simulated ADP Braze Cycle	154
70	Comparison of Beryllium-Copper Grain Size Prior to Brazing and After Brazing	155
71	Comparison of Nickel 270 Tube Grain Size in the Annealed Condition and After Simulated ADP Furnace Braze Cycle	156
72	Comparison of Nickel 200 Tube Grain Size in the Annealed Condition and After Simulated ADP Furnace Braze Cycle	157
73	Axial Load, Strain Cycle for a Thrust Chamber Tube	164
74	Mechanical Strain at Elevated Temperatures, Test Results on Brazed Nickel 200	166
75	Mechanical Strain at Elevated Temperatures, Test Results of Candidate Materials	167
76	Typical Tube Tester Thermal Fatigue Crack (47 CRES Specimen After 300 Cycles at 70 to 1100F)	168
77	Thrust Chamber Tube Tester (High Pressure)	169
78	ADP Inner Solid Wall Nozzle No. 1	178
79	ADP Outer Solid Wall No. 1	179
80	Solid Wall Inner Film Coolant Ring	180
81	Inner and Outer Thrust Chamber Tubes	182
82	ADP Thrust Chamber Tube Calibration Console	183
83	ADP Injector No. 1	184
84	250K Solid Wall Thrust Chamber Outer Body Assembly	185
85	250K Solid Wall Thrust Chamber Inner Body Assembly	186
86	250K Film Cooled Solid Wall Thrust Chamber	187
87	Chamber Locations of Pulse Gun Ports	190
88	Pulse Gun	191
89	Fuel Manifold Inlet Tee	193
90	ADP 250K Thrust Chamber Tube-Wall Assembly	194
91	Hydrogen Flow Circuit	195
92	Hypergol Tube	198
93	Block Diagram Representation of the ADP "Chug" Model	200
94	LOX Manifold Flow and Distribution Tests	201
95	Block Diagram Representation of the ADP "Chug" Model	203

TABLES

TABLE		PAGE
1	Preliminary Design Parameters	8
2	Operating Limits	12
3	Steady-State Tradeoff	17
4	Fuel Turbopump Operating Requirements	53
5	ADP Pump Parameters at Design Point	55
6	ADP Hydrogen Impeller Material Properties	57
7	ADP Two-Stage Impeller Weight Comparison	60
8	Turbopump Comparison	62
9	LOX Turbopump Operating Requirements	64
10	Design Comparison Study	65
11	Injector Characteristics, 250K Injector	77
12	Side Loading from Thrust Vector Control	101
13	Maximum Acceleration Loading	101
14	Structural Factors	102
15	Table of Hardware - 2.5K Segment Solid-Wall Evaluations	105
16	2.5K Segment Injector Test Summary	116
17	Adjusted C* Efficiencies for Gas Tapoff Tests	128
18	No. 2 250K Injector Candidate Selection Rating	139
19	Candidate Materials for Thrust Chamber Usage	150
20	Mechanical Property Tests: Summary of Results ...	153
21	Brazing Feasibility Tests, Nickel 200, 270, and Beryllium Copper	159
22	Brazing Feasibility Tests, OFHC Copper	161
23	Mechanical Strain at Elevated Temperature Fatigue Tests, Summary of Test Conditions	163
24	Hastelloy-X vs Stainless Steel Test Results	170

TABLES

TABLES		PAGE
25	Factors Affecting Selection of 20K-Segment Tube Material.....	172
26	Factors Affecting Selection of Long-Range Tube Materials	174
27	Tentative Test Schedule for Each Chamber	175
28	250K Chamber Instrumentation Provisions	206

NOMENCLATURE

A = area
 A_c = chamber cross-sectional area
 A_t = nozzle throat area
 $C_F(1-D)$ = one-dimensional thrust coefficient
 $C_F(2-D)$ = two-dimensional thrust coefficient
 E = Young's modulus
 F = thrust
 h = enthalpy
 $H-Q$ = pump head-flow
 k = specific heat ratio, thermal conductivity
 K = distance
 M = Mach number
 q = heat rate
 Q/A = heat flux
 R = radius
 T = temperature
 u = boundary layer velocity
 U = free stream velocity
 u/c = turbine wheel velocity to spouting velocity ratio
 \dot{w} = flowrate
 DN = bearing bore (millimeters) X rpm

NOMENCLATURE (Continued)

GREEK LETTERS

δ = boundary layer thickness
 ϵ = strain
 θ = boundary layer momentum thickness
 μ = viscosity
 ν = Poisson's ratio
 σ = stress

SUBSCRIPTS

B = bulk
c = chamber, curvature
e = nozzle exit, elastic
p = plastic
R = reference
TH = thermal
t = nozzle throat
 ∞ = free stream
aw = adiabatic wall
ST = Stanton Number
 Pr = Prandtl Number

SUPERSCRIPTS

$\bar{}$ = average value

CONFIDENTIAL

I. INTRODUCTION

(C) The Advanced Development Program (ADP) Aerospike Nozzle Concept started 1 March 1966 with a 17-month duration. The objectives are to evaluate critical technology associated with the Aerospike concept and produce the preliminary design of an advanced hydrogen-oxygen engine of the following characteristics:

1. 250,000-pound thrust (nominal rated) with throttling to 20 percent of rated thrust
2. 6:1 mixture ratio (nominal) with a range of 5 to 7:1
3. 96 percent (minimum) of theoretical shifting specific impulse at rated thrust; 95 percent (minimum) during throttling
4. 100-inch maximum overall diameter
5. 10-hours life between overhauls with 100 reuses
6. Restartable at altitude

The total effort is comprised of two major tasks:

Task 1, Analysis and Design

- A. Module Design
- B. Application Study

Task 2, Fabrication and Test

- A. Injector Performance Investigations
- B. Thrust Chamber Nozzle Investigations
- C. Thrust Chamber Cooling Investigations
- D. Segment Structural Evaluation

(U) Task 2 and Task 3 of the first quarterly report, Thrust Chamber Performance Evaluation and Thrust Chamber Durability Evaluation, respectively, are now combined into Task 2, Fabrication and Test.

CONFIDENTIAL

CONFIDENTIAL

(U) This second quarterly report presents the program status, technical progress, and problem areas and solutions as of the end of the second quarter of the ADP Aerospike, and a brief summary of planned effort for the third quarter.

CONFIDENTIAL

CONFIDENTIAL

II. SUMMARY

(U) In Task 1, work progressed on both demonstrator module design and flight module studies. The demonstrator engine balance was modified for defined operating limits and for component study results. The engine layouts were refined with definition of turbine drive hot-gas ducts, propellant feed arrangement, igniter configuration, and turbo-pump mounts. Thrust structure candidate designs were reduced to four. Study of control points was brought to selection of two hot-gas values for thrust and mixture control; however, studies of open- vs closed-loop control modes continue with either being satisfactory for the demonstrator module. A study of gas generator turbine drive against tap-off was initiated for completion in the next period. A trade study of hydrogen pumps was completed with selection of a two-stage centrifugal pump. The LOX pump design and turbine design features for both pumps were established. A thrust chamber structure trade study was completed with selection of a titanium structure and definition of the tie-bolts arrangement and cooling circuit. Gimbal design requirements were defined and the study nearly completed. Flight module preliminary parametric data was completed along with the preliminary layout of variations in the flight configuration.

(U) The Applications Study was initiated with requirements established and the parametric data completed. Studies of vehicle shroud and thrust structure variations are in progress.

(C) In the Injector Performance Investigation subtask of Task 2, all hardware scheduled for the period was delivered and all tests scheduled were conducted. The three candidate injectors were evaluated for performance, stability, durability, and chamber compatibility over the throttling range. The triplet pattern was selected for 250K injector No. 1 and is a strong contender for the high-performance 250K injector No. 2. This evaluation will be completed early in September. Results show the triplet, as developed in the 2.5K segment, to be stable over the operating range, to better the performance requirements, to be durable, and to produce acceptable throat heat flux. Tapoff data was taken and these tests are continuing. "Bomb" disturbed stability rating tests were conducted and will be completed in September.

(C) Progress was made in fabrication of the 250K experimental thrust chambers under the chamber-nozzle subtask of Task 2. All working drawings were released. The solid-wall chamber is undergoing copper throat deposit prior to final machining. Complete tubes were fabricated to check the process, and tube-wall bodies were partially machined. The injector body has completed manifold welding and is undergoing final machining prior to brazing. Injector strip drilling and baffle

CONFIDENTIAL

electroforming was initiated. Manifolds, igniter, thrust mount, and test equipment are partially fabricated. A stability computer model was constructed and test instrumentation defined. The test facility was activated with 40K aerospike thrust chamber.

(U) In the thrust chamber cooling investigations of Task 2, the laboratory and analytical material studies were completed. Tube tester simulation tests were conducted on stainless steel and nickel, and will continue in September. From all results, stainless steel was eliminated as a material for the demonstrator module tubes. Nickel 200 was selected for the 20K segment and, pending tube-wall segment hot-firing test results, for the demonstrator chamber. Life predictions from the combination of the analytical model and laboratory materials results corroborated tube tester results and actual chamber life experience on similar cooling tubes. The 2.5K tube-wall segment with nickel tubes was fabricated to the point of assembly preparatory to brazing. The copper tubes for the other 2.5K segment were formed and the body parts were nearing completion. Instrumentation for hot-gas side-wall temperatures and other variables was developed.

(U) In the segment structural evaluation subtask of Task 2, detailed design of the segment was initiated during this quarter. The titanium structural concept selected for the demonstrator chamber was incorporated into this segment along with the tie bolt and cooling circuit of the demonstrator chamber. Layouts and design specifications were completed and preliminary design review held. Tube material and structure material was ordered. Tube material was selected as nickel 200 from the cooling investigations subtask.

(C) The overall program is essentially on schedule with several subtasks ahead of the program plan and one behind, namely the 250K chamber nozzle investigations. Here, certain hardware fabrication is behind schedule; however, it will not affect the initiation of full-scale tube-wall tests on schedule. The No. 2 250K injector will be released in the first week of September instead of August as scheduled.

(U) Issuance of Demonstrator Module Design requirement specifications was delayed 2 weeks for refinement to include study results. Other program plan milestones were met in the second quarter.

CONFIDENTIAL

CONFIDENTIAL

SECTION III PROGRAM STATUS

A. TASK I, DESIGN AND ANALYSIS

1. MODULE DESIGN

a. Status

(1) System Analysis

(U) The steady-state analysis of the tapoff engine cycle was deepened during this report period to include a preliminary cycle balance reflecting the latest program ground rules. An analysis of the effect of the change in the requirement for constant thrust vs mixture ratio was undertaken, and a decision as to the recommended design direction will be made early in the next quarter. A preliminary study of the maximum operating limits of the various engine components was completed and is being used in establishing component design requirements.

(U) An investigation of possible thrust and mixture ratio control methods was conducted during this report period to determine the optimum control points consistent with operational requirements. It was concluded that the system utilizing two hot-gas valves to control turbine speed was preferable for the tapoff system.

(U) An open-loop vs closed-loop controls study was initiated, and concluding recommendations will be forthcoming early in the next report period. Preliminary results are that the engine will operate satisfactorily with both closed-loop and open-loop systems and that either can be designed to control the engine.

(U) A comparative analysis of a gas generator and tapoff cycle was brought near completion during this report period. Results to date indicate that as tapoff gas properties approach gas generator properties, the performance difference between the two cycles approaches zero. The tapoff cycle has fewer components, comparable weight, and somewhat better control characteristics at a higher estimated cost of development. This study will be concluded during the next report period.

(U) Start model updating and refining to include simulation of heat transfer and compressible, two-phase, hydrogen flow through the thrust chamber cooling tubes is currently being accomplished as is conversion of the digital engine model to the IBM 360 computer. Preliminary

CONFIDENTIAL

transient performance data have been obtained and some preliminary valve sequencing established.

(2) Preliminary Design

(U) A preliminary cut through the mechanical design and module general arrangement has been accomplished. In-depth design studies have been initiated and design sheets released on the major subsystems and components. Preliminary weights, envelopes, and interfaces have been established for the major components. A trade study on the thrust structure selection has narrowed candidates to four, and final selection will be made early in the next report period.

(C) Preliminary layouts of the 250K and 350K flight module have been completed. Parametric engine weight and performance data have been generated for the flight module. The thrust range covered was 150K to 350K, chamber pressure was varied from 750 to 2000 psia, and engine diameters investigated were 80, 100, and 120 inches. The nozzle length was 25 percent and mixture ratio was varied from 5 to 7.

(U) Performance specifications have been established for both the fuel and oxidizer turbopumps; preliminary turbine and pump operating envelopes were also established; an evaluation of the type of fuel pump configuration was completed. A two-stage centrifugal pump configuration has been selected, and preliminary layouts of both the fuel and oxidizer turbopumps initiated.

(U) Definition of the thrust chamber wall structure, including coolant circuit, attachment method, material selection, and fabrication technique has been finalized and the tube material tentatively selected. Nozzle contour and shroud geometry have been established and the theoretical calculation technique verified through a cold flow nozzle test series conducted under a separate program.

b. Progress During Report Period

(1) System Analysis

(a) Engine Balance

(U) The engine balance calculations for the tapoff cycle engine system, shown schematically in figure 1, were made using a nonlinear digital computer program. The program balances the engine at the nominal design point and then permits one or more of the design variables to be changed to determine off-design performance. Iterations between the steady-state cycle balance and component designs have been continually carried out. The current design point parameters are summarized in Table I.

CONFIDENTIAL

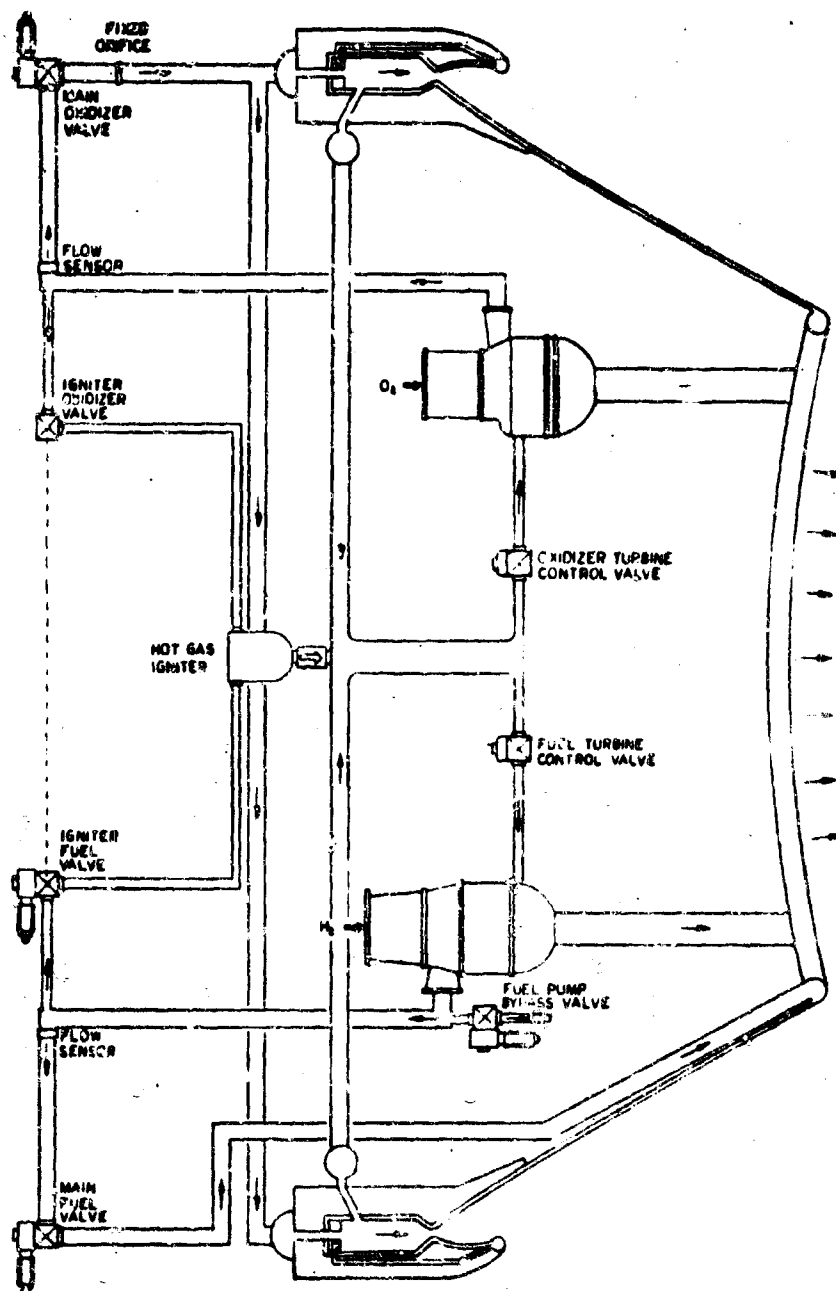


Figure 1. Demonstrator Module System Schematic

CONFIDENTIAL

CONFIDENTIAL

(C) Table 1. Preliminary Design Parameters

CONFIGURATION

Thrust, pounds	250,000
Specific impulse, second (vacuum)	450.8
Specific impulse efficiency, percent	97.0
Engine mixture ratio	6.0
Envelope:	
Diameter, inch	100
Length, inch	47
Area Ratio	76.9
Oxidizer flow, lb/sec	475.3
Fuel flow, lb/sec	79.2
Total propellant flow, lb/sec	554.5
Oxidizer inlet pressure, psia	40
Fuel inlet pressure, psia	35
Oxidizer inlet temperature, R	175.6
Fuel inlet temperature, R	41.3

THRUST CHAMBER

Thrust, pounds	242,600
Mixture ratio	6.45
Throat area, sq in.	81.71
Chamber pressure, psia	1500
Injector end pressure, psia	1531
Oxidizer flow, lb/sec	472.3
Fuel flow, lb/sec	73.2
Combustion efficiency, percent	96.5
Fuel injector pressure drop, psia	390
Oxidizer injector pressure drop, psia	390

BASE AREA

Thrust, pounds	7400
Base pressure, psia	3.86
Secondary flowrate, lb/sec	9.04

FUEL TURBOPUMP

Pump

Number of stages	2
Speed, RPM	36,000

CONFIDENTIAL

CONFIDENTIAL

(C) Table 1. Preliminary Design Parameters
(Continued)

FUEL TURBOPUMP (Continued)

Pump (Continued)

Discharge pressure, psia	2634
Efficiency, percent	75
Flowrate, lb/sec	79.2

Turbine

Number of stages	1
Pressure ratio	30
Inlet temperature, R	1960
Inlet pressure, psia	1225
Flowrate, lb/sec	6.45
Efficiency, percent	60

OXYGEN TURBOPUMP

Pump

Number of stages	1
Speed, RPM	20,000
Discharge pressure, psia	2055
Efficiency, percent	80
Flowrate, lb/sec	475.3

Turbine

Number of stages	1
Pressure ratio	15
Inlet temperature, R	1960
Inlet pressure, psia	600
Efficiency, percent	50
Flowrate, lb/sec	2.59

CONFIDENTIAL

CONFIDENTIAL

(C) A change in the thrust vs mixture ratio requirement was received during the second quarter. Previously, the requirement had called for constant thrust over a mixture range from 5 to 7:1. This required elevated pump speeds at the mixture ratio extremes, as shown in figure 2. At 5:1, the fuel pump speed required increased 8 percent over the nominal design point speed at mixture ratio of 6:1, while at 7:1 the oxidizer pump speed required increased 1.2 percent. Using a criterion which limits the pump speeds to the nominal design point (mixture ratio 6:1) speed, results in a thrust loss at both ends of the mixture ratio excursion as depicted in figure 3. This loss is only 1.6 percent at a mixture ratio of 7:1; however, it reaches approximately 10.4 percent at a mixture ratio of 5:1.

(C) Preliminary analysis indicates that the engine weight savings using the pump speed limit criteria is approximately 30 pounds with no change in specific impulse at vacuum conditions, while the thrust loss at a mixture ratio of 5:1 is significant. A decision on the design course to be taken will be made early in the next quarter. The engine balance shown reflects use of the pump speed limit criteria.

(b) Operating Limits

(U) Design of a rocket engine for a specific operating point and off-design capability results in nominal design values for all engine components. However, manufacturing tolerances result in component performance slightly different from the nominal design values. The cumulative effect of these tolerances must be statistically calculated to determine the maximum probable values at which each component must be capable of operating. These values are summarized in Table 2.

(U) Tolerances which were considered in determining maximum operating conditions included line and valve resistances, combustion and nozzle efficiencies, and turbomachinery performance. Component tolerances for the ADP demonstrator module were estimated based on current Rocketdyne production engines. An exception to this was the thrust chamber tolerance. Current production engines are bell-type thrust chambers, whereas the ADP engine is an annular-type thrust chamber. Therefore, it was necessary to analytically predict the throat gap tolerance. This tolerance was estimated to be larger for the annular chamber than for a bell chamber because of the narrow throat gap of the annular chamber.

CONFIDENTIAL

CONFIDENTIAL

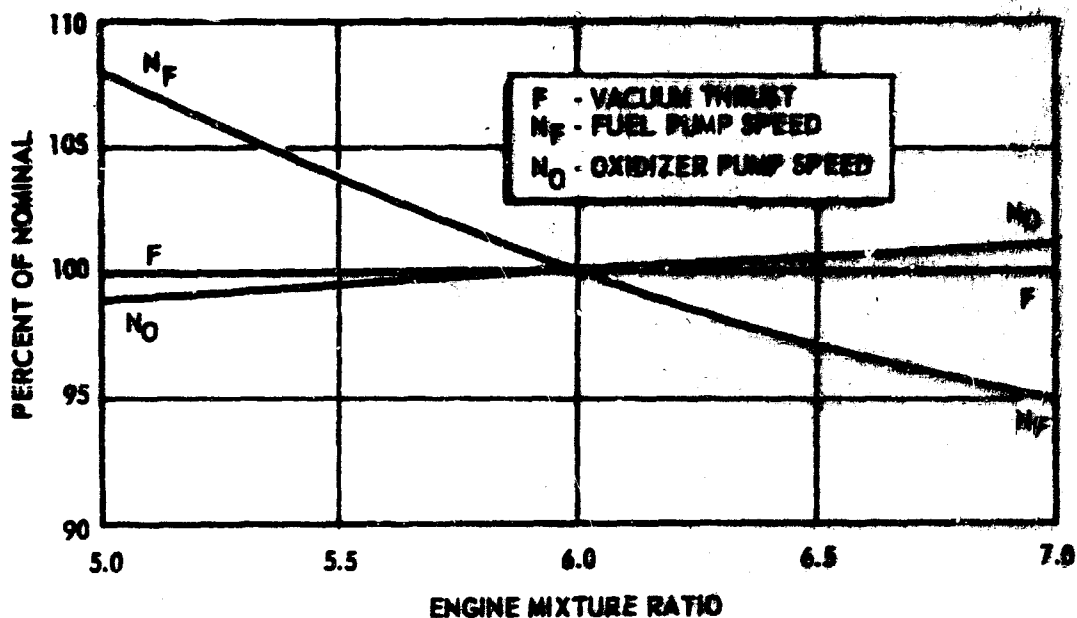


Figure 2 Constant Thrust Criteria

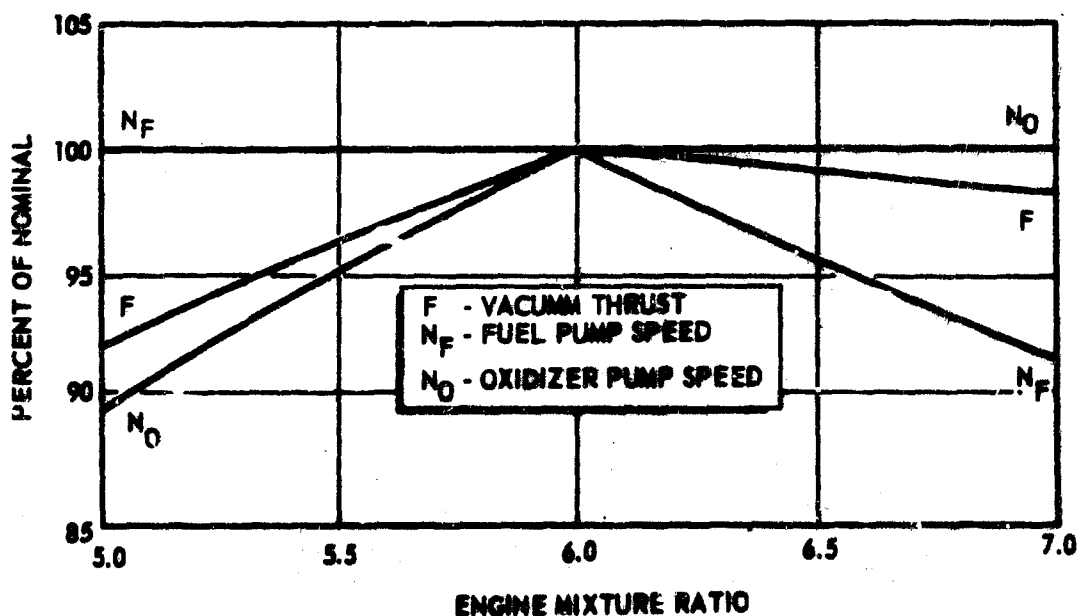


Figure 3 Maximum Speed Criteria

CONFIDENTIAL

CONFIDENTIAL

(C) Table 2. Operating Limits

	Nominal Mixture Ratio	2- σ Random Variation	Maximum
Engine thrust, pound	250,000	17,364	267,364
Engine mixture ratio	6,0000	0.3503	--
Thrust chamber injector end pressure, psia	1531.3	166.7	1698.0
Thrust chamber fuel flow, lb/sec	73.39	5.59	78.98
Thrust chamber oxidizer flow, lb/sec	473.05	44.75	517.80
Tapoff fuel flow, lb/sec	5.95	0.65	6.60
Tapoff oxidizer flow, lb/sec	2.97	0.33	3.30
Fuel turbine inlet temperature, R	1960	*	1960
Fuel turbine outlet temperature, R	1254	39	1293
Fuel turbine inlet pressure, psia	1226.8	140.9	1367.7
Fuel turbine outlet pressure, psia	39.9	4.1	44.0
Fuel turbine speed, rpm	35,986	1925	39,911
Fuel turbine torque, ft-lb	2292.5	232.0	2524.5
Fuel turbine flow, lb/sec	6.37	0.687	7.06
Oxidizer turbine inlet temperature, R	1960	*	1960
Oxidizer turbine outlet temperature, R	1449	33	1481
Oxidizer turbine inlet pressure, psia	599.6	70.2	669.8
Oxidizer turbine outlet pressure, psia	39.9	4.1	44.0

* The standard deviation of the tapoff gas temperature from the nominal value of 1960 R was not estimated because of the limited amount of test data on tapoff for this engine configuration. An estimate of this value will require sufficient testing to allow a statistical analysis. In place of the 2- σ turbine inlet temperature variation, an arbitrary variation of 100 F was selected to assess the criticality of this parameter. This variation was estimated to result in a 1.0 percent change in thrust, a 0.7 percent change in pump speed, a 1.0 percent change in propellant flowrate, and a 1.0 percent change in pump discharge pressure. The control system would then rebalance the engine at the nominal thrust and chamber pressure with a change in specific impulse of approximately 0.2 seconds.

CONFIDENTIAL

(C) Table 2 (Continued)

	Nominal Mixture Ratio	1- σ Random Variation	Maximum
Oxidizer turbine speed, rpm	28,000	1120	29,120
Oxidizer turbine torque, ft-lb	959	111	1070
Oxidizer turbine flow, lb/sec	2.56	0.29	2.85
Fuel pump discharge pressure, psia	2634.5	252.9	2887.4
Fuel thrust chamber inlet pressure, psia	2425.4	216.5	2641.9
Fuel injection pressure, psia	1921.4	195.0	2116.4
Oxidizer pump discharge pressure, psia	2055.7	226.3	2282.0
Oxidizer injection pressure, psia	1921.5	210.7	2132.2
Fuel pump head, feet	81,669	7447	89,116
Fuel pump volume flow, gpm	8449	653	9102
Fuel pump horsepower, bhp	15,708	2380	18,088
Oxidizer pump head, feet	4222	474	4696
Oxidizer pump volume flow, gpm	3107	217	3324
Oxidizer pump horsepower, bhp	4567	761	5328
Base pressure, psia	4.03	0.87	4.90
Base temperature, R	1310	34	1344
Base thrust, pound	7743	1679	9422

(U) Each tolerance was examined independently to determine its effect on the engine parameters shown in Table 2. The cumulative effect of all tolerances on each parameter was determined from

$$X_{\text{maximum}} = X_{\text{nominal}} + \sqrt{\sum_i \Delta X_i^2}$$

where the maximum expected value of the engine parameter, X , is determined from the nominal value and the deviations from the nominal because of the various component tolerances.

CONFIDENTIAL

(c) Control Points

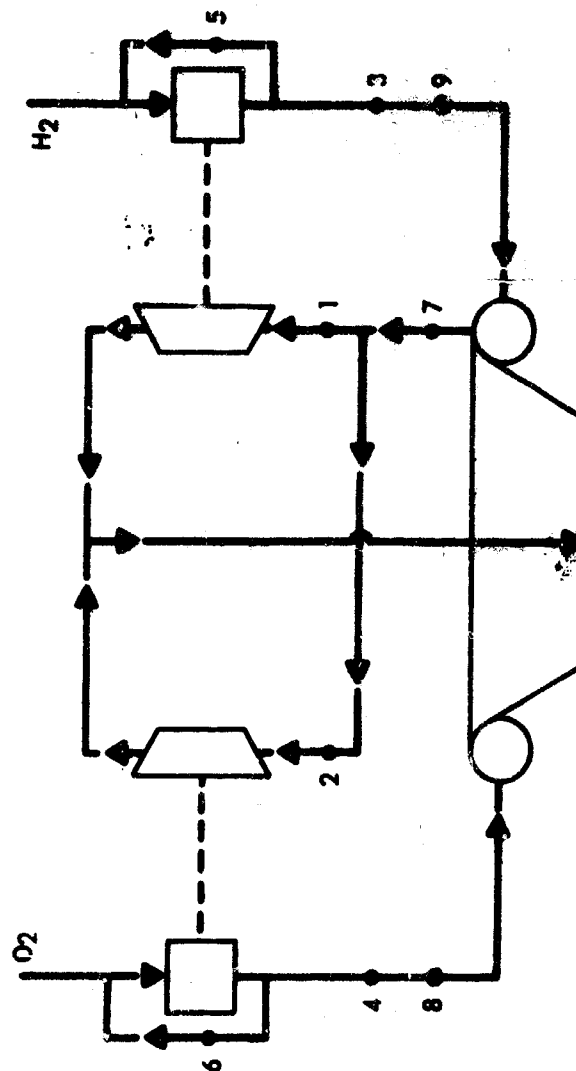
(C) An investigation of possible thrust and mixture ratio control methods was conducted during this report period to determine the optimum control points consistent with the flight and demonstrator module operational requirements. Schemes which involved multiple controllers for one function (i. e. , rough mixture ratio control achieved with a hot-gas valve and trimming with liquid valves) were eliminated from consideration because of the adverse effect upon system reliability. The control systems which merited consideration are listed below. The numbers in parenthesis correspond to the control points shown in figure 4.

1. Two hot-gas valves (1,2) or (2,7)
2. Main fuel valve and main oxidizer valve (3,4)
3. Two cavitating venturis (8,9)
4. One hot-gas valve and main oxidizer valve (7,4)
5. One hot-gas valve and fuel pump bypass (7,5)
6. One hot-gas valve and oxidizer pump bypass (7,6)
7. Main oxidizer valve and fuel pump bypass (4,5)
8. Main fuel valve and oxidizer pump bypass (3,6)

(U) The candidate systems were compared on the basis of performance effects, weight, engine dynamics, compatibility with other control functions, and design and development problems and costs. Table 3 summarizes the performance effects for all eight systems showing the values for pump discharge pressures, flowrates, pump speeds, thrust, and specific impulse. Undesirable levels for each parameter are asterisked. System number 3, consisting of two cavitating venturis, requires a 7000-psia fuel pump discharge pressure and a 3700-psia oxidizer pump discharge pressure. These are necessary to provide the extremely high pressure drops to maintain cavitation at the nominal condition.

CONFIDENTIAL

CONFIDENTIAL



- | | |
|---|-------------------------------|
| 1. FUEL TURBINE INLET VALVE (HOT GAS) | 5. FUEL PUMP BYPASS VALVE |
| 2. OXIDIZER TURBINE INLET VALVE (HOT GAS) | 6. OXIDIZER PUMP BYPASS VALVE |
| 3. MAIN FUEL VALVE | 7. TAPOFF VALVE (HOT GAS) |
| 4. MAIN OXIDIZER VALVE | 8, 9. CAVITATING VENTURES |

Figure 4 Control Point Schematic

CONFIDENTIAL

CONFIDENTIAL

This page is intentionally left blank

CONFIDENTIAL

CONFIDENTIAL

TABLE 3

STEADY-STATE TRAJECTORY

System No.	Operating Condition	Significant Parameters					
		Oxidizer Pump Discharge Pressure, psi	Oxidizer Flowrate, lb/sec	Oxidizer Pump Speed, rpm	Fuel Pump Discharge Pressure, psi	Fuel Flowrate, lb/sec	Fuel Pump Speed, rpm
1	Low mixture ratio	1800	405	23,065	2560	81	36,000
	Nominal	2056	476	25,016	2634	79.3	35,900
	High mixture ratio	2030	486	25,000	2420	69.1	33,600
2	Low mixture ratio	2391	456	26,342	2891*	91.3*	38,800
	Nominal	2242	477	25,914	3284*	79.6	38,800
	High mixture ratio	2118	505	25,646	3051*	74.5	36,900
3	Nominal	3700*			7000*		
4	Low mixture ratio	2706*	427	25,500	2566	82.8	36,000
	Nominal	2425	476	26,714	2635	79.4	36,000
	High mixture ratio	2064	482	23,650	2498	70.0	34,300
5,7	Low mixture ratio	2163	486.3	25,640	2916	98.1*	39,400
	Nominal	2054	476	25,013	2650	99.5*	38,000
6,8	Nominal	2055	606.4*	25,442	2634	79.4	35,900
	High mixture ratio	2516	589.3*	27,850	2918	83.7	37,000

*Undesirable value

TABLE 3

STEADY-STATE TRADEOFF

Significant Parameters					Remarks
Fuel Flowrate, lb/sec	Fuel Pump Speed, rpm	Specific Impulse, seconds	Thrust, pounds	Mixture Ratio	
81	36,000	453.5	224,000	5	Two hot-gas valves; 300 psi tapoff ΔP
79.3	35,986	450.2	250,000	6	
69.4	33,600	441.2	246,000	7	
91.7*	38,854	453	248,000	5	Two main valves; maximum differential pressure is 200 psi oxidizer and 670 psi fuel
79.6	38,873	449	250,000	6	
72.5	36,968	440.2	254,000	7	
					Two cavitating venturis
82.8	36,000		230,000	5.18	One hot-gas valve and main oxidizer valve; 400 psi differential pressure; oxidizer valve nominal
79.4	36,000	449.9	250,000	6	
70.9	34,344		248,000	6.84	
98.1*	39,440*	452.5	261,000	5.36	Hot-gas valve and fuel pump bypass; main oxidizer valve and fuel pump bypass
99.5*	38,071*	449.3	250,000	6	
79.4	35,992	449.8	250,000	6	Hot-gas valve and oxidizer pump bypass; main fuel valve and oxidizer pump bypass
83.7	37,830*	441.7	292,000	5.9	

CONFIDENTIAL

This page is intentionally left blank

CONFIDENTIAL

CONFIDENTIAL

(U) This area alone was sufficient to eliminate the cavitating venturiz from further consideration. The system using both main propellant valves (number 2) also required higher discharge pressures which translates into increased weight and decreased performance. Systems 5, 6, 7, and 8 (pump bypass systems) all require elevated pump flows and speeds. An associated pump weight increase and performance loss also occurs with the increased flows. The hot-gas valve system (number 1) has the best specific impulse; however, its advantage is small. The improved performance of the tapoff hot-gas control system results from the lower pump discharge pressures and flows achieved by removing the control point from the liquid system. This allows a reduction in the turbine hot-gas flowrate which is used as the secondary flowrate in the base region of the aerospike nozzle. The nature of the aerospike nozzle is such, that in the region of the nominal ADP operation, a reduction in secondary flowrate causes an increase in engine specific impulse.

(U) A dynamic analysis of the control system response favors liquid valve control over gaseous systems. However, the response requirements for the thrust and mixture ratio control systems do not preclude the use of the gaseous system. Another possible dynamics advantage of the liquid systems is the impedance it places between the feed system and thrust chamber. This would perhaps be of importance in throttling lower than 5:1 but is not judged of importance at the 5:1 design requirement.

(U) Two areas of possible interaction of system functions with the throttling and mixture ratio control systems are the start sequence and the hot-gas igniter mixture ratio control. The hot-gas control valve system may be useful for both of these other functions, because the hot-gas valves can be opened for additional turbine starting torque, can be used to control pump discharge pressure, and can be used to control mixture ratio. The main valve systems cannot be used for either of the first two applications, because they control flow only to the thrust chamber. A hot-gas valve and bypass system (number 5 or 6) could conceivably also accomplish the added functions.

(U) Rocketdyne experience favors the design and development of liquid control valves (particularly oxidizer) over the hot-gas valves. However, experience in design and development of large servocontrolled valves is not so far advanced in either case that there would be a significant difference in schedule.

(U) The conclusion to be deduced from the study is that the system utilizing two hot-gas valves is preferable because systems using main valves or cavitating venturiz imply undesirable increases in system

CONFIDENTIAL

CONFIDENTIAL

operating pressures, and systems using pump bypass imply undesirable increases in system propellant flowrate (on the order of 20 percent for full mixture ratio excursion at nominal thrust).

(d) Closed-Loop vs Open-Loop Control Systems

(U) During this report period, effort was directed toward the selection of closed-loop or open-loop control systems for thrust and mixture ratio control. The pertinent material required during this period is presented under topics which are important considerations in forming a basis of selection. The work to date has consisted of specific evaluation of open-loop mixture ratio control vs closed-loop mixture ratio control because this control system is most critical with regard to cost, versatility, safety, and reliability. Many of the same arguments apply also to open-loop vs closed-loop thrust control; however, for the purposes of discussion here the thrust control system is closed-loop.

(U) In order to evaluate system cost, it is necessary to formulate the system in terms of components. For the purposes of this discussion, a closed-loop system on mixture ratio is shown in figure 5, and an open-loop system on mixture ratio is shown in figure 6. All of the systems use a single hot-gas valve in the tapoff line for thrust control, and another hot-gas valve in the line to the oxidizer turbine for mixture ratio control. The closed-loop system uses two sensors for control by volumetric flow measurement (turbine-type flowmeter) or three sensors (one of which is the chamber pressure measurement also used in the thrust controller) for control by pressure measurement. The flowmeter system uses filters and a multiplier circuit to generate an error signal to drive the oxidizer turbine valve, while the pressure transducer system uses a function generator to compute the error signal to drive the valve. Both systems require servovalve compensation and incorporate valve position feedback circuitry to increase safety and reliability. The open-loop mixture ratio control system (figure 6) uses the same valves as the closed-loop counterpart, with a similar minor loop closed around valve position. However, some modification of the system with respect to thrust level is necessary, either with respect to operating chamber pressure or with respect to tapoff valve area (if both systems are open-loop). The need for modification of the control loop (shown by analog multiplier and function generator) is justified in figure 7. This figure shows two thrust vs mixture ratio control envelopes for an open-loop control system based upon constant oxidizer turbine valve area throttling. The two envelopes result from two turbomachinery designs which have roughly a 10 percent change in the pump H-Q curves and the turbine efficiency-u/c curves. The figure reveals the controls sensitivity to the turbomachinery characteristics, because a 3 unit change in mixture ratio at low thrust occurs between the two designs. Although the expected variation in pump curves from

CONFIDENTIAL

CONFIDENTIAL

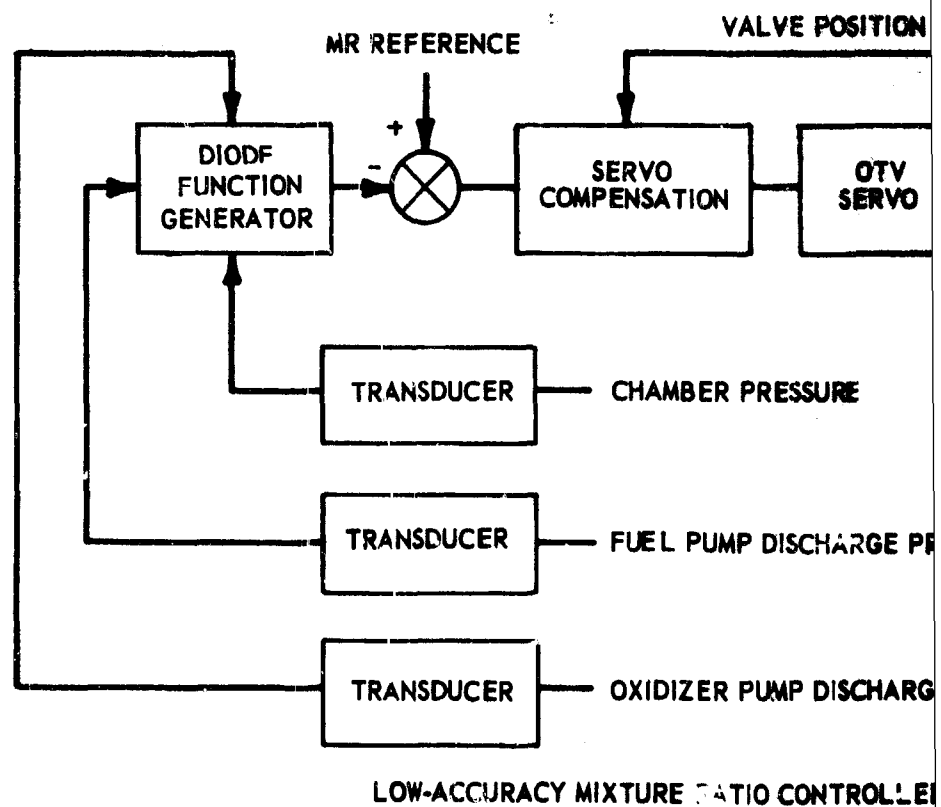
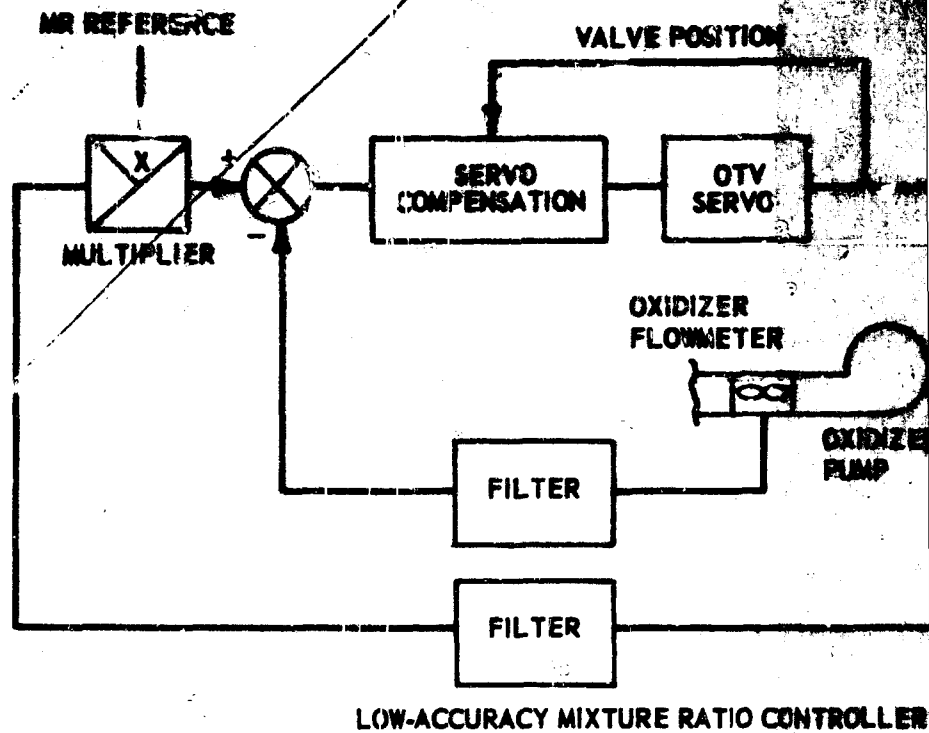
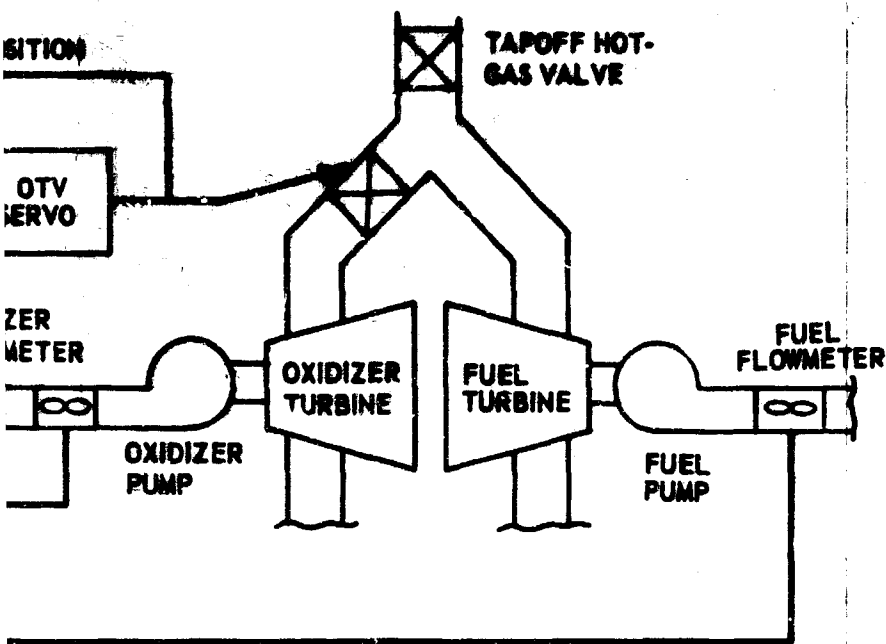
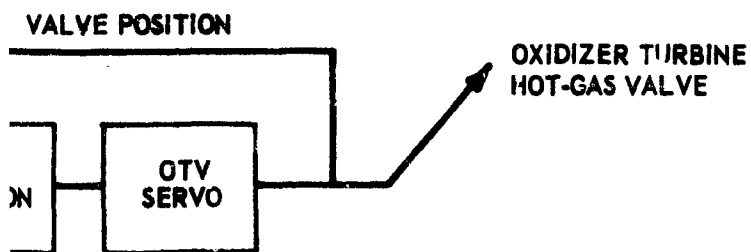


Figure 5



RATIO CONTROLLER USING TURBINE FLOWMETERS



ER PRESSURE

JMP DISCHARGE PRESSURE

IR PUMP DISCHARGE PRESSURE

RATIO CONTROLLER USING SYSTEM PRESSURES

Figure 5 Closed-Loop Mixture Ratio Control Systems

CONFIDENTIAL

This page is intentionally left blank

CONFIDENTIAL

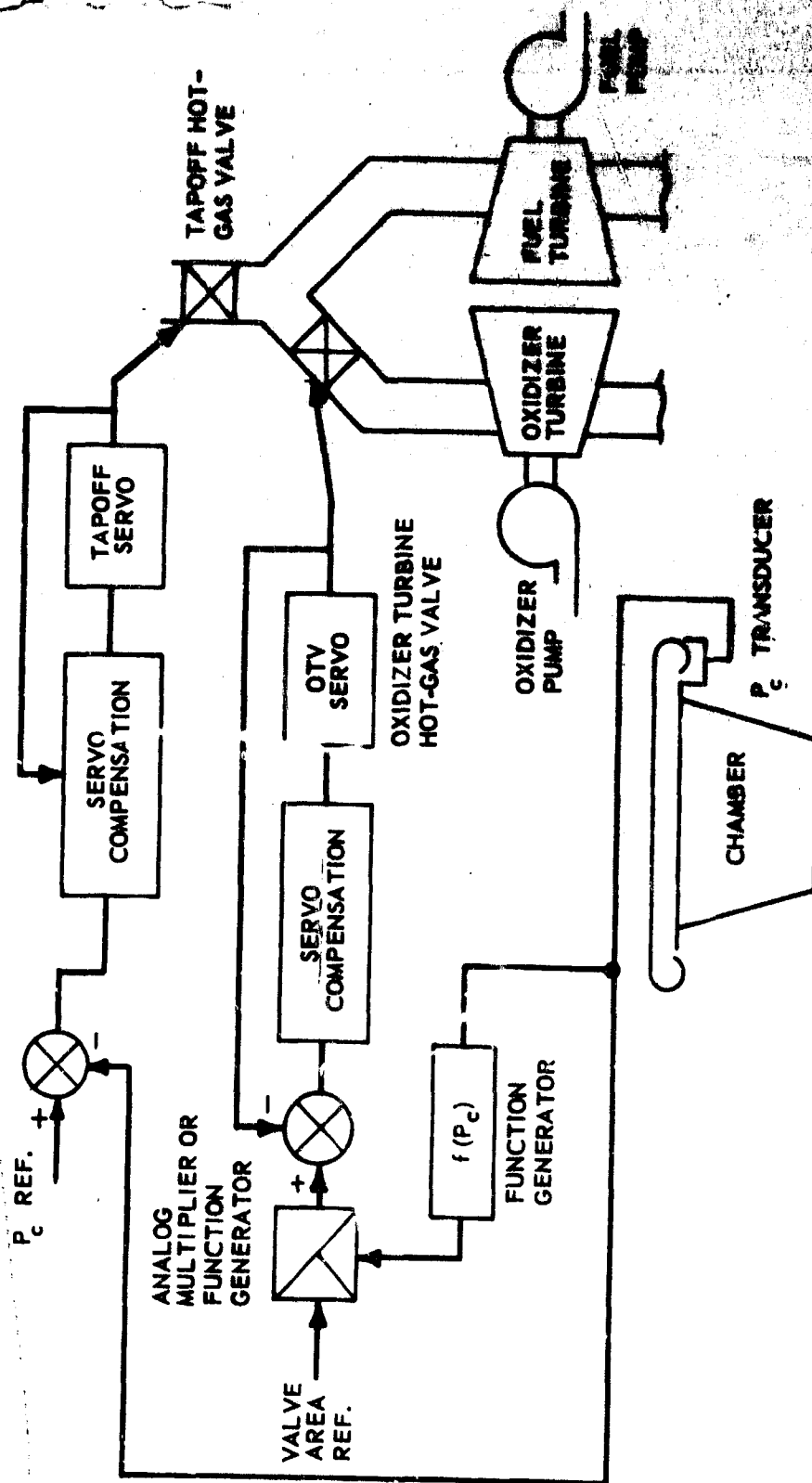


Figure 6 Open Loop Mixture Ratio Controller

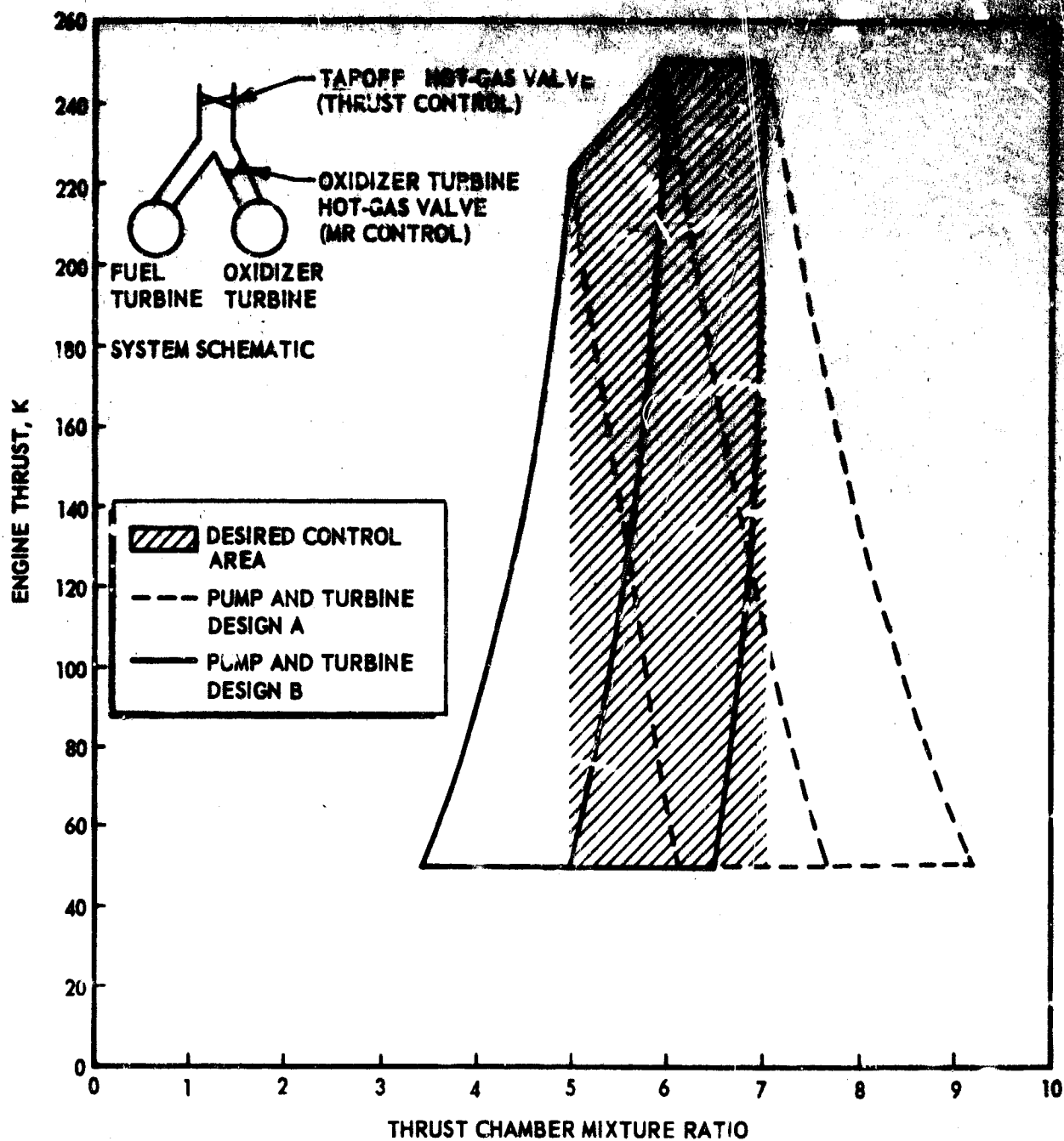


Figure 7 Effect of Pump and Turbine Curves on Open Loop Mixture Ratio Control System

CONFIDENTIAL

engine-to-engine is a factor of 3 less than shown and the expected variation in turbine efficiency is a factor of 5 less than shown, this will nevertheless produce an intolerable variation in mixture ratio during throttling unless some correction with thrust level is introduced. This can be introduced in a number of ways, such as mechanical linkage between valves, but electrical modification is depicted in the schematic since either tapoff valve area or chamber pressure will be available.

Cost

(U) The open-loop and the closed-loop mixture ratio system are judged to be identical in cost except for the addition of two turbine flowmeters and some increase in system compensation logic in the closed-loop system if all costs including additional testing for calibration purposes are considered. (This equates the cost of the closed-loop system filters and the multiplier with the function generator and multiplier required for valve area change with thrust level of the open-loop system.) The flowmeters may be required as standard flight instrumentation in any event, but for the purposes of this study, this is assumed not to be the case. Valve position control is included in both systems because of the increase in safety and reliability of the closed-loop system and because maintenance of constant area with input signal is essential for satisfactory open-loop system operation.

(U) Testing costs for the open-loop system will be greater. This cost could be minimized by development of a facility mixture ratio control system so that engine calibration can be accomplished in one test. With this assistance, extra engine testing would probably be increased by two tests, one for determination of the oxidizer turbine valve area vs thrust level function generator setting (or cam) for that particular engine, and one for checkout and verification. Some increase in cost of component testing would also occur for open-loop operation, because more component trimming will be required for insurance that correction of the oxidizer turbine valve as a function of thrust level can be obtained.

(U) In summation, closed-loop operation will require two flowmeters and increased compensation complexity as opposed to open-loop operation requiring development of a facility mixture ratio control system, two extra tests per engine, and some increase in component testing.

Versatility

(U) The closed-loop system is judged to be more versatile in that extensions in thrust or mixture ratio range are possible without engine recalibration. The same argument is present for component replacement. In addition, the closed-loop system has the greatest potential

CONFIDENTIAL

CONFIDENTIAL

for avoidance of undesirable operating points, if they are identified. Less modification is required for addition of other control parameters, such as pump speed. Also, if it is desired to run the closed-loop system in an open-loop mode for test or demonstration purposes, it can be done with minimal effort as opposed to running the open-loop system in a closed-loop mode.

Safety

(C) The closed-loop system is generally judged to be safer than the open-loop system as substantiated by the following arguments. Mechanical stops can be located on both hot-gas valves so as to restrict travel. Thrust can be restricted to values of 250K (with some sigma variation) by suitable location of an opening stop, and to values of 50K by suitable location of a closing stop. However, thrust variations greater than nominal or less than 20 percent can be considerable before failure is anticipated. The same is not true for mixture ratio; variations on the high side can result in burnout, and variations on the low side can result in flameout, either of which may be catastrophic. It is not possible to locate fixed mechanical stops in the oxidizer turbine valve for mixture ratio variation protection without seriously reducing the operating region.

(C) If stops are located based on the nominal thrust region, then it is possible to exceed allowable mixture ratio variation at the 20 percent thrust level. If stops are located based on the 20 percent thrust level, then mixture ratio variation from 5 to 7 is not possible at nominal thrust. These considerations apply to both closed-loop and open-loop systems. The closed-loop system will give some indication that mixture ratio is entering an undesirable region; the open-loop system will only indicate that oxidizer turbine valve position is entering an undesirable region. Dynamics may preclude considerable separation between valve position and engine mixture ratio. In the proposed systems, failure of the valve position transducer will result in failure of the engine for the open-loop system for most instances; in the closed-loop the engine failure will be caused only if both the mixture ratio loop and the valve position minor loop fail simultaneously. Although a vehicle mixture ratio controller may serve to protect the engine in some cases, in cluster applications mixture ratio failure in one engine may be masked by the other engines.

Reliability

(U) There is expected to be some penalty in reliability of the closed-loop system over the open-loop system because of the increase in components; however, this will be offset to a certain extent by the redundancy of mixture ratio and valve position discussed above. According

CONFIDENTIAL

CONFIDENTIAL

to flight instrumentation systems reliability data for the J-2 engine (which is similar to the ADP engine), the failure rates are 0.0004 per exposure for turbine flowmeters and 0.0021 for exposure for pressure transducers (about 50 percent of these were out-of-calibration only) for the period of June 1964 through April 1966. These rates are suitable for this application.

Static Accuracy

(U) The static accuracy of the closed-loop system is expected to be on the order of 7 percent in mixture ratio. The object of the closed-loop system is not to accurately control engine mixture ratio; that is left to the vehicle guidance computer. During this report period, work was accomplished describing expected accuracy of volumetric flow measurements relative to true mass flow measurements for computing mixture ratio. Volumetric mixture ratio is expected to be within 5 percent of true mass mixture ratio over the range of thrust. The flowmeters each contribute 0.3 percent (J-2 experience), and the filtering and multiplication process is expected to contribute another 1 percent. If pressure measurements are used, less accuracy is expected because of the transducers (2 percent accurate, J-2 experience) and method of computation to yield an estimated 10 percent. The open-loop system is expected to yield an accuracy of 15 percent for a given input current.

Dynamic Performance

(U) Presently, no problem in dynamic performance are anticipated with either the closed-loop or open-loop systems. One possible criterion may arise in the ratio of fuel turbine time constant to oxidizer turbine time constant; too large a discrepancy will cause a large change in mixture ratio during fast changes of input for the open-loop system. Another disadvantage of the open-loop system is a loss in flexibility of manipulation of the engine transfer function. The ability to change this function might prove advantageous in the advent of a POGO problem or other vehicle/engine interface instability problems.

(e) Gimbal Actuator Study

(U) During this report period, a preliminary study of estimating gimbaling loads, sizing actuators and servovalves, and determining the output power required of a hydraulic pump was completed. The results are preliminary ones because the engine thrust structure configuration and exact location of the gimbal bearing and actuator attach points are not yet determined; however, one of the four candidate thrust structure designs was selected for study purposes. Some of the study assumptions and results are listed below.

CONFIDENTIAL

CONFIDENTIAL

GENERAL OPERATING CHARACTERISTICS

Gimbal Angle (in circular pattern), degrees	7
Gimbal Rate (maximum), degree/sec	30
Gimbal Acceleration (maximum), radians/sec ²	30
Longitudinal Acceleration, g	5
Lateral Acceleration, g	1.5
Engine Moments of Inertia, in-lb-sec ²	5900 Pitch Axis 5600 Yaw Axis
Gimballing Loads (maximum), in-lb	
At 30 deg/sec rate	332,000
At stall	500,000

ACTUATOR

Moment Arm (assumed), inches	31.25
Area, sq in.	5.33
Stroke (for ± 7 deg), inches	± 1.82
Rate (maximum), in/sec	16.36
Maximum Differential Pressure, psi	
At 332,000 in-lb load moment	1992
At 500,000 in-lb load moment	3000
Maximum Force, pound	
At 332,000 in-lb load moment	10,600
At 500,000 in-lb load moment (stall)	16,000
Power (maximum), hp	26.34

SERVOVALVE

Flow at 30 deg/sec gimballing, gpm	22.67
Flow Rating, gpm	
At 1000-psi differential pressure	22.60
At no load	39.25

CONFIDENTIAL

HYDRAULIC PUMP

Differential Pressure (nominal), psi	3000
Hydraulic Fluid	MIL-H-5606
Power (gimballing in actuator plane), hp	39.67
Power (gimballing at 45-degree plane), hp	
32 gpm at 3000 psi	56.1
32 gpm at 2000 psi	37.4

(U) The study reveals that the thrust structure concepts being considered will permit a substantial moment arm (31 inches) and thereby minimize the actuator force requirements. If the gimbal bearing location is raised above the plane of the injector, the engine moment of inertia will increase and raise the power demands; however, even the worst case does not present a design problem.

(U) At the Air Force/RD coordination meeting of 29 August 1966 a diagram was presented of the acceleration loads to be used in designing the demonstrator and flight modules. These loads are greater than those used in the study to date. This new data will be incorporated into the gimbal and actuator load definition during the next quarter.

(f) Alternate Engine Cycle, Gas Generator

(C) During the second quarter, a study was undertaken to compare two different aerospace engine systems. The variations involved tapoff vs gas generator line drive gas sources, with hot gas used to ignite the main thrust chamber. The effort was initiated to provide backup data based upon recent experimental results and design studies to be used in a final system configuration selection. Because the two systems have many common components, the design effort currently being conducted on the tapoff configuration will be useful for either system regardless of the final selection.

(C) The two candidate systems are shown schematically in figure 8. The first is the tapoff driven cycle with a hot-gas igniter for thrust chamber ignition. Thrust and mixture ratio control are achieved with hot-gas valves in the turbine inlet lines. The igniter temperature is controlled during the start transient by the use of a liquid oxygen regulator, and a hot-gas igniter isolation valve is required in the igniter discharge line to prevent tapoff gases from circulating into the gasifier body during mainstage.

CONFIDENTIAL

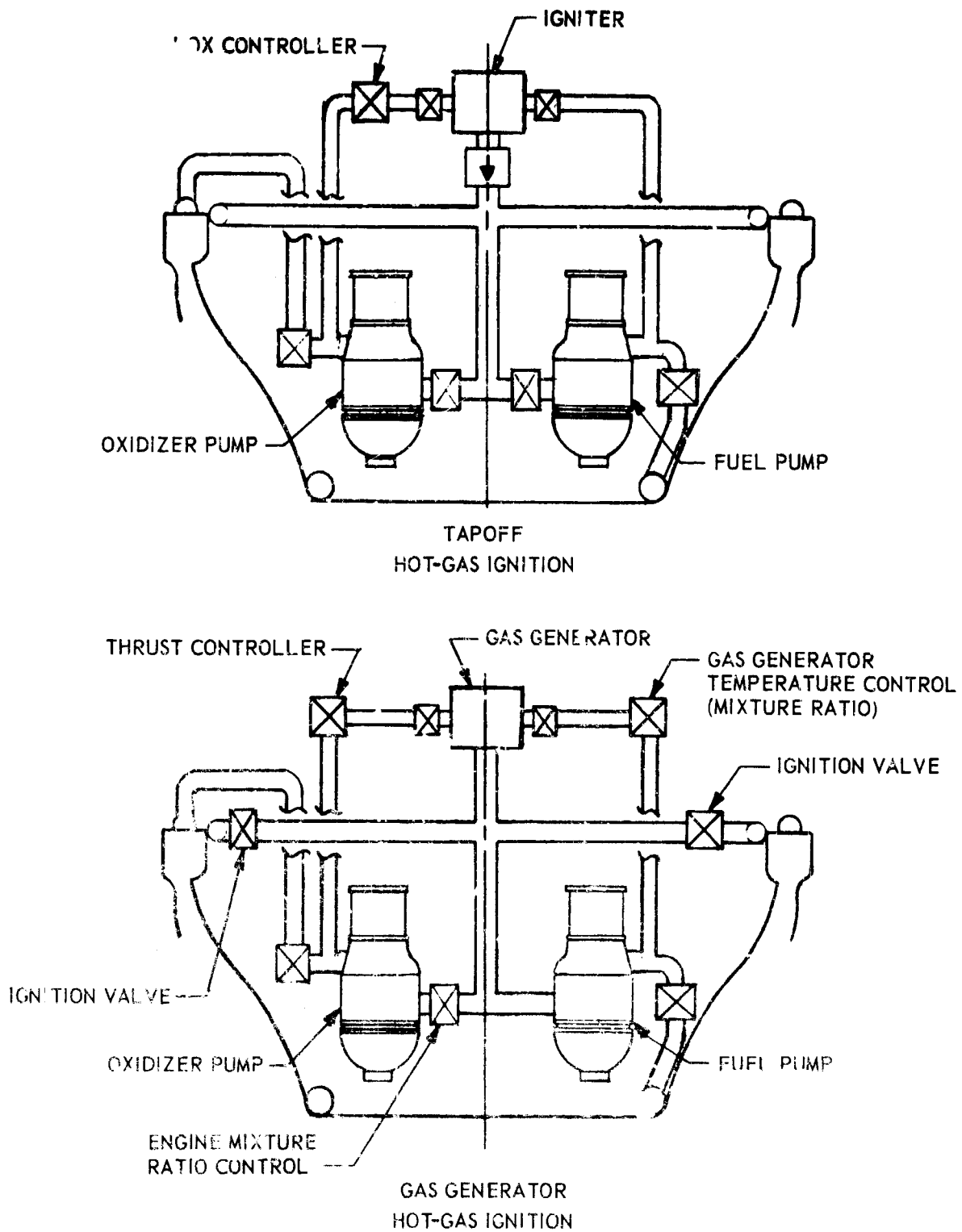


Figure 8 Cycle Schematics

CONFIDENTIAL

CONFIDENTIAL

(C) The second system is the gas generator driven cycle also using hot-gas as the thrust chamber ignition source. One hot-gas valve is used for engine mixture ratio control, while valves in the gas generator liquid lines are used for thrust control. Two additional hot-gas shutoff valves are required in the thrust chamber ignition lines, while the igniter isolation valve is eliminated from the system.

(C) The two systems will be compared on the basis of performance, weight, reliability, cost, risk, and operability. Preliminary results have indicated that the tapoff cycle provides a small (1 second) performance advantage over the gas generator cycle; however, current test results have raised the possibility that the tapoff gas properties may have a lower energy content than used in the performance calculations. If the tapoff gas properties should turn out to be closer to gas generator properties, then the performance difference will become even smaller.

(C) From a weight standpoint, the two systems differ only in their ignition systems, controls, and turbine drive gas systems. Preliminary weight comparisons have indicated that the two are virtually identical. The two systems both require the same hot-gas manifold because it is sized for the start condition, and the gas generator and hot-gas igniter have no significant weight difference. Both of the combustors are sized for the start condition and only the injector design will differ between the two. While the gas generator system employs one extra valve, the weight of those valves found only in the gas generator system appears less than the weight of those valves found only in the tapoff system. Both systems use the same four-way hot-gas distribution manifold at the combustor exit together with the same hot-gas ducting design.

(U) From the schematic comparison, it can be seen that the differences between the two systems lie almost entirely in controls. The tapoff system employs eight valves and the gas generator system nine. Five valves are common to both systems. An analysis of the module layout indicates that the valve changes can be made with virtually no alteration to the engine packaging arrangement. This fact greatly enhances the tapoff development program, because the design is flexible and could be converted to a gas generator design with a minimum of effort and time. The layouts also emphasize the fact that much in-depth design on common components can be initiated early in the ADP program without the risk of lost effort.

(U) Preliminary thrust and mixture ratio control studies indicate that dynamics of the system controlled with turbine hot-gas valves is better than that controlled with gas generator liquid propellant valves. Preliminary studies also indicate operation and control of the gas generator at low thrust levels may present a problem because of the low allowable

CONFIDENTIAL

injector pressure drops. On the other hand, the attainment of acceptable turbine drive gas properties in the tapoff system over the mixture ratio and thrust range of interest may present a significant development problem.

(U) The factors of reliability, cost, risk, and operability have not been studied quantitatively; however, a preliminary qualitative assessment can be made. The tapoff system has the potential of being the simplest and most reliable because of the elimination of the gas generator operation during mainstage and the simpler control problem. But it may also be the most expensive, and involves the most risk, as an unknown development quantity. However, the development risk factor is reduced by the flexibility of the system and its ability to be readily converted to a gas generator design.

(U) The main development advantage of the gas generator system is the avoidance of the development of a thrust chamber tapoff port design. This permits the hot-gas ignition ports to be designed for only one function without compromise. It also reduces the extent and complexity of thrust chamber testing, with a resultant decrease in development cost. However, because much of the tapoff development testing will be conducted on low thrust level segments and in conjunction with normal thrust chamber testing, the actual dollar difference will be difficult to determine. Further effort to evaluate the two systems will continue during the next quarter and a design decision will be made at that time.

(g) Start Dynamics

(U) A dynamic simulation of the fuel feed system was developed during this report period. A deep chill of the cooling tubes (-400F) was assumed in this first analysis. Also, pump surge (a region of positive H-Q slope or discontinuity) was not simulated. As the study progresses, effects of coolant tube initial temperature, pump surge, and other system parameters will be added to the scope of the analysis.

(C) The description of the central ignitor, hot gas, and turbine flow system was modified to reflect current configurations but remained in a simplified form. Transient performance of this system is shown in figures 9 and 10. The valve sequencing is shown in figure 11.

(C) Pump speeds rise steadily until they reach 9044 rpm (LOX pump) and 14240 rpm (fuel pump). These speeds are those required for the 20 percent thrust level performance. They are almost 40 percent of those required for 250K thrust (because the flow coefficient is 50 percent of nominal) due to the flat H-Q characteristics. A controller which affects turbine valve area is responsible for this speed profile. Fuel turbine valve area was made a function of the difference between

CONFIDENTIAL

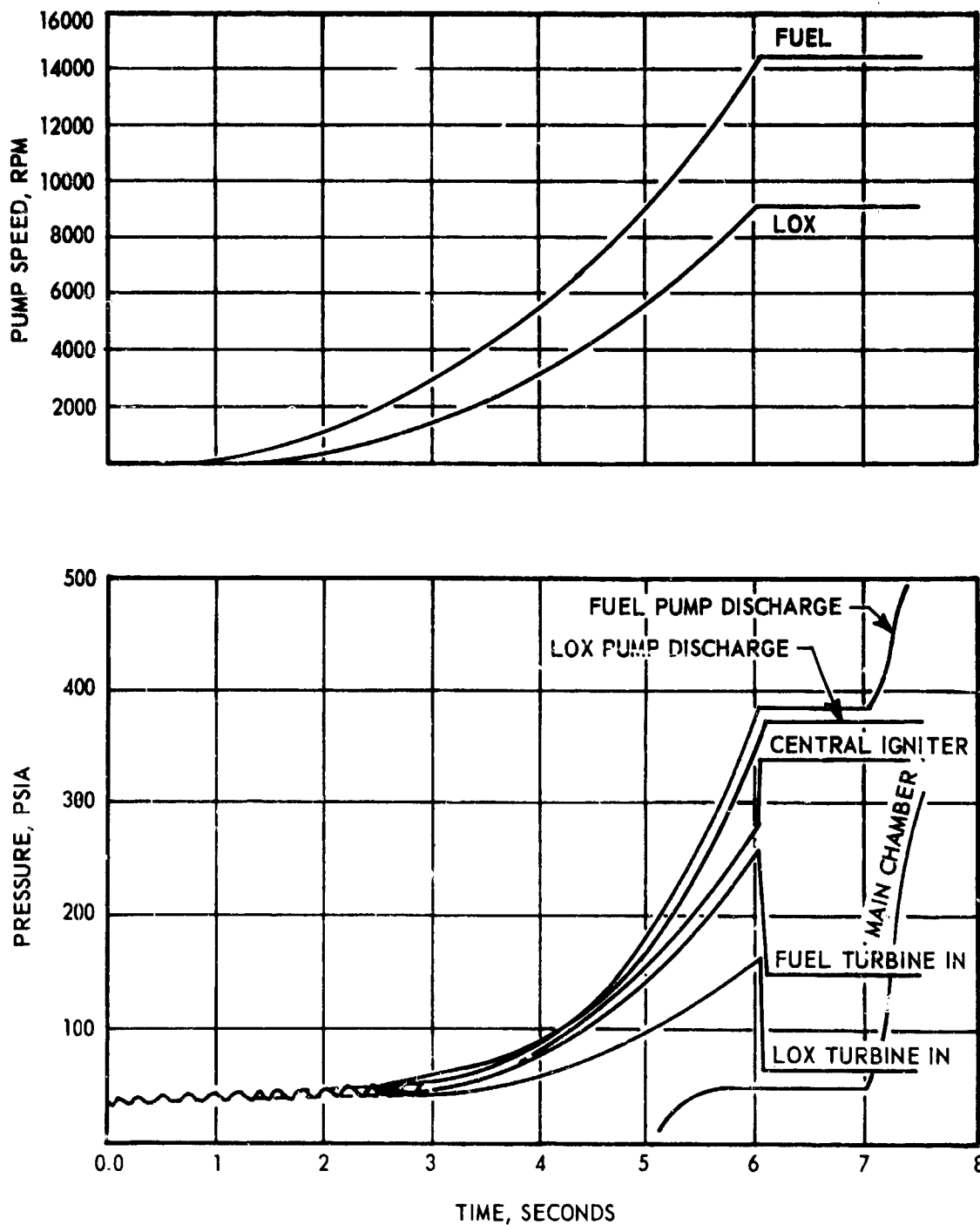


Figure 9 Transient Performance, Pressure and Pump Speed vs Time

CONFIDENTIAL

CONFIDENTIAL

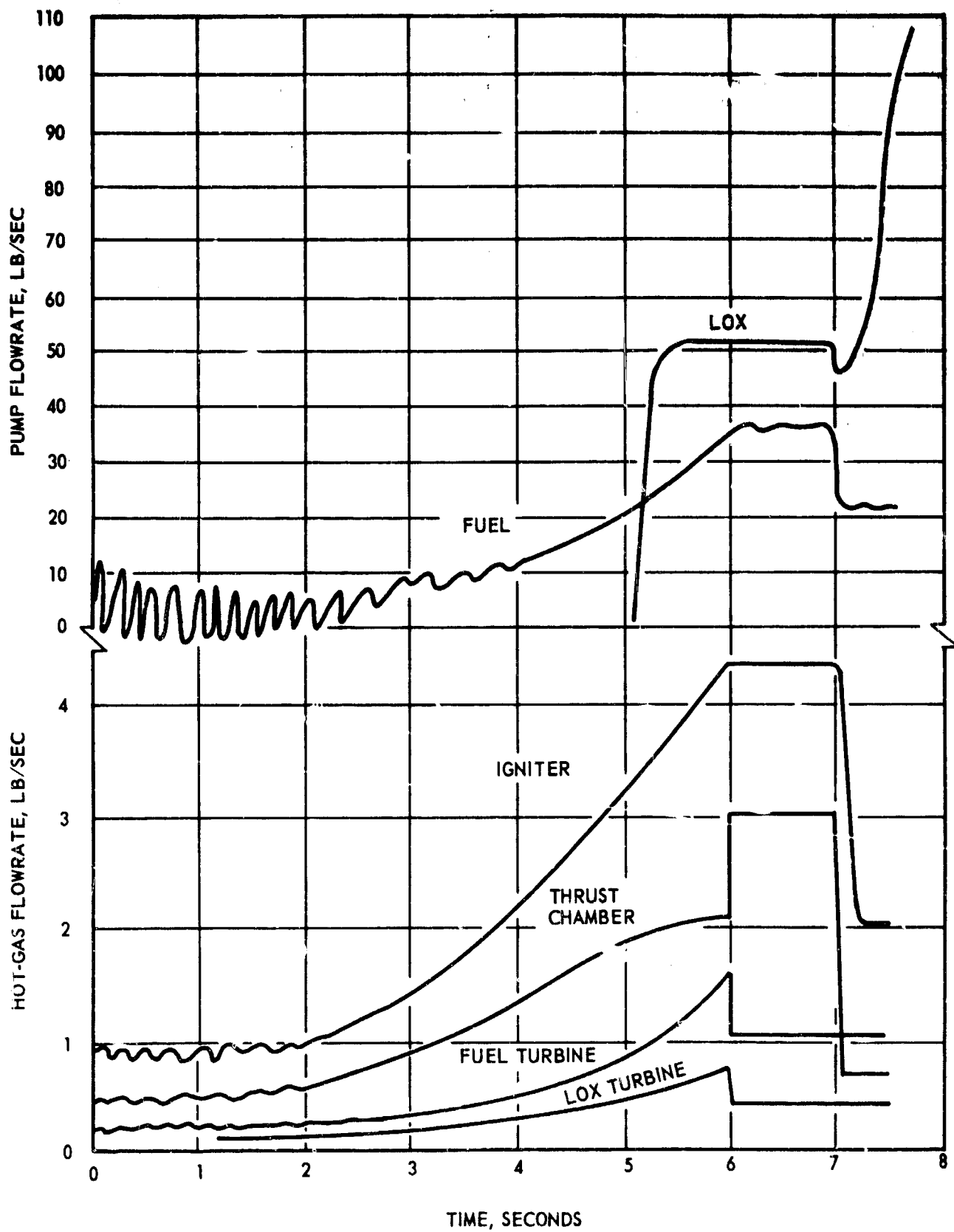


Figure 10 Transient Performance, Hot-Gas and Pump Flowrate vs Time

CONFIDENTIAL

CONFIDENTIAL

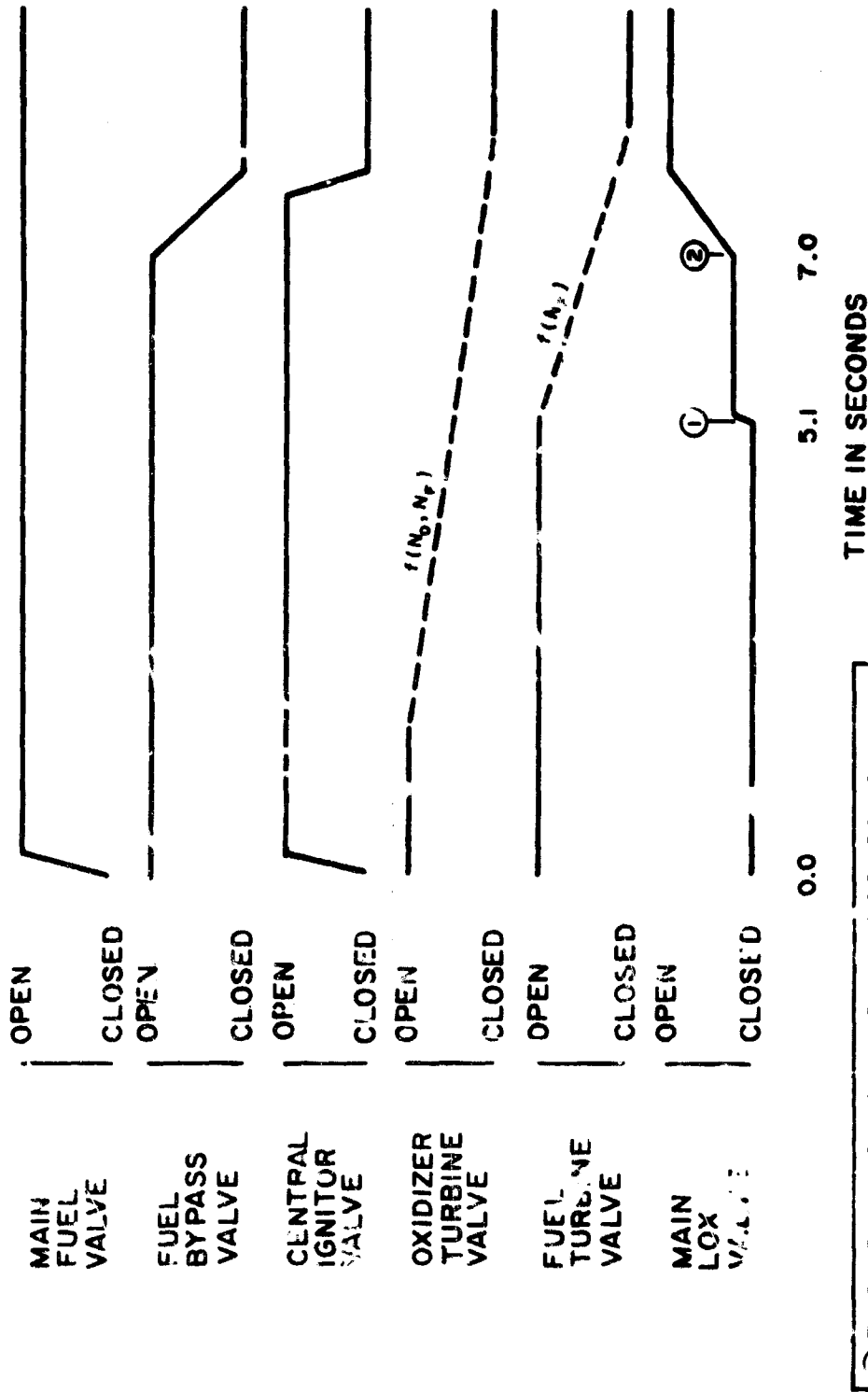


Figure 11 Valve Sequencing for ADP Start

CONFIDENTIAL

CONFIDENTIAL

14240 rpm and actual speed. LOX turbine valve area was function of the difference between the ratio 9044 rpm/14240 rpm and actual ratio of LOX and fuel pump speeds. As a result, LOX and fuel discharge pressure are very close to each other during the start. The LOX is actually slightly lower during most of the start. This pressure profile reduces demands on the central igniter mixture ratio controller and enhances the possibility of removing the requirement entirely. However, as long as oscillations exist in the fuel feed system, a controller will be required.

(U) Developments in the NASA SDI program are being continually reviewed for state-of-the-art applicability to the ADP program. Recently a test program was conducted investigating the priming and distribution characteristics of the LOX manifold utilizing water and gas-water in three 0.25-scale transparent models. With four tangential lines feeding a toroidal manifold, symmetrical rapid priming occurred. With two symmetrical radial arms and four 90-degree tapered manifold sections, a high velocity impact against the end of each section occurred, creating a pressure wave which swept back through the manifold. This characteristic may be undesirable at engine start. However, evaluation of the water flow data from a manifold using 2-tangential inlets indicates it primes uniformly. In addition to the transparent model manifolds, a full-size four-tangential inlet manifold was constructed. This manifold was water-flow tested at the high-flow facility, and tests results have indicated excellent priming and fluid distribution characteristics. As additional results are obtained from the SDI program, they will be utilized in the design of the Demonstrator Module.

(2) Preliminary Design

(a) Demonstrator Module

(U) The demonstrator module layout was updated during the quarter and is shown in figure 12. It incorporates the parallel turbine arrangement established during the last quarterly effort and several minor changes since that time. Line sizes and routings were altered and the main propellant valves are installed in a vertical plane rather than horizontal, while the hot-gas igniter design has been integrated with a single isolation valve and a distribution manifold.

(U) During the second quarter, in-depth design was begun on the engine subsystems and components. This effort was undertaken to reveal some of the design problems which would arise and require additional tradeoff studies, and to establish subsystem envelopes and interfaces. However, to avoid wasted effort on configurations which may later be ruled out, the areas currently receiving attention are components and subsystems which are either common or very similar to the alternate module designs under consideration.

CONFIDENTIAL

CONFIDENTIAL

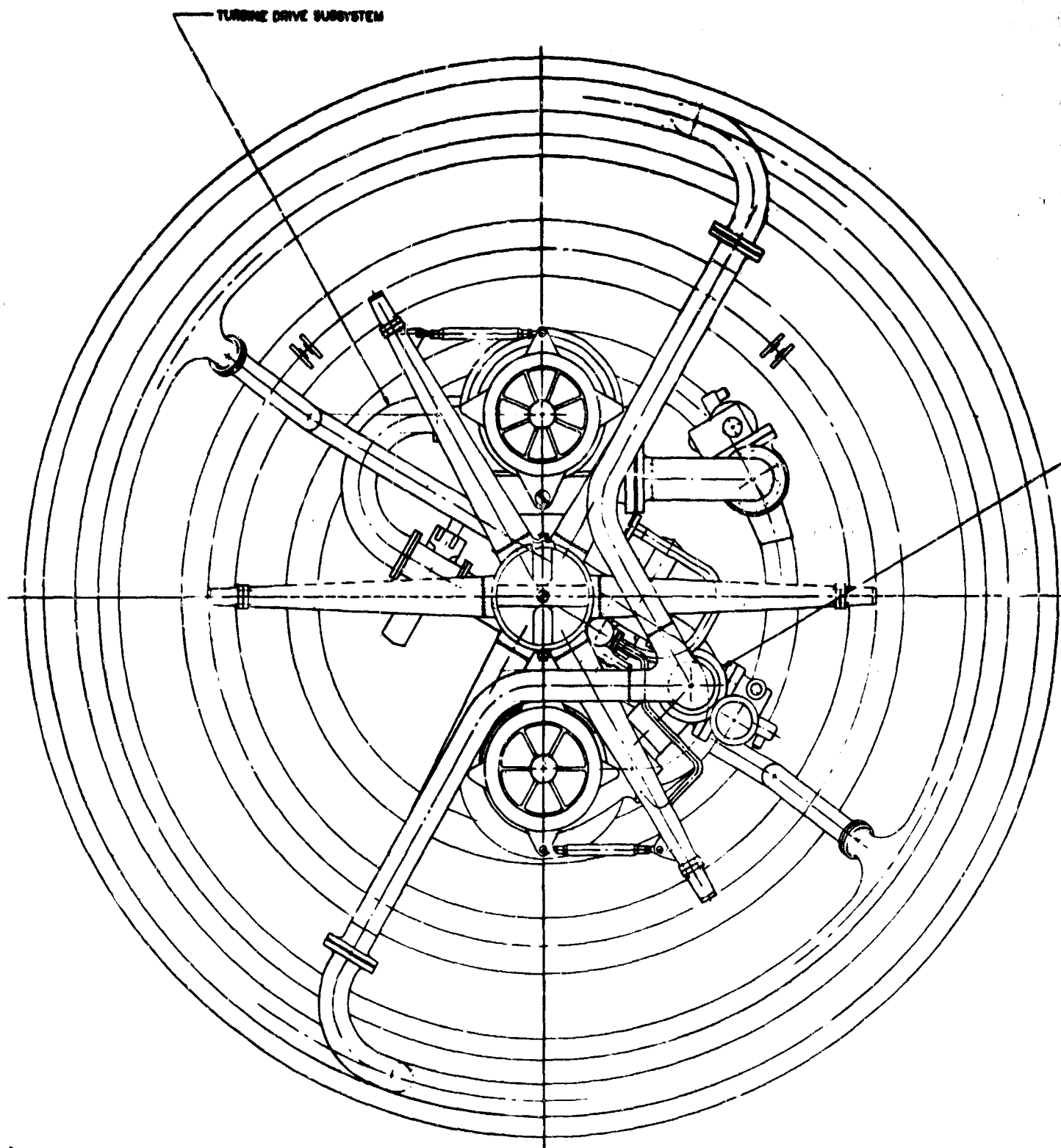
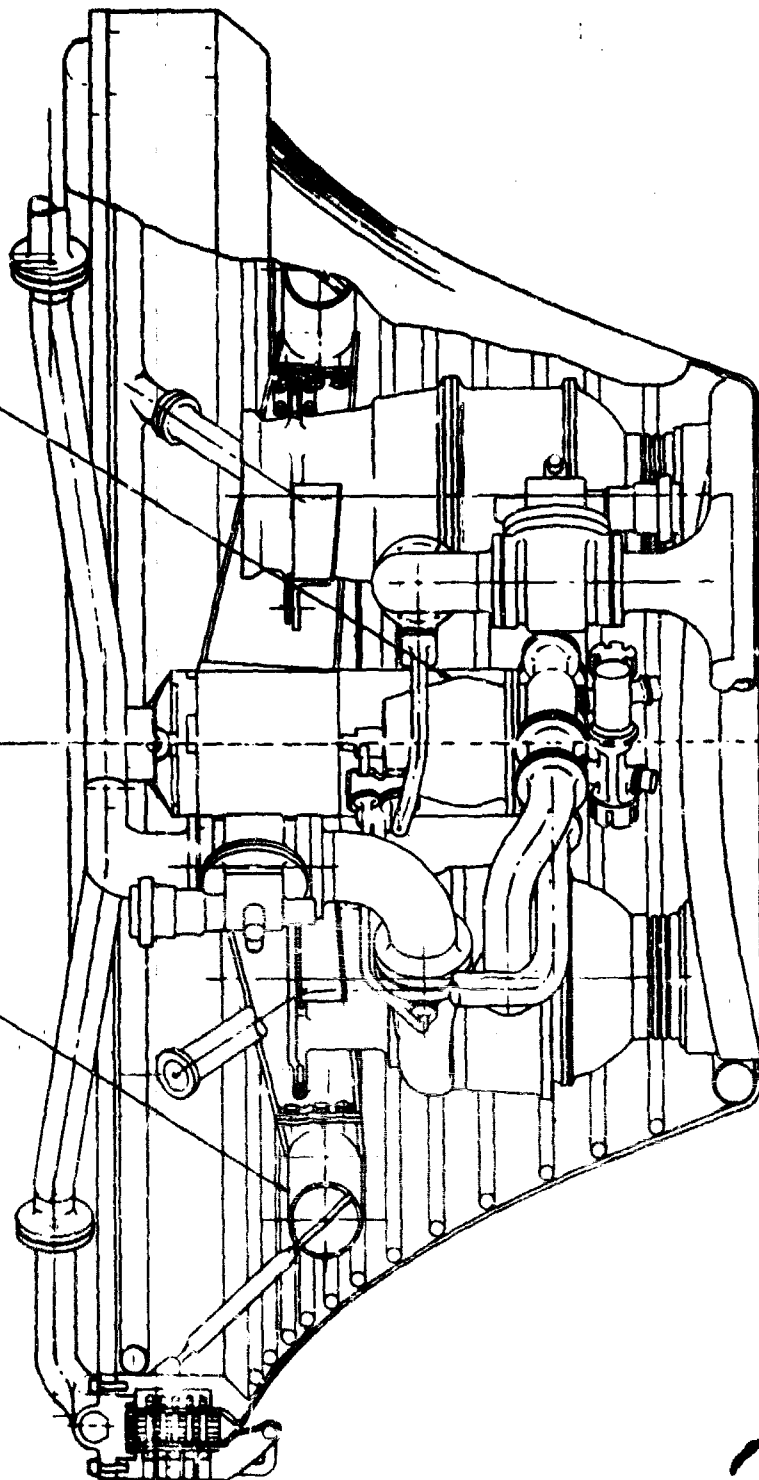


Fig 1

IGNITER HOT-GAS SUBSYSTEM

PROPELLANT FEED SUBSYSTEM

THRUST SUBSYSTEM



37

Figure 12. Preliminary Layout Demonstrator Module

2

CONFIDENTIAL

CONFIDENTIAL

This page is intentionally left blank

CONFIDENTIAL

CONFIDENTIAL

(U) The four main engine subsystems (turbine drive, propellant feed, igniter, and thrust) were studied to establish the criteria for the initial release of the preliminary component design sheets, and to define the subsystem envelopes and interfaces. Subsystem schematics and functional grouping diagrams were prepared and incorporated in a subsequent revision to these design sheets.

Turbine Drive Subsystem

(U) Analysis of the turbine drive subsystems determined that the hot-gas ducts and manifolds must be sized for the start condition. Further study was made of the tapoff duct configuration from a cost and manufacturing standpoint. The results indicate a mirror image design which sacrifices a few pounds of weight for an ease in fabrication may be the most attractive.

Propellant Feed Subsystem

(U) Deepening of the propellant feed subsystem design covered a cryogenic seal study, a propellant duct material trade-off study, and a preliminary study of the oxidizer "Y" branch line. Five types of static seals were considered:

1. Elastomer O-rings
2. Metal O-rings (vented and pressurized)
3. K-seals
4. Con-o-seal
5. Naflex

(U) The Naflex seal was selected because of previously conducted Rocketdyne evaluation studies which determined that the Naflex seal performs as well or better than other cryogenic static seals available at this writing, and because previous Rocketdyne usage and service experience is strongly in favor of the Naflex seal.

(U) The propellant duct materials considered in the design study were 347 CRES tubing, 6061-T6 aluminum extruded tubing, and Inconel 718 welded tubing. The Inconel 718 tubing was selected on the basis of a higher strength-to-weight ratio and superior capability to resist thermal stresses and deflections.

CONFIDENTIAL

(U) The study of the oxidizer branch line included an evaluation study to determine the optimum manufacturing method to use on the Y-fitting. The methods considered were:

1. One-piece forged billet, 3-D machined
2. Sheet stock, 4-piece weldment
3. One-piece precision investment casting

Controlling factors, weight, cost, ease of manufacture, tooling costs, reliability, delivery, and simplicity influenced the decision to design this part as a (3-D machined) one-piece configuration. Braided wire flexible hoses were also considered in the design evaluation of the oxidizer branch line assembly. High weight and pressure loss were the significant reasons for rejection of this configuration.

Igniter Subsystem

(U) Analysis of the igniter subsystem was made to help define conditions during the start transient and also to define the igniter gas/tapoff gas inter-relationships. Through this study, it was determined that it was desirable to isolate the hot-gas igniter body and injector from the tapoff gases flowing during mainstage. At this time, it appears that a check valve as previously envisioned is unsatisfactory because pressure in the igniter is always greater than that in the tapoff duct until the igniter is sealed off. This led to a tentative design of an integrated hot-gas igniter body and poppet valve. The design shown in figure 13 also integrates the hot-gas plenum chamber distribution manifold with the igniter body and valve. The manifold has four openings with each tapoff duct inlet co-linear with a turbine drive duct outlet. This design thereby minimizes the steady-state tapoff hot-gas pressure drop through the distribution manifold.

Thrust Subsystem

(U) The thrust subsystem was studied to improve accessibility and to analyze the thrust structure. The accessibility study determined that the oxidizer and tapoff ducts should be designed with a joint at a diameter greater than the central thrust structure beams. This would permit the thrust chamber to be detached from the structure and dropped free of the components mounted in the well with no interference.

CONFIDENTIAL

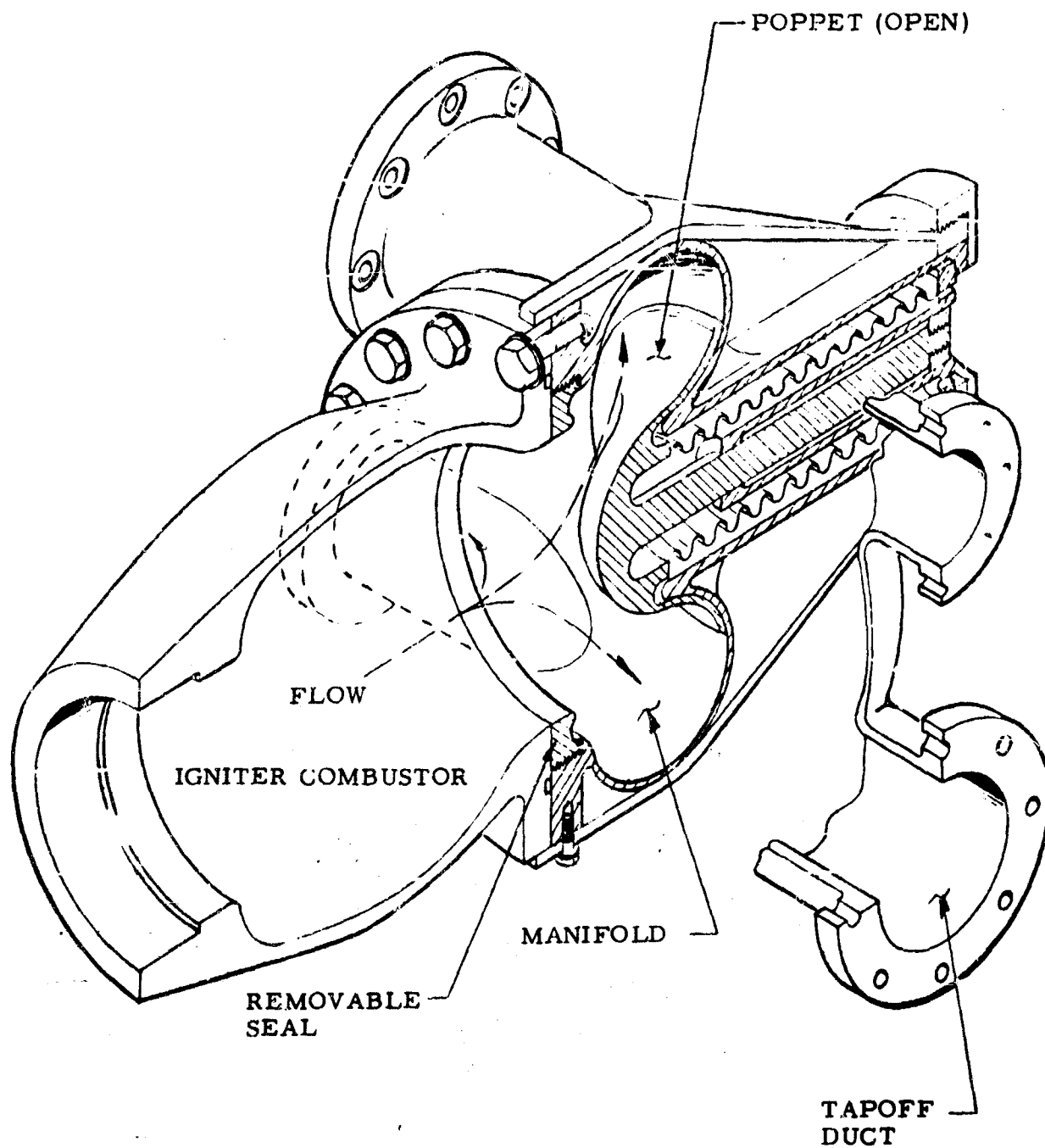


Figure 13. Igniter Hot-Gas and Isolation Valve/Manifold Assembly

CONFIDENTIAL

CONFIDENTIAL

(U) The method of mounting the pumps on the thrust structure was studied, and a preliminary concept which features adjustability in all three axes is shown in figure 14.

(U) A deeper thrust structure trade study was initiated primarily to re-evaluate the weight, assembly, and accessibility aspects of this component assembly. Figure 15 depicts 25 basic concepts in three basic categories using the module gimbal point as a means of classification: (1) locating the gimbal point at the elevation of the injector face, (2) and (3) locating the gimbal point at increasing elevations above the injector face. A limit of 13 inches was placed on the lowest elevation to be occupied by the structure, because of volume requirements for module components within the thrust chamber centerbody cavity. The upper limit is established by dynamic envelope and engine length requirements from module application considerations. Out of the 25 concepts, four candidates (figure 16) have been selected for more extensive evaluation preparatory to the final selection. Figure 17 shows the plot of weight vs height for the truss configuration and is the same in general for the beams. Figure 18 shows the dimensional geometry of the module related to available space for the thrust structure. A plot of the module dynamic envelope radius vs gimbal point elevation is shown in figure 19 for the 7-degree circular gimbal pattern.

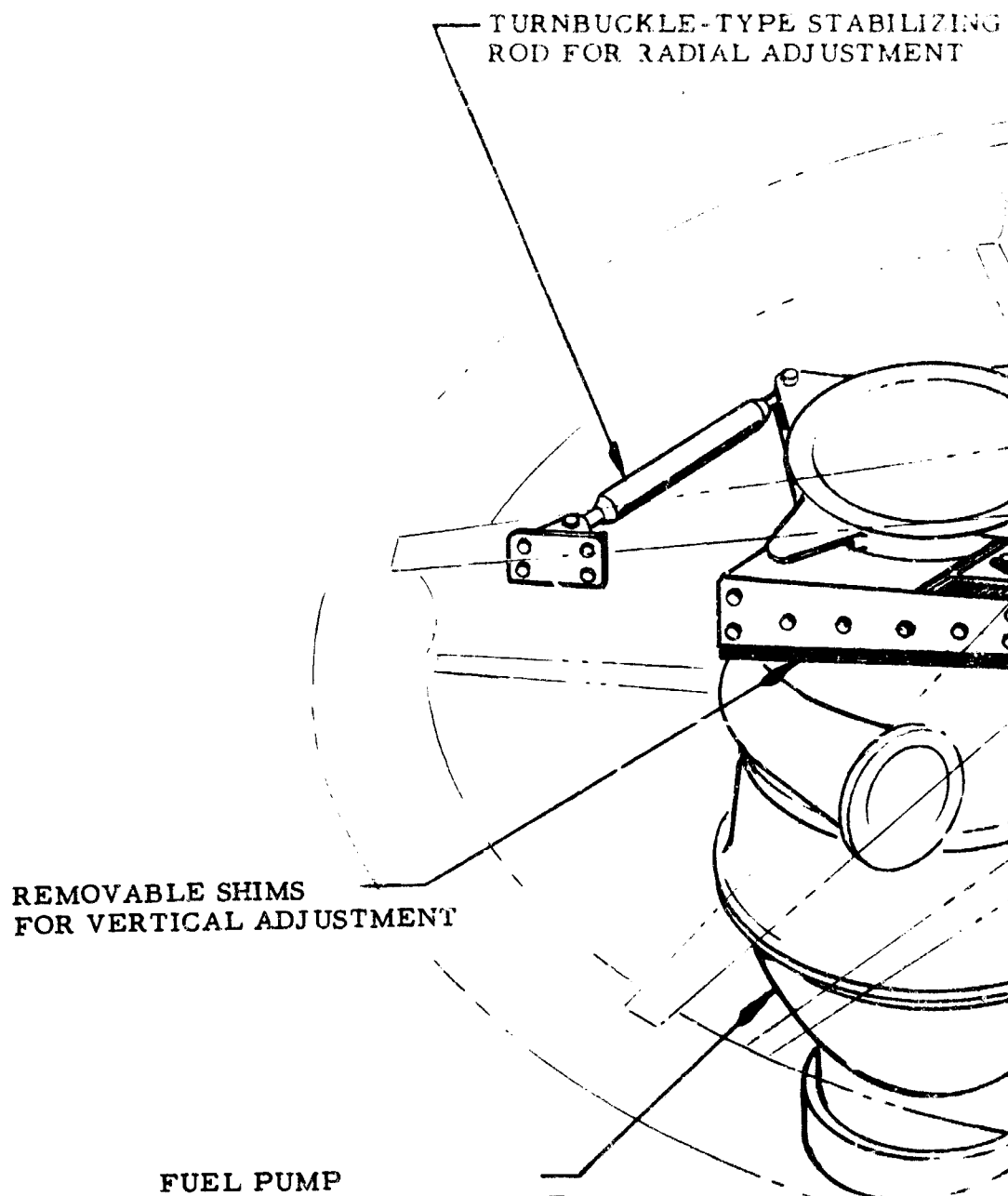
(U) Final analysis and evaluation of the thrust structure trade study will be completed next quarter.

(b) Flight Module

(C) Preliminary layouts of the 250K and 350K flight modules were prepared for use in the applications study. A nominal 350K engine is shown in figure 20. This engine delivers a vacuum thrust of 350K operating at an engine mixture ratio of 6:1. The annular combustion chamber operates at 1500 psia (nozzle stagnation), and the products of combustion are expanded along a shrouded, truncated, 25-percent length spike nozzle.

(C) As shown in the general arrangement drawing, the gimbal point is in the plane of maximum diameter and, thus, the dynamic diameter during gimbaling is the same as the static diameter for this configuration.

CONFIDENTIAL



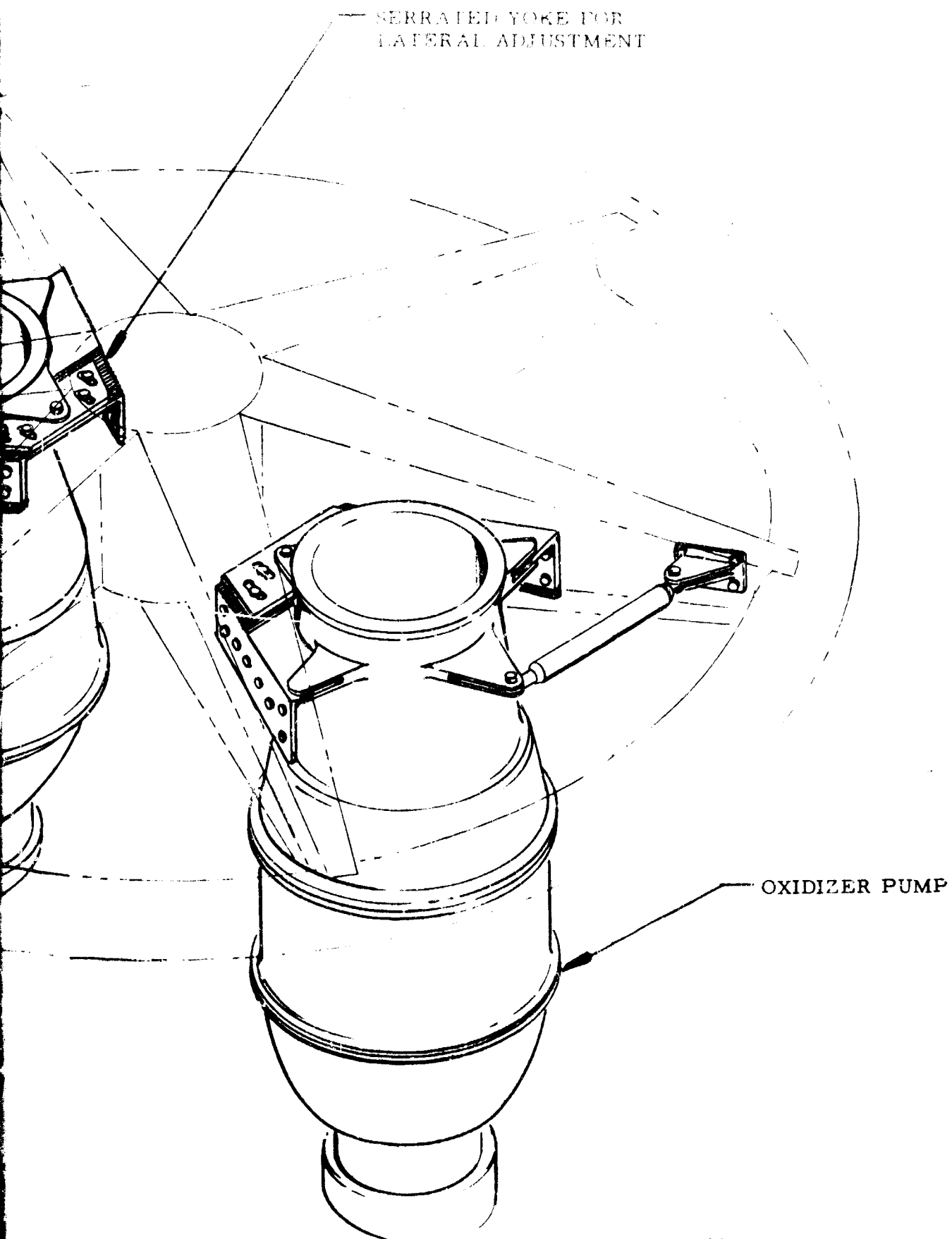


Figure 14. Proposed Adjustable Pump Mounting Concept

CONFIDENTIAL

This page is intentionally left blank

CONFIDENTIAL

CONFIDENTIAL




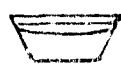







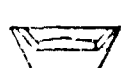



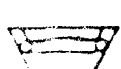


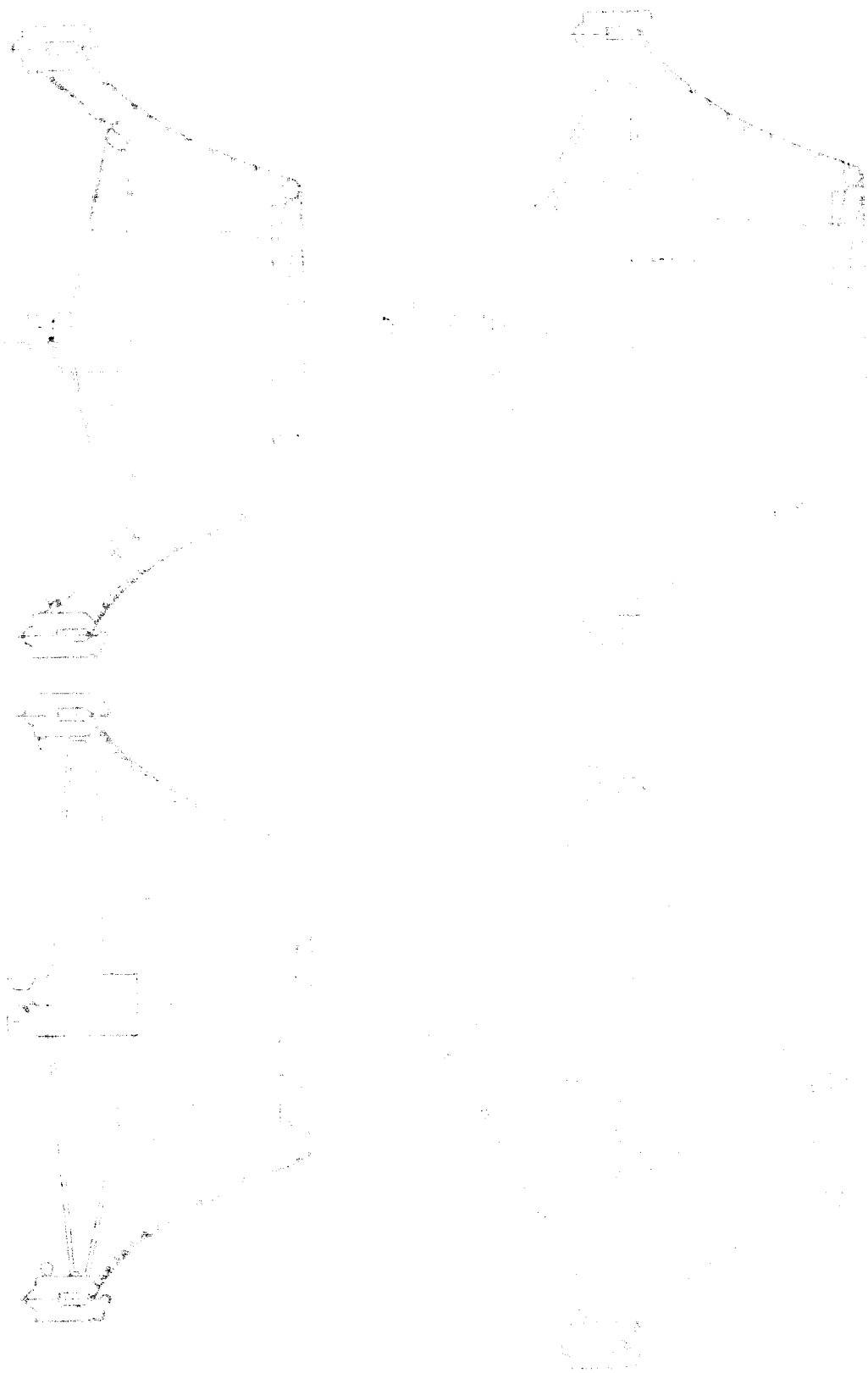
1		2		3	
A	 Disk	A ₁	(Basic Design Modified)	L	 Cone
B	 Disk Cone	B ₁	Disk Cone	M	 Beam Ring
C	 Beam	C ₁	Beam	N	 Beam Cone
D	 Beam Ring	D ₁	Beam Ring	O	 Beam Cone
E	 Beam Cone	E ₁	Beam Cone	P	 Beam Ring Cone
F	 Beam Ring Cone	F ₁	Beam Ring Cone	Q	 Beam
G	 Beam Ring Cone	G ₁	Beam Ring Cone	R	 Truss
H	 Cone Cone	H ₁	Cone Cone		
		I ₁	Beam Cone		
		J ₁	Truss		

Figure 15. Thrust Subsystem Designs

CONFIDENTIAL



CONFIDENTIAL

CONFIDENTIAL

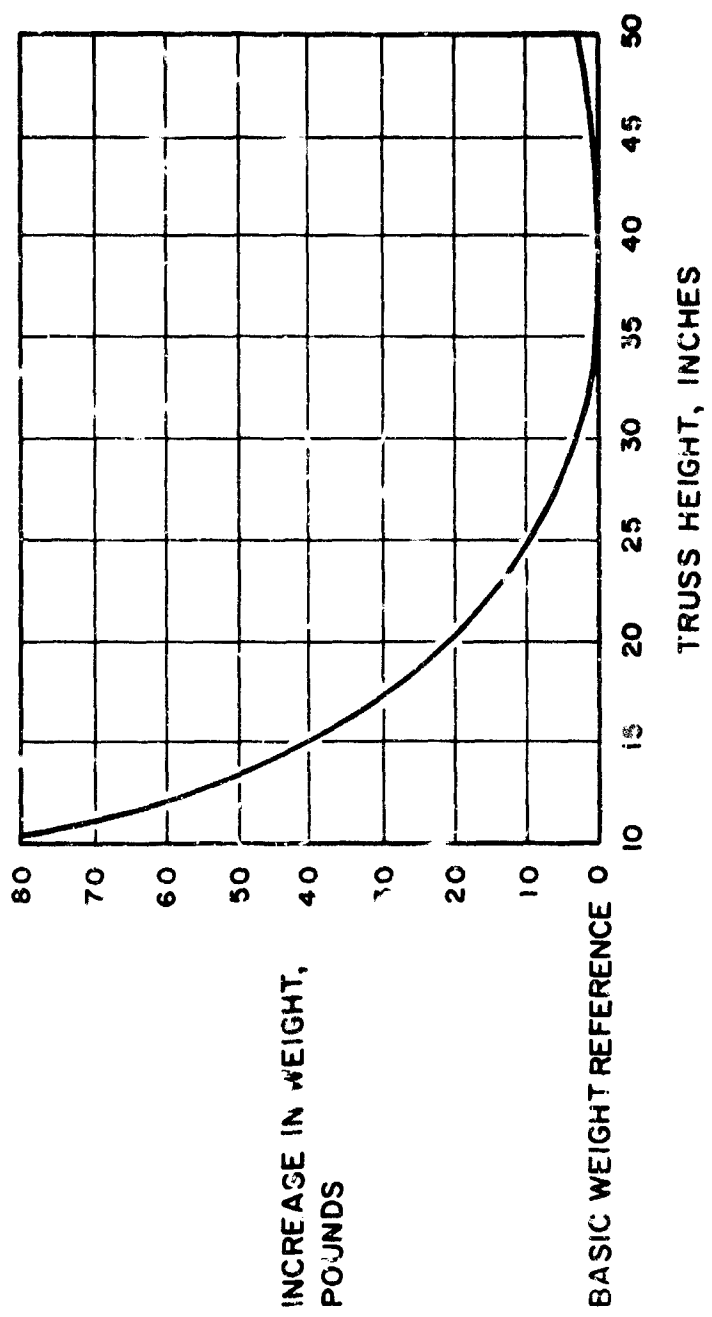


Figure 17. Titanium Thrust Structure Weight vs Depth of Truss Structure

CONFIDENTIAL

CONFIDENTIAL

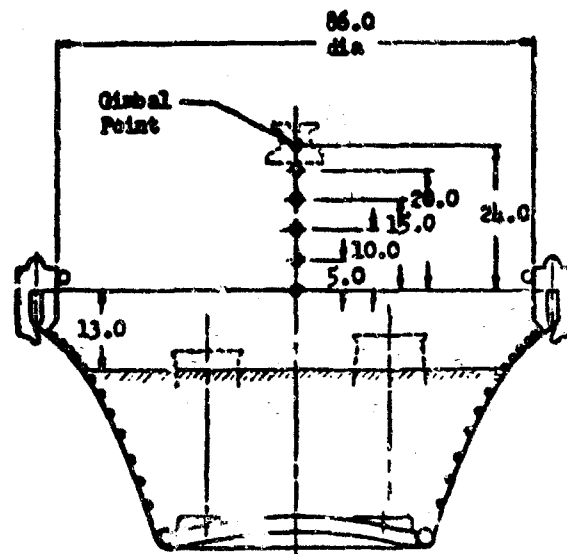


Figure 18. Gimbal Height and Thrust Structure Space Limitation Diagram

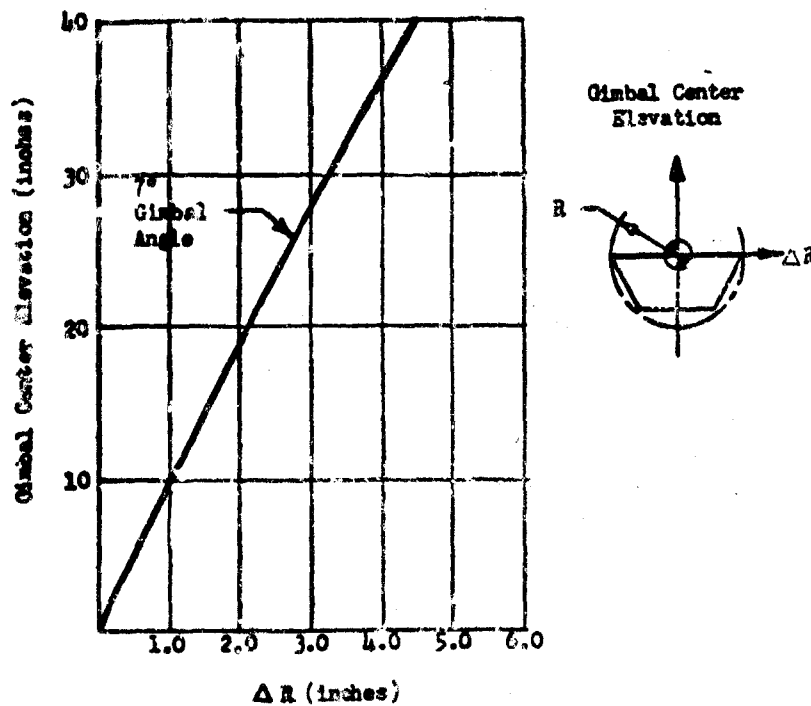
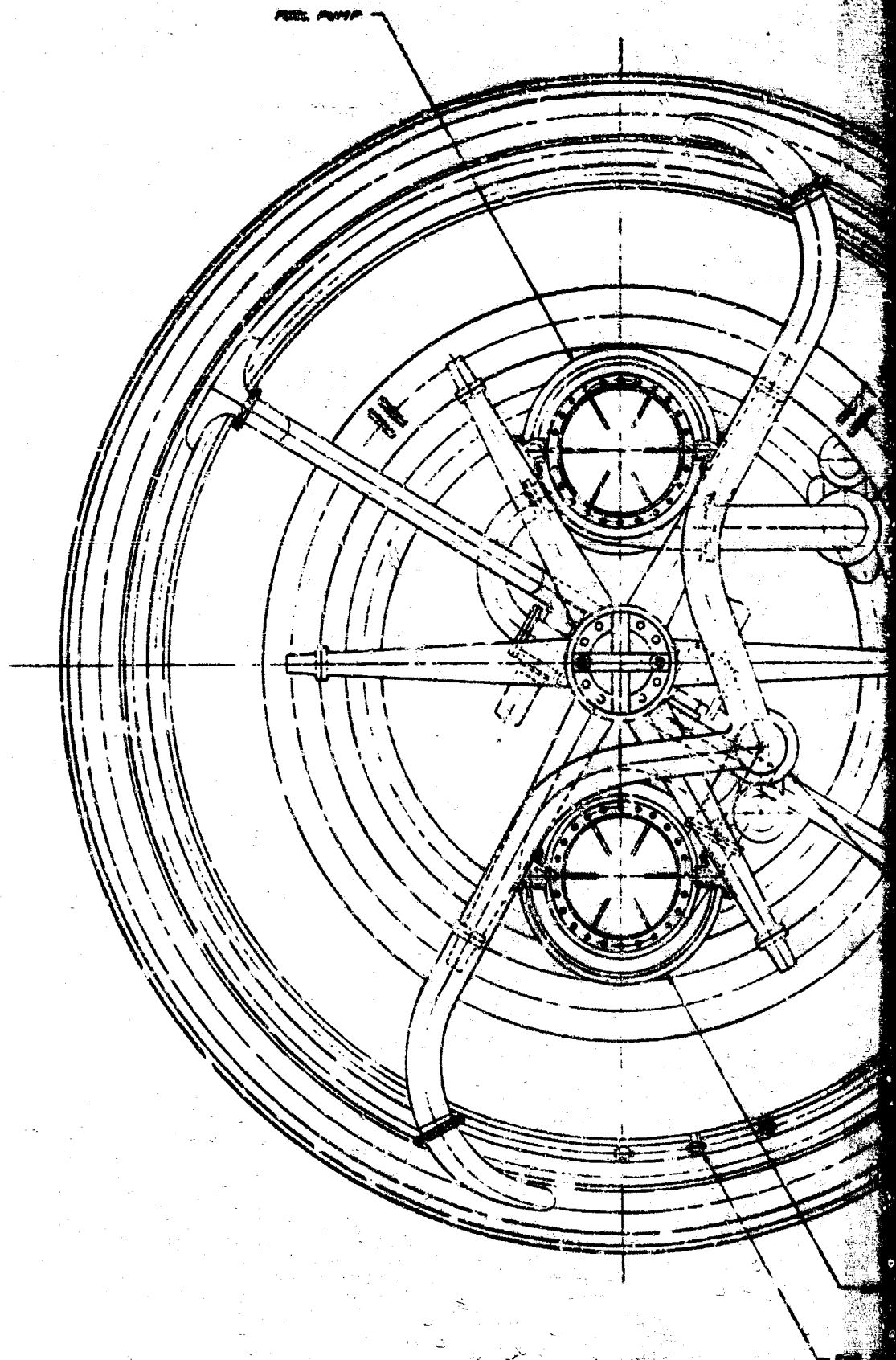


Figure 19. Increase in Dynamic Envelope Requirement With Gimbal Center Elevation Above Position where $R_{static} = R_{dynamic}$

CONFIDENTIAL

CONFIDENTIAL



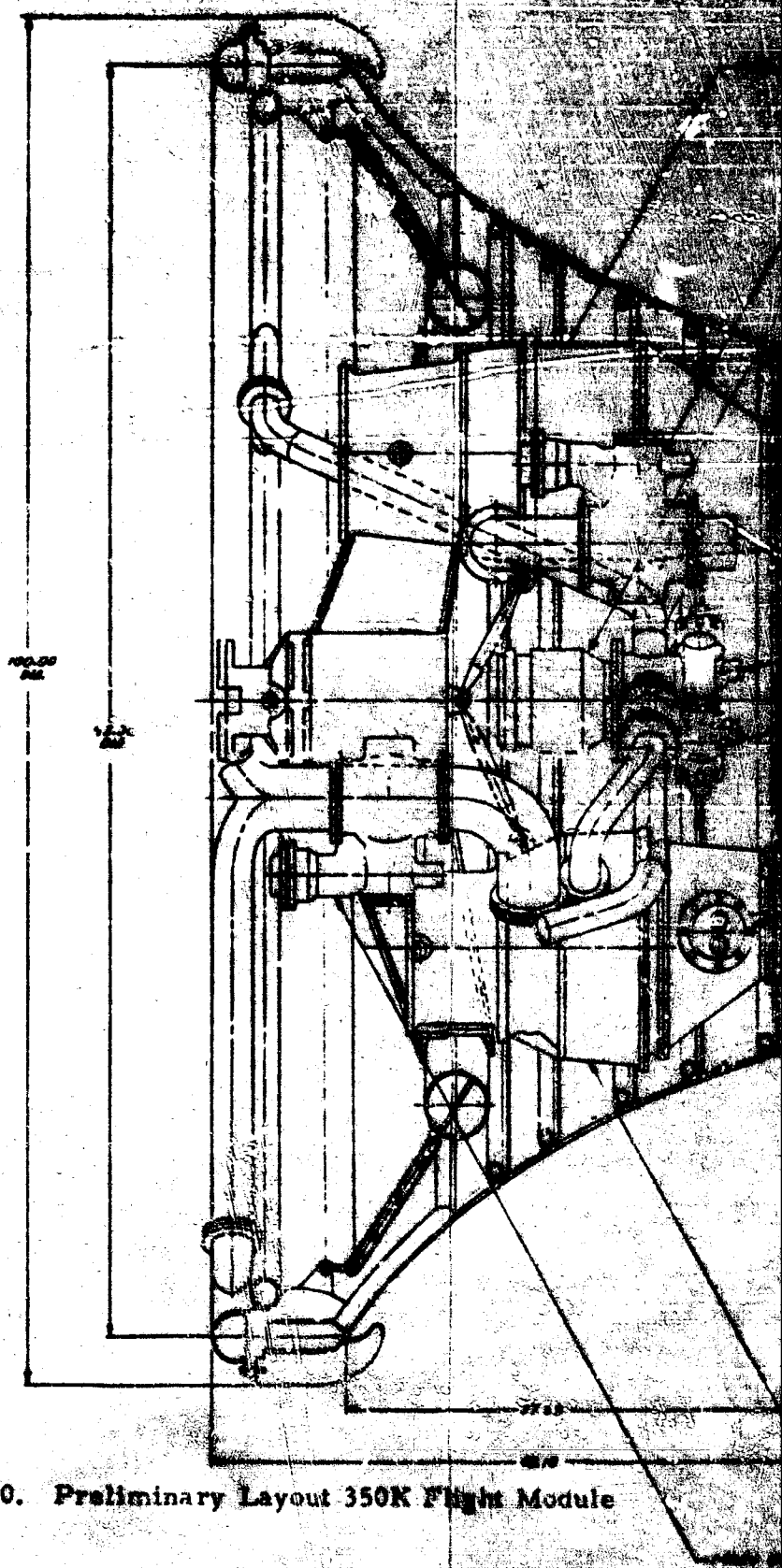
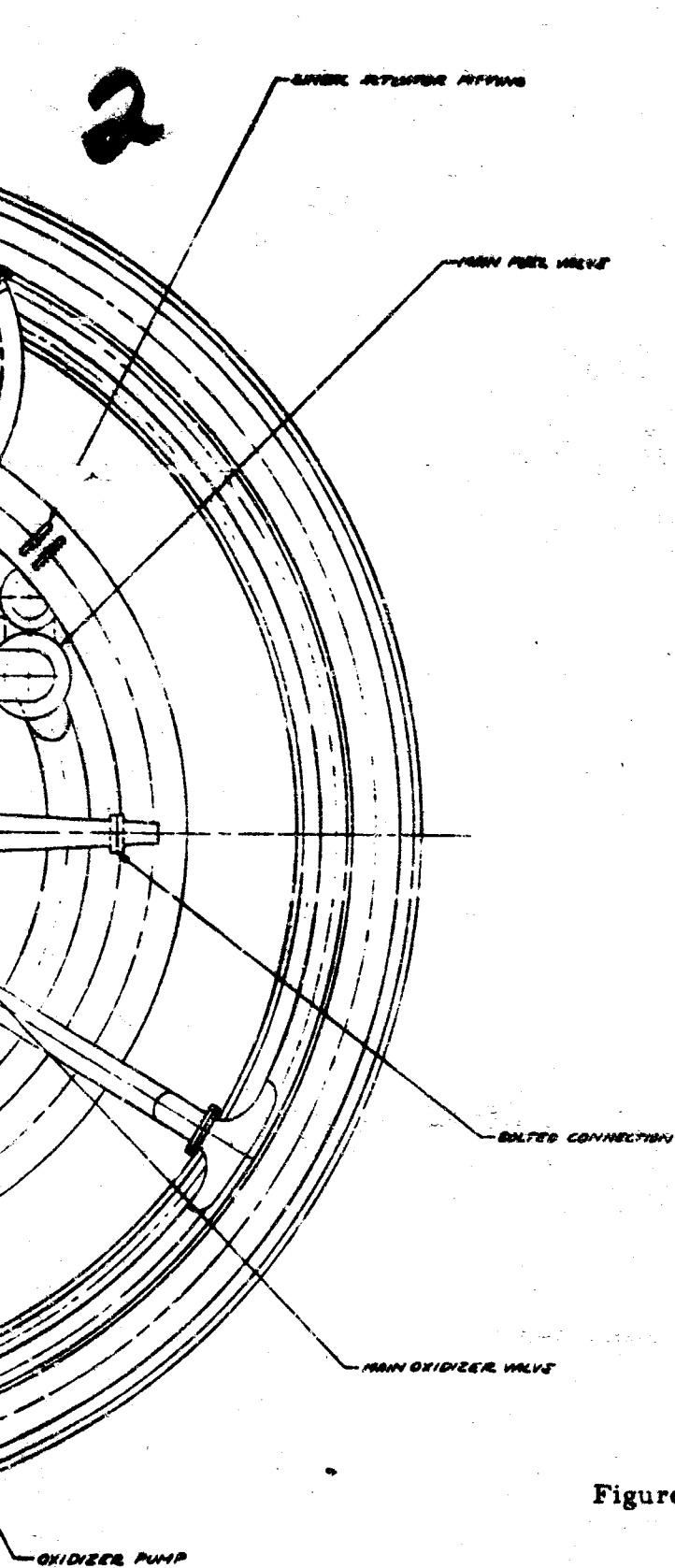
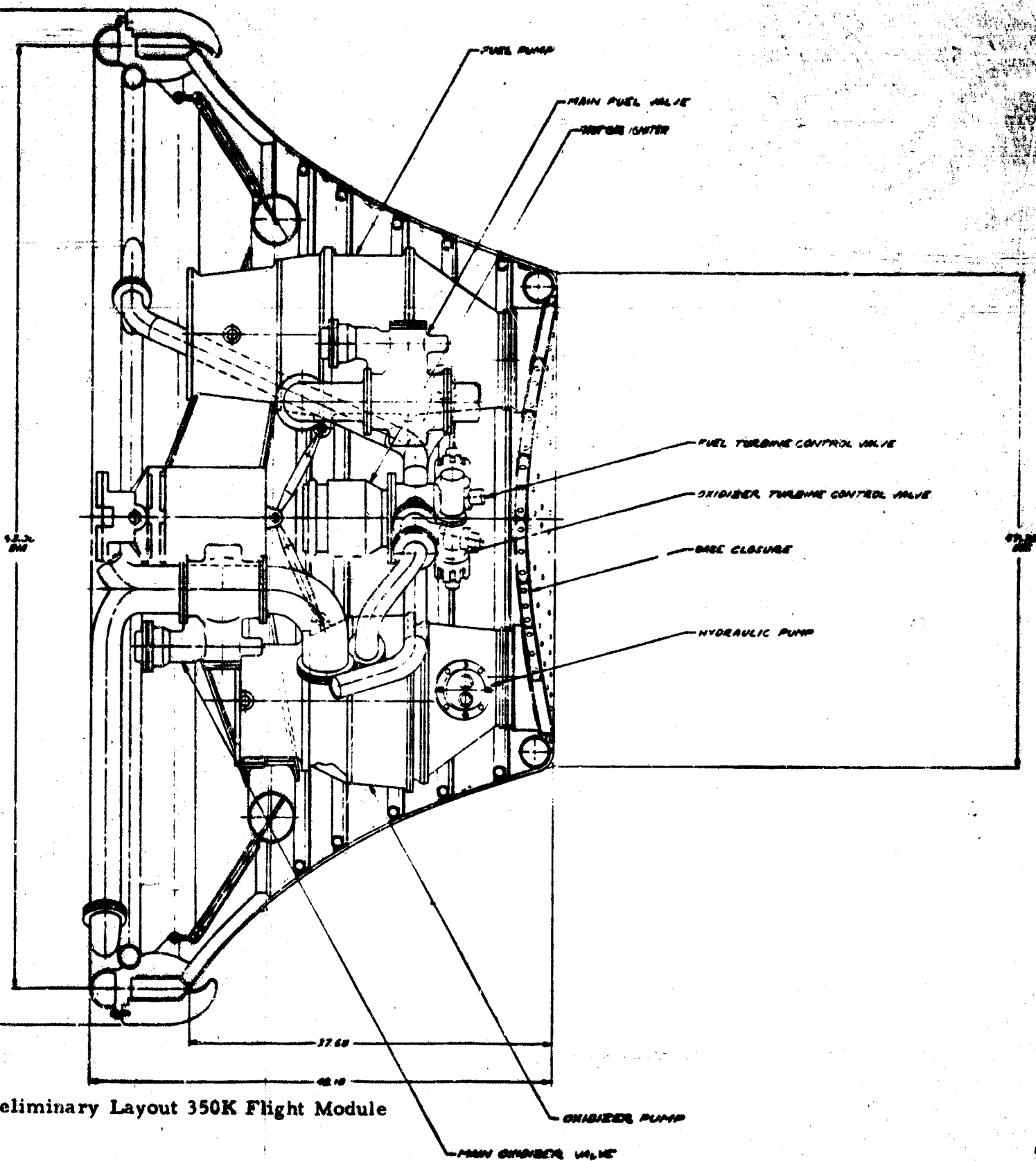


Figure 20. Preliminary Layout 350K Flight Module

FIR FANOUT LINE CONNECTION (40 PLACES)



Preliminary Layout 350K Flight Module

CONFIDENTIAL

This page is intentionally left blank

CONFIDENTIAL

CONFIDENTIAL

(C) Parametric engine performance, weight, and geometry data was generated for combinations of the following parameters and given to RPL on 9 August 1960.

Thrust, pounds $\times 10^3$	150, 200, 250, 300, 350
Chamber Pressure (nozzle stagnation), psia	750, 1000, 1250, 1500, 1750, 2000*
Engine Mixture Ratio	5.0, 5.5, 6.0, 6.5, 7.0
Engine Diameter, inches	80 to 120

(C) The data are based on the premise that each engine will be capable of operating at the design thrust level over a mixture ratio excursion from 5 to 7 with a nominal at 6. System geometry was, therefore, established in each case for a mixture ratio of 6, and performance was then determined over the required mixture ratio range for each geometry. The nominal chamber pressures used in the study were established to exist at mixture ratio of 6. Because of performance changes which resulted from mixture ratio variation, chamber pressure must vary when thrust is held constant. The effect of mixture ratio variation on chamber pressure at constant thrust is shown in figure 21. It should be noted that this figure applies to all values of nominal thrust and diameter. Variations over the thrust and diameter range considered here were shown to be insignificant.

Subsequent to the preparation of the parametric data, the program was reoriented by RPL to remove the requirement for constant thrust capability over the mixture ratio excursion. The design direction to be taken in response to this change is currently being evaluated.

(c) Turbopumps

Hydrogen Pump

(C) A summary of the fuel turbopump operating requirements is shown in Table 4. The establishment of the maximum operating head of the fuel pump at 89,116 feet (Table 4), required a re-evaluation of the selection of the type of pump best able to meet this requirement. The three types of configurations re-evaluated were:

1. Single-stage, inducer/centrifugal pump (1-1/2 stages)
2. Single-stage, multivaned centrifugal pump (multistage radial)
3. Two-stage, centrifugal pump

*The data will be extended to include 2250 psia next quarter.

CONFIDENTIAL

CONFIDENTIAL

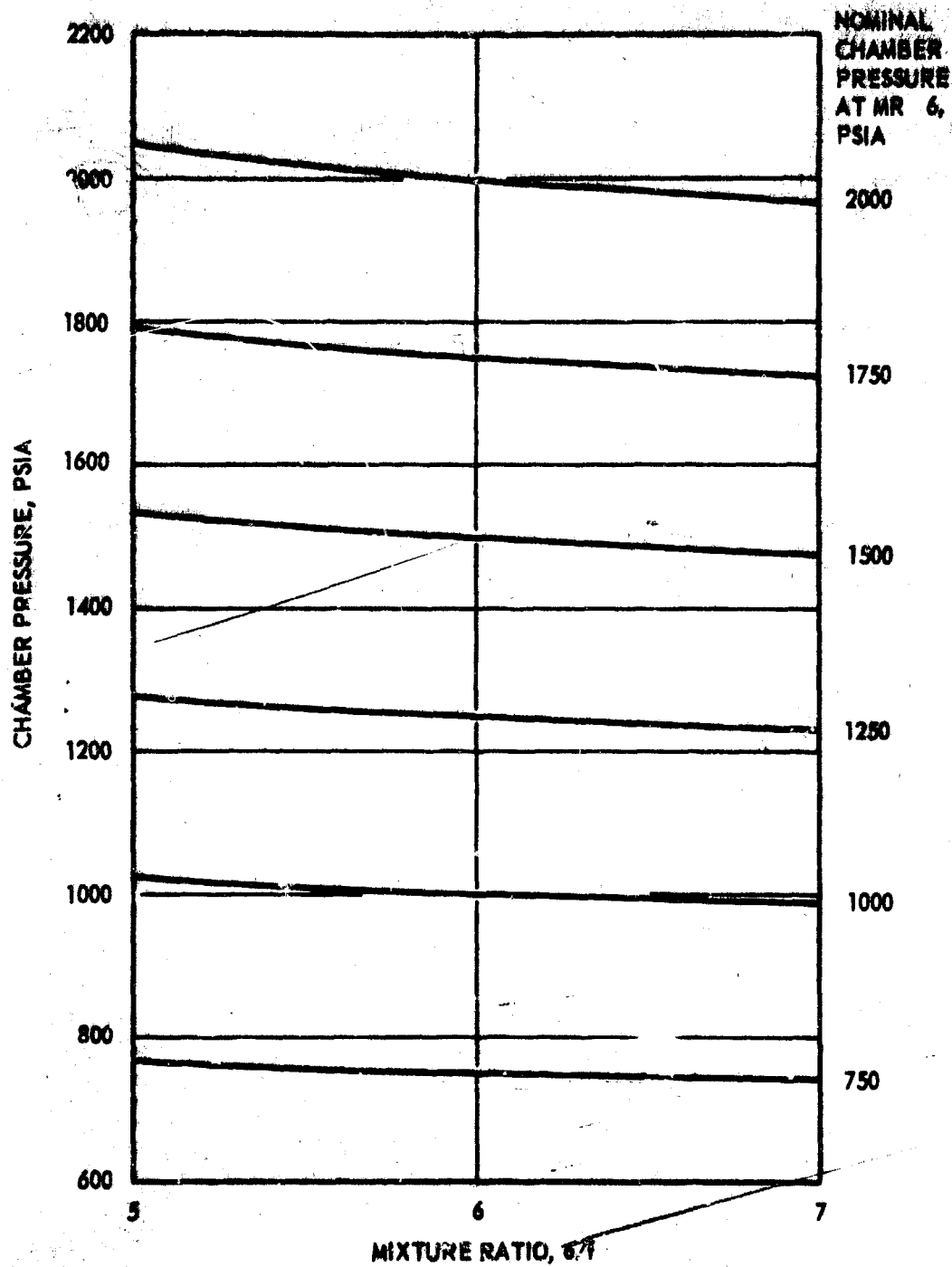


Figure 21. Chamber Pressure vs Mixture Ratio

CONFIDENTIAL

CONFIDENTIAL

TABLE 4

FUEL TURBOPUMP OPERATING REQUIREMENTS

	Nominal Mixture Ratio	Maximum % σ
Pump		
Flowrate, lb/sec		
Discharge Pressure, psia	2635	3014
Head, feet	81,669	92,840
Flow, gpm	8449	9428
NPSH, feet	60	60
Turbine		
Inlet Pressure, psia	1017	1438
Inlet Temperature, F	1500	1500
Horsepower	15,708	19,278

NOTE: TBO 10 hours
Restarts 100
Throttling ratio 5:1

CONFIDENTIAL

CONFIDENTIAL

The pump parameters at the design point are shown in Table 5 and H-Q and efficiency curves for the three types are shown in Figure 22. The evaluation of the pumps was made on the basis of:

- Life
- Weight
- Hydrodynamic Performance
- Up-rating Capability
- Manufacturing Difficulty
- Efficiency
- Off Design Performance
- Structural Design
- Maximum Bearing DN
- Maximum Seal Speed
- Overall Dimensions

(U) Table 6 is a compilation of properties of possible impeller materials. Titanium and several aluminum alloys were chosen for their good strength-to-weight ratio. Ductility, ease of fabrication, and history of successful use as impeller material were also considered. Figures 23 and 24 indicate maximum allowable tip speed for various impeller back plate configuration and materials. These tip speeds were calculated in accordance with established Rocketdyne burst speed policy; i. e., the maximum allowable speed equals to 75 percent of the burst speed. The effect of peak stress due to bending was not included, and may decrease these allowable speeds somewhat. A weight comparison of the two-stage impeller configurations for aluminum and titanium is shown in Table 7.

(U) One of the important considerations with respect to the multistaged radial pump is the maintenance of minimum tip clearance, and to evaluate this a preliminary structural analysis of a volute configuration for one radially staged LH₂ pump was undertaken. Figure 25 is a representation of the deflected shape of the volute due to internal maximum pressure. The magnitude of the calculated deflections are shown in several locations. These values may be reduced by increasing the thickness of the volute in certain areas and by designing the volute inlet guide vanes to carry compressive loads. Other sources of structural displacement affecting the tip clearance, are also tabulated in figure 25.

(U) A summary of the comparison of the three LH₂ pump configurations is shown in Table 8. Based on weight, efficiency, up-rating capability and off-design performance characteristics, the 1-1/2-stage pump was eliminated from further consideration. The choice between the two-stage centrifugal and the radial-staged pump was more difficult. Weight efficiency were about equal. Reliability and long life, achieved through

CONFIDENTIAL

TABLE 5

ADP PUMP PARAMETERS AT DESIGN POINT
(Mixture Ratio = 6)

Parameter	Oxidizer	Fuel 1-1/2 Stage	Fuel 2 Stage	Fuel Multistage Radial
Impeller Speed, rpm	20,000	36,000	36,000	36,000
Preinducer Speed, rpm	6000	14,600	14,600	14,600
Overall Head Coefficient	0.465	0.820	1.23	0.820
Impeller Discharge Diameter, inches	6.25	11.4	9.50	11.4
Impeller Inlet Diameter, inches	5.0	6.75	6.0	5.5
Preinducer Inlet Diameter, inches	9.0	9.0	9.0	9.0
Preinducer Head, feet	155	700	700	700
Impeller Required NPSH, feet	100	600	600	600

CONFIDENTIAL

CONFIDENTIAL

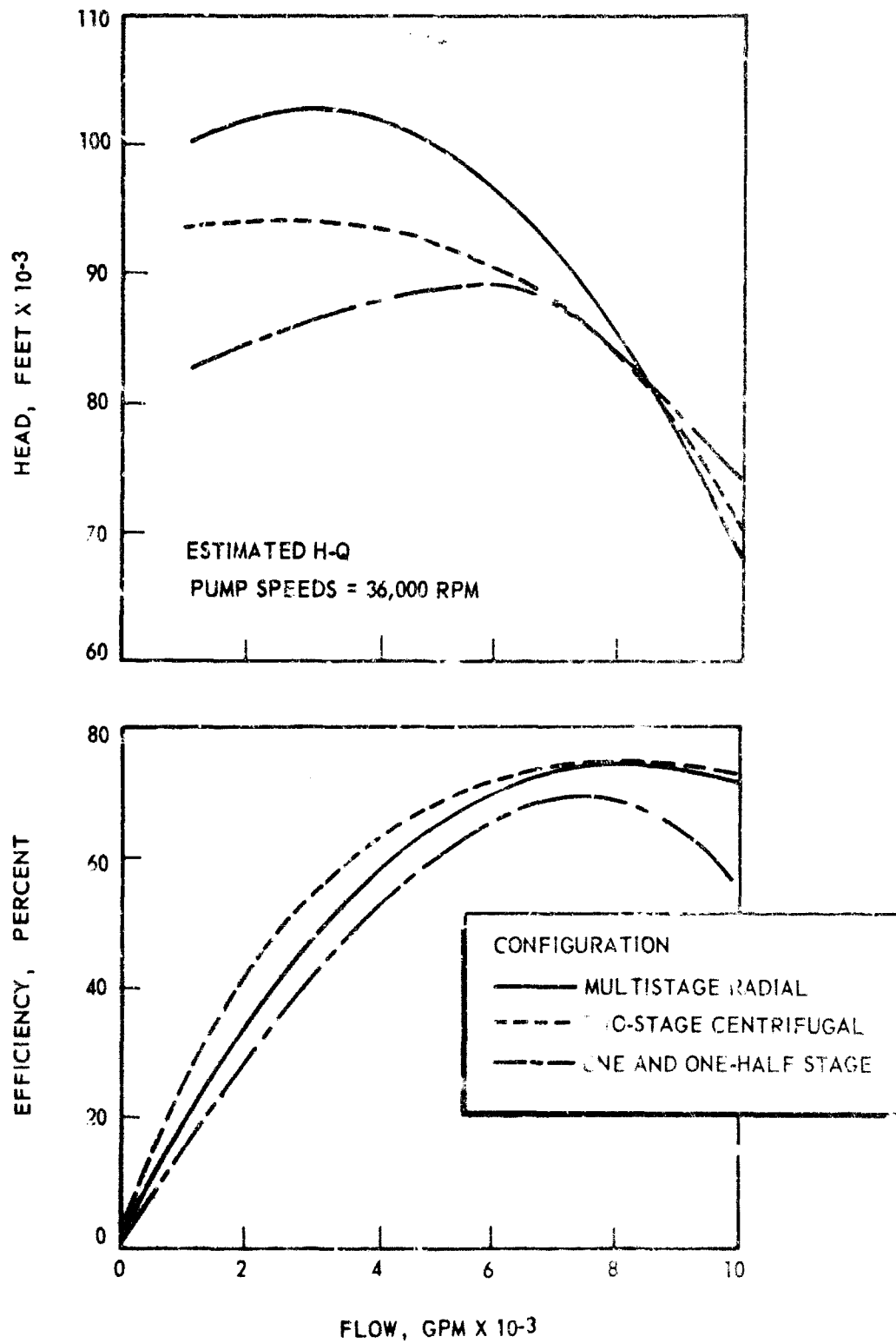


Figure 22. Mark 30 H-Q and Efficiency Curves

CONFIDENTIAL

CONFIDENTIAL

TABLE 6
ADP HYDROGEN IMPELLER MATERIAL PROPERTIES
(At -200 F)

Material	Ultimate Tensile Strength, psi	Yield Strength (0.2 percent offset), psi	Elongation, percent	Specific Weight, lb/in. ³
Tens-50-T60 (Premium Strength Aluminum)	51,800	40,500	3.8	0.10
7075-T73 Aluminum	66,500	57,000	3.0	0.10
6061-T6 Aluminum	44,500	33,000	9.2	0.10
6061-T6B Aluminum	50,500	40,700	11.0	0.10
6070-T6 Aluminum	56,500	42,700	11.0	0.10
ALIC-AT-ELI (5Al-2.5Sn) Titanium	126,000	111,000	9.5	0.16

CONFIDENTIAL

CONFIDENTIAL

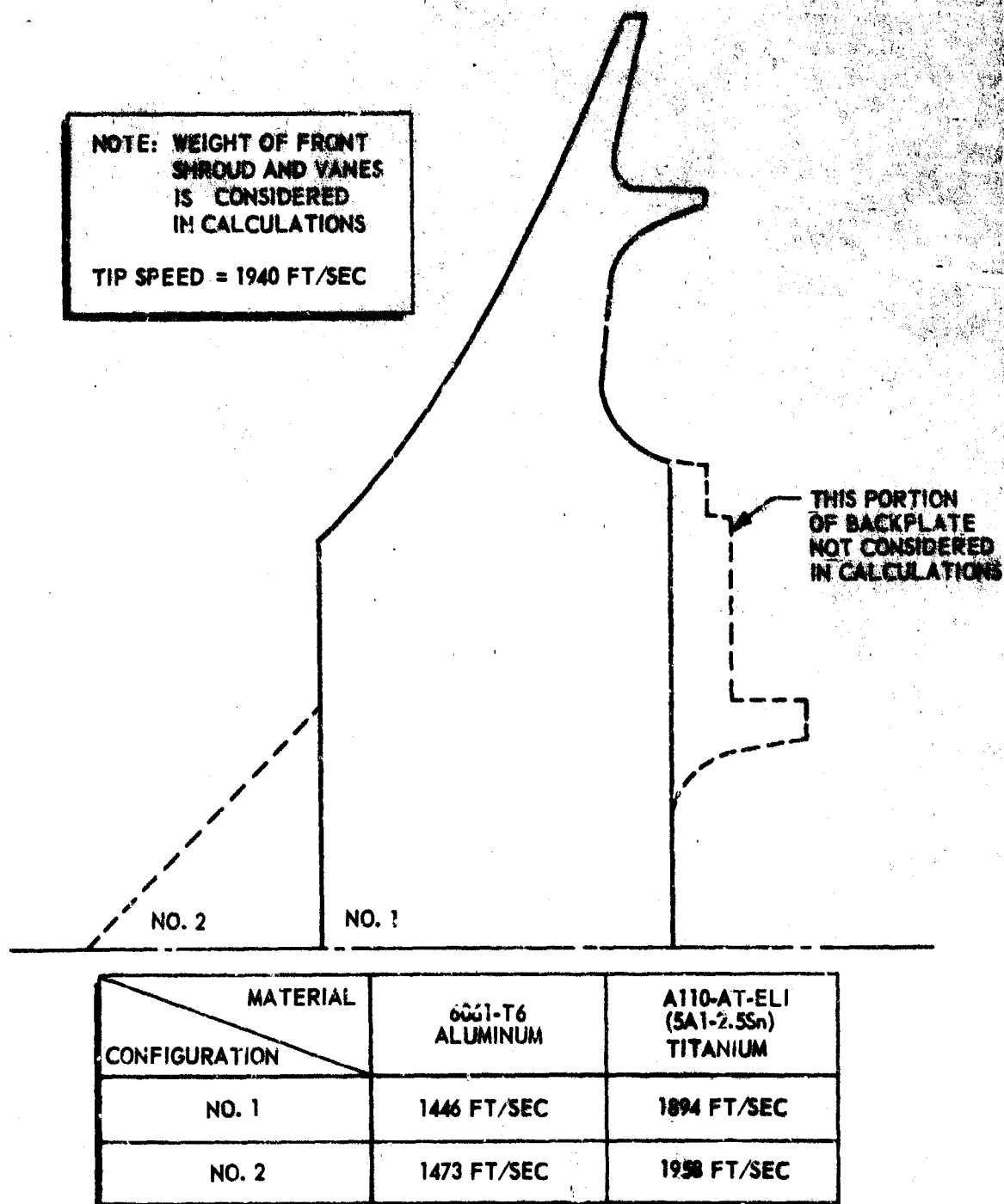


Figure 23. One and One-Half-Stage Hydrogen Impeller Backplate Allowable Tip Speeds

CONFIDENTIAL

CONFIDENTIAL

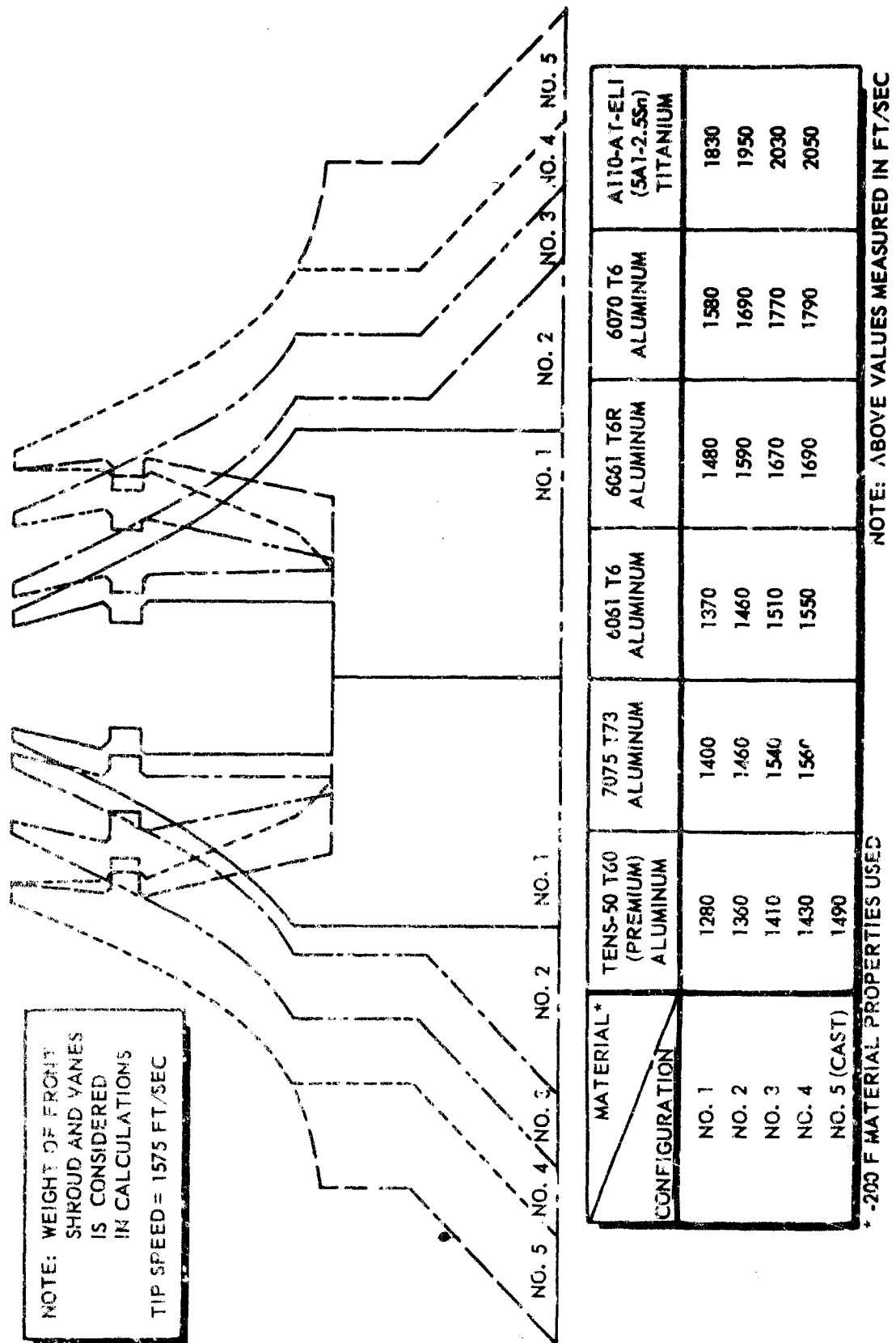


Figure 24. Two-Stage Hydrogen Impeller Backplate Allowable Tip Speeds

CONFIDENTIAL

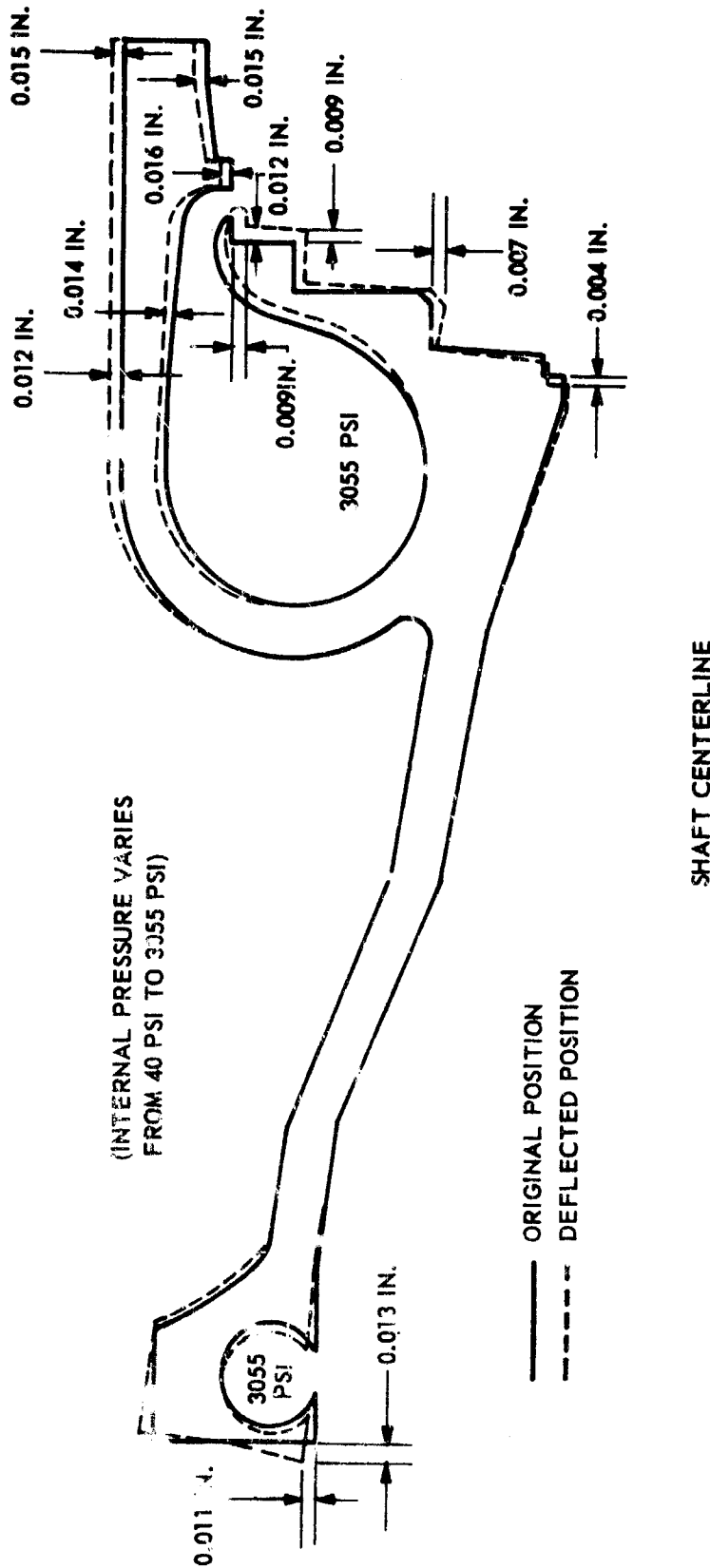
CONFIDENTIAL

TABLE 7
ADP TWO-STAGE IMPELLER WEIGHT COMPARISON
(In Pounds)

Configuration No.	Aluminum			Titanium		
	Preimpeller	Impeller	Total	Preimpeller	Impeller	Total
1	2.1	7.8	9.9	3.4	12.6	16.0
2	2.1	7.9	10.0	3.4	12.7	16.1
3	2.1	8.9	11.0	3.4	14.3	17.7
4	2.1	10.3	12.4	3.4	16.6	20.0
5	2.1	9.3	11.4	3.4	15.0	18.4

CONFIDENTIAL

CONFIDENTIAL



SOURCES INFLUENCING RADIALLY STAGED IMPELLER VANE TIP CLEARANCE (PERFORMANCE):

1. VOLUTE AND BACKPLATE DEFLECTION (DUE TO PRESSURE, LOAD, AND TEMPERATURE)
2. BALANCE PISTON DISPLACEMENT (DUE TO FLUID, STATIC, AND DYNAMIC PRESSURES)
3. SHAFT DEFLECTION (DUE TO STATIC AND DYNAMIC LOADS)
4. IMPELLER DEFLECTION DUE TO CENTRIFUGAL AND HYDRODYNAMIC LOADS
5. IMPELLER DEFLECTION DUE TO VANE AND DISK DYNAMIC RESPONSE

Figure 25. Deflections of Hydrogen Volute due to Internal Static Pressure

CONFIDENTIAL

CONFIDENTIAL

TABLE 8

TURBOPUMP COMPARISON

	1-1/2-Stage Impeller	2-Stage Impeller	Radial
Life, hours	10	10	10
Weight, Less Turbine (optimum), pounds	158 (Aluminum impeller not possible)	150	152 (Titanium impeller)
Weight (possible), pounds	171 (Titanium impeller)	150	226 (Titanium volute)
Maximum rpm	38,900	38,900	38,900
Impeller Tip Speed (38,900 maximum rpm)	1940 (surrounded radial)	1575	1940 (unshrouded)
Head Coefficient	0.795	1.2	0.795
Hydrodynamic Performance	Depends on 1/2-stage performance	Least number of problems	Depends on maintaining blade clearance; stall characteristic unknown
Operating Capability	None (unless impeller is made unshrouded)	Yes	Yes
Manufacturing	Difficult to machine vanes	Casting of cross-over lines difficult	No problem
Efficiency, percent	69	74	74
Off-Design Performance	Flat because of radial vanes	In between	Steepest
Structural Design	Impeller marginal	No problem	Stiff structure required to maintain clearance
Maximum Bearing DN	1.556	1.556	1.576
Maximum Seal Speed, ft./sec	760	760	760

CONFIDENTIAL

CONFIDENTIAL

the design approach of as few parts as possible, a minimum number of joints and high-pressure leak paths, elimination of stress areas and material selection for adequate strength, was roughly equivalent. The problem area of the cross over lines on the two-stage design was balanced by the problem of maintaining rotor tip clearances on the multistaged radial. Seal speeds and bearing DN values were almost identical; however, the H-Q characteristic of the radial-staged pump was steeper, which is more desirable from a throttling standpoint.

(U) The final decision, the selection of the two-staged centrifugal pump, was not based, therefore, on any technical superiority, but on the lack of empirical data on the stall characteristics of the radial-staged pump which would require additional testing.

Oxidizer Pump

(C) The preliminary LOX pump parameters are summarized in Table 9. The LOX turbopump, is proposed, operated at a speed of 25,000 rpm and utilized an outboard bearing on the turbine end of the shaft which was lubricated with liquid hydrogen. The problem of distortion in the hot bearing support and the complexity of piping liquid hydrogen to the LOX turbopump bearing resulted in the evaluation of an overhung turbine design. The required small inlet diameter of the pump at 25,000 rpm resulted in a critical speed problem with the overhung design which was resolved by decreasing the pump speed to 20,000 rpm. This increased the pump inlet diameter, thus increasing the shaft diameter; however, it reduced the turbine u/c ratio and resulted in an increase in turbine weight flow. A larger turbine diameter is currently being investigated, which will add weight but re-establish the lower turbine weight flow. Evaluation of the two configurations is continuing.

(d) Thrust Chamber

(U) The demonstrator module thrust chamber design effort was deepened to include detailed analysis of the structure, combustor, injector, heat transfer, and nozzle.

Structure

(C) During this report period, the design approach to the chamber wall structure has been defined. The design selected embodies a chamber wall structure of titanium alloy (6Al-4V). Nickel coolant tubes will be brazed to a thin Inconel 718 backup member (either bands or a complete sheet) which in turn will be epoxy-bonded to the titanium structural wall. In addition, the chamber walls will be linked together by bolting through the 40 chamber baffles. This structural tie will maintain the

CONFIDENTIAL

TABLE 9

LOX TURBOPUMP OPERATING REQUIREMENTS

	Propellant	Nominal Mixture Ratio	Maximum 3 σ
Pump			
Flowrate, lb/sec	476.7		
Disk Pressure, psia	2055	2056	2395
Head, feet	4225	4222	4933
Flow, gpm	3110	3107	3432
NPSH, feet	16	16	16
Turbine			
Inlet Pressure, psia	600	800	800
Inlet Temperature, F	1500	1500	1500
Horsepower	4570	4570	5709
Maximum DN	1.12	1.2	1.2
Seal Speed, ft/sec	316	375	375

Note: TBO 10 hours
 Restarts 100
 Throttling ratio 5:1

CONFIDENTIAL

CONFIDENTIAL

throat gap within acceptable limits during firing and will result in a significantly lower chamber weight over an unlinked design.

(U) This design approach resulted from a parallel and competitive design study which compared a conventional Inconel 718 structure (figure 26), the selected machined titanium alloy configuration (figure 27), and more advanced structural concepts of honeycomb (figure 28) and press diffusion-bonded titanium (figure 29). The criteria for selection in this design study were weight, manufacture and assembly, cost, and experience as seen in Table 10. The more advanced honeycomb and diffusion-bonded titanium designs will require development of the specific fabrication method which would require more time than available for the demonstrator module. They were therefore eliminated for the demonstrator and 20K segment. They do point out the potential of advanced fabrication techniques for the flight module.

(U) Table 10. Design Comparison Study

Design	Chamber Weight	Experience	Manufacture and Assembly	Cost
Machined Inco 718	990	State-of-the-Art	Difficult to machine	Moderate
Machined Titanium	750	Semiadvanced	New assembly techniques required for epoxy assembly	Moderate
Titanium Honeycomb	650	Advanced	Difficult to machine and assemble	High
Diffusion-Bonded Titanium	600	Advanced	Extremely difficult to assemble	High

(U) Titanium was selected for the chamber wall structure because of its extremely high strength-to-weight ratio. Approximately 200 pounds weight savings can be effected with titanium over an Inconel 718 configuration. Fabrication of the titanium wall will be achieved by machining a ring forging to the configuration required to yield the highest

CONFIDENTIAL

CONFIDENTIAL

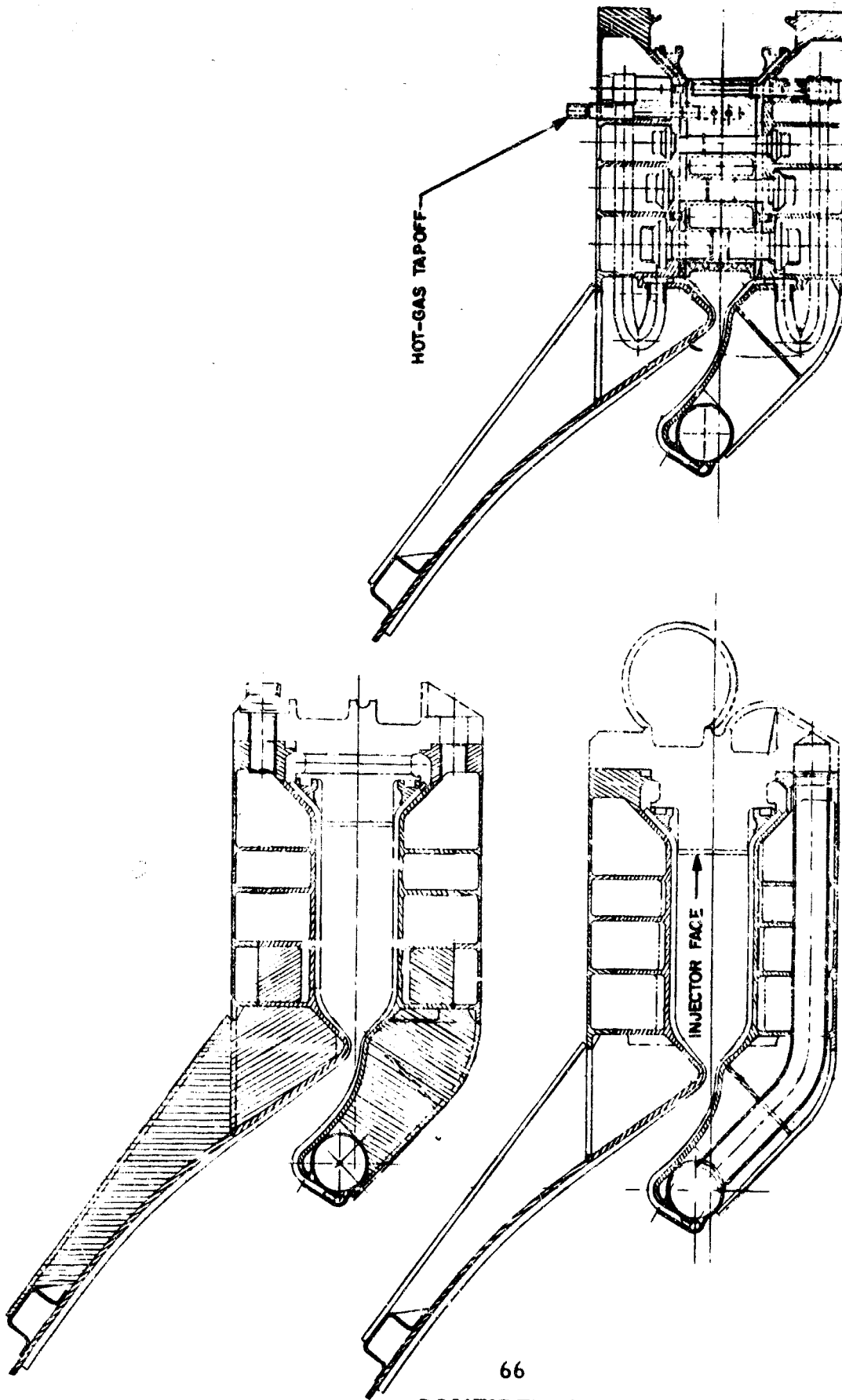
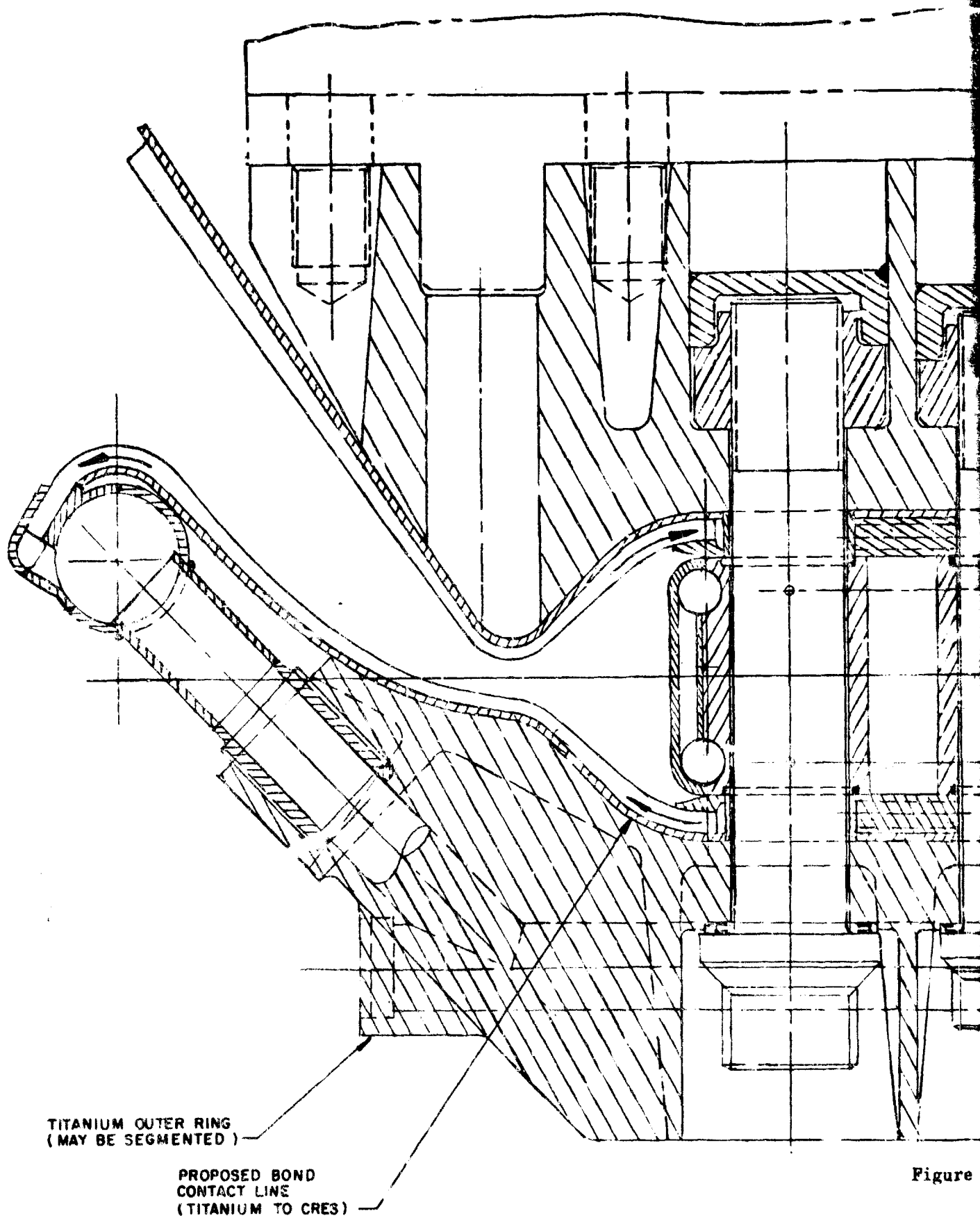


Figure 26. Structural Concept, 250K Aerospike Thrust Chamber Demonstrator Module

CONFIDENTIAL



Figure

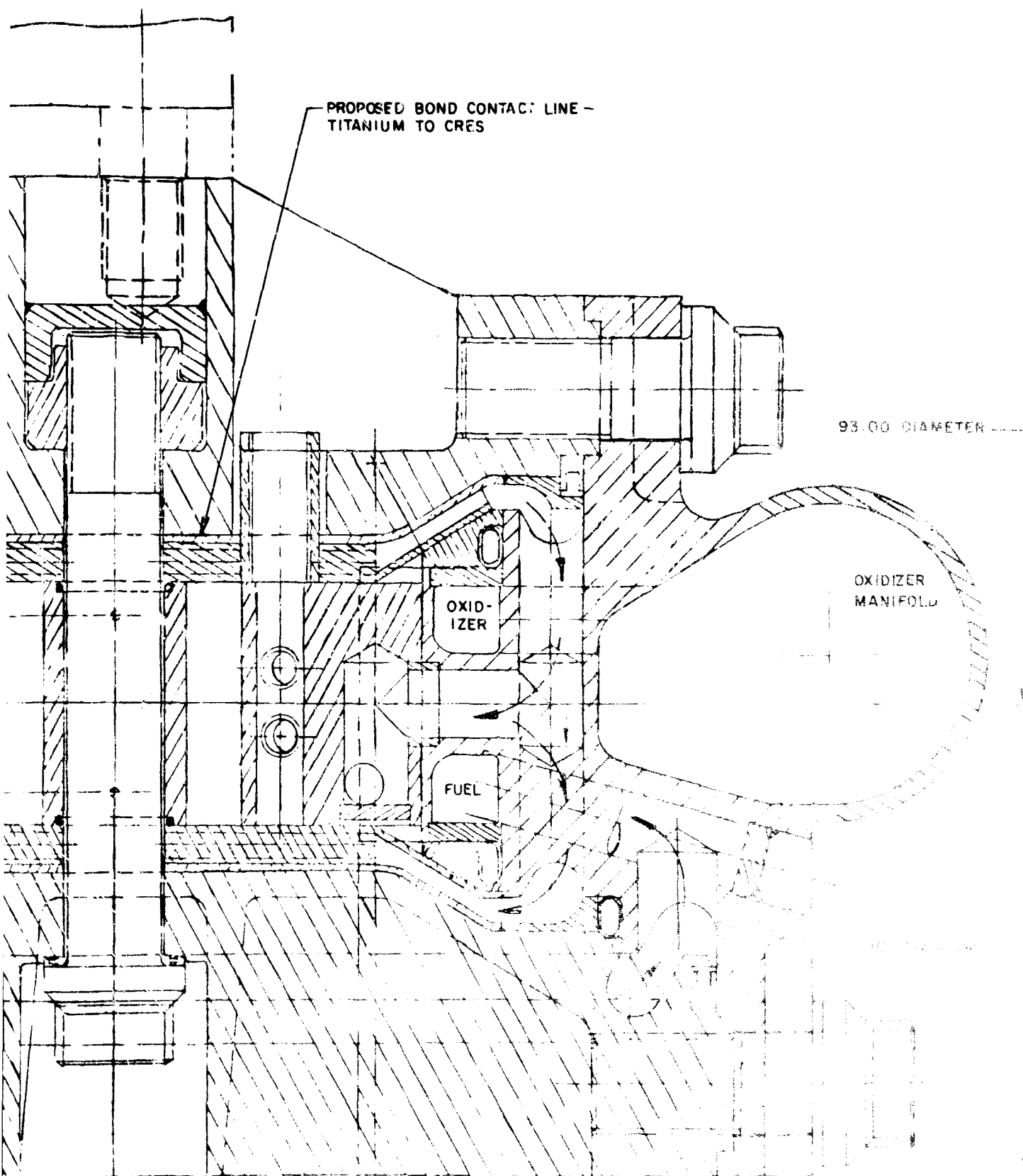


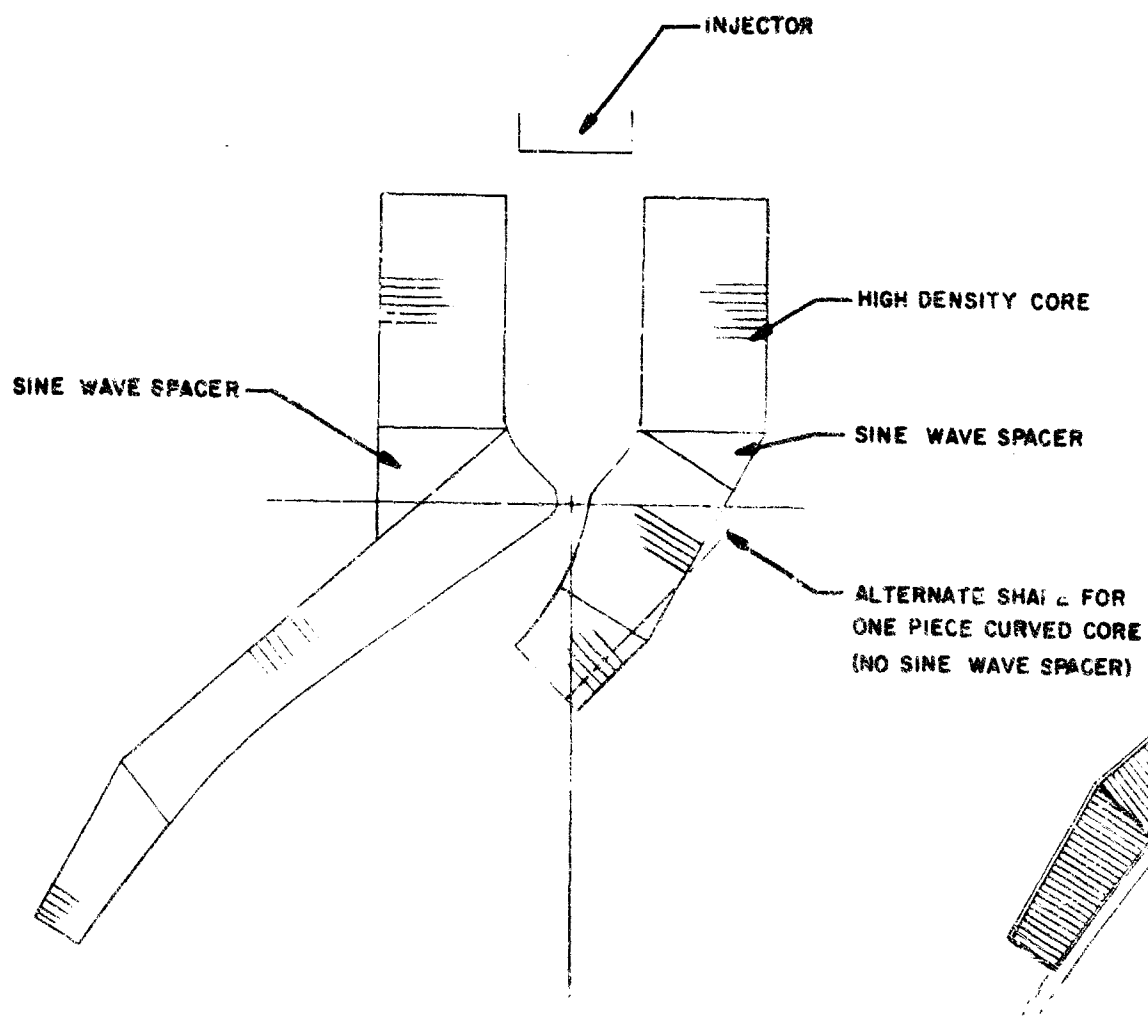
Figure 27. Proposed 250K Aerospike Thrust Chamber,
Two Belt Integral Baffle Injector Con-
figuration (40 Places)

CONFIDENTIAL

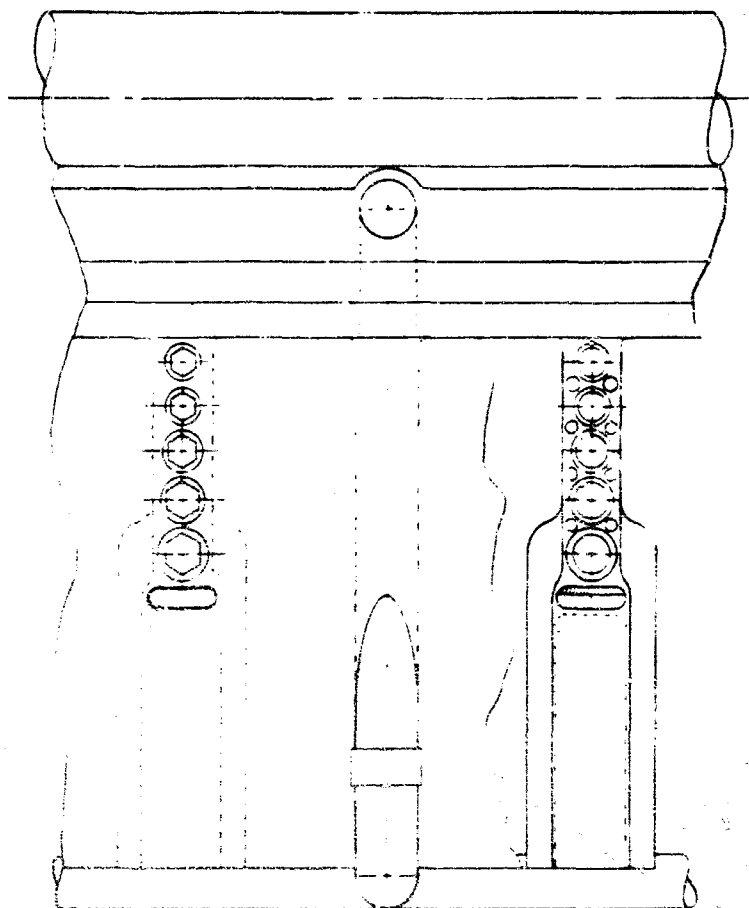
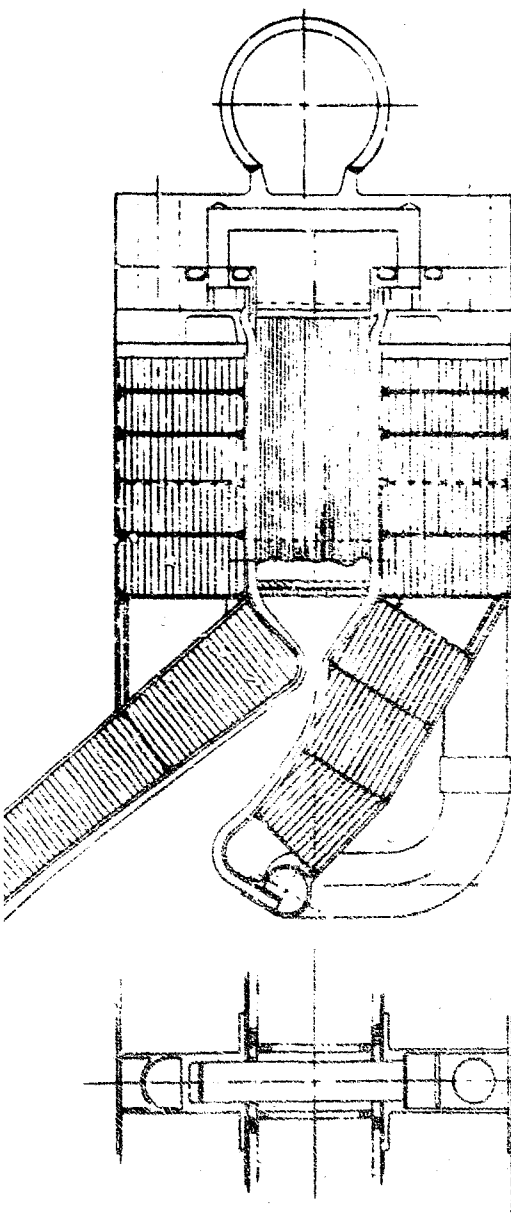
This page is intentionally left blank

CONFIDENTIAL

CONFIDENTIAL



HIGH DENSITY HONEYCOMB



LOW DENSITY HONEYCOMB

Figure 28. ADP Demonstration Chamber Study
(Honeycomb Structure)

This page is intentionally left blank

CONFIDENTIAL

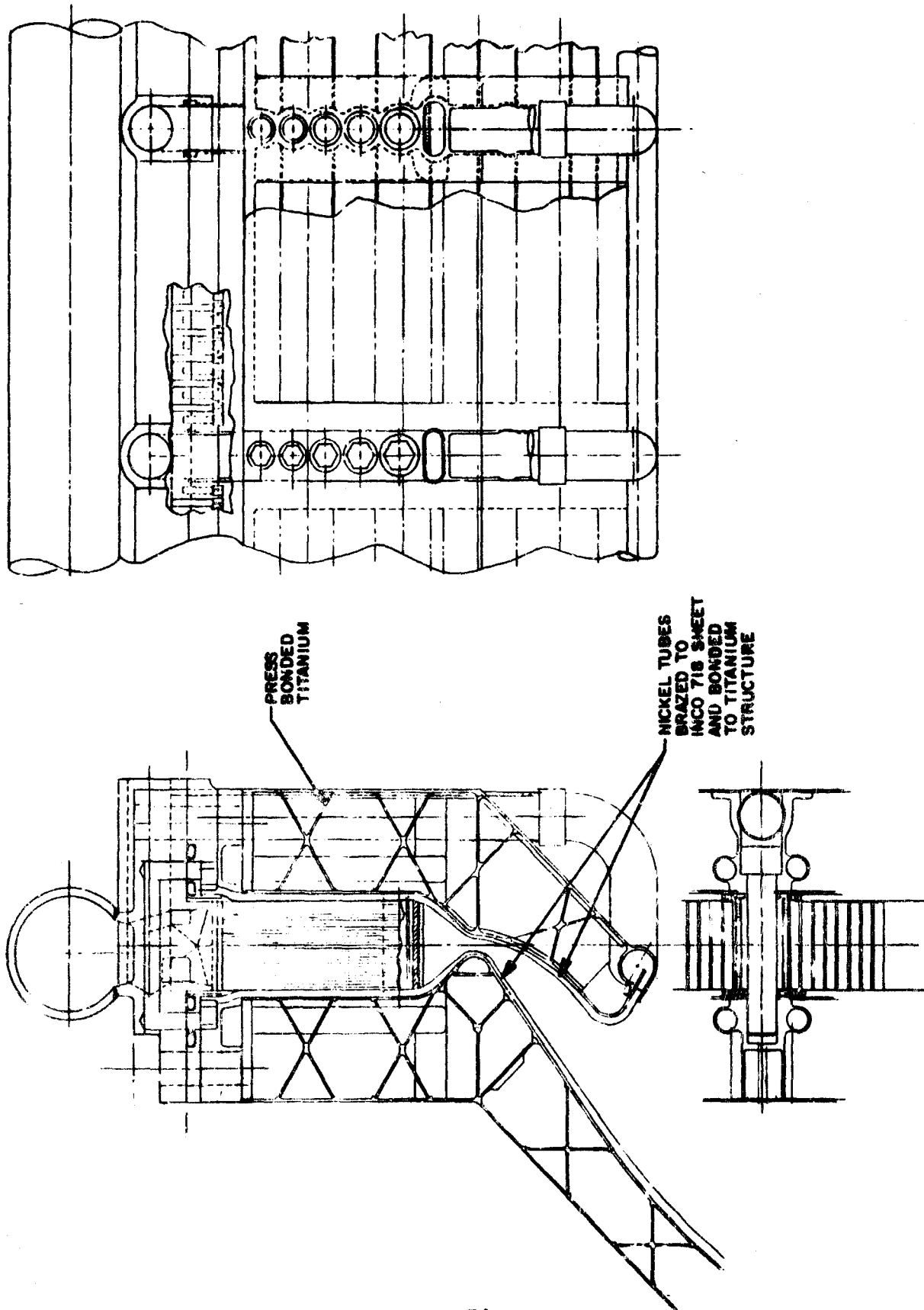


Figure 29. ADP Demonstration Chamber, Pressure Diffusion-Bonded Titanium

CONFIDENTIAL

CONFIDENTIAL

strength-to-weight design. This method was selected over a machined and welded assembly because it can be designed to higher stress levels due to the absence of welding.

(U) The selected baffle coolant circuit is shown in figure 30. Pressure drops shown represent increases above conditions that already exist in the chamber as a result of cooling of the tube bundle. This circuit combined the most desirable features of the two alternate configurations shown. In this design, both the pressure drop and bulk temperature rise of the separate flow paths have been balanced before they are combined in cooling of the outer wall immediately upstream of the throat. Furthermore, the baffle is separated from the injector assembly which ensures easier installation of the injector on the chamber wall assembly.

(C) Two concepts (figure 31) were studied for the structural tie between the inner and outer chamber bodies. The first was the selected tie through the chamber baffles as seen in figure 27, while the second was to employ structural ties in the subsonic portion of the combustor immediately upstream of the throat (figure 32). Chamber stability baffles would still be required with this design.

(C) The initial results of this study indicated that 80 subsonic ties together with 40 stability baffles would yield the lightest weight chamber assembly. Detailed design and analysis revealed that with 80 pre-loaded ties the predicted weight increased, while the amount of chamber blockage increased the heat flux on this tie from approximately 15 Btu/in²-sec-F to 28 Btu/in²-sec-F, and therefore increased the coolant pressure drop required to cool the tie. Furthermore, with both a subsonic tie and a stability baffle to cool, the hydrogen coolant circuit became undesirably complex. For these reasons, the 80 separate structural tie design was abandoned in favor of using bolts through the 40 baffles.

Combustor Configuration

(C) The combustor as described in the first quarterly report is identical to that of the 250K experimental thrust chamber, and it is 2 inches wide and 6 inches from the injector face to the throat. The combustor side walls are parallel and the range angle of approach to the throat is 40 degrees. The effective contraction ratio is 7.1:1, and the effective L* is 40 inches. The combustor volume is divided into 40 compartments by full-length structural baffles.

CONFIDENTIAL

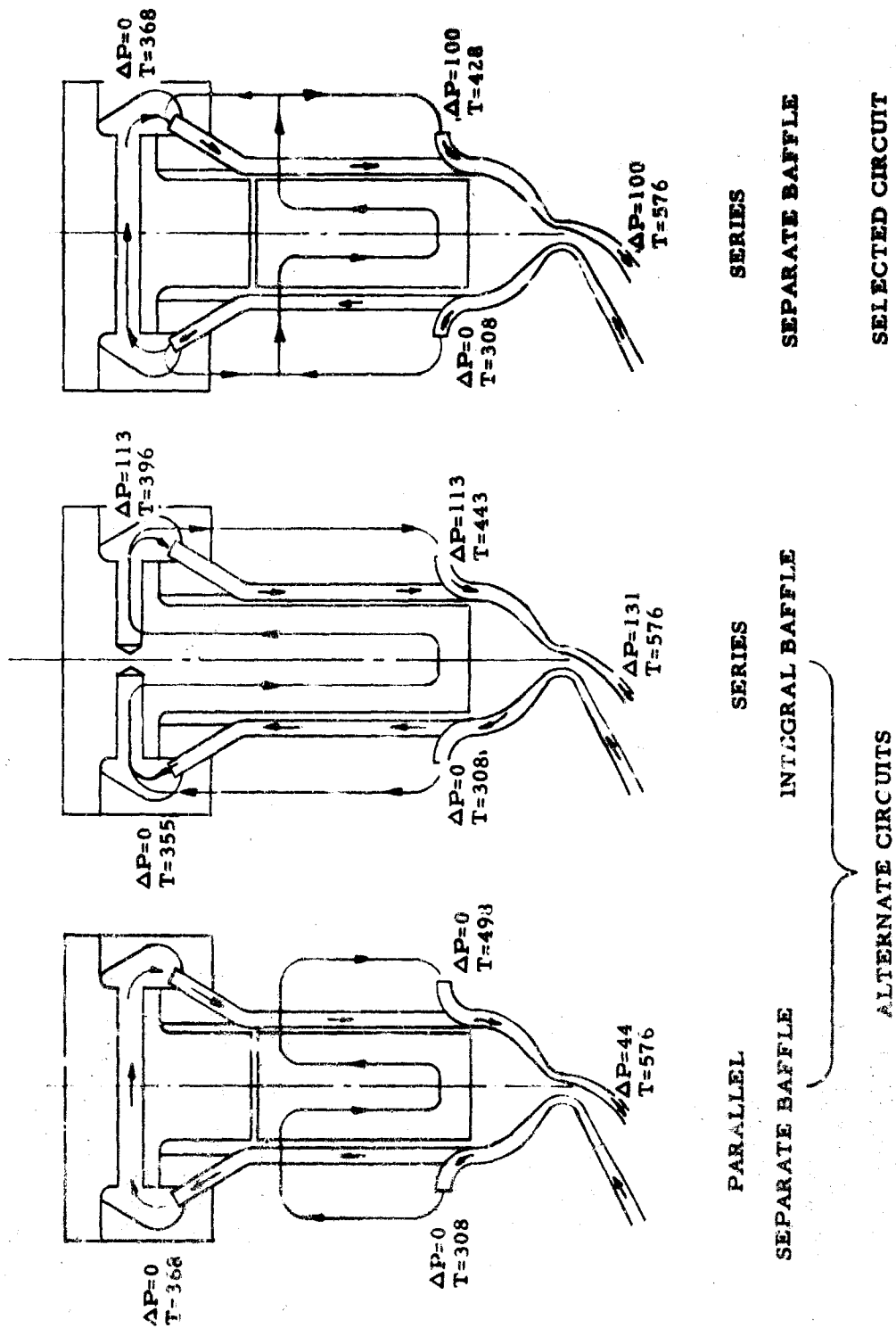


Figure 30. 250K Flow Circuits

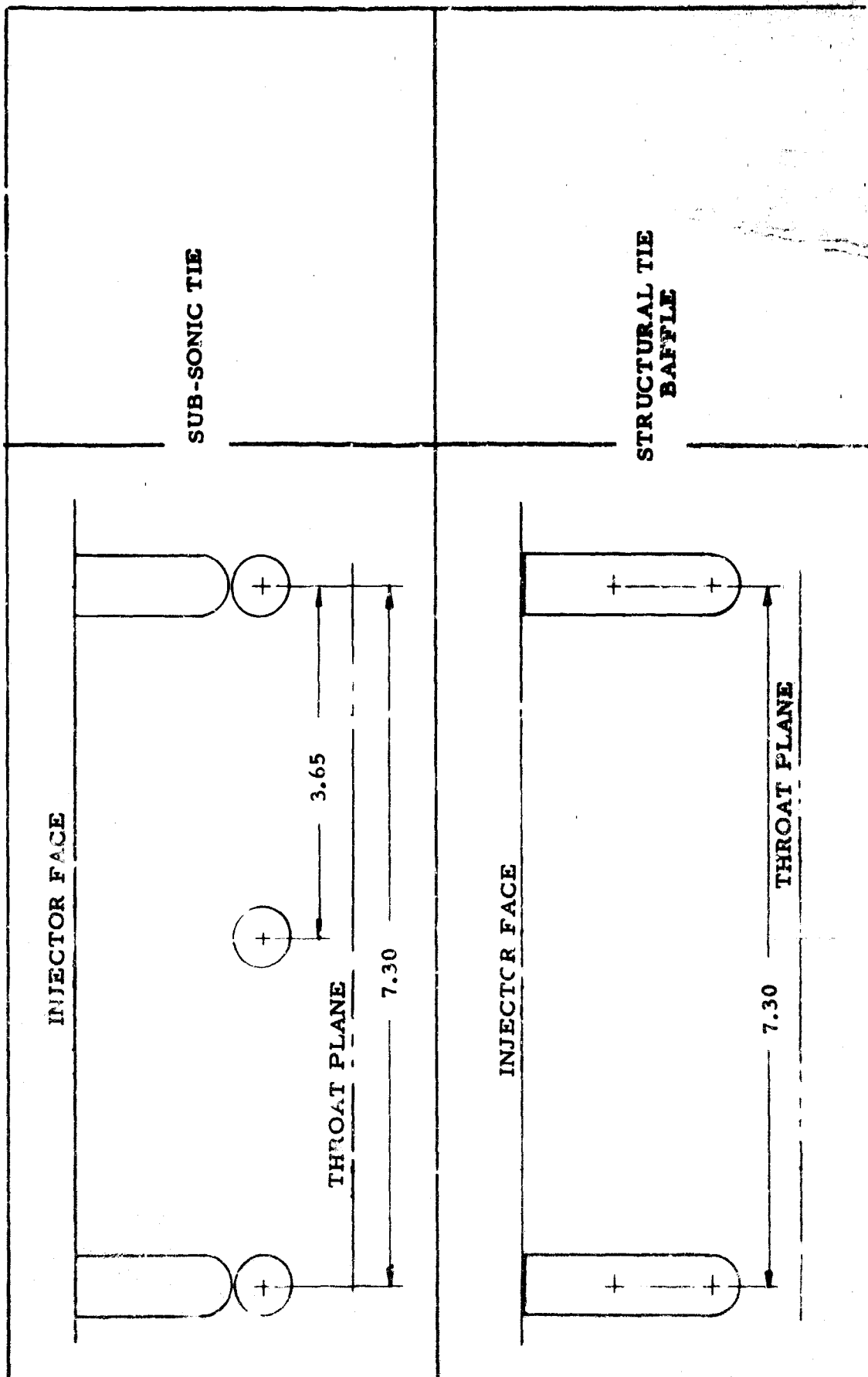
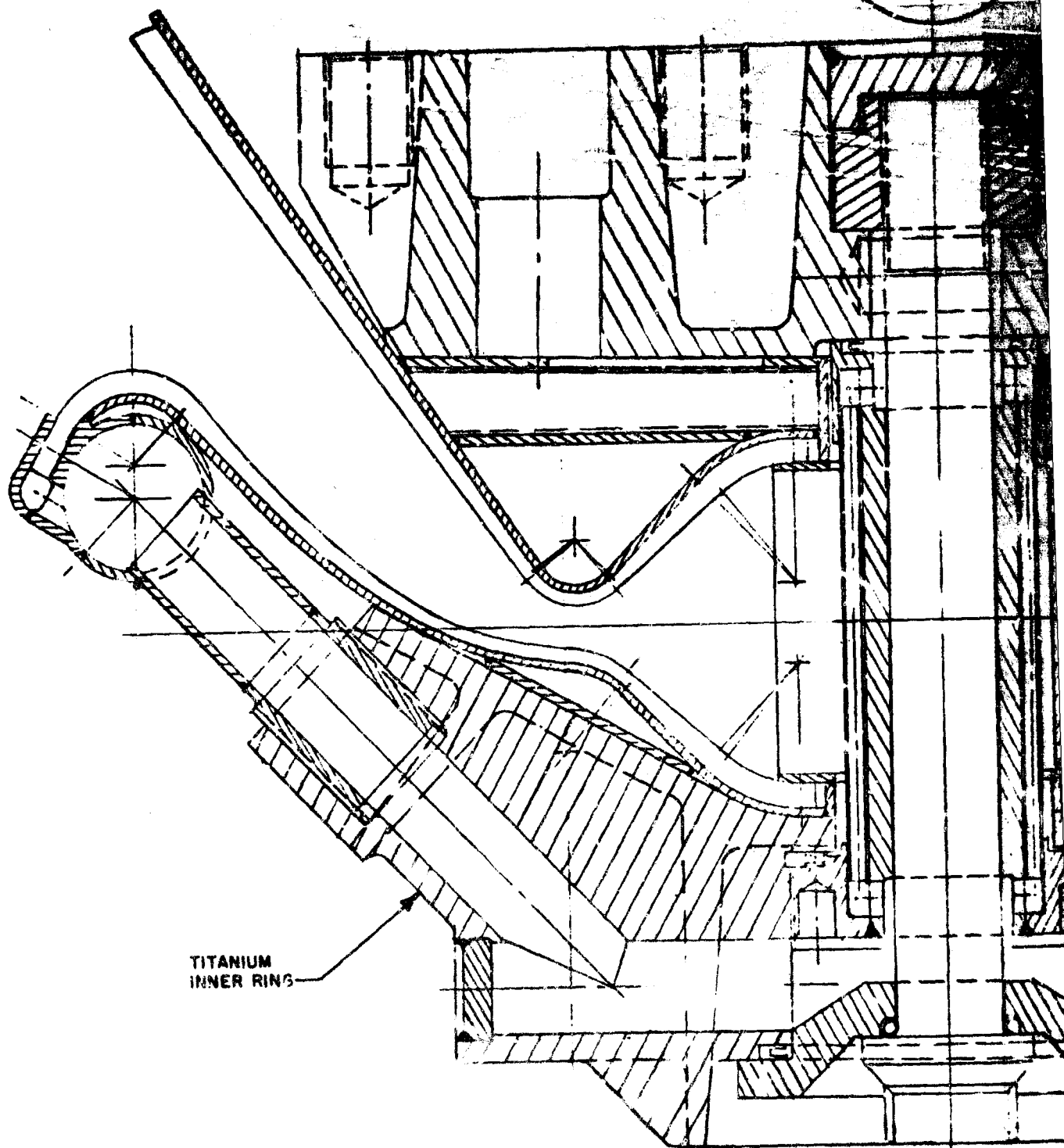


Figure 31. Structural Tie Concepts

CONFIDENTIAL



TITANIUM
INNER RING

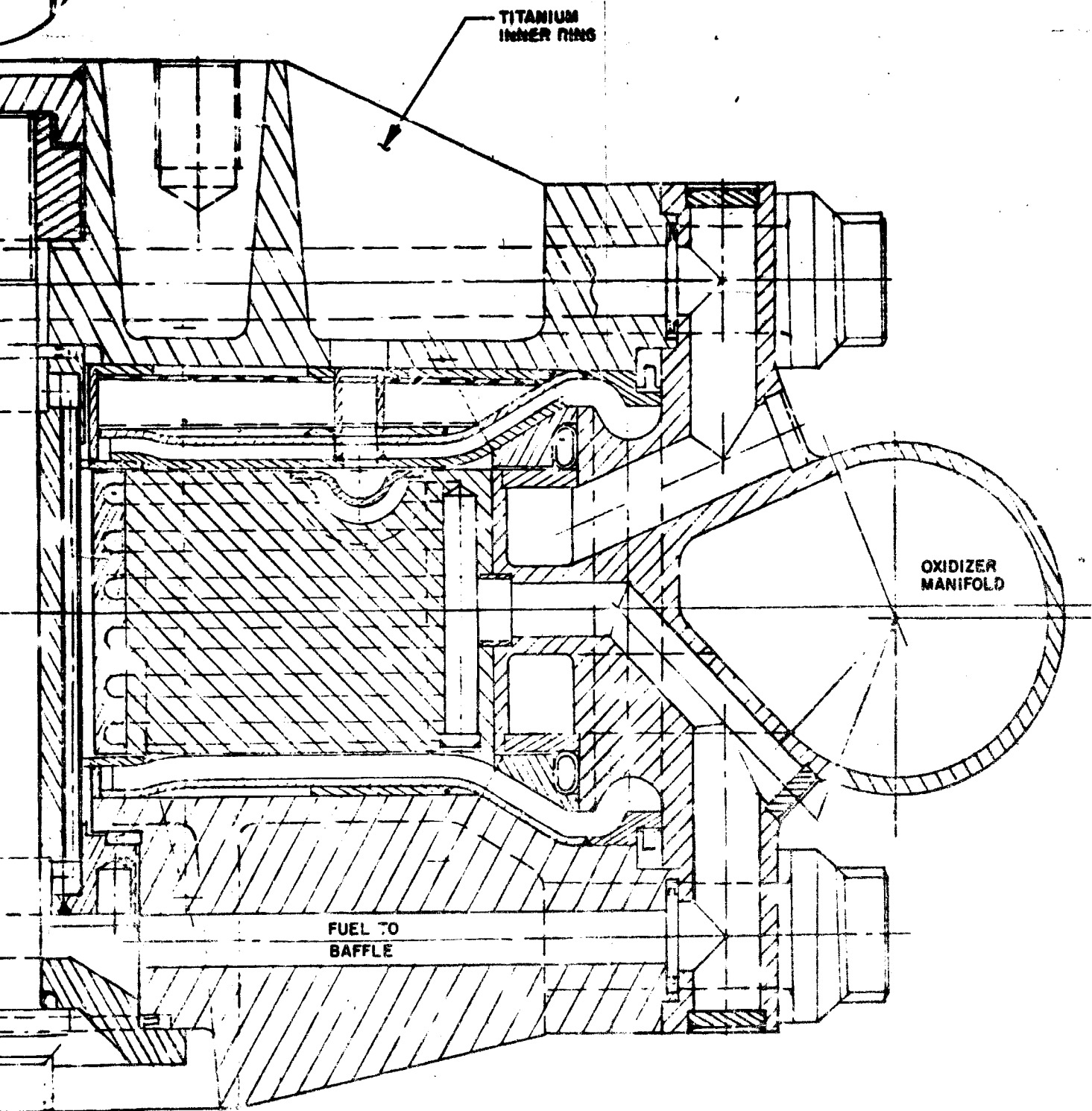


Figure 32. Proposed 250K Aerospike Thrust Chamber, 80-Subsonic Strut Configuration

CONFIDENTIAL

This page is intentionally left blank

CONFIDENTIAL

CONFIDENTIAL

Injector Configuration

(C) The demonstrator module injector pattern will be the same as the 250K experimental injector with modifications found necessary in the test program. The design characteristics are given in Table 11. The pattern features a continuous raised hydrogen post which is located between recessed LOX flat strips. Two LOX jets impinge below the hydrogen post to form a LOX fan.

Table 11. Injector Characteristics,
250K Injector

Characteristic	H ₂ System	O ₂ System
\dot{w}_{total}	79.21 lb/sec at 1500 psia P _c	475.26 lb/sec at 1500 psia P _c
Δp	400 psi at 1500 P _c	375 psi at 1500 P _c
T _{oH₂}	400 R	--
P _{O2}	--	70 lbf/ft ³
No. of orifices	2800 (includes bias)	4,480
D _{hole}	0.070 inch	0.0368 inch
A _{total}	9.07 sq in.	4.77 sq in.
C _d	0.90	0.92

STRIP GEOMETRY

H ₂ Post Height	0.238 inch above LOX strip
H ₂ Post-to-Impingement Distance	0.160 inch
Angle (LOX to LOX included)	60 degrees
Overall Height of Strip	0.498 inch
No. of elements per strip	8

CONFIDENTIAL

Thrust Chamber Heat Transfer

(U) The design for the 250K demonstrator engine cooling tubes will commence in the next quarter. It will incorporate the latest information concerning heat flux, choice of wall material and operating temperature limits for long life, tube roughnesses which can be reasonably expected based on 2.5K tube segments, and coolant curvature enhancements. Effects of baffle design which is currently in progress on the tube cooling requirements will be considered.

Nozzle Contour

(U) The contour and shroud configuration for the demonstrator module thrust chamber were selected on the basis of high performance at all altitudes and heat transfer considerations. The latter involved a shock-boundary layer interaction phenomenon which could possibly lead to local boundary layer separation and adverse local heat fluxes. Both the performance estimates and the prediction of the shock-boundary layer effect are highly dependent on the predicted wall pressure profiles.

(U) To verify the theoretical calculation techniques employed to predict the wall pressure profile an experimental cold flow nozzle test series was conducted under separate task. The cold flow model employed in the test series was a two-dimensional quarter-scale segment of the 250K experimental thrust chamber. Both analytical and experimental wall pressure profiles for a typical data run are shown in figure 33. The results of these tests confirms that the analytical model employed to predict wall pressure profiles of the 250K experimental thrust chamber is more than adequate. Based on these model tests, it can be concluded that high nozzle performance will be obtained at all altitudes and that no adverse heat transfer conditions will occur as a result of shock-boundary layer interaction.

c. Problem Areas and Solutions

(1) Off-Nominal Performance

(C) Problem areas may exist in the off-design performance of the combustion process as related to the properties (such as temperature and heat capacity) of the tapoff gases at off design conditions. Currently it is assumed that these efficiencies and properties remain constant throughout off-design operation. These assumptions will be modified if necessary as test results become available. The magnitude of such changes was anticipated by calculating engine performance at the 50K thrust and mixture ratio of 6.0 operating point assuming a 600 K temperature decrease in tapoff gas temperature at this throttle.

CONFIDENTIAL

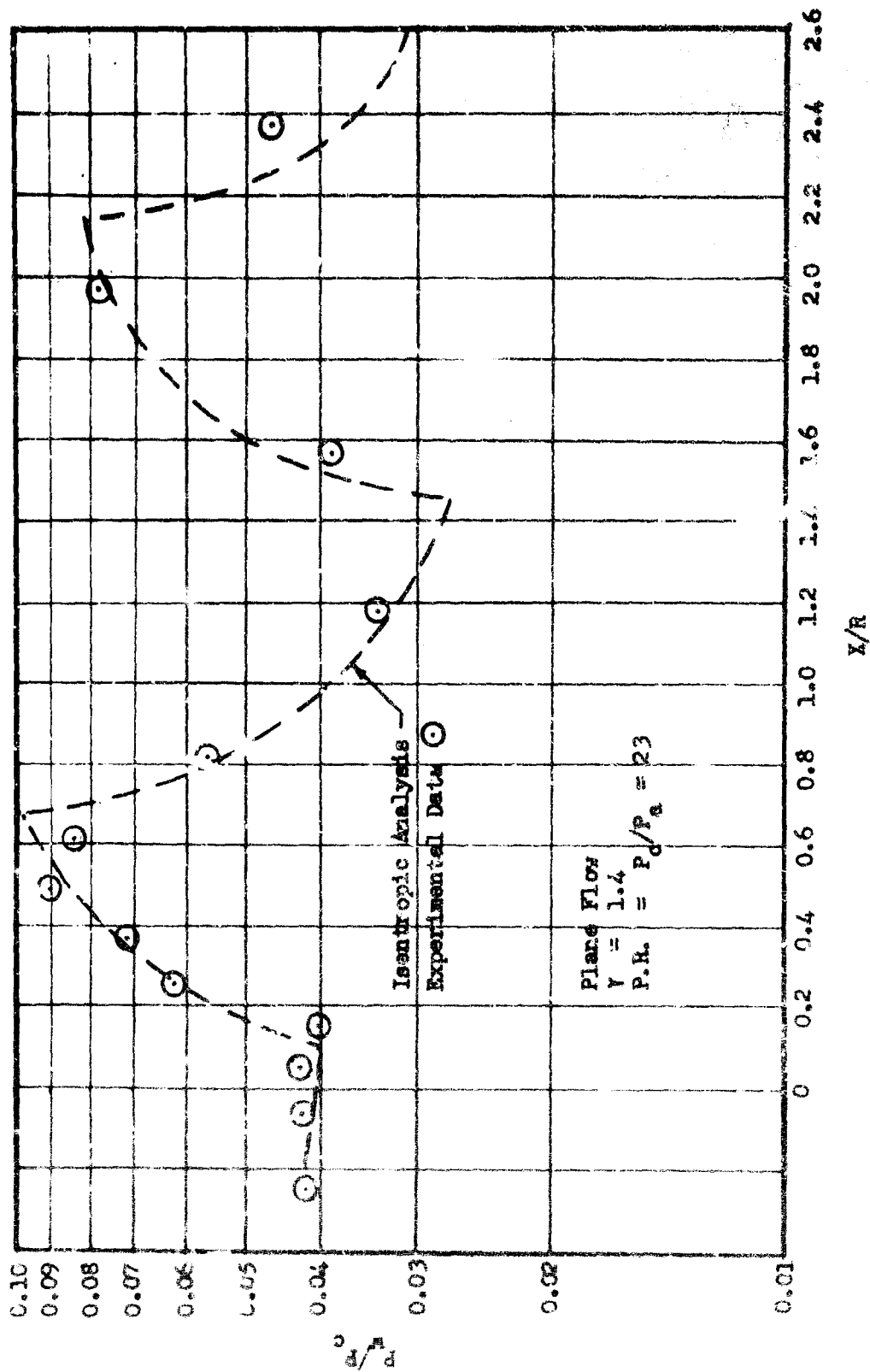


Figure 33. Full-Length Shroud Pressure Profile

CONFIDENTIAL

CONFIDENTIAL

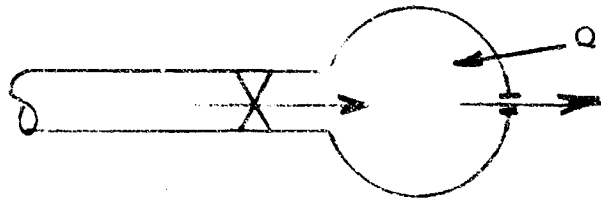
condition. The results showed a 1.1 second decrease in specific impulse, indicating that a very substantial decrease in the energy content of the tapoff gases at throttled conditions will not seriously penalize engine performance.

(2) Hot-Gas Ignition

(C) Hot-gas ignition of the main chamber has been a problem area which is being studied under a separate test program. The required hot-gas and liquid propellant conditions for smooth repeatable starts are being determined. Problems in igniting liquid hydrogen earlier in the quarter have been overcome, and results to date have been quite satisfactory. Ignitions have been achieved with a hot-gas temperature as low as 1370 F at the proper sequence mixture ratio and with liquid hydrogen. Data from this program will be used to finalize the thrust chamber and ignition system designs.

(3) Hydrogen Feed System Start Transient

(U) A major start transient problem area may be large flow oscillations in the main fuel feed system. An analog of this system could be a line filled with a cryogenic fluid, a valve, and a large bottle with a small hole discharging to atmosphere (as shown below). The bottle



is the cooling tubes and the small hole is the throat section of the tubes. When the valve is opened, liquid flows into the warm container and turns to gas which is compressed at relatively high pressure. Being a gas, it cannot escape rapidly enough out of the small hole, therefore a flow reversal or oscillation occurs in the line. Two things can happen to stabilize the system. The container chills to liquid temperature reducing gas formation, or line pressure increases decreasing capacitance.

(U) If these oscillations are severe enough, they can drive the pump into an unfavorable operating region such as a "surge" or "stall" region from which recovery may be difficult. It appears that some sort of auxiliary flow system will be required to maintain pump flowrate above some minimum value. This system may take the form of fuel pump recirculation, or fuel dump into the fuel turbine discharge, LOX turbine

CONFIDENTIAL

CONFIDENTIAL

discharge, base plenum, base region, or fuel injector. A trade-off study will be made on these systems. The system will be sequenced full-open at start with ambient temperature cooling tubes, and sequenced closed as cooling-tube impedance decreases and cooling-tube heat transfer and required cooling increases.

(4) Oxidizer Priming and Valve Sequencing

(U) The problem of main oxidizer system priming is being studied under the NASA Systems Dynamics Investigation Program Contract NAS 8-19. This study is investigating LOX priming volumes and times and is considering the technical problems of multiple lines, symmetrical and unsymmetrical configurations, baffles, and orificing.

(C) Priming the main oxidizer system and sequencing the main LOX valve will be a critical point in the start sequencing. With a relatively flat H-Q pump curve, fuel flowrate drops into the surge region and may not recover. Thus, a two-step with ramp secondary opening main LOX valve as used in J-2 type engines may be required and is shown in figure 11. Increasing the negative slope of the H-Q map will decrease the criticality of these requirements.

(5) Hot-Gas Priming

(U) Gas dynamics and heat transfer is expected to be important in the hot-gas system. This system is sized to have minimum pressure drop to maximize available turbine starting torque. Its flow capacity is actually larger than that required to drive the engine at 100-percent thrust. This large capacity creates a large priming volume and heat transfer area, signifying that gas dynamics and heat transfer will be important as it was with the J-2 crossover duct.

(6) Oxidizer Propellant Feed Line Configuration

(U) The oxidizer propellant feed line configuration is still an unresolved problem area. The current layout shows two symmetrical branch lines from the pump to the thrust chamber manifold. The LOX priming studies being conducted on the NASA Systems Dynamics Investigation program are considering two, four, symmetrical, and unsymmetrical branch lines. The latter design appears to decrease the priming time and provide a more uniform oxidizer distribution in the manifold. The effects of unsymmetrical lines has not yet been determined, and the packaging problem of more than two lines has not been assessed. The final design configuration must therefore await further results from the Systems Dynamics investigation together with design trade-off studies.

CONFIDENTIAL

CONFIDENTIAL

(7) Thrust Chamber/Thrust Mount Thermal Growth

(U) Another problem area arises in the design of the thrust chamber/thrust mount interface. The thrust chamber will undergo a radial contraction as a result of introducing liquid hydrogen into the regenerative cooling circuit prior to main chamber ignition. However, the thrust mount structure will remain at approximately ambient temperature, resulting in a tendency toward relative radial movement between these two components which produces loads on the thrust mount cone structure. The two components must therefore be isolated mechanically. This may be accomplished through the use of a thermal expansion connection concept at the component's circumferential interface which will allow unrestrained radial movement during component temperature differences with no effect on concentric alignment. The technique will still provide a rigid load path during engine thrust, dry gimbaling, shipping, and handling.

(8) Fuel Turbine Seal

(U) A problem area in the fuel turbopump is the rotating seal between the second stage pump inlet and the turbine. In this location, the pressure difference between the fuel pressure and the turbine pressure is greater than can be handled by the seal bellows. A partial solution to the problem is to use a conventional turbine arrangement instead of the reversed flow turbine as this puts the higher pressure stage next to the pump inlet, decreasing somewhat the pressure difference. To further decrease the pressure differential, additional labyrinth and a seal may be required.

(9) Preinducer Drive

(U) The LOX turbopump design requires the LOX preinducer to generate a relatively high load. This, combined with the NPSH specification, is causing matching problems between the preinducer and the main impeller. During throttling operation, the preinducer flow coefficient decreases more rapidly as the pump flow is dropped. One solution would be the use of a high-speed inducer attached to the main pump; however, this will increase the largest of the unit as well as add weight. Additional matching studies are underway.

d. Summary of Planned Effort

(1) System Analysis

(U) The nominal engine design point balance will be continually updated as component designs become final. A criteria for establishing the upper limit of thrust over the mixture ratio range will be established

CONFIDENTIAL

CONFIDENTIAL

early in the next report period and component design requirements modified as necessary to reflect this decision.

(U) Selection of the control loop for mixture ratio and thrust will be accomplished in the next report period. Analog computer design parameter studies will be completed and control component parameters requirements defined. Design of the control system will be initiated.

(U) The evaluation of tapoff vs gas generator cycle will be completed and component design requirements modified as necessary to reflect the decision.

(U) Conversion of the digital model to the IBM 360 system will be completed early in the next quarter. Evaluation of candidate hydrogen dump and bypass schemes to minimize hydrogen cooling tube instability and avoid pump operation in the surge region will be conducted. Hot-gas valve transient requirements for balanced speed buildup under both sea level and altitude conditions will be determined. The dynamics of the hot-gas igniter, including priming transient and tendencies towards chugging, and control response requirements will be evaluated. A simulation of the shutdown sequence will be accomplished to evaluate cutoff problems and establish valve rates.

(2) Preliminary Design

(U) A study of propellant feed subsystem assembly and maintainability will be made in addition to a study of duct routing that will provide for better system isolation. In-depth design studies will be performed to optimize the number of oxidizer branch lines (utilizing inputs from the NASA SDI program), to determine the optimum method for supporting the turbopumps, to further evaluate cryogenic seals for static applications, and to select the best technique for thermal isolation of hot components.

(U) The thrust structure trade study will be completed and a thrust structure selected for the module. The thrust subsystem design layout will be carried through a second iteration. The engine general arrangement will be modified as necessary to reflect the pending decision relative to type of control loop and turbine drive gas source.

(C) The 250K and 350K module parametric performance and weight data will be modified as necessary to reflect design decisions during the course of the study. Sensitivity of system performance to component variation, such as turbine inlet temperatures, turbopump efficiencies, system ΔP nozzle percent length, and etc. will be investigated during the next quarter.

CONFIDENTIAL

CONFIDENTIAL

(U) Optimization of the preinducer drive design will continue to arrive at minimum weight and size and maximum overall efficiency. Design problems and advantages of the following configurations are being investigated.

1. Through flow preinducer
2. High-pressure tip turbine preinducer
3. Gear driven preinducer
4. Separate gas turbine driven preinducer

The turbopump design effort will be deepened to include more comprehensive and detailed hydrodynamic, turbine, stress and dynamic analysis, and the problems of the fuel turbine rotating seal and oxidizer turbine diameter will be resolved.

(U) During the next report period, design definitions of the titanium structural wall will be achieved. Finalization of this component will involve consideration of such factors as structural tie baffle attachment, load paths, coolant circuit manifolds and transfer ducting, hot-gas tap-off, and the interfaces between the chamber wall and the injector, base closure, fuel inlet, and thrust mount. Design of the coolant tube bundle attachment to the structural wall will be supported by data on various epoxy compounds.

(U) Further definition of the injector assembly will also be conducted. Primary emphasis will be placed on seal type and bolt location.

(U) Preliminary design of the hot-gas valves, main oxidizer valve and main fuel valve will be initiated during the next quarter.

CONFIDENTIAL

2. APPLICATIONS STUDY

a. Status

(U) The applications study task was initiated during the last half of this quarter (mid-July). Preliminary vehicle layout drawings were made and structural studies began to generate preliminary parametric surface areas and engine installation weights as defined by the Air Force application packages. The structural effort during the report period was concentrated on studying the details of "state-of-the-art" thrust structures and related systems that are required to complete the vehicle installation. These data combined with engine module parametric data will be fed into a high-speed computer program to generate the defined performance index data required for all the vehicles. As the preliminary parametric data is refined, it will be fed back into the program to help converge on the recommended common engine modules; one for the 250K and one for the 350K vehicles.

b. Progress During Report Period

(1) Performance Index Analysis

(U) In comparing module concepts and optimizing engine parameters, the performance index is used as a basis of evaluation. The equation, presented in the application packages which defines the performance index is shown below:

$$W_x = \left\{ \frac{W_g - 2A_i}{W_g} \right\} \left\{ W_{bc} - K \left[W_e + 1.5 A_f + 0.02 (W_g - W_{bc}) \right] \left(1 + \frac{5}{R} \right) \left(\frac{500,000}{W_b - W_{bc}} \right)^{1/3} \right\}$$

The performance index approximates the stage burnout weight decreased by the weight of the engine modules and engine-dependent weights, with consideration of growth potential for the reusable stages. The engine module performance is reflected in the term burnout weight, W_b . Other factors, such as module geometry, weight, interstage and fairing structure, etc., are also accounted for.

(U) With the aid of the Rocketdyne-designed IBM computer programs, the performance index technique is being utilized to optimize engine and engine-vehicle integration component characteristics. Using preliminary estimates of engine installation weights, interstage and

CONFIDENTIAL

CONFIDENTIAL

fairing surface areas, etc., exchange factors were first generated. These exchange factors are being employed to facilitate the formulation and selection of design concepts regarding module location and arrangement, thrust structure configuration, feed line routing, interstage and fairing areas. During this report period, the performance index programs have been designed for use for both the 250K and the 350K modules.

(U) A consistent procedure for maintaining records on performance index calculation inputs and results has been established. A continuous log is being kept to document all pertinent information that went into the computation for each series of performance index calculations. Summary records, graphs, and charts are also maintained for quick reference and rapid comparison.

(2) Installation

(U) Examination of each of the six Advanced 250K Vehicles was initiated and preliminary conceptual installation layouts prepared. Factors, such as fairing and interstage surface areas, maximum skirt diameter, and installation weight, which influenced the performance index are being evaluated with the aid of exchange factors. The range of engine diameters under investigation are from 80 to 120 inches.

(U) The two candidate engine arrangements evaluated to date for cases 1 and 3 are shown in figure 34. Each vehicle was evaluated with respect to overall engine diameter and engine arrangement. Performance index reductions due to increases in fairing area and maximum fairing skirt diameter were computed. Results for Cases 1 and 3 are shown in figures 35 and 36, respectively. These graphs are based on arrangements A (one inboard/four outboard engines) and B (five engines in a circular pattern). A comparison of both engine arrangements for each vehicle indicates that mounting the engines in a circular pattern results in lower losses; however, this configuration has the disadvantage of not being symmetrical with respect to thrust vector control (TVC) about the pitch and yaw axes. During the Air Force coordination meeting of 29 August 1966, Rocketdyne was directed to limit the clustering arrangement to be studied for all 5 engine clusters to that depicted in figure 34, arrangement 1.

(U) A candidate Arrangement 1 thrust structure, similar to the concept used on the Saturn S-II stage, is illustrated in figure 37. The thrust structure consists of skin-stringer conical shell. This shell transfers engine thrust loads to the perimeter of the main structural ring. The four outboard engine thrust loads are applied directly through the gimbal block to the longerons. The center module thrust is reacted by two cross beams. These beams transfer the load to the

CONFIDENTIAL

CONFIDENTIAL

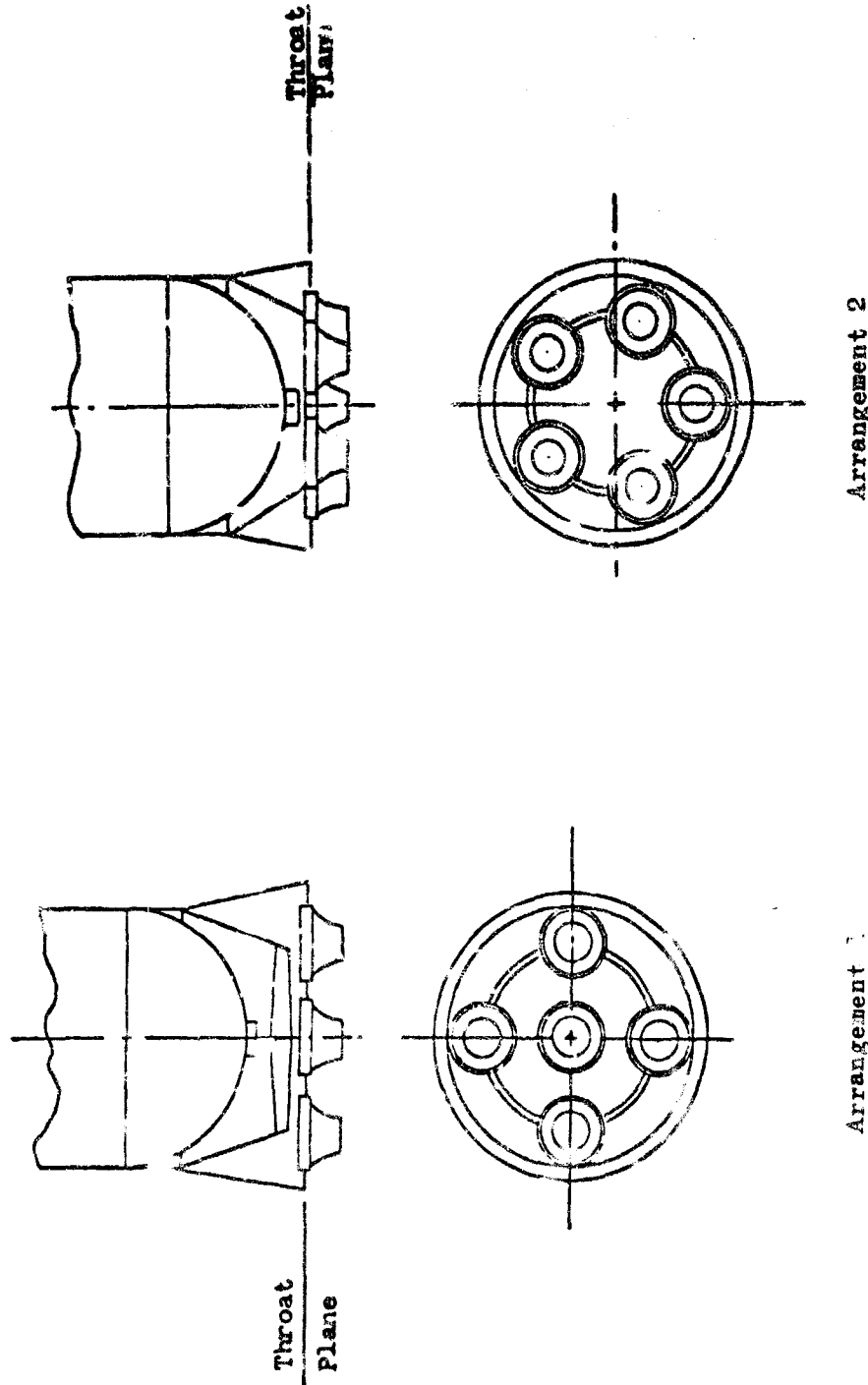


Figure 34. Candidate Engine Arrangements: Case 1, Expendable First Stage;
Case 2, Expendable Single Stage to Orbit

CONFIDENTIAL

CONFIDENTIAL

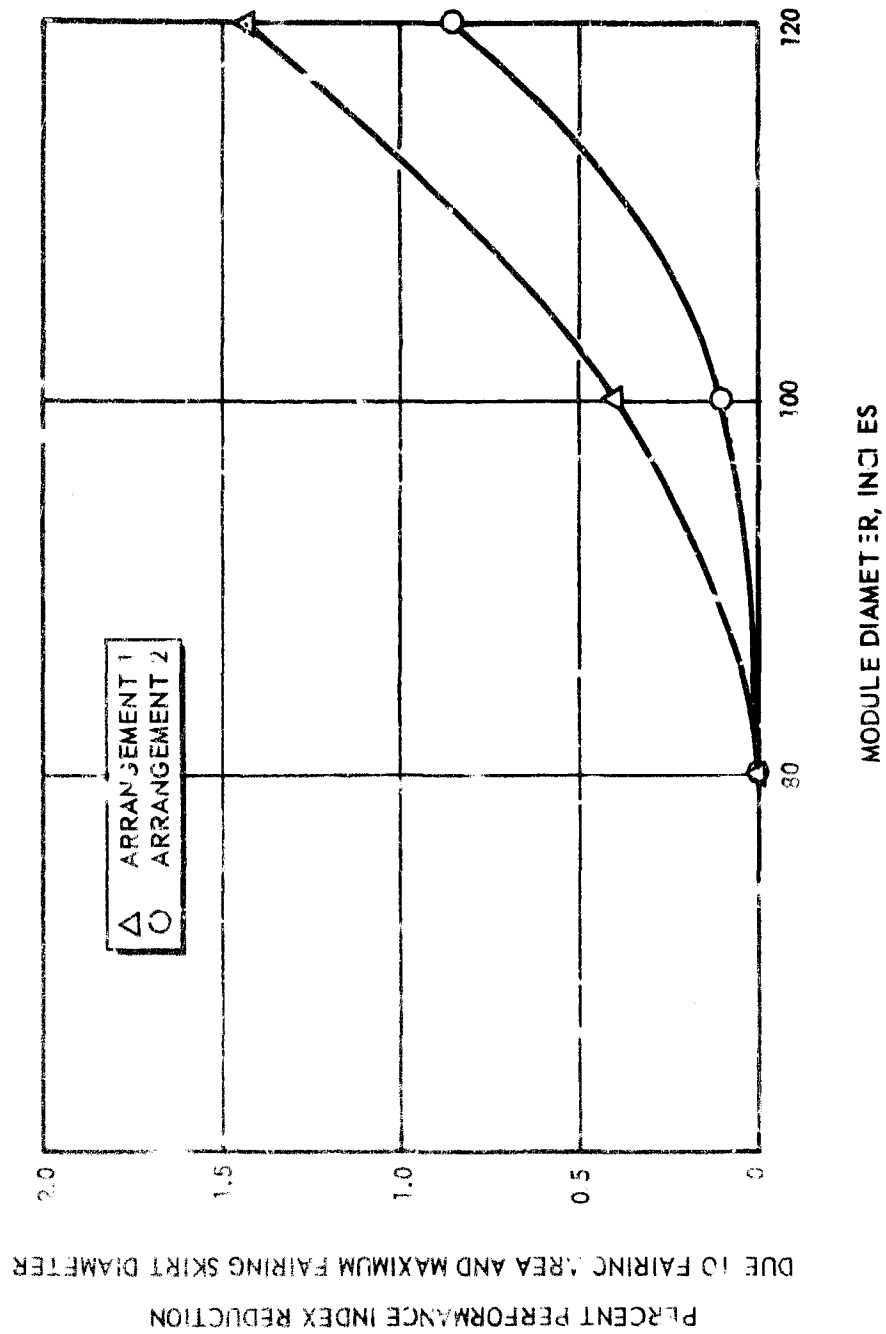


Figure 35. Case 1, Relative Performance Index Decrease Module Diameter

CONFIDENTIAL

CONFIDENTIAL

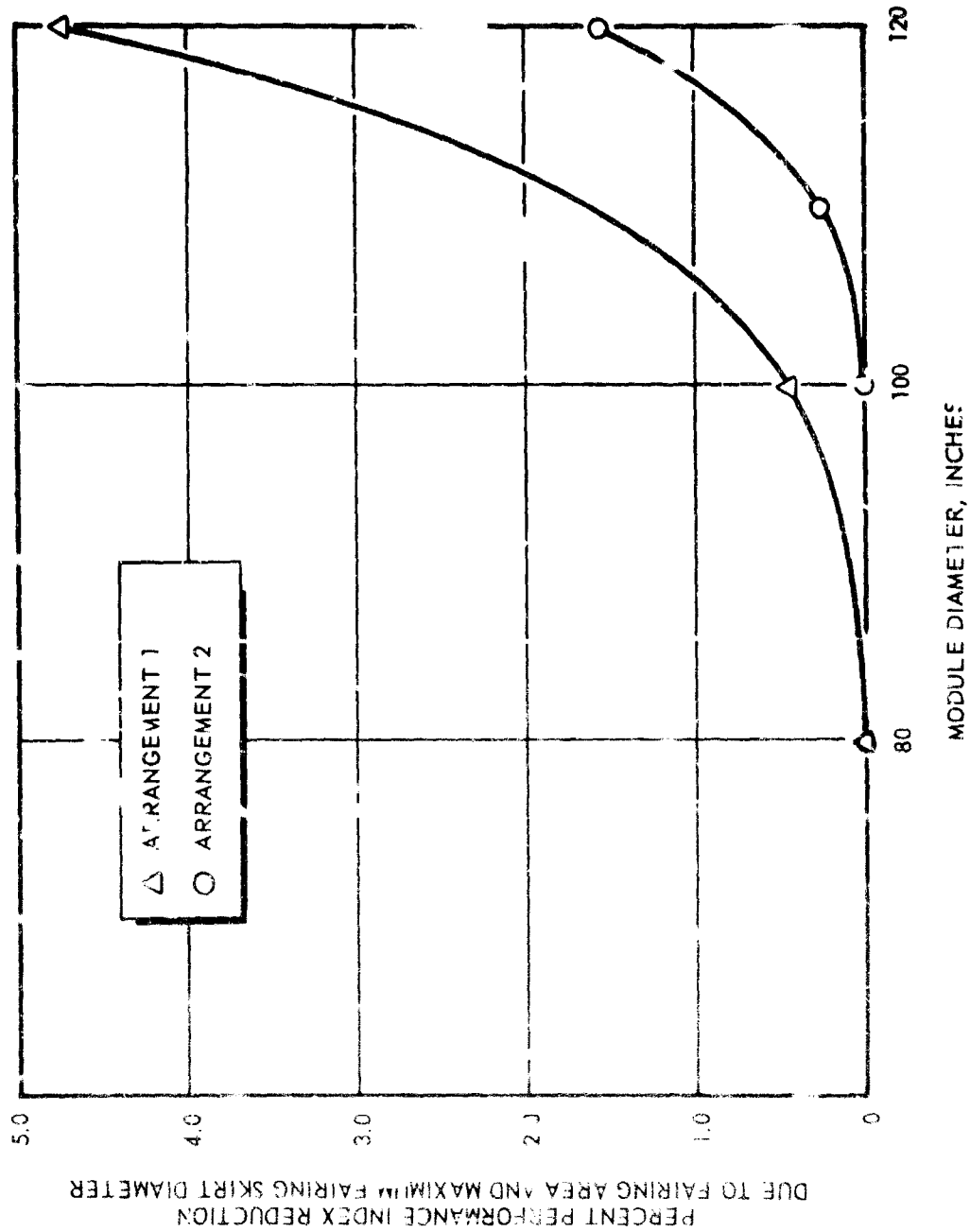
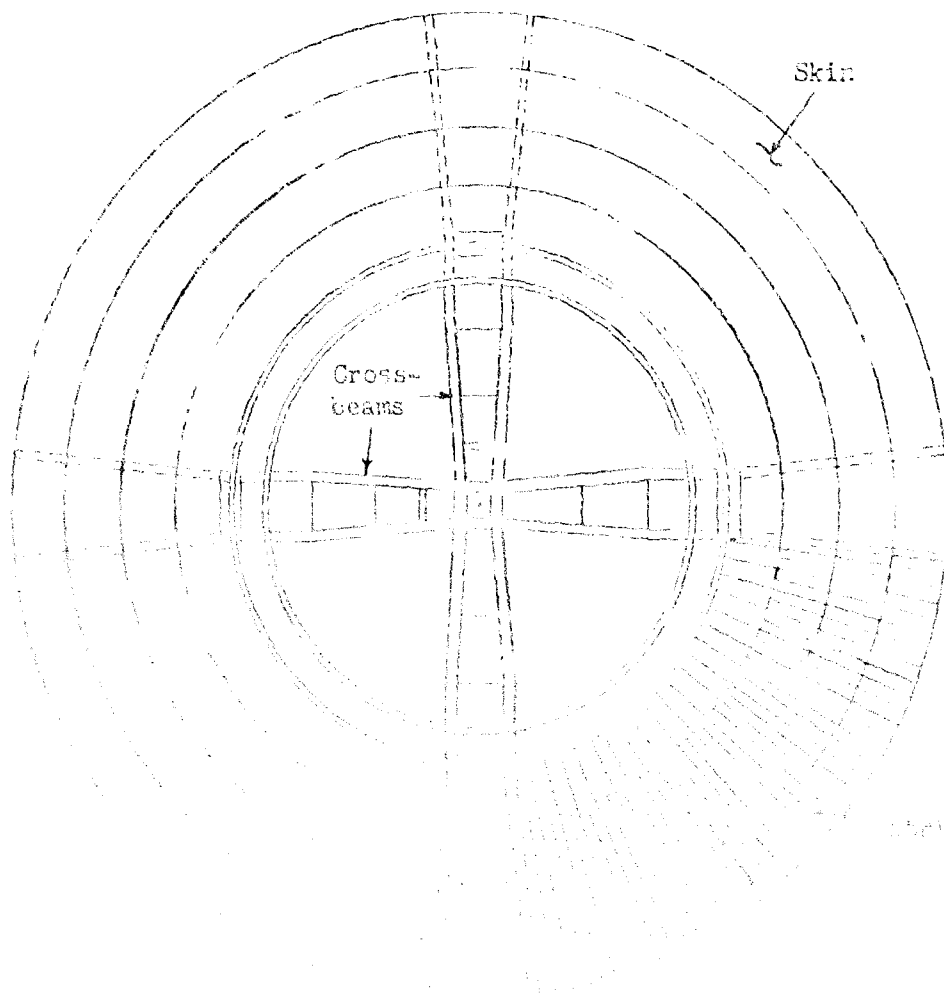
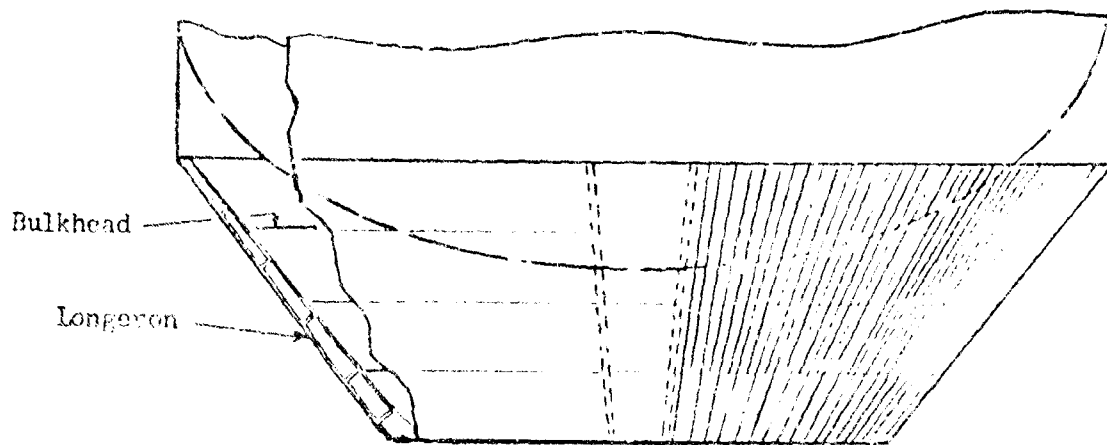


Figure 3a Case 3, Relative Performance Index Decrease Module Diameter

CONFIDENTIAL

CONFIDENTIAL



CONFIDENTIAL

CONFIDENTIAL

longerons. The cross beams also react the horizontal force component of the module thrust load at the longerons. The total thrust loads are thus sheared into the skin-stringer shell. Frames are provided on the thrust structure for general shell stability. Kick loads from the longerons and from the conical shell also have to be considered in the design of the frames.

(U) Parameters affecting the frames, longeron and cross beam design are the magnitude and sense of the module kick loads. The kick loads are dependent upon the (1) location of the frames at the extremities of the longerons, (2) the location of the cross beam to longeron attachment, and (3) the TVC actuator attachment location. The longeron-to-shell stiffness ratio influences the conical shell compression load distribution (determined through a shear lag analysis). The shell skin-stringer axial load carrying capability is also determined by the frame locations.

(U) Cases 2 and 6 are single engine installations and were evaluated differently than the multiengine installations. In Case 2, performance index reduction caused by increases in interstage area as a function of engine/vehicle thrust structure mount height is shown in figure 38. Minimum mount heights for each engine diameter occur at that height for which the overall interstage length is approximately 8 feet. Figure 38 indicates that for a given mount height, the larger performance index reduction occurs with the 120-inch-diameter engine. Preliminary analysis revealed that Case 6 interstage area is independent of thrust structure mount height because of the fixed 20 feet diameter at the aft end of interstage and the limiting 15-degree surface angle. In case 6, performance index reduction caused by increases in fairing area is shown in figure 39. The range of module diameters does not fully utilize the envelope generated by the interstage surface. Thrust structure and feed line weight as a function of mount height is being determined.

(U) Design effort on the Case 4 vehicle during this period was concentrated on determining the module arrangement which would minimize the engine mounting height and fairing area. Three candidate module arrangements which were evaluated are shown in figure 40. Based on layouts of the module arrangements, 100-foot-diameter engine mounting height and fairing area were compared with arrangement C which utilized one inward and seven outward modules. The installation of arrangement A, consisting of four inward and four outward modules, resulted in square patterns, resulting in maximum values of mounting height and fairing area. The installation of the circular module Arrangement B, resulted in values between A and C.

CONFIDENTIAL

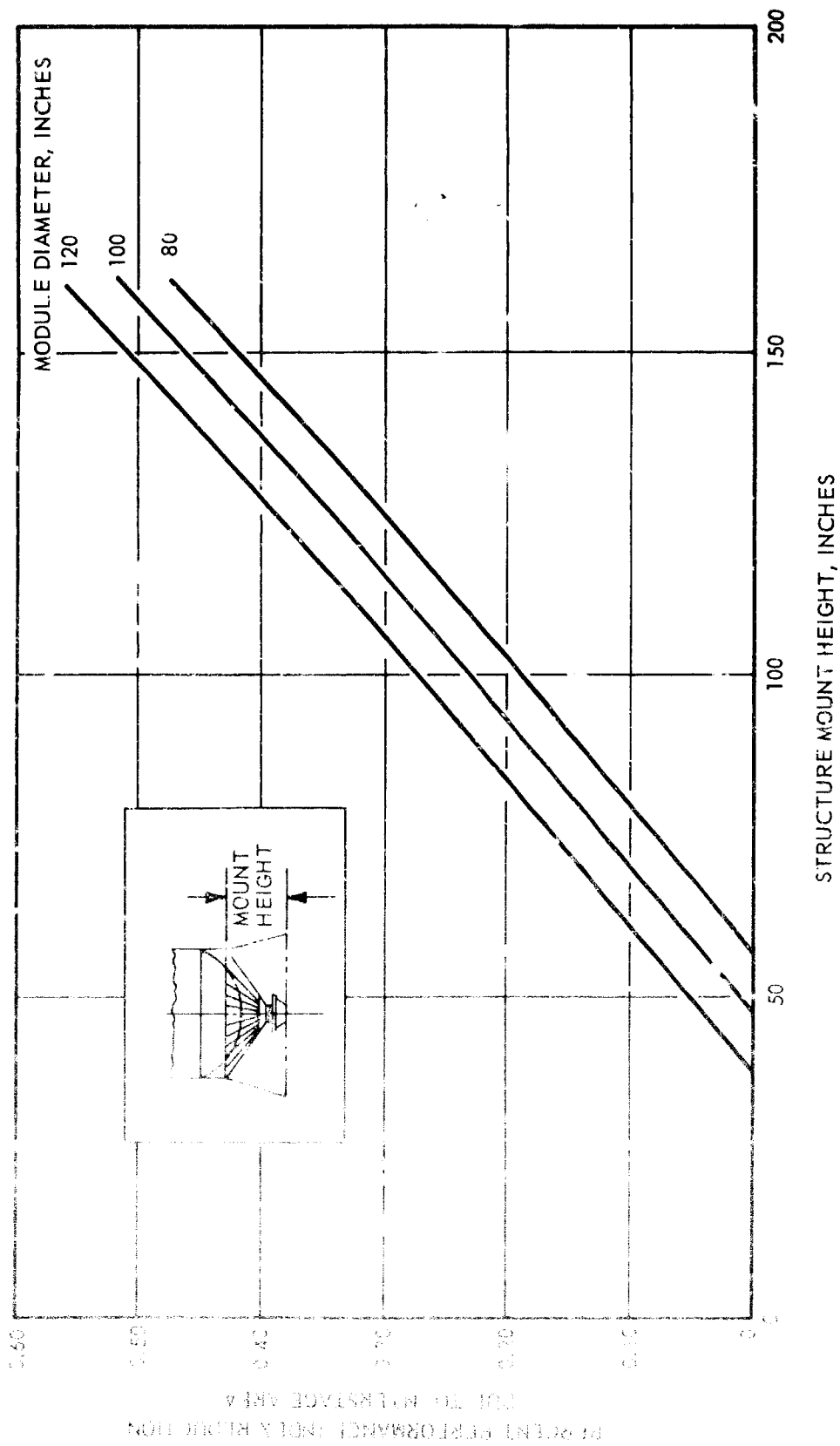


Fig. 10-24. Case 2, Relative Performance Index Decrease vs Mount Height

CONFIDENTIAL

CONFIDENTIAL

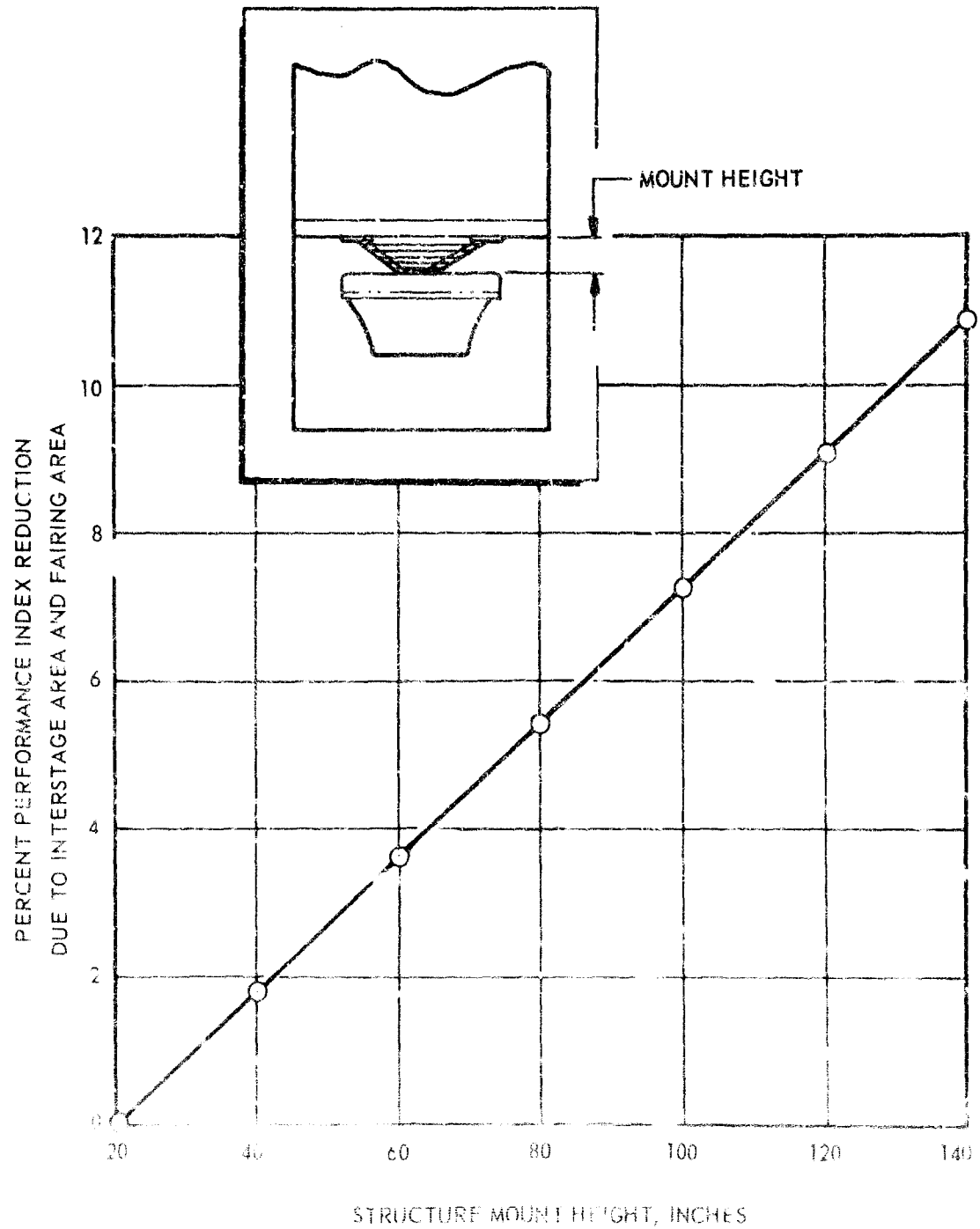


Figure 39. Case 6, 25% Relative Performance Index vs. Mount Height

CONFIDENTIAL

CONFIDENTIAL

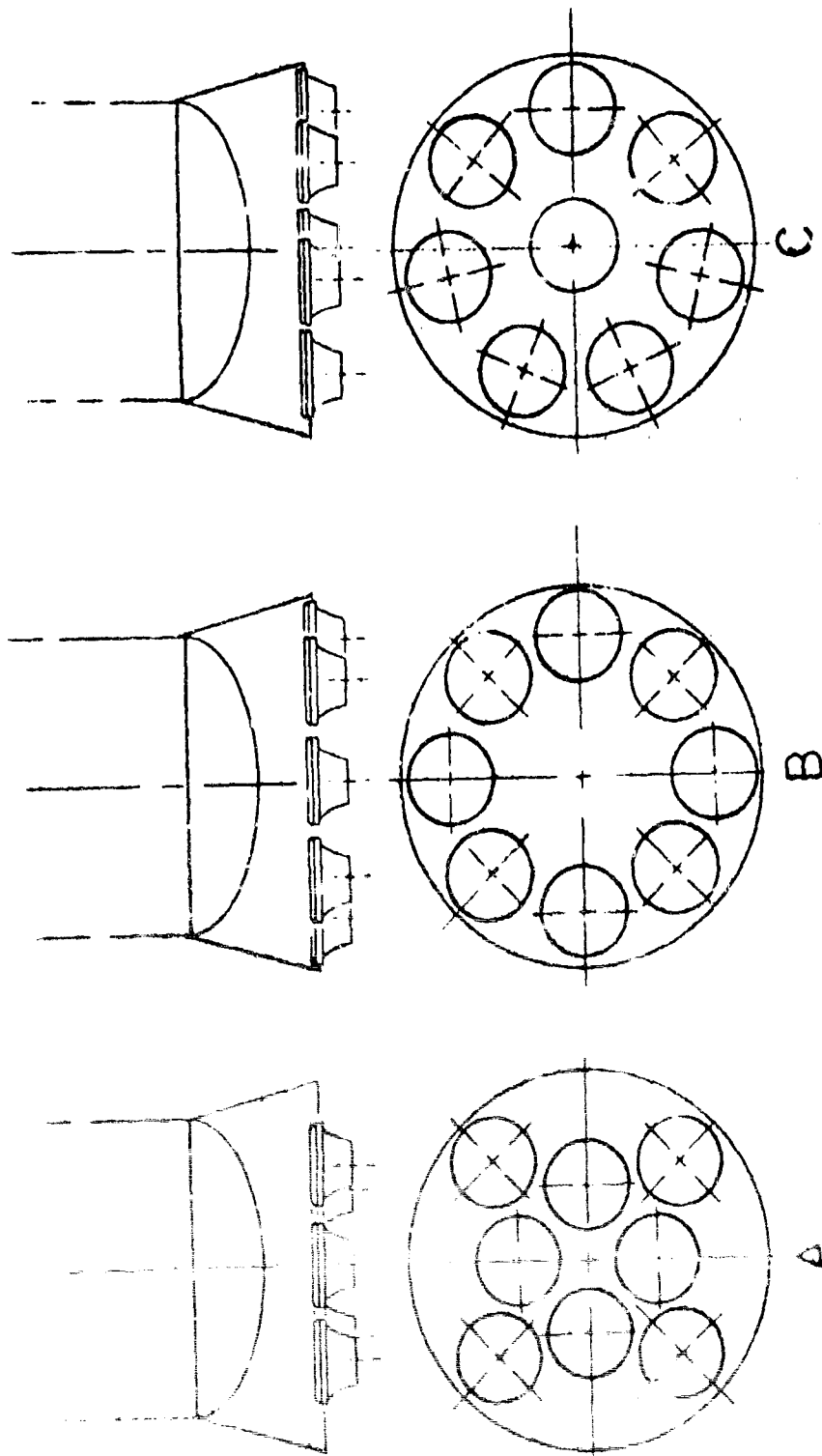


Figure 40. Candidate Engine Arrangements: Case 4, Recoverable First Stage (VTOHL)

CONFIDENTIAL

CONFIDENTIAL

(U) The variation in performance index were studied with respect to fairing area and maximum fairing skirt diameter. A graph (figure 41) of relative performance index decrease vs module diameter for the three arrangements shows that the smallest losses with respect to fairing area and maximum skirt diameter occur with Arrangement C for the range of module diameters considered however, Arrangements A and B have the advantage of being symmetrical with respect to thrust vector control about the yaw and pitch axis. On 31 August 1966, AFRPL provided the study ground rule that multiengine installations must be symmetrical about the pitch axis and the yaw axis, thus eliminating Configuration C from further consideration.

(U) Two engine arrangements are being evaluated for Case 5. Figure 42 shows the tank-end and between-tank mounting configurations. The between-tank installation has a smaller fairing area compared to the tank-end design; however, it has a higher propellant feed line weight. A study is underway to establish the optimum installation configuration.

(U) Two concepts of pyramidal thrust structure have been studied for this case. One concept, the tubular design, carries module loads in four main compression members from the thrust forging to the vehicle (figure 43). The other concept, a sheet-stringer design, carries module loads to the vehicle by means of longitudinal stringers stabilized by a thin skin (figure 44).

(U) The tubular design is governed primarily by column buckling considerations. The main thrust members have hollow circular-tube cross sections. The hollow circular tube is the most efficient section in column buckling because, in a column free to buckle about any axis, it provides the greatest stiffness per unit area. Tubular cross-members are employed to break the relatively long unsupported length of the main members into a number of shorter columns, thus increasing the critical buckling load of the main members.

(U) The sheet-stringer design utilizes several Z-section stringers to carry the module loads to the vehicle. Thin sheet is riveted to the stringers. A potential weight advantage exists for this type of structure over the tubular design. This advantage arises from the fact that the thin sheet acts to prevent the stringer from buckling about their axis of minimum stiffness. Thus, a deep section (such as the Z-sections), with a stiffness/weight ratio greater than tubular members, can be used.

CONFIDENTIAL

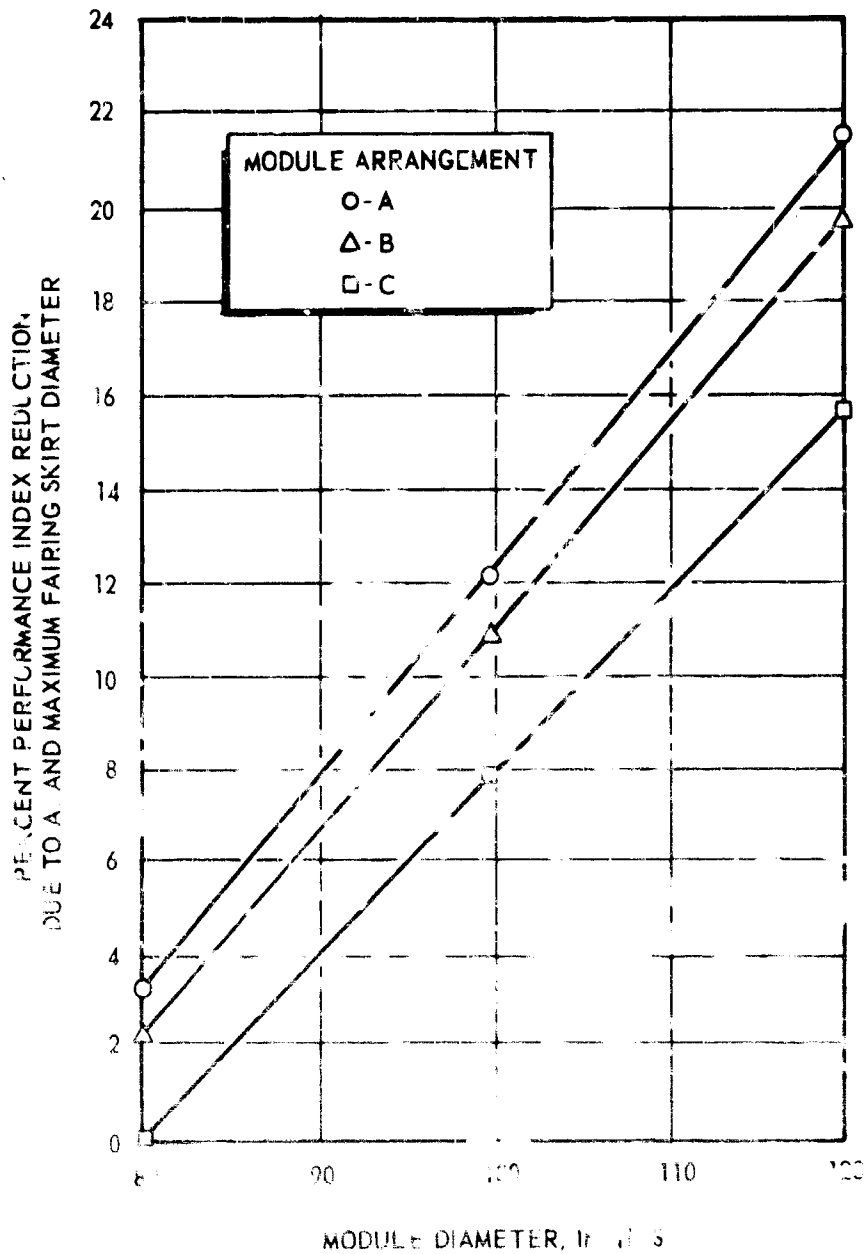


Figure 41. Case 4, 250K Modules Relative Performance Index Decrease vs Module Diameter

CONFIDENTIAL

CONFIDENTIAL

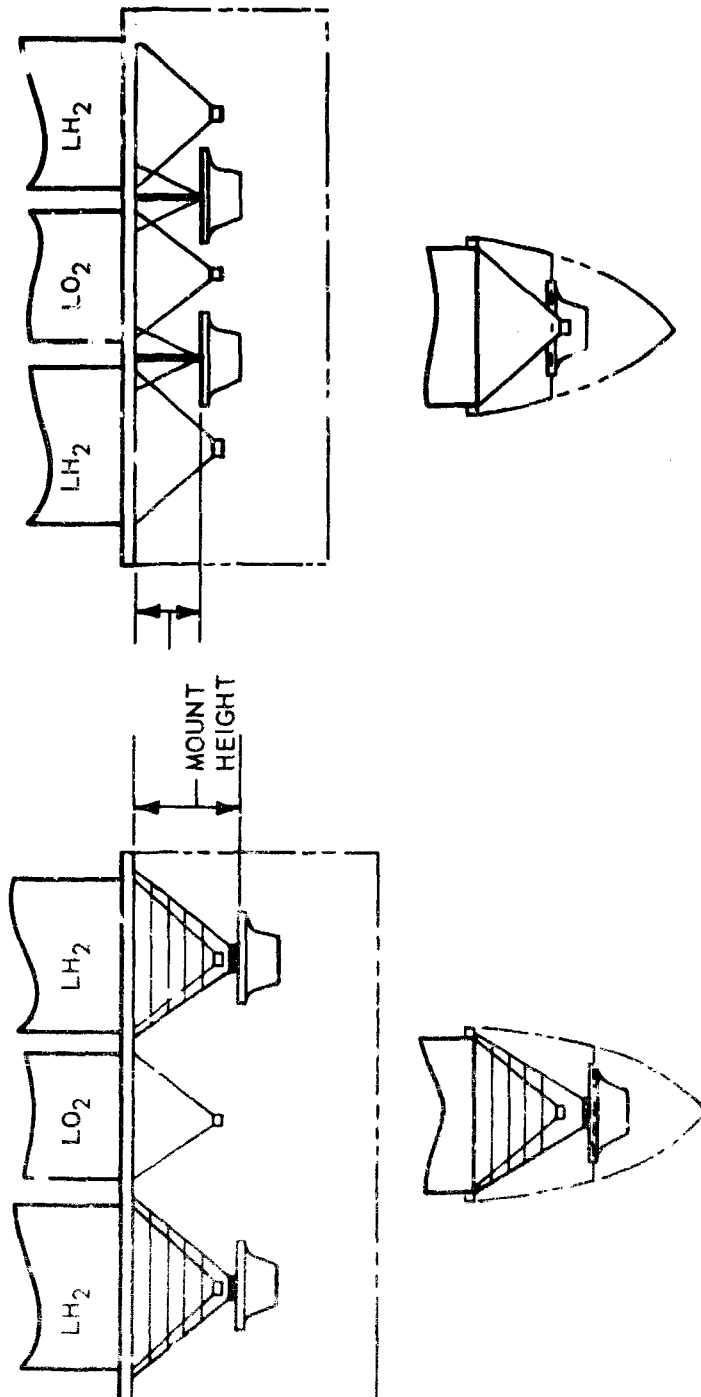


Figure 42. Candidate Engine Arrangements: Case 5, Recoverable Second-Stage Pickaback

CONFIDENTIAL

CONFIDENTIAL

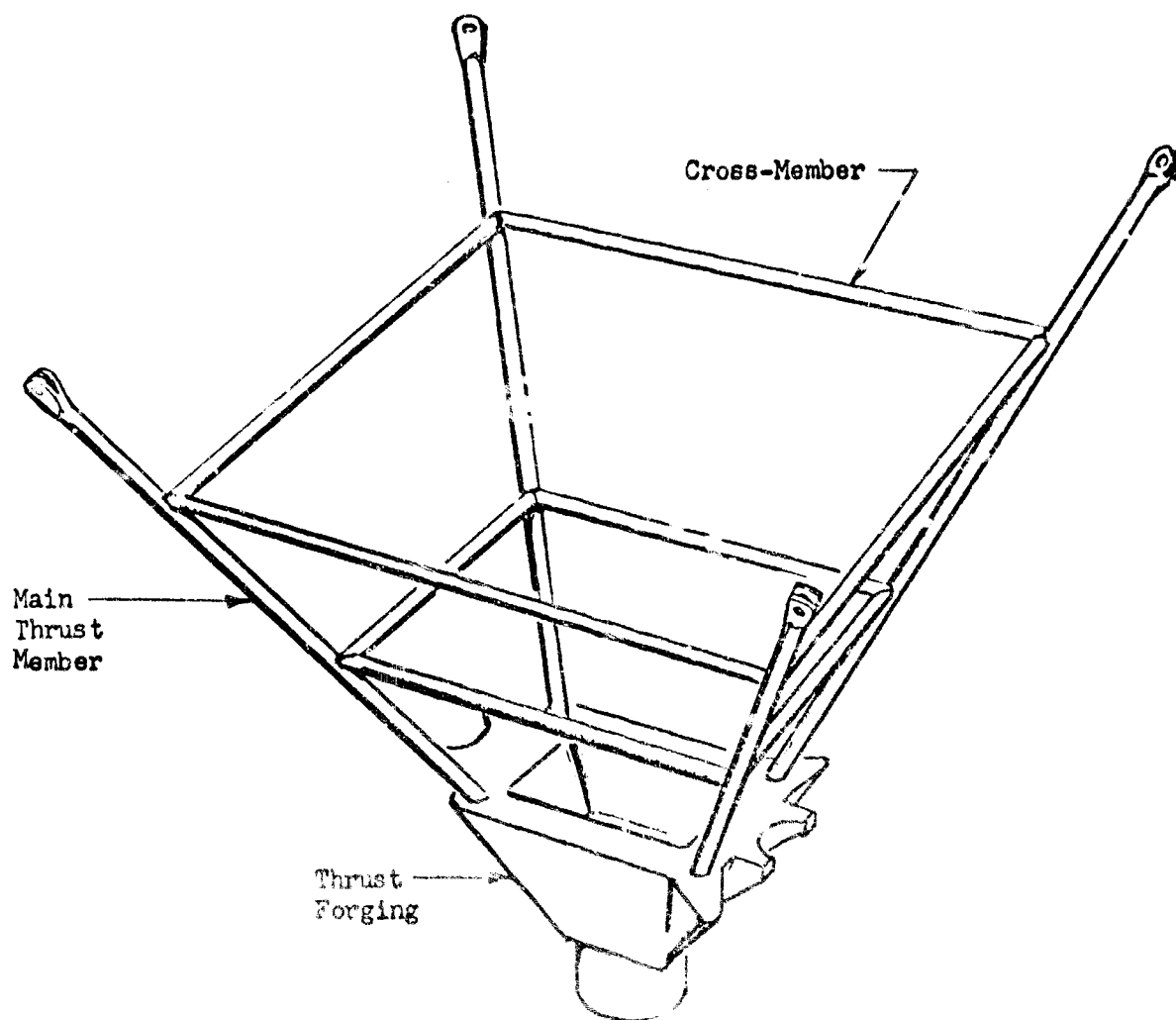


Figure 45 Tubular Design With Cross-Member

CONFIDENTIAL

CONFIDENTIAL

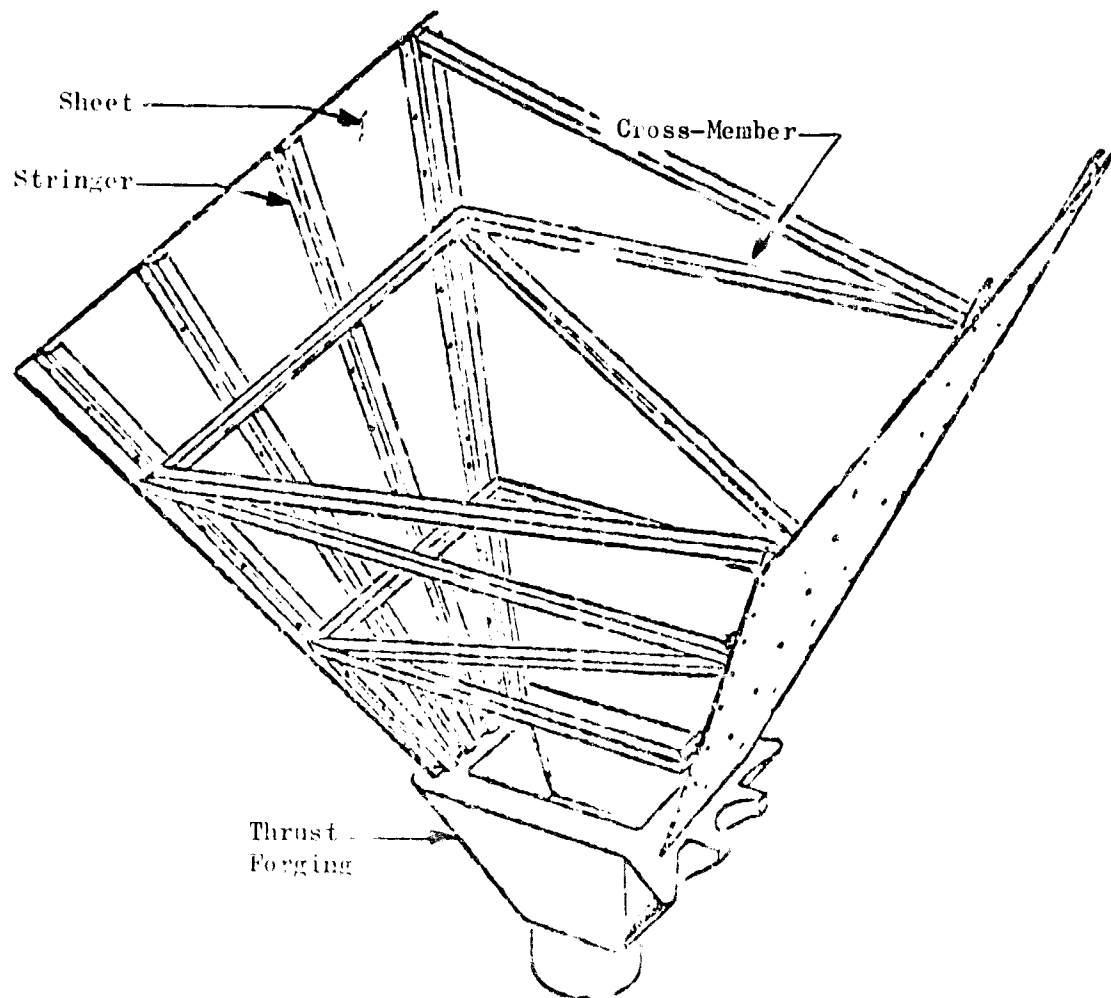


Figure 11. Sheet-Stringer Design With Cross-Members

CONFIDENTIAL

CONFIDENTIAL

(U) Because of the mounting requirements, several departures from a standard sheet-stringer design are necessary. First, the vehicle mounting provisions are two parallel channels. Thus a conical structure, which would provide the most efficient structure, cannot be used. Second, the vehicle mounting channels are not connected by cross-members. For this reason, stringers cannot be used on two faces of the pyramidal structure, because there would be nothing to react their loading. On these two faces, necessary shear stabilization will be provided by diagonal braces, or possibly sheet attached to the buckling support members.

(U) The safety factor and loading criteria to be used in the design of the vehicle installation components were derived. The safety factor on ultimate material strength and the maximum side loading from the thrust vector control system were specified. To this basic criteria were added the required safety factor on material yield strength and column buckling load, the maximum acceleration that would be encountered, the limit load factor to be used in conjunction with these acceleration, thrust, and other loads, and the proof-pressure factor for pressurized components. The criteria derived are shown in Tables 12, 13, and 14 for the 250,000-pound module. A similar approach is being utilized for the 350,000-pound module installations.

(c) Problem Areas and Solutions

(U) There were no significant problems or delays in the application study during the first quarter.

(d) Summary of Planned Effort

(U) During the next report period, the parametric weight analysis of engine installation items such as vehicle thrust structures, propellant lines, heat shields, pressurization system and etc. will be completed. Based on these data, refined Performance Index analysis will be conducted to determine the optimum installation geometry and engine operating parameters for each of the vehicles.

CONFIDENTIAL

CONFIDENTIAL

TABLE 12

SIDE LOADING FROM THRUST VECTOR CONTROL

Case	Maximum Altitude Thrust Total, pound	Mechanical	Side Injection
1	1,250,000	150,000	87,500
2	250,000	30,000	17,500
3	1,250,000	150,000	87,500
4	2,000,000	240,000	140,000
5	500,000	60,000	35,000
6	250,000	30,000	17,500

TABLE 13

MAXIMUM ACCELERATION LOADING

Case	Maximum Acceleration Loading, g		
	Forward	Alt	Lateral
1	1	2	1
2	1	2	1
3	1	2	1
4	1	2	1
5	1	2	1
6	1	2	1

CONFIDENTIAL

CONFIDENTIAL

TABLE 14
STRUCTURAL FACTORS

	Factor
Safety Factor on Material Ultimate Strength	1.5
Safety Factor on Material Yield Strength	1.1
Safety Factor on Buckling Load	1.5
Limit Load Factor (thrust, acceleration, etc.)	1.0
Proof Pressure	1.2

CONFIDENTIAL

B. TASK 2: FABRICATION AND TEST

1. 2.5K SEGMENT INJECTOR PERFORMANCE INVESTIGATION

(C) The 2.5K segment injector investigation effort was designed to utilize the segmentation potential of the Aerospike thrust chamber for the development of injector patterns for the 250K injector. Candidate injector patterns for this program were made available through in-house and previous contracted efforts. The primary criteria used to determine acceptability of a pattern were selected as:

1. Durability
2. Performance
3. Peak Throat Heat Transfer
4. Fabricability
5. Stability

Previous effort and ADP analysis indicated that durability at 1500 psi would be a major problem. The performance problem would manifest itself primarily in the low chamber pressure regions. Heat transfer in annular combustors has been shown to be primarily a function of chamber contour; however, injector effects on throat heat transfer have been experienced and were expected on the ADP effort. Fabricability of the selected patterns restricted the choice of candidate injectors to those which could be readily produced for the 250K injector.

(C) Stability of the patterns was also considered to be important; however, it is recognized that the 2.5K segments, representing approximately one-half of a 250K compartment will probably not support any acoustic modes, the nearest mode being the first longitudinal at ~ 5500 cps. The possibility of low frequency buzzing could not be discounted, however.

a. Status

(U) During this report period, the final three candidate injector patterns were extensively evaluated to obtain data on durability, performance, heat transfer, tapoff, and stability. A total of 103 runs have been conducted; 101 runs were conducted this quarter.

(C) Based upon the favorable performance results obtained in the early part of the quarter with the triplet injector, this injector pattern was

CONFIDENTIAL

selected as the pattern for the first 250,000 lb/thrust injector. Data indicates that the C* efficiency of this pattern will exceed 97 percent during full throttling and approaches 100 percent above 1000 psia. Operation was stable over the throttling range of 20 percent to 100 percent, and at mixture ratios of 5 to 7.

(C) The triplet, the reverse flow, and the LOX fan patterns have provided excellent performance. Some buzzing has occurred with the LOX fan pattern. The reverse flow patterns (both 60 deg and 80 deg) were eliminated from further consideration when accumulated durability data at 1500 psi indicated the face of the injector was overheated and erosion of the ends of the injector strips were severe.

(C) Heat transfer results have isolated the cause of early observed heat transfer anomalies and indicate throat heat flux of 52 - 54 Btu/in.²-sec at 1500 psi P_c . These values agree closely with earlier theoretical predictions.

(U) Final selection of the pattern for the second 250K injector will be made early in September.

b. Progress during the Report Period

(1) Method of Evaluation

(C) Evaluations were conducted in the basic 6-inch long by 2-1/8-inch wide segment hardware described in the First Quarterly Progress Report. When the safe operating heat flux of the water-cooled segment (40 Btu/in.²-sec) was approached, auxiliary hydrogen film cooling was provided in the combustion chamber convergent section to facilitate duration runs at high pressures. The total hardware available to the ADP program for the 2.5K segment evaluation is indicated in Table 15. The candidate injectors for the 250K injectors were the 60-deg LOX triplet, the LOX fan triplet, and the reversed pattern (figure 45, 46, 47, and 48).

(U) The method of approach to injector evaluation was in the order indicated on Table 15. Low chamber pressure performance and heat transfer tests were conducted, followed by high pressure runs (1500 psia) in uncooled hardware for 250 ms. Surviving candidates were then run through additional performance runs over the range of operation, and heat transfer data are acquired. Bomb tests were made to check stability and more are scheduled. Buzzing evaluation was made upon its spontaneous appearance anywhere in the pressure range of operation.

CONFIDENTIAL

TABLE 15
TABLE OF HARDWARE - 2.5K SEGMENT SOLID-WALL
EVALUATIONS

Injectors*	No. of Units	Type
1-1	1	Stagger fan triplet; 90-deg LOX angle
1-2	1	Reversed flow flat face; 30-deg LOX impingement, 60-deg hydrogen impingement
1-3	1	60-deg triplet (No. 2 H ₂ post); 60-deg LOX impingement
1-4	1	60-deg triplet (No. 5 H ₂ post); 60-deg LOX impingement
2-1	1	60-deg triplet (No. 1 H ₂ post); 60-deg LOX impingement
2-2	1	60-deg triplet (No. 3 H ₂ post); 60-deg LOX impingement
3-1	1	LOX fan pattern; 90-deg relative LOX impingement
3-2	1	Revised LOX fan; 60-deg relative LOX impingement
4-1	1	Reversed flow flat face; 60-deg LOX angle, 80-deg hydrogen angle
4-2	1	60-deg triplet (No. 4 church steeple); 60-deg LOX angle
5-1	1	Showerhead type; 13 strips; 30-deg LOX self-impingement

*The first number reflects injector body number and the second number the strip pattern. Letter designations indicate basic modifications.

CONFIDENTIAL

TABLE 15

TABLE OF HARDWARE - 2.5K SEGMENT SOLID-WALL
EVALUATIONS (Continued)

Water-Cooled Chamber Sections	No. of Units	Type
Injector mounting block	3	347 CRES; mounting block. Chamber to injector
FWD body assembly	2	OFHC copper; first water-cooled section
Spacer	7	OFHC copper; second water-cooled section
Film cooled spacer	2	Same as spacer with H ₂ film passages
Throat assemblies	6	OFHC copper; forms throat, convergence and divergence of 2.5K chamber (water-cooled)
Film-cooled throat assemblies	1	Same as throat assembly with wall H ₂ film passages
15-deg spacer	1	OFHC copper; forms 15-deg convergent section (water-cooled)
15-deg convergence throat assembly	1	OFHC copper; rework of throat assembly to produce 15-deg convergence. Use with above spacer and standard chamber sections (water-cooled)
Forward body - tapoff	1	OFHC copper; uncooled, accommodates two tapoff inserts. Interchangeable with standard forward body.
Tapoff insert	6	OFHC copper - 347 CRES; form actual tapoff hole configuration

CONFIDENTIAL

CONFIDENTIAL

TABLE 15
TABLE OF HARDWARE - 2.5K SEGMENT SOLID-WALL
EVALUATIONS (Concluded)

Uncooled Chamber Hardware	No. of Units	Types
Chamber shell	2 sets	347 CRES; chamber structural uncooled sections; forms complete body shell
Combustor insert	4	Graphite; uncooled combustion zone insert
Uncooled throat	6	OFHC copper; replaceable throat section-injector durability check
Bombing insert	1	OFHC; replaces graphite-mounts bomb for instability testing

(2) Theoretical Basis and Background for Injector Designs

(U) The injector segment work conducted under Contract NAS 8-19 provided the background for the injector designs advanced to the ADP effort. The results of that program showed that the attainment of high performance with LOX and H_2 propellants in short toroidal chambers was solely dependent upon achieving maximum atomization through use of the potential energy of both the LOX and the H_2 . The best performing injector of that study was a LOX fan pattern (similar to one evaluated in the ADP effort and reported in the First Quarterly Progress Report). In this design, the LOX impinged on itself as a doublet on both sides of a series of hydrogen orifices. Primary atomization was accomplished through this process. The atomized LOX fans were then further atomized through passing into the path of the hydrogen gas.

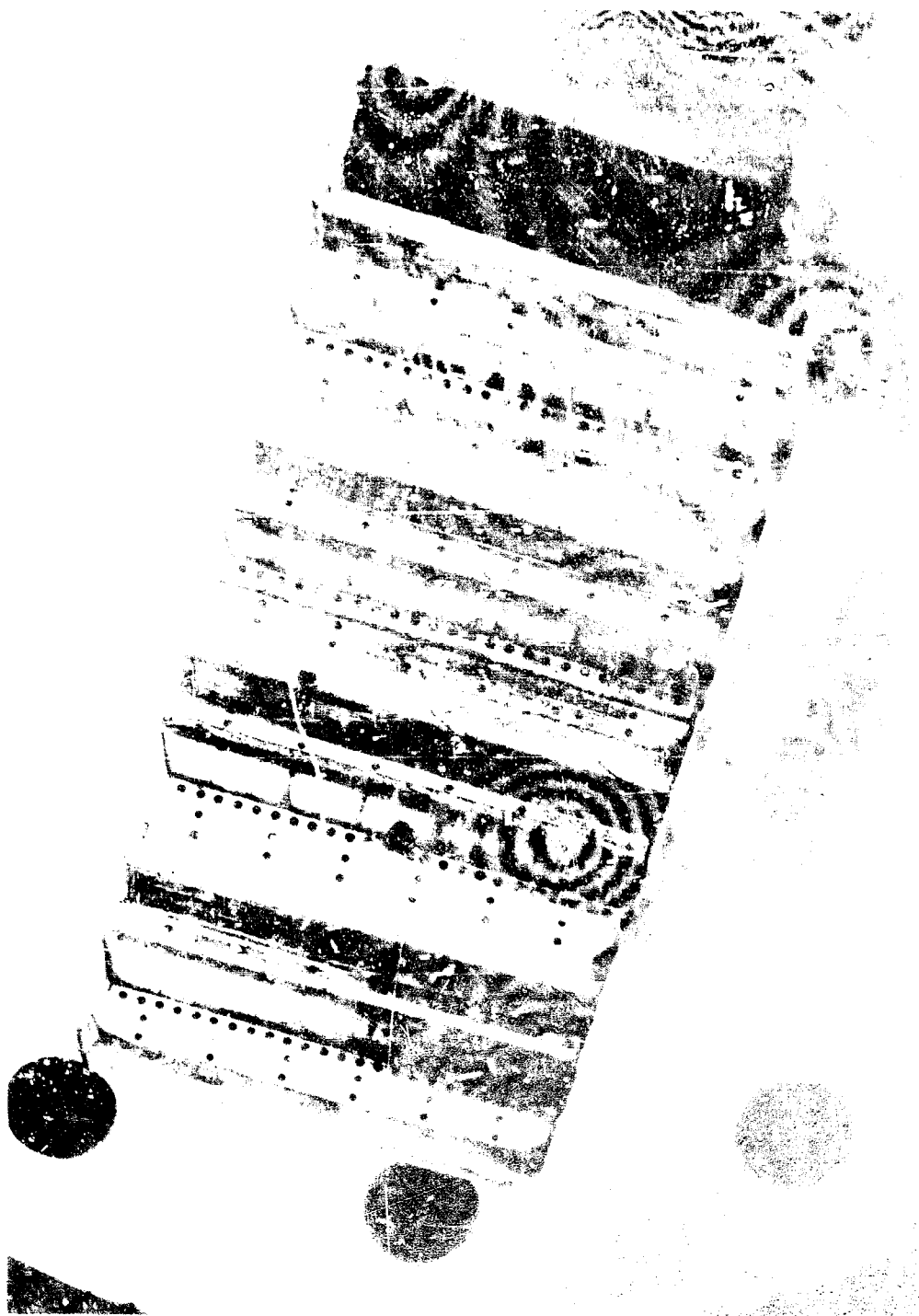
(U) Theoretical analysis shows that the same effect of a self-impinging doublet can be attained through control of the liquid jet length before impingement. For a given jet momentum, the jet has a length at which surface instabilities will appear which lead to atomization. This characteristic was designed into the basic triplet element.

CONFIDENTIAL



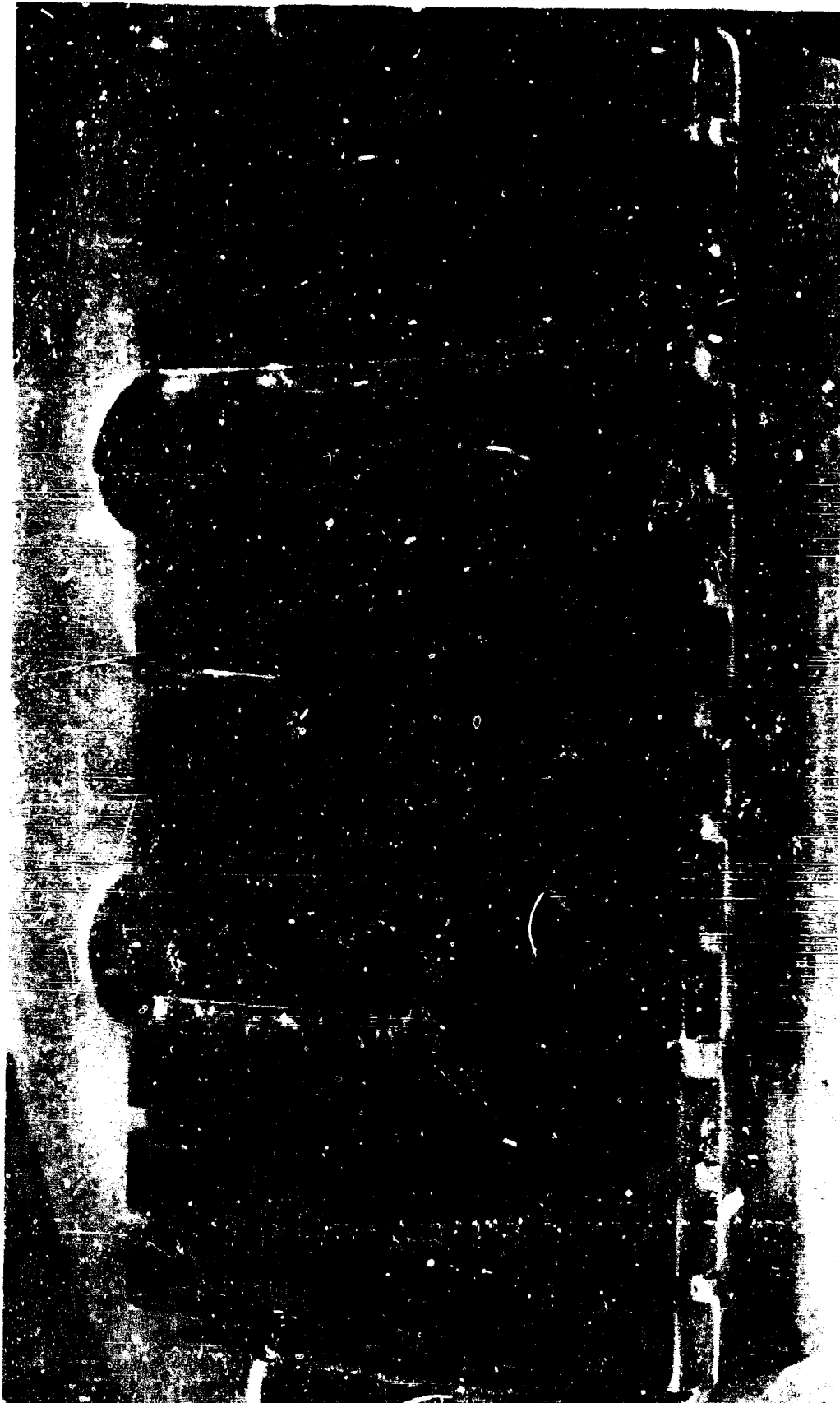
5AA34-8/24/66-SLA

Figure 45. 60 degree 10X Impinging Triplet With Shell Post Extended and
Both Chamfered and Nonchamfered 10X Strips



CONFIDENTIAL

CONFIDENTIAL



LXV3-5/19/66-81D

Figure 47. Reversed Pattern, 60-Degree Fuel on 10X Fan

CONFIDENTIAL

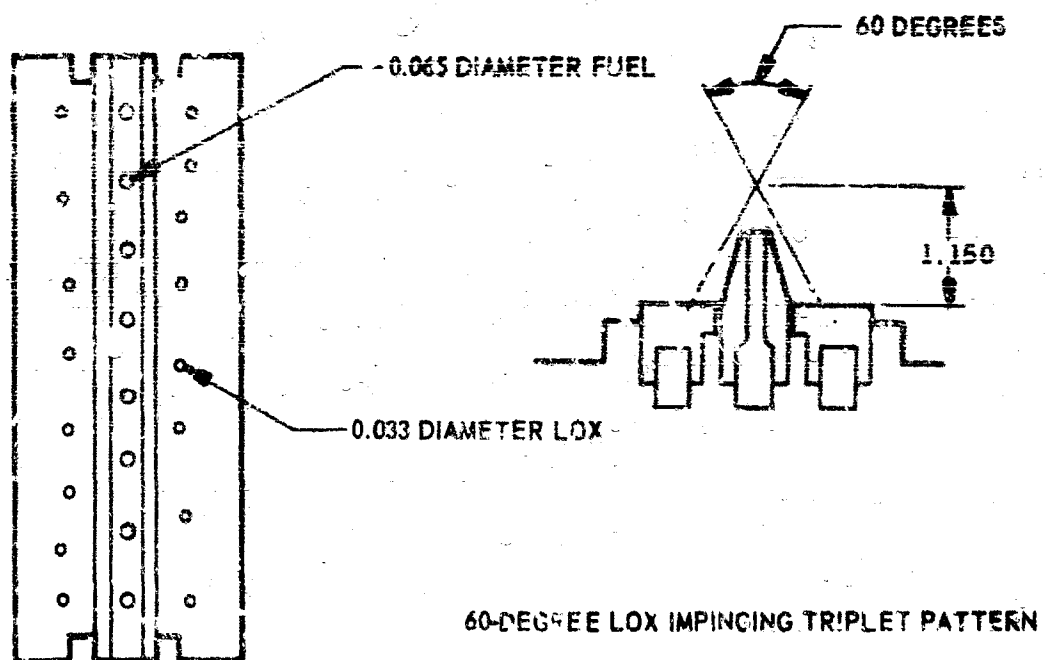
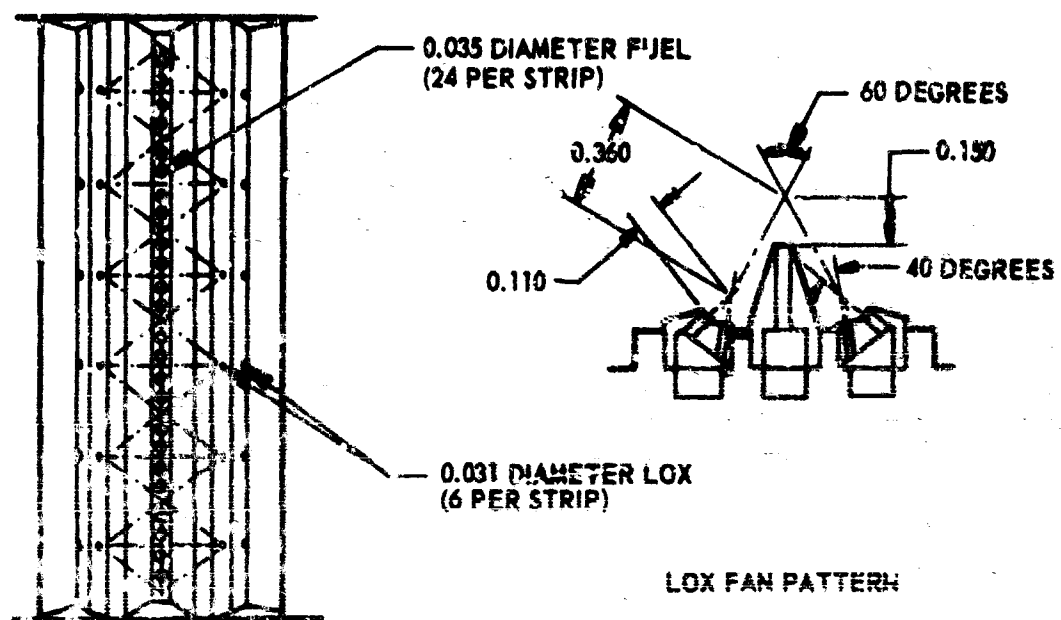


Figure 48. Primary 250K Injector Patterns Candidates

CONFIDENTIAL

(U) Theoretical analysis shows that the primary atomization produces mean drop sizes on the order of 150 microns. Secondary atomization by the hydrogen under proper impingement produces mean drop sizes on the order of 50 microns. However, the attainment of this small drop size requires careful control of the hydrogen jet dynamics. Cold-flow studies revealed that the jet dissipates rapidly and if the point of LOX impingement is too far away, the H₂ escapes around the combustion field. If the jet is too close to the point of impingement, the H₂ spreads the LOX fans (or jets) apart and never mixes. Best atomization occurs when the H₂ jet to LOX impingement distance is ~ 2-4 jet diameters for the ADP operation. This results in an impingement distance of ~ 0.150 inch. This is the distance designed into the ADP injectors. The use of this distance and matching the ΔP to peak performance has resulted in a nominal 1-1/2 to 2 percent improvement over the performance results obtained in the NAS8-19 program.

(U) The NAS8-19 program was conducted at ~650 psi, and no injector heat transfer problem was encountered. It was expected that injector heat transfer at 1500 psi might be a major problem because of the high recirculation potential of the GH₂/LOX designs. Jet dynamic calculations show that as much as 53 percent of the total propellant flow through the injector will be recirculated in the ADP at 1500 psi for the proposed injector designs. Such high recirculation provides an added basis for high performance but it also presents a potential heat face transfer problem. The basic approaches to the heat face transfer problem were considered: (1) use of a raised fuel post to prevent face recirculation and also control impingement distance, and (2) use of a face pattern with predominant hydrogen face cooling. The basic triplet patterns use the raised face, while the reverse-flow pattern provides for maximum hydrogen face cooling.

(U) Thermochemical calculations on the LOX drops show that below ~1100 psi the drops actually exist as liquid droplets throughout their consumption. Above 1100 psi, the drops rapidly rise to and exceed their critical temperature. Because of the high contraction ratio of the toroidal engine combustion, induced turbulence along with GH₂ jet turbulence is high and persists. This turbulence above 1100 psi results in rapid eddy diffusive mixing of the LOX vapor, and, therefore, once fine atomization is achieved, near theoretical performance can be expected.

(3) Candidate Pattern Evaluation

(C) 60-deg LOX Impinging Triplet Pattern. The basic triplet pattern consists of a showerhead fuel stream (from a raised fuel strip) impinging on a 60-deg LOX doublet (figure 45). The purpose of the raised fuel post is to place the fuel stream exit point close to the point of LOX

CONFIDENTIAL

impingement to obtain good primary propellant atomisation. The post also acts to prevent recirculation from causing high face heat transfer.

The injector strips are oriented perpendicular to the chamber circumference with eight propellant elements per strip. Modifications to the basic triplet pattern consisted of:

1. Addition of fuel bias at fuel strip ends (incorporated into 250K injector pattern)
2. Extending raised fuel strips to chamber wall-square ends (incorporated into 250K injector pattern)
3. Beveling LOX strip ends (found to be unnecessary with square end fuel strips)
4. Introduction of fuel bias along sides of injector (found to be unnecessary)
5. Enlarging fuel orifices to lower injection pressure drop (found to be unnecessary)

(C) LOX Fan Pattern with Fuel Post. The LOX fan pattern with a raised fuel strip is also considered as a candidate for the 250K injector pattern. Satisfactory performance and durability were demonstrated with this pattern; however, the chamber throat heat flux was found to be slightly higher with the LOX fan pattern than with the triplet. The hot gas tapoff temperature with the selected 250K tapoff port was considerably lower than the tapoff temperature using the triplet injector pattern.

(C) An element of the LOX fan pattern consists of two pairs of LOX doublets forming doublet fans impinging at 60-deg above a raised fuel strip (figure 46). Four showerhead fuel streams were directed at the line of impingement of the doublet fans. Each set of strips contained six propellant elements.

(C) Modification of the basic pattern consisted of enlarging the fuel orifices and providing fuel bias of the main orifices at the fuel strip ends.

(U) The LOX fan pattern with the raised fuel strip was an improved version of the LOX fan concept tested during the first quarter which featured 90-deg LOX impinging fans and no raised fuel strip. Severe burning of the LOX strips was sustained in these tests.

CONFIDENTIAL

(C) Reversed Pattern. The reversed pattern (figure 47) was so named to indicate that the point of introduction of propellants was reversed from that of the other patterns tested (fuel on the outside and LOX in the center of an element of the reversed pattern). The reversed pattern element consisted of a LOX fan (formed by a LOX doublet) impinging on an 80-deg impinging fuel doublet. The pattern was placed on a flat face injector.

(C) Modification of the basic pattern consisted of enlarging the fuel orifices to lower the injection pressure drop.

(U) Erosion of the strip ends was sustained during high chamber pressure tests, and the face appeared to be overheating to the point of being marginal.

c. Problem Areas and Solutions

(C) Three problems were encountered during the injector evaluations; (1) slight edge erosion of the primary candidate pattern occurred on early tests. This was eliminated by extending the posts to the edge; (2) heat transfer anomalies were observed run to run, clouding the influence of injectors and of operating parameters; these heat transfer anomalies were determined to be caused by sporadic gross surface roughness caused by deposits of a melted CTF ignition tube tip; retraction of this tube eliminated this problem; (3) tapoff gas temperatures with the selected post configuration were excessively high. Solution by injector-bias is being studied for future evaluation.

d. Testing

(1) Test Results

(U) Thrust Chamber Performance. Thrust chamber testing was conducted to evaluate: (1) performance, (2) injector durability, (3) heat transfer, and (4) hot gas tapoff. Thrust chamber performance was determined only for those tests that achieved steady-state operation.

(U) The performance parameter that measures combustion efficiency is the characteristic velocity. This performance parameter is calculated from chamber pressure and from thrust, thereby obtaining a check on the internal consistency of the data. Characteristic velocity is calculated from chamber pressure as follows:

$$C^* = \frac{P_c A_t g}{\dot{w}} \eta_1 \quad (1)$$

CONFIDENTIAL

where

P_c = injector end chamber pressure

A_t = geometric area of nozzle throat

$g = 32.174 \text{ lbm} - \text{ft/lbf-sec}^2$

\dot{w} = total propellant flowrate

η_1 = influence coefficient

(C) The influence coefficient η_1 accounts for stagnation pressure loss, nozzle discharge coefficient, heat loss to the coolant water, and thermal shrinkage of the nozzle throat. In the range of ADP thrust chamber operating conditions, η_1 has an average value of 0.9831.

(U) Calculation of characteristic velocity from thrust is accomplished as follows:

$$C^* = \frac{g F}{\dot{w} C_F} \eta_2 \quad (2)$$

where

F = thrust

C_F = thrust coefficient

η_2 = influence coefficient

(C) In Eq. 2, the influence coefficient η_2 accounts for thrust degradation due to heat loss to the water coolant, frictional drag, and nozzle divergence. The average value for η_2 over the ADP conditions was taken as 1.0344. A complete discussion of the influence coefficients and the calculation technique for evaluating these factors is presented in Appendix A.

(C) Thrust chamber performance data from those tests judged to be suitable for obtaining reliable performance data are summarized in Table 16. Excellent agreement between characteristic velocity from thrust and characteristic velocity from chamber pressure is indicated. From Table 16, it may be seen that the triplet injector, U/N 2-1B and U/N 1-3B (the selected No. 1, 250K configuration), delivers an average characteristic velocity efficiency of 98.3 percent over the chamber pressure range of 325 to 973 psia.

CONFIDENTIAL

TABLE 16

2.5K SEGMENT INJECTOR TEST SUMMARY

Test Run No.	Test Date, 1966	Injector Number	Duration, seconds	Throat Area, sq in.	Chamber Pressure, psia	Mixture Ratio, o/g	V_c , lb/sec	ΔP (Fuel)	ΔP (Oxidizer)	c_p	η_{sp}	η_{sp}	η_{sp}	Throat Peak Heat Flux, Btu/in. ² -sec	Influence Coefficient For c_p (%)	Influence Coefficient For Specific Impulse (%)
016 to 026*																
Uncooled Hardware - Injector Durability Tests																
027*	5-21	2-1A	3.7	0.990	937	5.81	2.658	253	53	7635	0.989	7788	1.008	30.1	0.983	1.056
028*	5-21	2-1A	3.9	0.990	1015	6.50	4.038	348	133	7337	0.998	7506	0.994	31.5	0.982	1.053
029*	5-21	2-1A	3.7	0.990	1020	5.04	1.225	154	9	7750	0.989	7884	1.004	14.4	0.985	1.059
030*																
Nozzle Throat Eroded																
031 and 032																
Uncooled Hardware																
033	6-6	2-1B	4.3	0.980	896	5.91	2.545		39	7695	1.000	7716	1.003	25.8	0.985	1.057
034	6-6	2-1B	4.3	0.980	1377	6.43	4.947		118	7662	1.012	7473	0.988	42.7	0.985	1.055
035	6-6	2-1B	4.0	0.980	1330	5.69	1.340		8	7531	0.979	7332	1.956	13.7	0.984	1.058
036 to 045																
Nozzle Throat Eroded																
046	6-16	2-1D	4.3	0.980	1446	5.79	1.394	66	14	7373	0.965	7277	0.959	13.2	0.984	1.058
047	6-16	2-1D	4.4	0.980	955	6.07	2.753	123	55	7666	1.002	7560	0.988	33.1	0.985	1.054
048	6-16	2-1D	4.3	0.980	933	5.94	2.749	124	54	7657	0.996	7556	0.983	33.2	0.985	1.054
049	6-16	2-1D	4.3	0.980	920	5.80	2.653	128	54	7671	0.995	7568	0.979	34.8	0.985	1.057
050	6-21	2-1E	4.2	0.965	1025	5.38	1.304	63	15	7635	0.980	7509	0.984	11.9	0.984	1.059
051	6-21	2-1E	4.3	0.965	909	5.62	2.599	11.1	35	7879	0.988	7654	0.985	33.2	0.985	1.057
052	6-21	2-1E	4.3	0.965	911	5.63	2.531	123	33	7644	0.984	7579	0.975	33.7	0.985	1.057
053	6-22	2-1E	4.2	0.965	118	5.31	1.254	61	12	7736	0.994	7693	0.986	12.3	0.982	1.059
054	6-22	2-1E	4.3	0.965	672	5.79	1.970	84	30	7665	0.994	7567	0.988	31.1	0.984	1.057
055	6-22	2-1E	4.3	0.965	898	5.90	2.666	116	32	7525	0.977	7392	0.960	27.4	0.985	1.057
056 to 071																
Injector Strip-To-Land Separation and No Throat Zero Shifts																
072	7-5	1-3A	4.0	0.990	745	6.84	2.270	128	53	7870	0.979	7505	0.971	33.8	0.985	1.056
073	7-5	1-3A	4.3	0.990	1062	5.70	3.096	254	95	7585	0.977	7452	0.968	45.0	0.985	1.056
074	7-5	1-3A	4.3	0.990	1037	5.15	2.942	245	88	7598	1.005	7883	0.993	41.9	0.984	1.057
075																
Nozzle Throat Eroded																
076	7-8	1-3B	4.4	0.990	870	5.64	2.382	174	64	7567	0.975	7543	0.977	34.1	0.985	1.057
077	7-3	1-3B	4.4	0.990	886	5.88	2.622	172	65	7477	0.969	7435	0.964	28.9	0.985	1.057
078	7-8	1-3B	4.4	0.990	846	5.59	2.488	174	58	7527	0.967	7341	0.969	28.6	0.984	1.056
079	7-12	1-3B	14.3	0.940	1079	6.11	3.094	194	91	7500	0.980	7338	0.988	36.8	0.987	1.054
080	7-12	1-3B	14.3	0.940	1061	6.21	3.055	185	83	7484	0.982	7337	0.989	32.9	0.985	1.054

*Data pertinent to AEP program

CONFIDENTIAL

TABLE 16
(Continued)

Run No.	Test Date, 1966	Injector Number	Duration, seconds	Throat Area, sq in.	Thrust, pounds	Chamber Pressure, psia	Mixture Ratio, o/f	\dot{V}_t , lb/sec	ΔP (Fuel), lb/sec	ΔP (oxidizer), lb/sec	$\eta_{c,p}$, %	$\eta_{c,p}$, %	$\eta_{c,p}$, %	Throat Peak Heat Flux, Btu/in. ² -sec	Influence Coefficient For $\eta_{c,p}$	Influence Coefficient For Specific Impulse
001		3-0A														
002	7-15	3-0A	12.7	0.94	1111	805	6.72	3.172	260.2	56.7	7570	1.004	7540	1.000	0.905	1.057
003	7-18	1-3B		0.94	369	285	5.76	1.419	106.0					13.1	0.904	1.059
004	7-18	1-3B		0.94		304	6.16	1.637	93.5	16.9				13.2	0.904	1.059
005	7-18	1-3B	1.4	0.94	572	440	5.22	1.860	159.5	27.7				22.6	0.904	1.059
006	7-18	1-3B	1.2	0.94	822	615	5.73	2.554	169.1	39.6				30.5	0.905	1.057
007	7-18	1-3B		0.94	410	317	5.87	1.373	92.6	32.4				13.5	0.904	1.058
008	7-21	1-3B	1.5	0.94	830	609	5.33	2.489	193.0	49.6				30.5	0.904	1.057
009	7-21	1-3B		0.94	547	412	5.43	1.683	126.5	37.4				19.6	0.904	1.058
090	7-22	1-3B		0.94	505	387	5.20	1.574	127.9	28.4				19.6	0.904	1.058
091	7-22	1-3B	1.7	0.94	679	506	5.65	2.104	155.5	45.0				29.2	0.904	1.058
092	7-22	1-3B	1.8	0.94	964	685	5.72	2.777	194.5	86.5				28.8	0.905	1.058
093	7-27	1-3B	1.5	0.94	929	678	4.96	2.744	241.7	85.7				32.7	0.904	1.057
094	7-27	1-3B		0.95	937	688	6.32	2.916	171.1	104.5				35.5	0.905	1.057
095	7-27	1-3B	1.5	0.95	924	668	5.74	2.818	200.5	86.6				35.8	0.905	1.055
096	7-27	1-3B	1.8	0.88	866	705	5.10	2.593	193.6	77.5				14.2	0.904	1.056
097	7-29	1-3B	1.8	0.88	896	798	4.52	2.265	229.1	81.4				14.2	0.904	1.056
098	7-29	1-3B	1.9	0.88	892	779	6.28	2.705	157.7	104.5				14.2	0.905	1.056
100	8-2	1-3B	3.4	0.95	982	720	5.22	2.536	186.6	94.7				7.6	0.904	1.056
101	8-2	1-3B	3.5	0.95	1385	1004	4.88	3.389	276.6	101.1				14.2	0.904	1.056
102	8-2	1-3B	3.5	0.95	1617	1169	5.16	4.082	315.4	149.8				16.4	0.905	1.055
103	8-2	1-3B	3.5	0.95												
104	8-5	1-3B	3.5	0.95	2130	1494	6.85	5.346	287.8	295.3				20.8	0.905	1.048
105	8-5	1-3B	3.5	0.95	2153	1505	7.65	5.699	441.4	214.4				23.2	0.908	1.054
106	8-5	3-0A	3.2	0.95	2169	1507	8.05	6.032	231.1	165.1				20.4	0.908	1.054
107	8-9	4-1B	3.7	0.95	1007	794	6.97	3.025	179.4	45.7				30.6	0.905	1.055
108	8-9	4-1B	3.7	0.95	515	379	6.87	1.983	129.5	38.5				20.7	0.905	1.058
109*	8-9	5-1A	4.4	0.95	2168	1493	6.87	5.706	393.9	404.8				20.7	0.904	1.055
110*	8-9	5-1A	0.8	0.95	385	294	4.54	1.104	174.2	5.6	7741	0.967	7775	0.971	0.905	1.058
111	8-12	3-0A	4.9	0.97	405	304	5.72	1.269	134.7	8.4	7395	0.961	7357	0.961	0.905	1.055
112	8-12	3-0A	4.8	0.97	1378	969	6.03	3.650	337.3	94.5				19.4	0.905	1.055
113	8-12	3-0A	4.6	0.97	1378	969	6.03	3.650	337.3	94.5					0.905	1.055
114	8-12	3-0A	3.4	0.97	1339	946	6.16	3.651	331.4	93.9					0.905	1.055
115	8-12	3-0A	3.4	0.97	2308	1562	7.38	6.335	400.2	237.0					0.904	1.055

*Data pertinent to AMP program

CONFIDENTIAL

CONFIDENTIAL

TABLE 16
(Concluded)

Test No.	Test Date	Injector Number	Duration, seconds	Thrust Area, sq in.	Thrust, pounds	Chamber Pressure, psia	Mixture Ratio, o/g	V_e lb/sec	ΔP (Fuel)	ΔP (oxidizer)	$c^*_{f/c}$	$\eta_{f/c}$	c^*_f	$\eta_{f/c}$	Exhaust Exit Flow, lbm/in. 2 sec	Influence Coefficient For c^* (%)	Influence Coefficient For η (%)
116	8-17	2-2A	2.1	0.95	547	411	6.15	1.640	269.5	21.5	7956	0.997	7880	1.000	22.1	0.983	1.078
117	8-19	3-2A	3.9	0.985	866	659	5.14	2.390	275.2	25.8	7956	0.997	7880	1.000	31.6	0.984	1.077
118	8-19	3-2A	3.9	0.985	875	650	6.95	2.615	331.2	30.5	7853	0.982	7247	0.980	34.7	0.983	1.076
119	8-19	3-2A	4.5	0.985	105	518	4.73	1.199	130.6	4.9	7853	0.981	7897	0.984	16.3	0.981	
120	8-19	3-2A	4.5	0.985	395	310	5.92	1.216	108.0	5.0	7875	0.980	7491	0.982	17.5	0.984	1.078
121	8-23	3-2B	3.5	0.925	867	649	5.57	2.466	150.0	40.9	7700	0.991	7776	0.991	30.8	0.985	1.057
122	8-25	3-2B		0.925	1415	1042	5.90	3.658	196.4	82.1	7677	0.990	7605	0.991	38.3	0.983	1.073
123	8-26	4-2A	3.9	0.925	817	615	5.65	2.356	140.7	50.9	7677	0.990	7605	0.991	28.3	0.983	1.077
124	8-26	4-2A	3.8	0.925	791	596	5.55	2.842	194.1	51.1	7757	0.990	7764	0.991	27.0	0.984	1.077
125	8-26	4-2A	3.0	0.985	1356	1035	5.36	3.285	201.1	105.3					35.8	0.983	1.056
126	8-26	4-2A	2.4	0.985	1786	1322	5.24	4.470	304.0	199.2					36.8	0.982	1.074
127	8-26	4-2A	2.9	0.925	2029	1492	6.34	5.239	265.9	281.0					40.8	0.982	1.054

Data reduction in process

CONFIDENTIAL

CONFIDENTIAL

TABLE 16
(Concluded)

Run No.	Test Date, 1966	Injector Number	Duration, seconds	Thrust Area, sq in.	Thrust, pounds	Chamber Pressure, psia	Mixture Ratio, o/f	\dot{V}_t , lb/sec	ΔP (Fuel)	ΔP (Oxidiser)	c^*_c	$\eta_{c^*_c}$	c^*_g	$\eta_{c^*_g}$	Thrust Peak, lb	Influence Coefficient For c^*_g (%)	Influence Coefficient For Specific Impulse (%)
116	8-17	2-2A	2.1	0.95	547	411	6.15	1.640	269.3	21.3	7856	0.997	7680	1.000	22.1	0.985	1.038
117	8-19	3-2A	3.9	0.925	860	639	5.14	2.590	275.2	25.8	7856	0.997	7680	1.000	31.6	0.984	1.037
118	8-19	3-2A	3.9	0.925	873	690	6.93	2.615	191.2	30.5	7262	0.982	7247	0.980	34.7	0.983	1.036
119	8-19	3-2A	4.5	0.925	505	318	4.73	1.199	150.6	4.9	7853	0.981	7657	0.984	16.4	0.981	
120	8-19	3-2A	4.5	0.925	395	310	5.92	1.216	108.0	5.0	7475	0.980	7491	0.982	17.5	0.984	1.038
121	8-23	3-2B	3.5	0.925	867	649	5.57	2.466	150.0	40.9	7700	0.991	7770	0.991	30.8	0.983	1.037
122	8-23	3-2B	3.9	0.925	1415	1042	5.90	3.638	198.4	82.1	7677	0.990	7685	0.991	38.3	0.983	1.035
123	8-24	4-2A	3.8	0.925	791	615	5.65	2.336	149.7	50.9	7677	0.990	7685	0.991	28.3	0.983	1.037
124	8-24	4-2A	3.8	0.925	791	596	5.35	2.442	154.1	51.1	7757	0.990	7764	0.991	27.0	0.984	1.037
125	8-24	4-2A	3.0	0.925	1354	1005	5.36	3.285	201.2	193.3	7757	0.990	7764	0.991	35.8	0.983	1.036
126	8-24	4-2A	2.4	0.925	1786	1322	5.24	4.470	304.0	199.2	7757	0.990	7764	0.991	36.0	0.982	1.034
127	8-24	4-2A	2.9	0.925	2029	1492	6.34	5.239	263.9	281.0	7757	0.990	7764	0.991	40.8	0.982	1.034
128	8-26	4-2A															
129	8-26	4-2A															
130	8-26	3-2B															
131	8-31	4-2A															
132	8-31	4-2A															
133	8-31	4-2A															
134	8-31	4-2A															
135	8-31	4-2A															
136	8-31	4-2A															
137	8-31	4-2A															

Data reduction in process

CONFIDENTIAL

CONFIDENTIAL

(U) Performance results without regard to mixture ratio are plotted as a function of P_c for both the triplet and the drilled out LOX fan injector in figure 49. It is observed that both injectors are comparable in performance, with the triplet, perhaps, holding a slight statistical edge.

(U) Injector Performance Results at Pressures Above 1000 psi. A number of data runs were conducted on which film cooling was employed. These runs are in the process of being reduced to obtain the injector performance results. The influence of film cooling the thrust chamber must be factored out to properly evaluate the injector performance. Several techniques are being considered:

1. Include film cooling in overall performance calculation (base theoretical values on overall flows), vary the amount of film coolant, and extrapolate to zero film cooling.
2. Ignore film cooling in performance calculation (ie., base theoretical values strictly on injector flows), vary the amount of film coolant, and extrapolate to zero film cooling.
3. Treat injector contribution and film cooling contribution as additive effects to total combustion performance and obtain injector performance.
4. Perform energy balance on film coolant and back calculate injector performance.

(C) Preliminary results show that the range of injector calculated performance by these four techniques above 1000 psi ranges from 98 to 102 percent for both the triplet and LOX fan injectors; however, further examination of the four techniques is required to determine the most valid method.

(C) Hot-Gas Tapoff. The feasibility of hot-gas tapoff was investigated in the 2.5K chamber segment. The objectives of the tapoff tests were to determine the dependence of chamber pressure, mixture ratio, and tapoff geometry on the tapoff temperature with several tapoff variations. The configurations evaluated to date are indicated in figure 50. The first design was a single-hole configuration and the second, a two-hole unit, both units designed for a tapoff exit velocity of a Mach number equal to 0.2 for a nominally 1500-deg F fuel-rich gas. The tapoff temperature as a function of chamber pressure is shown in figure 51 for both of these configurations. The first test results indicate an increase in temperature with increasing chamber pressure and increasing mixture ratio (5 to 7). The third configuration under current evaluation is shown in figure 52. This configuration straddles the

CONFIDENTIAL

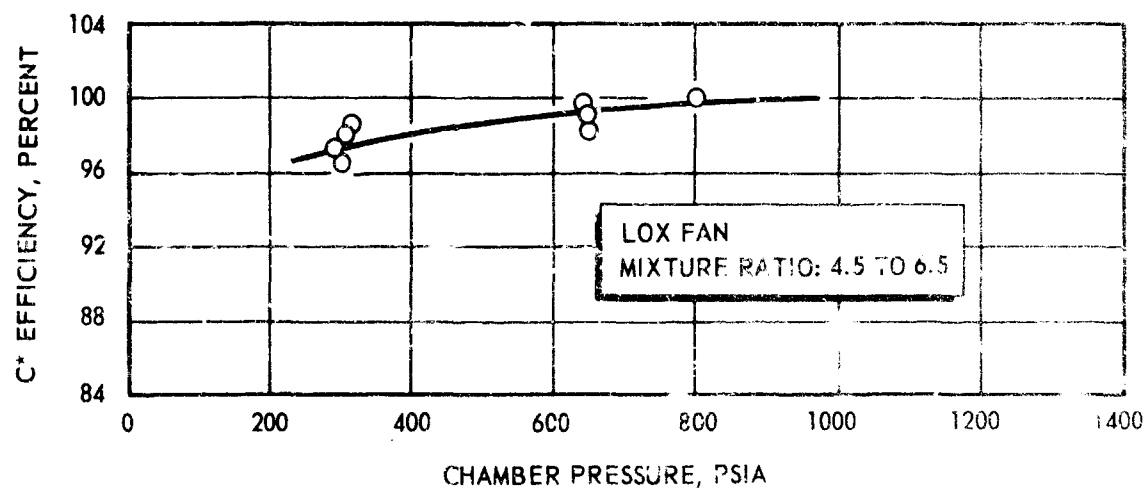
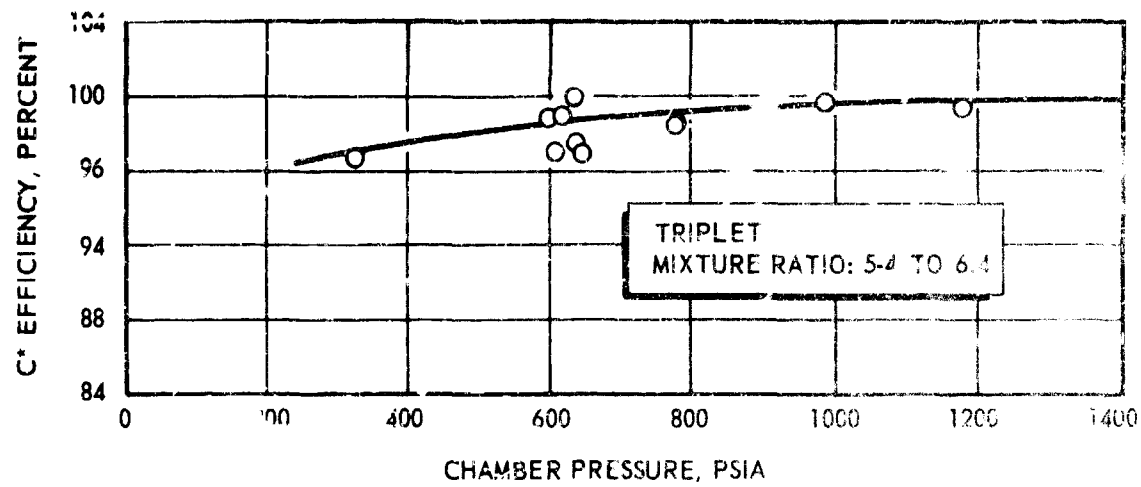
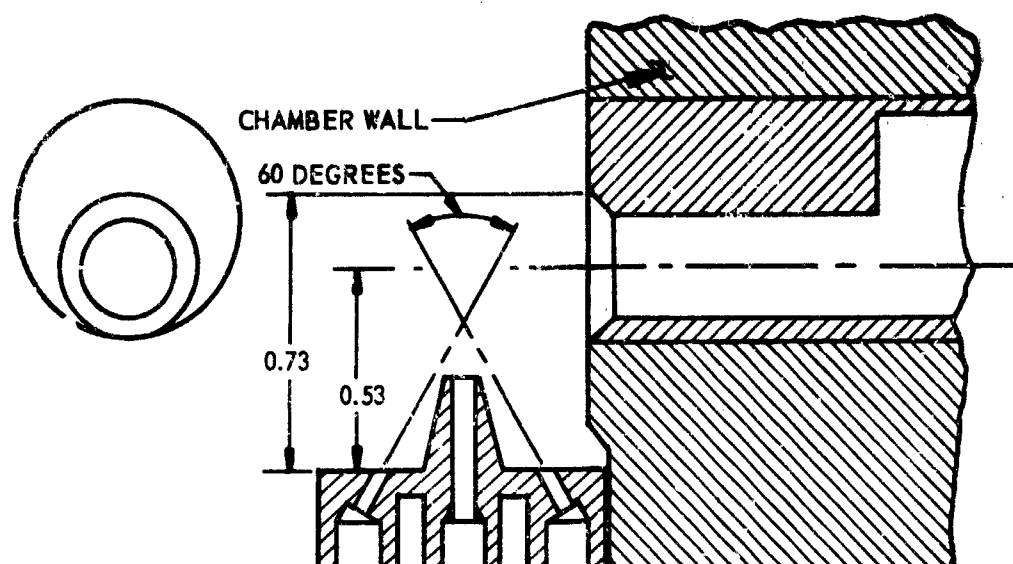


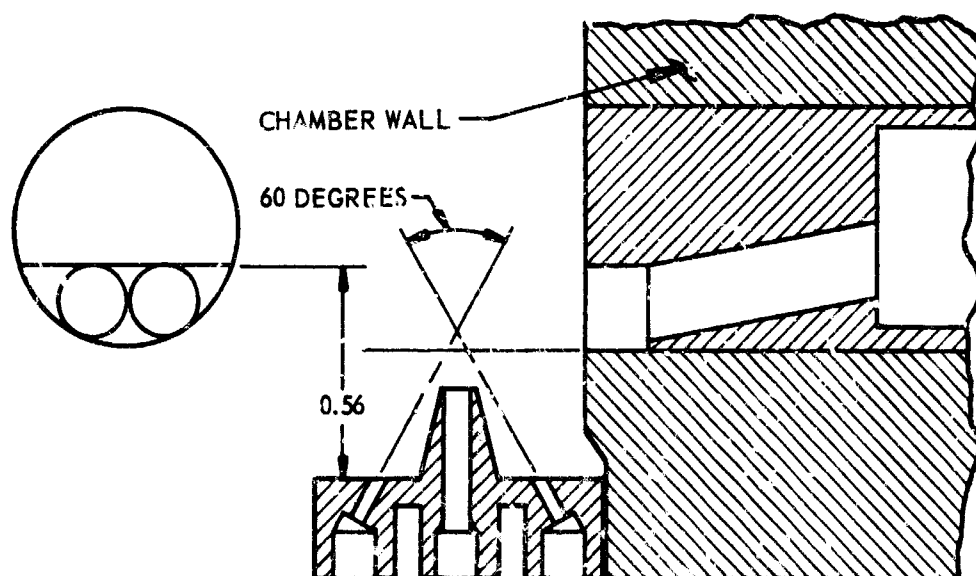
Figure 49. Performance Comparison. 250K Candidate Injector

CONFIDENTIAL

CONFIDENTIAL



ONE-HOLE HOT-GAS TAPOFF CONFIGURATION



TWO-HOLE HOT-GAS TAPOFF CONFIGURATION

Figure 50. 2.5K Hot-Gas Tapoff Configuration

CONFIDENTIAL

CONFIDENTIAL

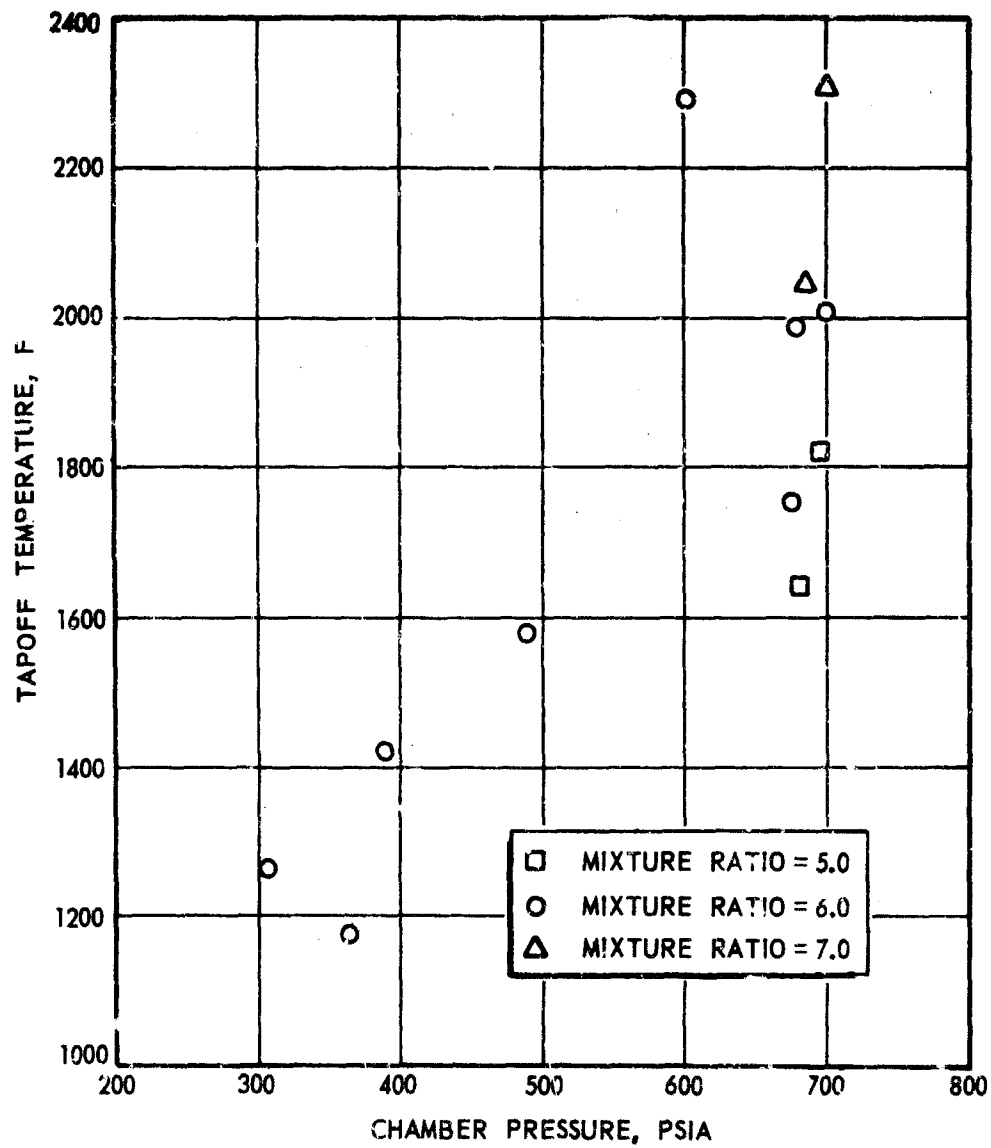


Figure 51. Measured Hot-Gas Tapoff Characteristics (2.5K Chamber)

CONFIDENTIAL

CONFIDENTIAL

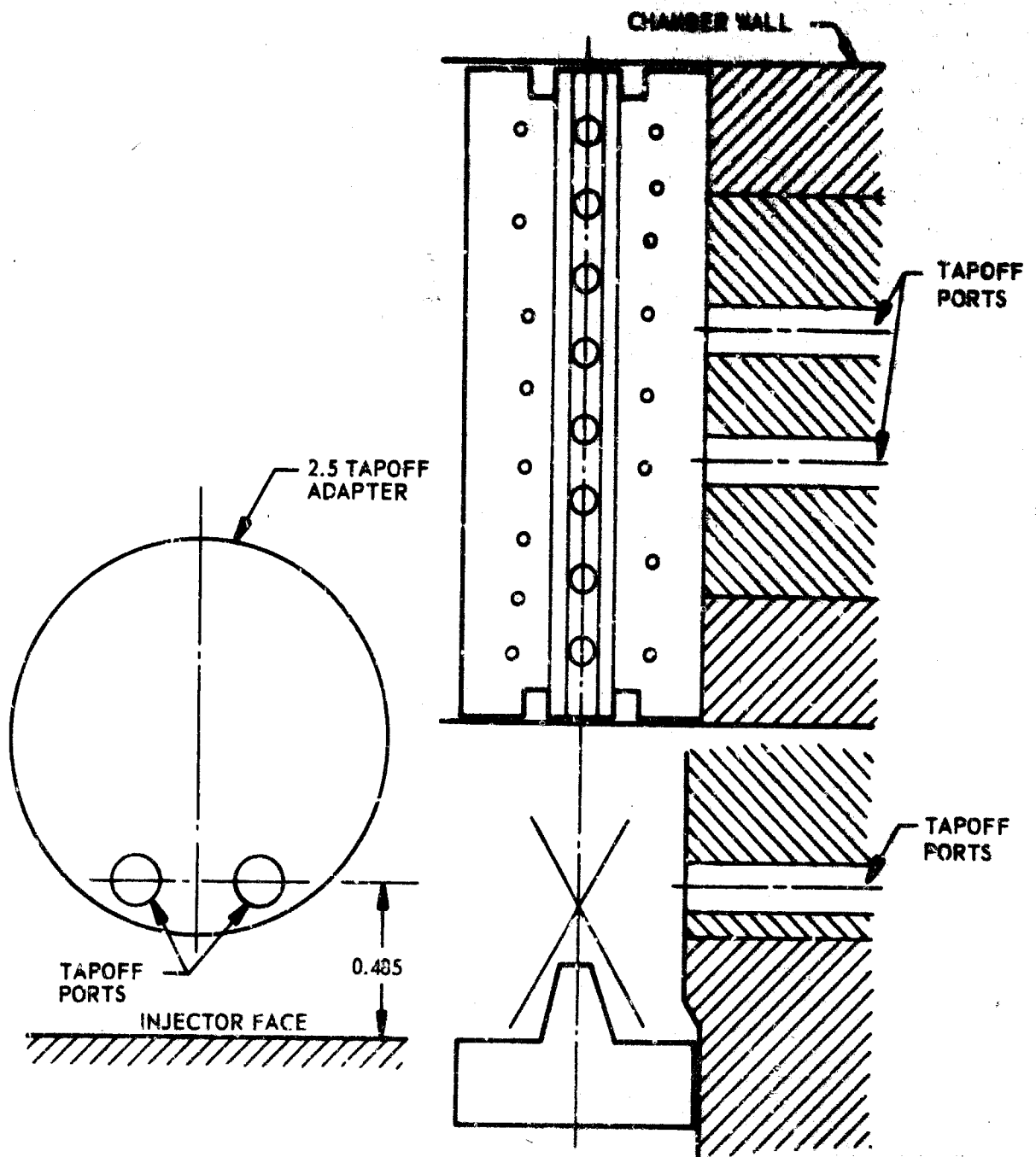


Figure 52. Simulated 250K Hot-Gas Tapoff Pores in 250K Thrust Chamber

CONFIDENTIAL

CONFIDENTIAL

injector pattern as shown and is designed to provide for a more positive flow of fuel-rich gas than were the first two configurations. Should this configuration indicate strong P_c and MR dependence, also, local mixture ratio control in the vicinity of the tapoff holes will be built into the injector strip by providing GN_2 jets sized and directed into the tapoff zone. Five initial gas tapoff tests were judged to be suitable for determination of meaningful thrust chamber performance. These were tests number 089, 091, 092, 093, and 095, all of which utilized injector U/N 1-3B. Gas tapoff configuration and instrument locations for these tests are shown in figure 53 and 54.

(U) The gas tapoff thrust chamber data reduction was accomplished in three steps. First, the oxidizer and fuel flowrate through the injector was determined. Second, the gas tapoff flowrate was calculated, and finally the net thrust chamber flowrate was calculated by taking the difference between the injector flowrate and the gas tapoff flowrate gas. Tapoff was evaluated as described in Appendix C.

(U) Gas tapoff flowrates were deducted from thrust chamber injector flowrates and adjusted thrust chamber performance was then determined. These data are presented in Table 17, and it may be seen that the results for tests 089, 091, and 092 are in excellent agreement with prior data for this injector. The adjusted results for tests 093 and 095 are subject to some question due to an indeterminate GN_2 purge. Additional tapoff data are in process of data reduction, and additional tests at higher chamber pressure are planned.

(C) Stability. Related experience with propellant injection pressures less than 10 percent of chamber pressure have indicated that careful attention must be given to the injection, combustion, and feed system characteristics to avert the occurrence of low-frequency instability. In throttling to 20 percent of rated thrust, the selected triplet injector pattern will experience an oxidizer side ΔP of 15 psi (5 percent) at a chamber pressure of 300 psi (figure 55). Furthermore, a mathematical analog of the test stand and 250K thrust chamber (discussed in the 250K nozzle test preparation section) indicated possibility of low-frequency modes of oscillation with certain assumed feed system and injection characteristics. Accordingly, stability as well as performance was evaluated with the 2.5K segments over the throttling and mixture ratio range.

(C) The triplet injection pattern (U/N 1-3B), which will be utilized for the No. 1 250K injector assembly, was throttled from rated chamber pressure of 1500 psia to 300 psia without evidence of combustion instability. This evaluation consisted of 13 tests in the 300- to 600-psia chamber pressure range where the nominal oxidizer injection pressure drop falls below 10 percent of chamber pressure.

CONFIDENTIAL

CONFIDENTIAL

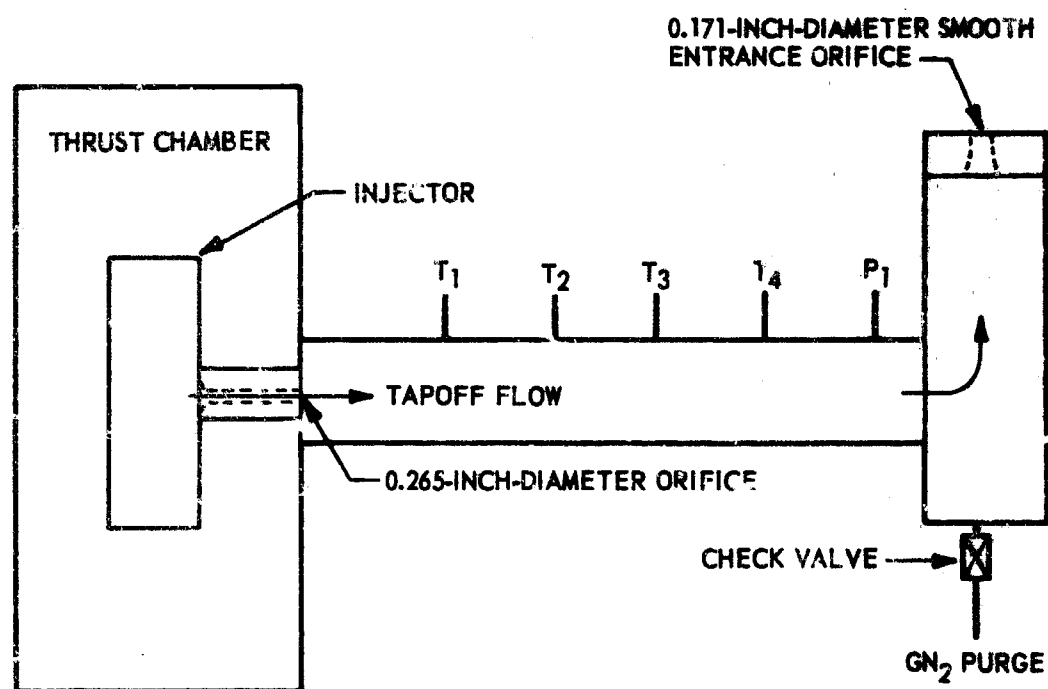


Figure 53. Gas Tapoff Configuration for Tests 088 Through 092

CONFIDENTIAL

~~CONFIDENTIAL~~

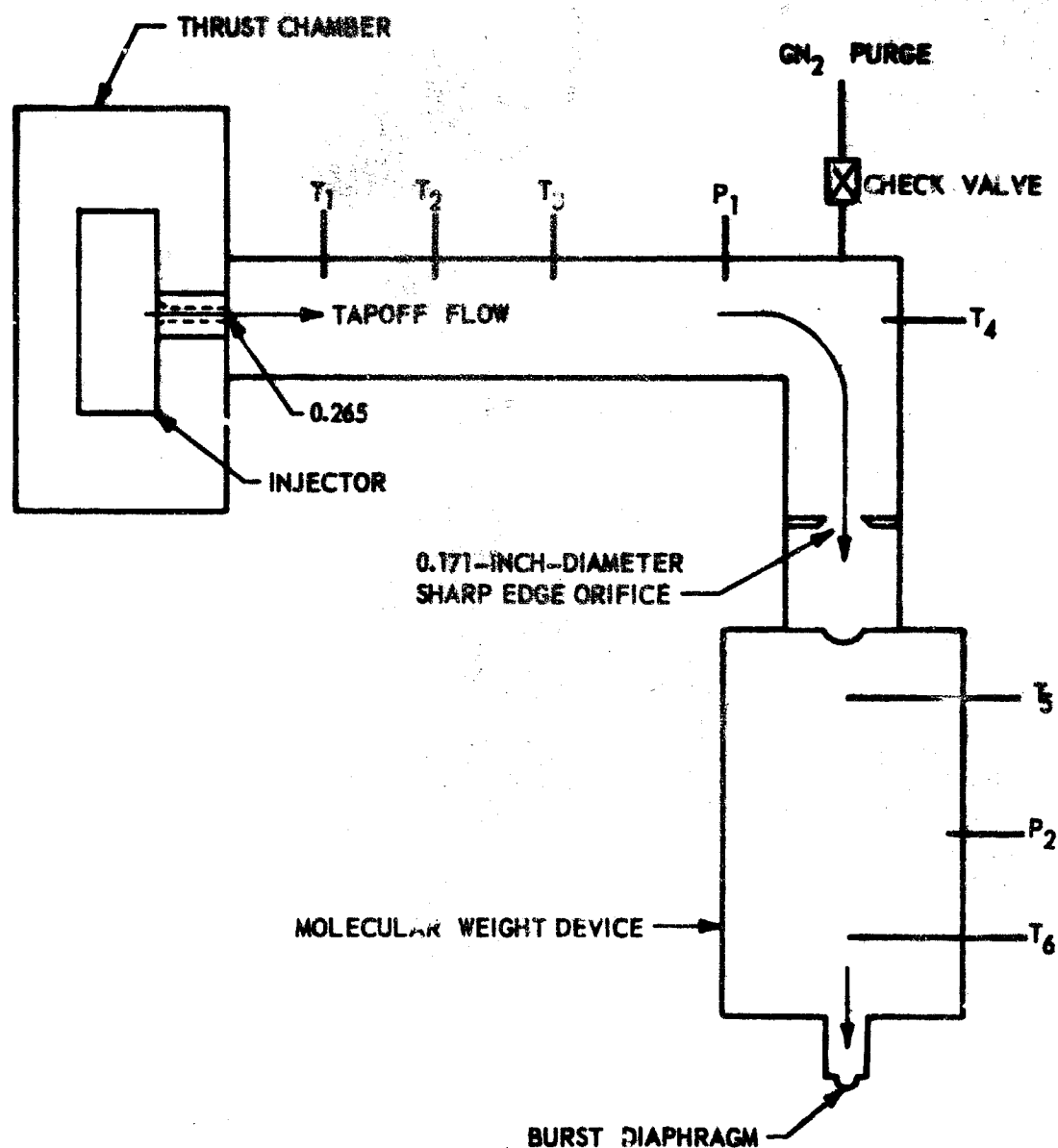


Figure 54. Gas Tapoff Configuration for Tests 093 Through 099

~~CONFIDENTIAL~~

CONFIDENTIAL

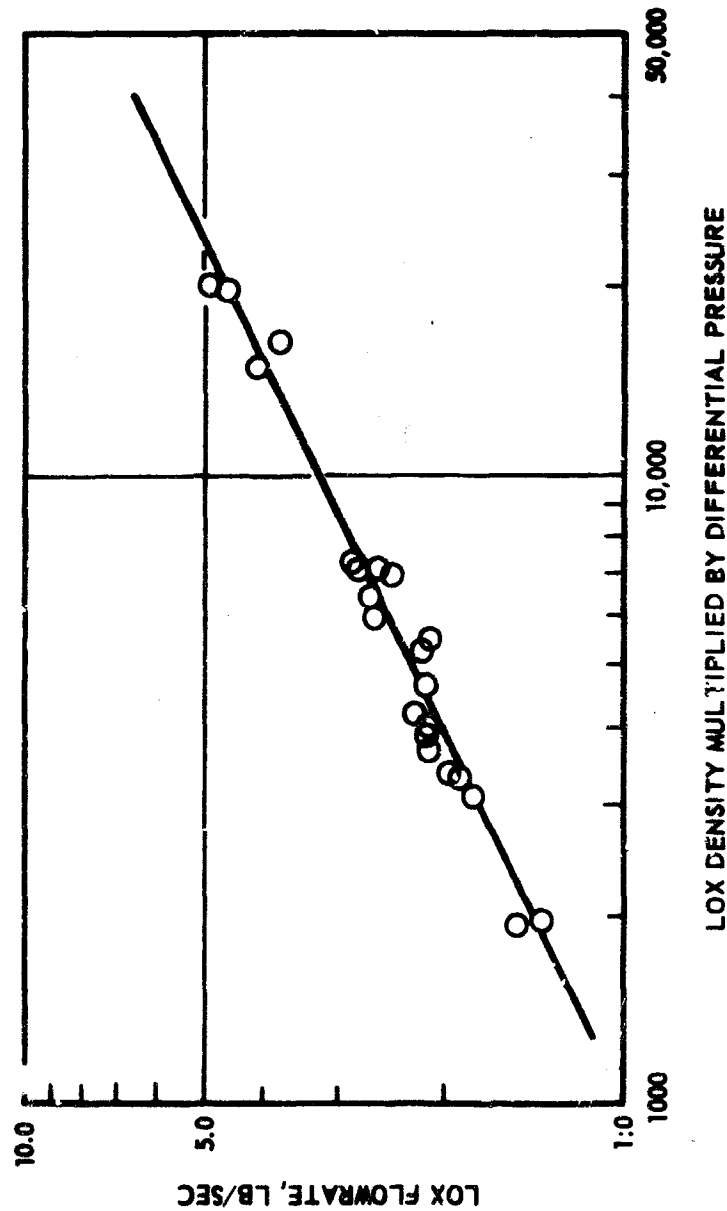


Figure 55. Correlation of LOX Flow Data for the No. 1 Selected 250K Injector Configuration

CONFIDENTIAL

CONFIDENTIAL

TABLE 17
ADJUSTED C* EFFICIENCIES FOR GAS TAPOFF TESTS

Test No.	Injector	Chamber Pressure, psia	Tapoff Flowrate, lb/sec	T/C MR	η_{C*}
089	U/N 1-3B	609	0.056	5.61	0.972
091	U/N 1-3B	387	0.037	5.56	0.966
092	U/N 1-3B	506	0.043	5.91	0.962
093	U/N 1-3B	685	0.065	6.02	0.992
095	U/N 1-3B	688	0.058	6.38	0.982

(C) Another 27 tests with the triplet injection pattern have demonstrated good stability characteristics in the 600- to 800-psia chamber pressure range. The nominal fuel injection pressure drop remains greater than 20 percent of the chamber pressure value throughout the throttle range.

(C) Instances of low-frequency buzzing were encountered with both the reverse flow (U/N 4-1A/B) and the LOX fan triplet (U/N 3-2A) injectors. With the reverse flow injector, the buzzing occurred at frequencies near 200 cps with occasional 300 cps. The amplitudes were high at 300 psia (100 psi peak-to-peak) and diminished to being nearly imperceptible at 1500 psia). The LOX fan showed occasional low-level buzzing in the 600- to 900-psi range at a much lower amplitude.

(U) Efforts were made to isolate the facility propellant systems from the chamber through placement of the hydrogen sonic flow venturi at the injector and adding as much as 1000 psi ΔP on the LOX side directly behind the injector. Neither of these changes particularly affected the observed buzz frequencies or amplitudes, and it was concluded that the frequencies must be primarily injector driven and sustained.

(U) No "bomb" stability tests were conducted during this quarterly report period.

(C) Overall Durability Results. The most durable injector of the three injectors is the LOX fan injector which appears to run extremely cool. The reverse flow injector not only experienced edge burning

CONFIDENTIAL

CONFIDENTIAL

but appeared to run very hot in the face, the appearance being such that engineering judgement resulted in the finding that the injector would be unacceptable for a large number of repeated firings.

(C) The triplet unit experienced some edge burning of the LOX strips with no burning or overheating of the core of the injector. Two steps were taken to correct this. The LOX strips were beveled at the edges to improve heat transfer cooling, and the hydrogen post was extended to the edge of the chamber to prevent edge recirculation. To separate the effects of the two changes, one side of the injector LOX strips was beveled and the other half left as before. The hydrogen post was extended on both ends. No erosion occurred in repeated firings, and it was concluded that recirculation past the previously beveled hydrogen post had resulted in the LOX strip burning. The extended hydrogen post has been incorporated into the design of the number 1 250K injector unit. This results in an added feature of simplicity by removing one machining operation.

(C) Injector Pressure Drop Characteristics. The injector pressure drop characteristics for the No. 1 250K configuration (U/N 1-3B) are shown in figure 55 and 56 for both LOX and GH_2 at ambient temperature. The data correlate quite well against the parameter $\rho\Delta P$, indicating that the hydraulic characteristics are well-behaved over the operating range. The expected 250K operating conditions are indicated below:

250K Injector Pressure Drop Summary

LOX Side	P_c	ΔP
	1500	375
	300	15
H_2 Side*	P_c	ΔP
	1500	375 ⁺⁶⁵ -00
	300	75

*Design data based upon hydrogen temperature available at injector.

CONFIDENTIAL

CONFIDENTIAL

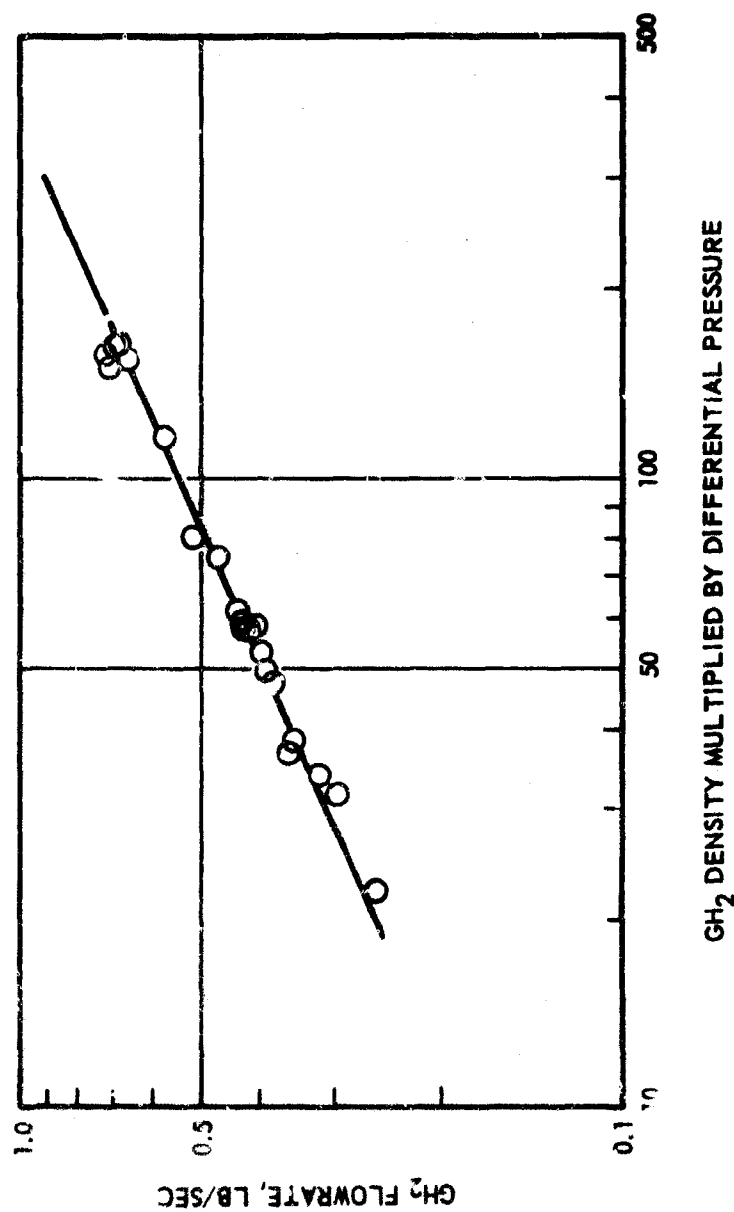


Figure 56. Correlation of GH₂ Flow Data for the No. 1 Selected 250K Injector Configuration

CONFIDENTIAL

CONFIDENTIAL

(U) **Heat Transfer Results.** To obtain heat transfer data in the 2.5K solid-wall segment effort, a water-cooled chamber is utilized as described in the First Quarterly Progress Report. This chamber is provided with coolant passages as shown in figure 57 with letter designations indicating passage location. The water flows into the passages are measured, and the bulk temperature rises indicated by three element chromel-alumel thermopiles. Primary emphasis is placed on the nozzle contour passages. The method of data reduction is outlined in Appendix B.

(U) The reduced throat heat flux values are indicated in Table 16. These values are subject to additional interpretation to obtain expected peak throat heat flux values for the ADP operation. Early in the performance program it was observed that certain throat heat transfer abnormalities were occurring. Repeated firings under identical operating conditions of mixture ratio and chamber pressure indicated nonrepeatable heat fluxes. The general characteristics observed were that the heat flux increased from one run to the next run. A number of hypotheses were postulated for exploration of this phenomena. These included corrosive attack of the copper chamber by the CTF ignition technique, thermal mechanical roughening of the contour surface, gross injector effects, and a segment contour mismatching disrupting the boundary layer.

(U) For ease of interpreting the results, the heat transfer data was reduced to a dimensionless Stanton and Prandtl number parameter,

$$N_{ST} N_{Pr}^{2/3}$$

and this parameter was plotted as a function of run number for a series of runs during which various specific surface effects were investigated. Particularly, it was observed that the throat surfaces appeared to be roughened after a series of firings. Following the hypothesis of surface roughening through CTF ignition product attack, the throat was electroplated with nickel on one side and mechanically smoothed on the other side, a number of times. The results are indicated in figure 58. It is observed that the Stanton number parameter increased more rapidly on the uncoated side than on the coated side. The limiting values coincide. Also of interest is the fact that the act of simply smoothing the throat resulted in a decrease in heat flux. The nickel surfacing did not appear to solve the problem.

(U) Further analysis of the data indicated that the increase in heat flux from run to run appeared to take place in discrete jumps rather than in a smooth manner. This led to a hypothesis of the effect being caused primarily during ignition. Two long-duration tests were

CONFIDENTIAL

CONFIDENTIAL

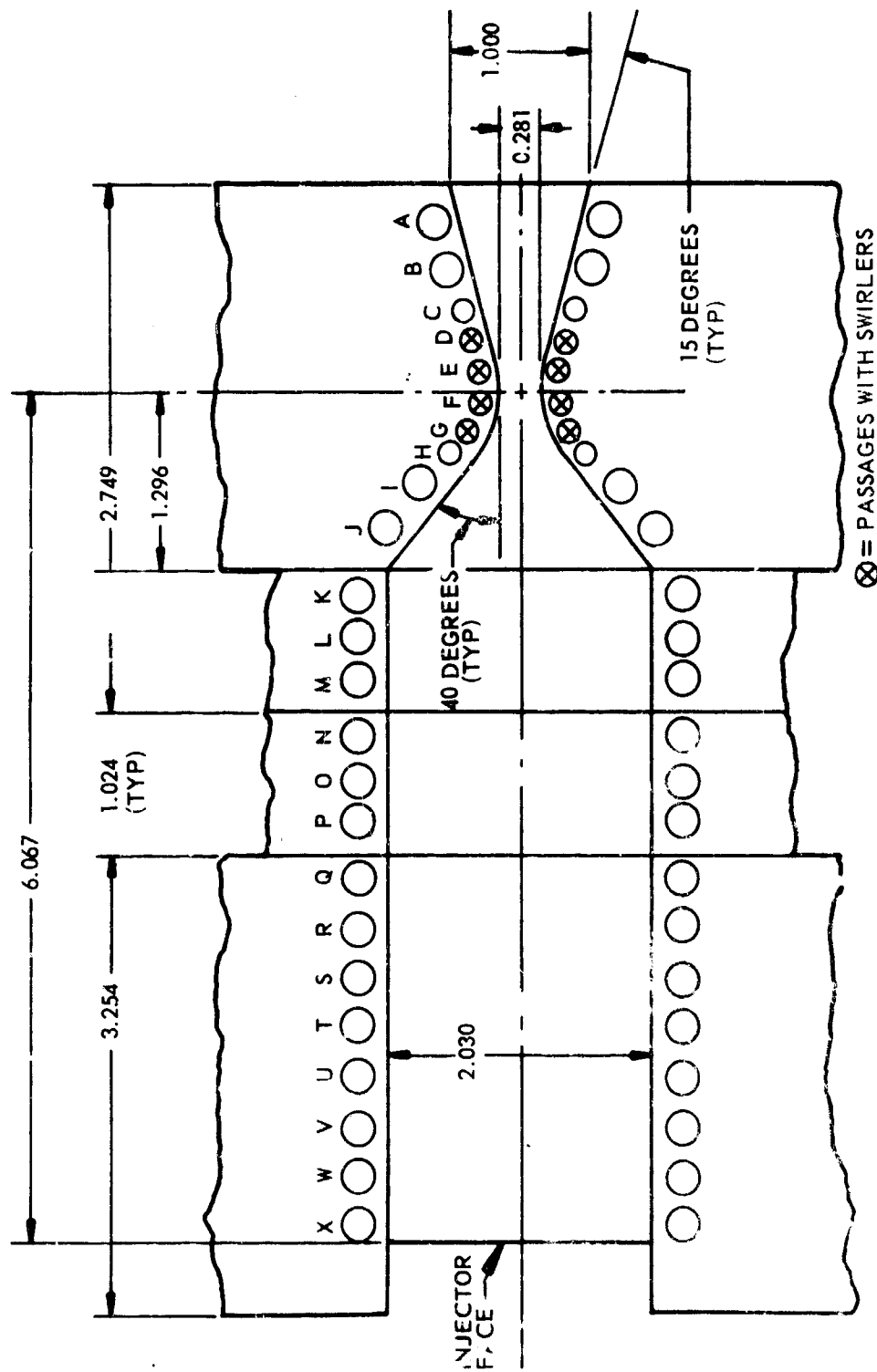


Figure 57. 2.5K Film-Cooled, Solid-Wall Segment
Coolant Passage Location

CONFIDENTIAL

CONFIDENTIAL

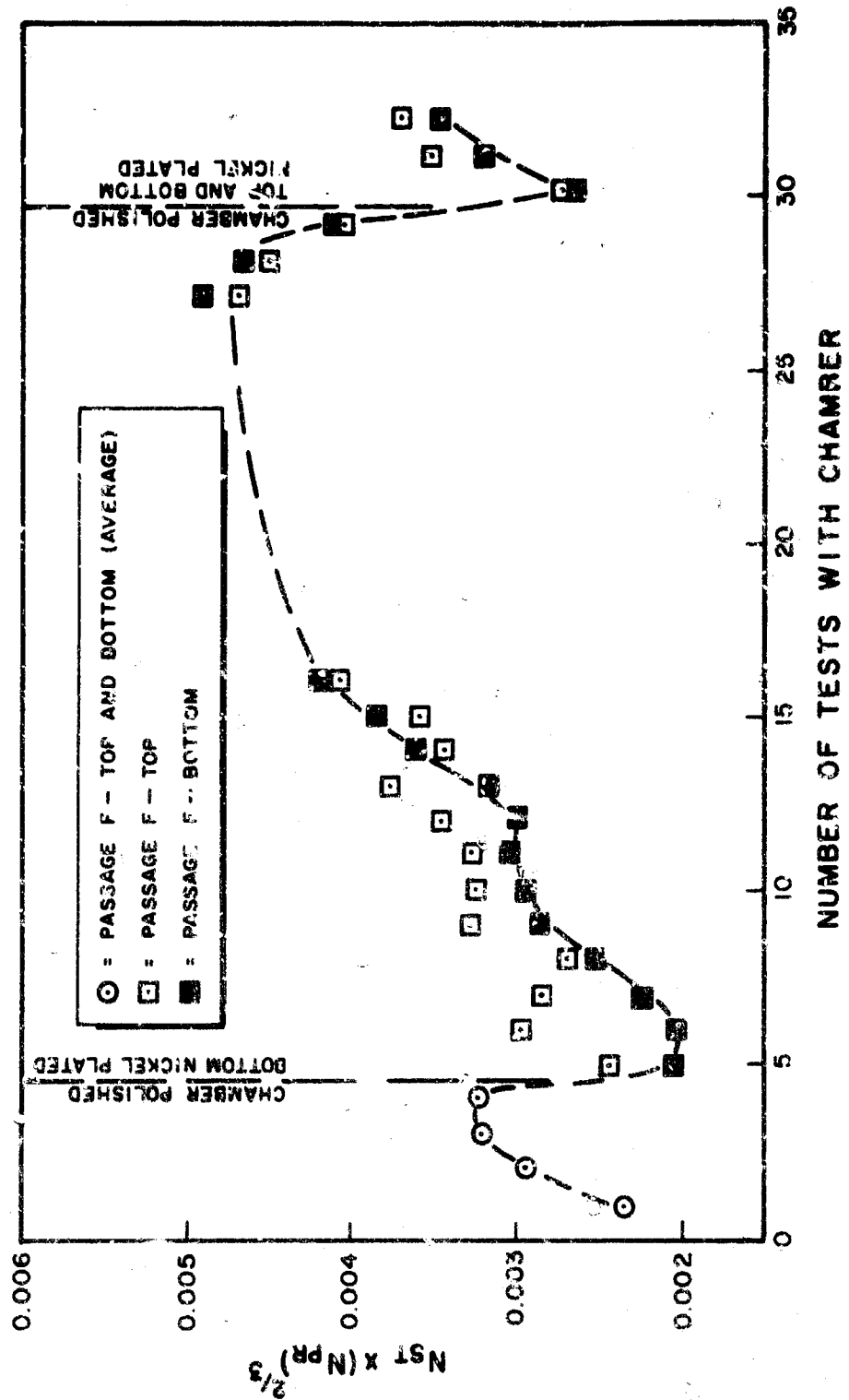


Figure 58. Variation in Heat Transfer Rates Into Passage Immediately Upstream of Throat

CONFIDENTIAL

CONFIDENTIAL

conducted to determine if this was so, and the results are given in figure 59. It is observed that a large increase in heat flux was incurred, and it apparently was associated with ignition.

(C) At this time a chemical analysis was conducted of the roughened throat surface, and it was found that the deposits were primarily nickel. Further close examination of the nozzle contour and throat surfaces showed that the roughening effects could not be described by distributed roughness, but instead would best be described by discrete surface protuberances. The CTF tube used as an igniter tube in the injector face was found to be pure nickel and the end eroded 1/16-inch to 1/8-inch behind the injector face. This small amount of erosion was found to be sufficient to account for most of the deposit coverage of the throat. To eliminate further difficulty, the CTF ignition tube was retracted to a position 0.125 to 0.200-inch behind the injector face.

(C) With these results in mind, a series of tests with a chrome plated (0.0005 inch) throat was conducted to determine if reproducibility of heat transfer data could be obtained. The results are tabulated below for both the triplet injector and the LOX fan injector both as raw data and as normalized data to one common operating point.

	<u>LOX Fan Injector</u>		<u>Triplet Injector</u>	
Run No.	<u>117</u>	<u>121</u>	<u>123</u>	<u>124</u>
P_c (psia)	639	649	635	596
MR	5.14	5.57	5.63	5.35
Q/A_{Exp}	31.6	30.8	28.3	27.0
Normalized Q/A (at 6.0 MR and 650 P_c)	29.7	30.2	27.8	26.3

(U) Run number 118 was a run at nominally 600 psi, but instrumentation read out in the throat was lost. Runs 119 and 120 were conducted at 300 psi with repeatable heat flux. Run 122 was a nominally 1000-psi run. This series of runs were considered to be as severe a test of the ignition hypothesis as could be devised in the hardware. The nominally 600-psi runs with the normalized values to a MR of 6.0 and a P_c of 650 psi indicate that the previously observed run-to-run increases in heat flux had been eliminated.

CONFIDENTIAL

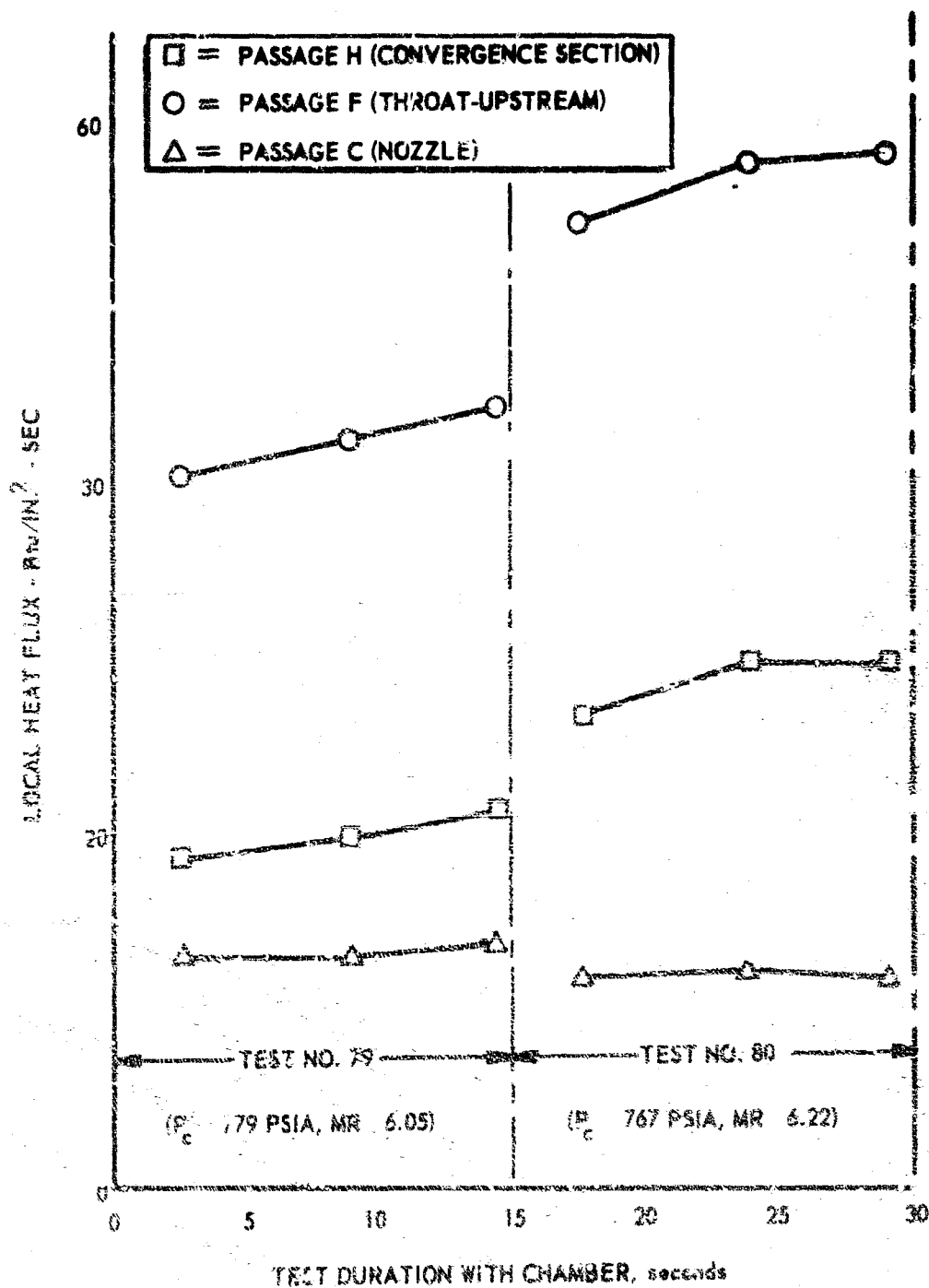


Figure 59. Variation in Local Heat Fluxes During ADP 2.5K Water Cooled Segment Firings (Tests No. 79 and 80)

CONFIDENTIAL

CONFIDENTIAL

(U) It is noted here that these heat fluxes are higher than the results for a smooth contour. It was found that this particular throat contained flats in the throat region. The results, however, serve to prove that burning of the CTF tube tip was responsible for the increased heat fluxes. Of interest also is the fact that the chromium plate was virtually lost on the first two runs of the series and cannot be considered as a part of the improved heat flux behavior.

(C) To obtain a true comparison and prediction of the heat fluxes for the candidate injectors only data for known smooth contours should be used. These include data for plated throats and those cases where the throat was purposely smoothed. The chromium-plated throat was smoothed after the above-discussed series of runs to eliminate the flats and utilized to obtain additional heat transfer data. The results obtained to date are shown in figure 60 for the copper segment as a function of total flowrate. The data correlate quite well and show an average prediction of 54 Btu/in.²-sec at the ADP operating conditions. Reduction of the data to effective Stanton numbers shows that the ADP heat flux in the stainless steel chamber will be 52 to 56 Btu/in.²-sec with an average value of 54 Btu/in.²-sec.

(U) P_c Injector Tap Investigation. The 2.5K solid-wall segment hardware is provided with three pressure taps, two in the chamber side wall approximately 0.5-inch downstream of the injector face, and one unit located in the injection face. It has been observed that the injector tap readout is always about 0.6 to 1.0 percent less than the side wall units. This is important to instrumenting the 250K injector in the tube wall chamber since in this unit instrumentation for P_c data acquisition can only be placed through the injector. The injection velocities of the hydrogen (1200 to 2000 fps) result in aspiration of the P_c tap if no provision is made to allow for diffusive effects around the tap. A short investigation conducted in the 2.5K effort showed the configuration shown in figure 61 to be adequate to reduce the aspiration effect to a negligible value.

(C) Summary Rating of Candidate Injectors. Based upon results obtained to date, exclusive of tapoff results, the three candidate injectors may be rated as indicated in Table 18. Also included is a rating based upon fabricationability which includes cost. The summary rating indicates the triplet as an overall superior injector for the No. 2 candidate injector. Final reduction of data along with tapoff data will be used to make the final selection.

CONFIDENTIAL

CONFIDENTIAL

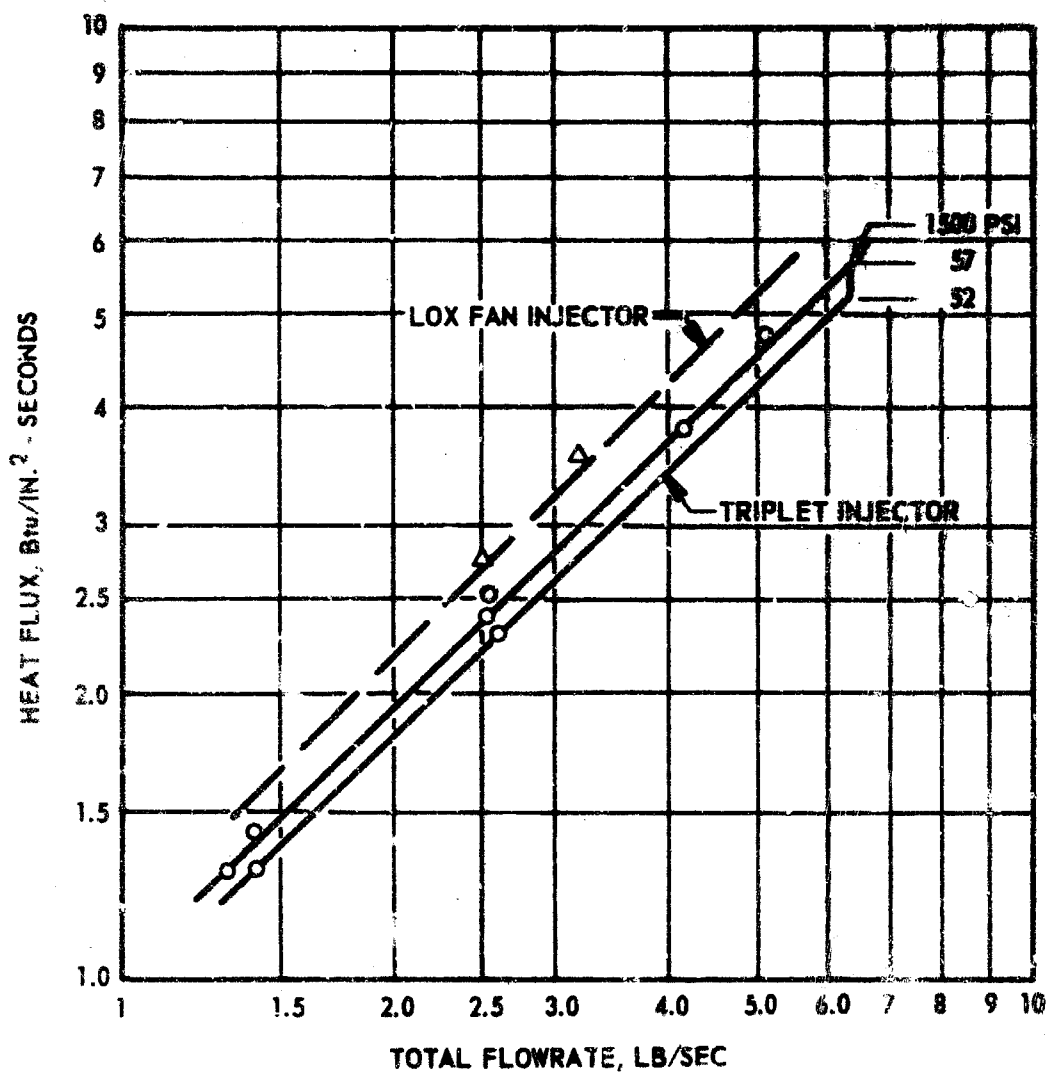


Figure 60. Comparison of Q/A for Triplet and Fan Injectors

CONFIDENTIAL

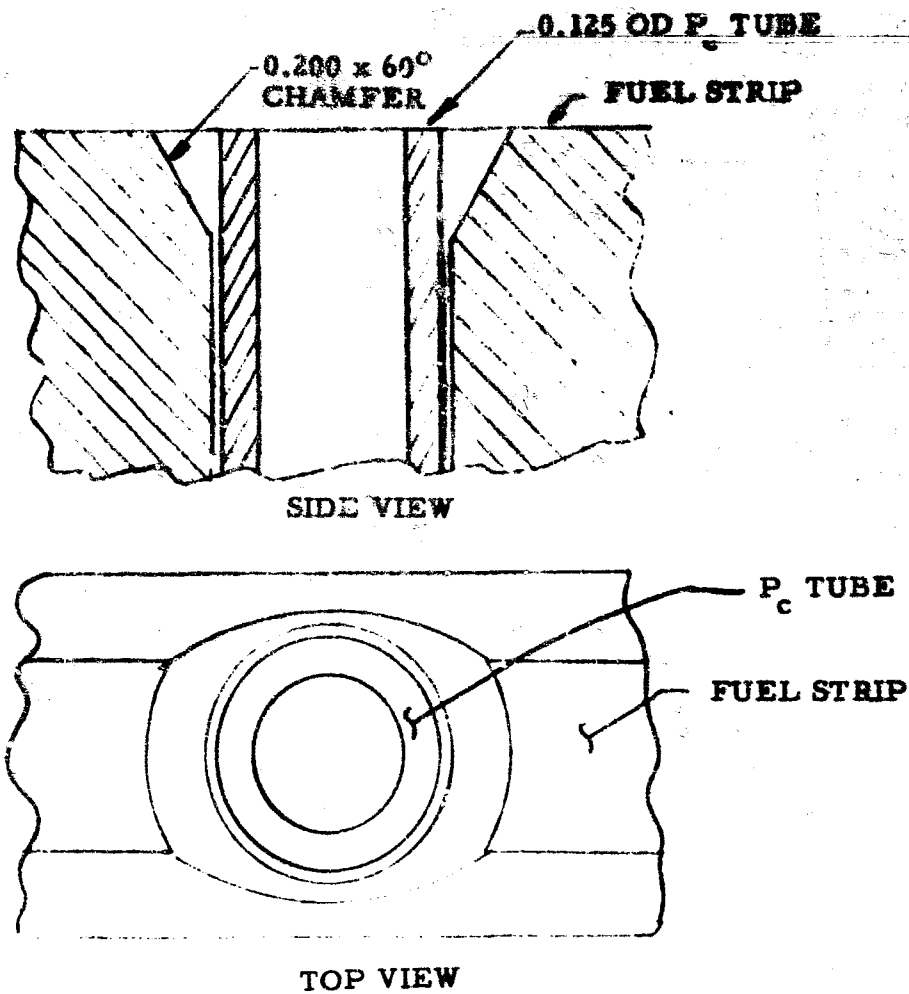


Figure 61. 250k Injector Chamber Pressure Tap Configuration

TABLE 18

NO. 2 250K INJECTOR CANDIDATE SELECTION RATING

	Performance	Heat Transfer Face and Throat	Durability	Fabricability	Stability
Triplet	1	1	2	1	1
Reverse Flow	2	2	3	2	3
Lox Fan	1	3	1	3	2

e. Summary of Planned Effort for Next Quarter

(C) The primary experimental activity will be completed early in the quarter. Other experimental activity with the 2.5K solid-wall segment will include tapoff runs to 1500 psia, several selected bombing stability runs on the selected No. 2 injector pattern, and, if necessary, supporting effort for the 250K injector in the fourth quarter. Complete reduction of data will be accomplished early in the next quarter to finalize the results. The No. 2 injector pattern selection will be made early in the report period based upon the final data analysis.

2. THRUST CHAMBER COOLING INVESTIGATIONS

(C) The thrust chamber cooling investigation consists of an evaluation of the regeneratively cooling limits for the Aerospike chamber, a determination of the operating point for a cyclic fatigue life of 100 reuses and 10 hours between overhauls, a selection of a tube material to cool and meet the life requirements properly, and a prediction of the cyclic fatigue life of the selected material. These objectives are being met by a combination of heat transfer analysis, stress and materials analysis, materials laboratory evaluations, a tube tester simulating hot-fire conditions and actual hot fire of 2.5K tube-wall segments. Three materials were initially to be evaluated--stainless steel, copper, and nickel. The limits of regeneratively cooling will be evaluated on the 2.5K hot-fire segments. The fatigue life of the various materials and, therefore, of the selected material, are to be evaluated through the combination of the analytical effort and experimental results. This combination is further checked by comparison to life results on

current thrust chambers (J-2). The 2.5K segment has previously proved itself as an effective test unit for combustion and cooling investigations.

a. Status

(U) All design effort on these segments has been completed and released for fabrication.

(U) The hardware fabrication status is as follows:

Nickel Tubes -- Complete and ready for braze assembly

Copper Tubes -- Complete and ready for braze assembly

Injector Support Block -- first unit being nickel plated; second unit in final machining

Throat Support Beams -- Complete and ready for braze assembly

End Plate Assembly (See figure 62) -- first set complete and ready for braze assembly; second set being furnace brazed

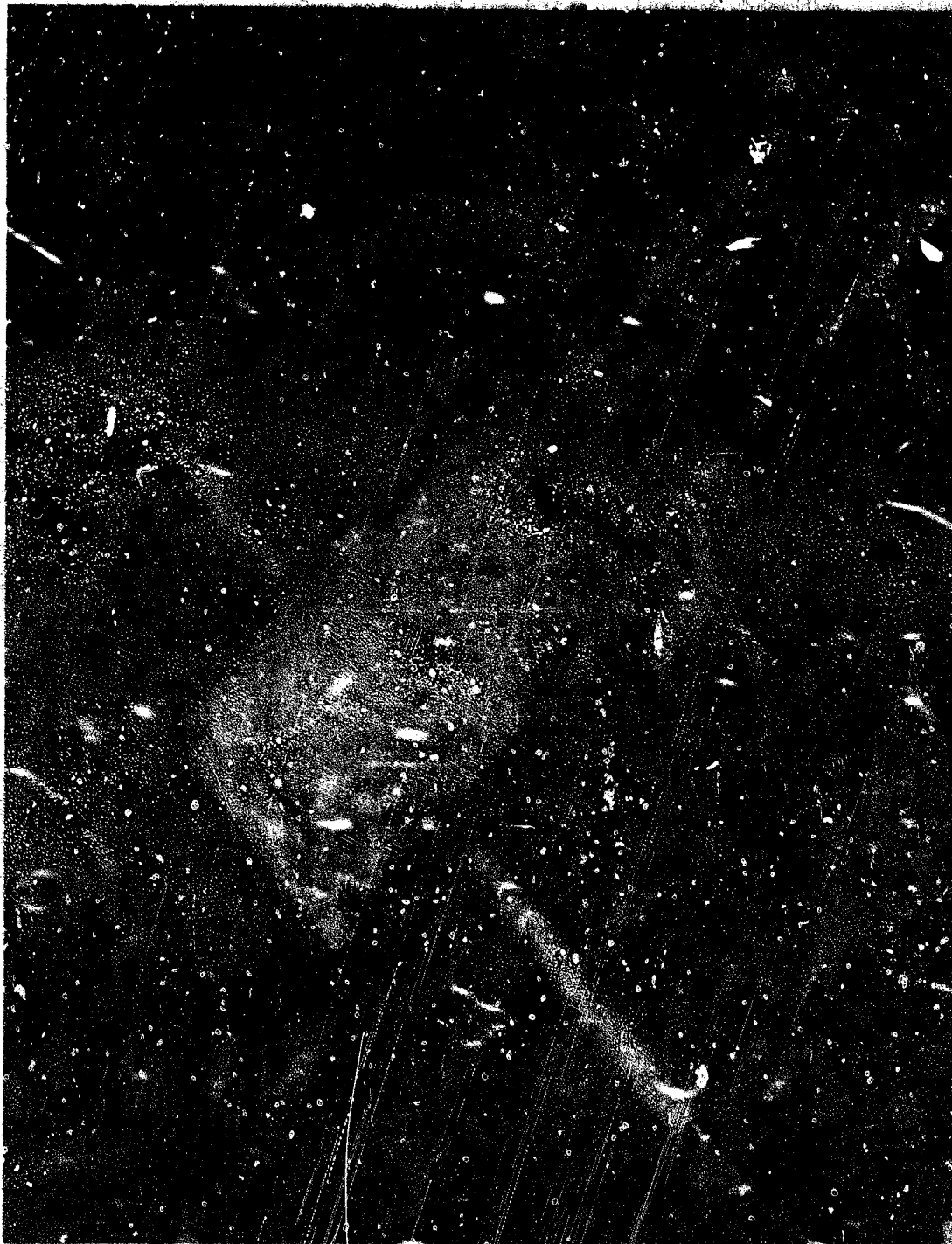
Exit Manifolds - Machining complete, being nickel plated

Assembly of the nickel chamber (figure 63) began during the last week of the quarter.

(U) This effort which was directed toward the evaluation and selection of long-life tube materials has been completed. This effort included an initial material selection based on analysis, material tests intended to develop fatigue and mechanical property data, and a review of the literature and conduct of basic studies.

(U) As a result of this effort, the tube material and a manufacturing process cycle for the demonstrator segment thrust chamber has been selected. In addition, two very promising long-range tube materials have been chosen.

CONFIDENTIAL



UNCLASSIFIED-7/12/66-012

Figure 62. 2.5K Segment End Plate Prior to Assembly

CONFIDENTIAL

CONFIDENTIAL

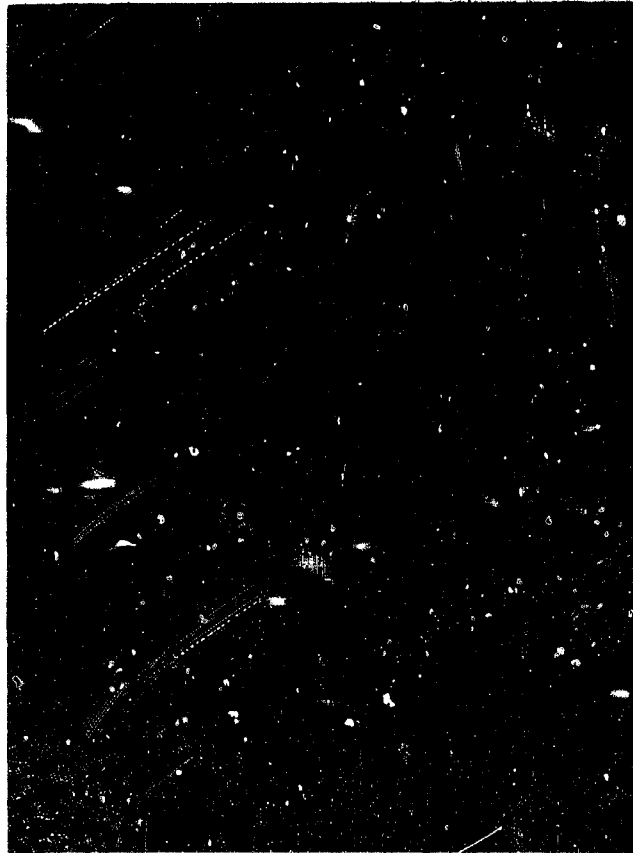


Figure 63. Nickel Segment Brazed Assembly

CONFIDENTIAL

CONFIDENTIAL

b. Progress During the Report Period

(1) Design

As reported in the First Quarterly Technical Report, three 2.5K chamber segments were designed to accommodate 347 CRES nickel 200 and OFHC copper tubes. Based on further material evaluations reported in a later section of this report, stainless steel was eliminated, and only the nickel and copper segments will be fabricated. The geometry of the combustor will be the same as that for the demonstrator module.

(2) Fabrication

(U) The final design, shown in figure 64, consists of a brazed assembly of tubes, forming the contoured walls; copper end plates, with drilled coolant passages; a 347 CRES injector end block; and 347 CRES exit end manifolds. The brazed assembly is reinforced by a 4130 steel backup structure bolted in place. Transfer of loads from the tube stack to the backup structure is through a bearing block bolted to the backup structure and making intimate contact with the tubes through an epoxy and glass fiber filler.

(U) Drawings of all detail components, as well as braze and chamber assemblies, were completed and released for fabrication. The first nickel assembly unit began during the last week of August. The balance of the components backup structure, manifolds, and inlet and outlet tubes are in work and will be completed in time to support an estimated completion of the nickel segment early in October. The copper segment will follow by 2 weeks.

(3) Cooling Limits

(C) A study of the heat flux capability of materials, OFHC copper (0.020 inch) and nickel 200 (0.013 inch), showed that the heat flux capability of these materials was in this order indicated, copper being the best. The results are shown in figure 65 and 66. For the purposes of this study, a coolant bulk temperature of 450R was used (this approximates the anticipated value in the outer body throat of the 250K thrust chamber), and a tube roughness of 50 microinches was assumed. Coolant mass velocity of 11 lb/in.²-sec is based on a coolant Mach number of about 0.5 for 450R and 2200 psia (total pressure) hydrogen.

(C) The results for nickel 200 indicate it can conduct with a 1600F wall temperature, a heat flux of 44, and 60 Btu/in.²-sec for curvature enhancements of 1.0 and 1.75, respectively. Thus, nickel 200 can operate at conditions of the engine currently being designed which has

CONFIDENTIAL

CONFIDENTIAL

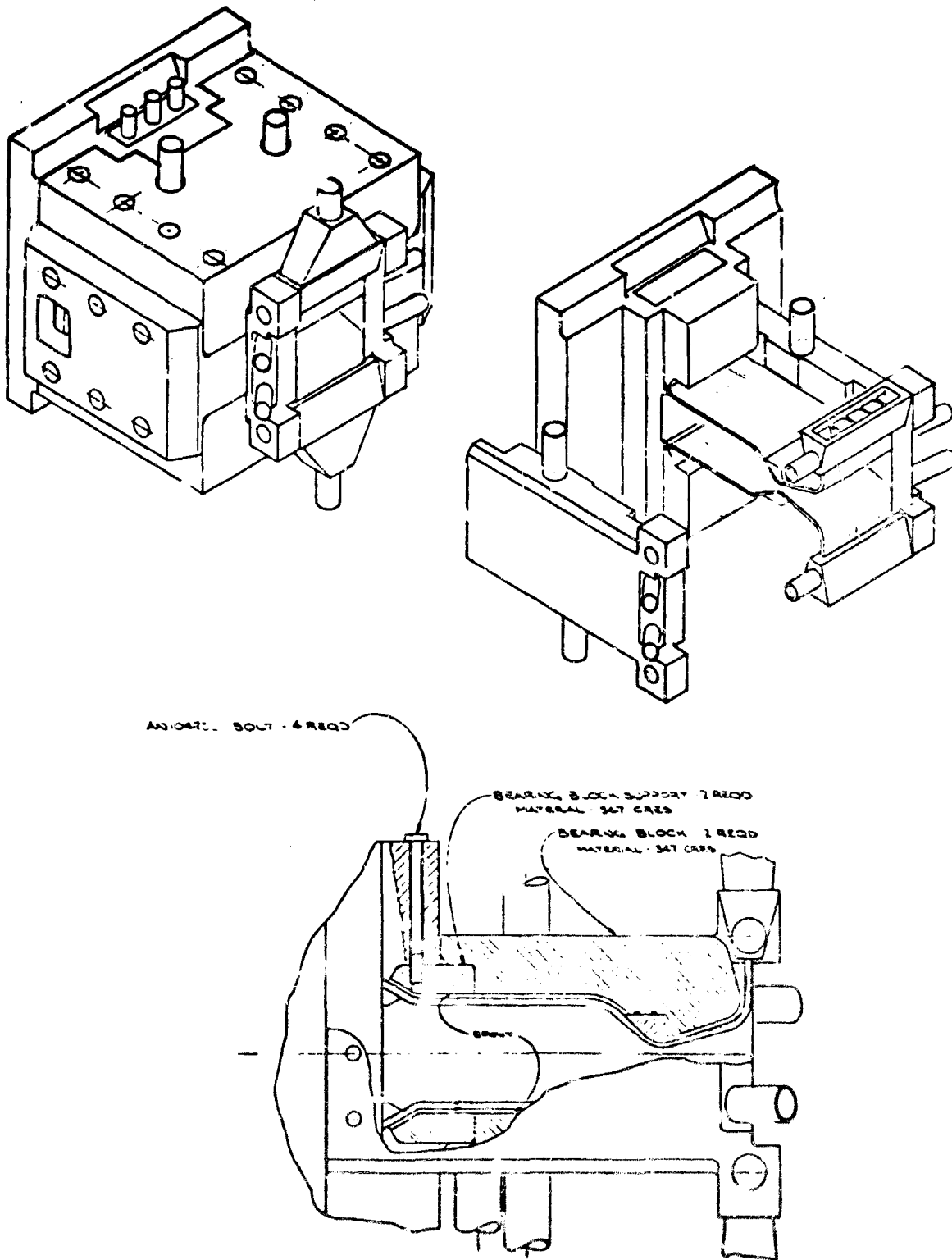


Figure 64. 2.5K Tube-Wall Segment

CONFIDENTIAL

CONFIDENTIAL

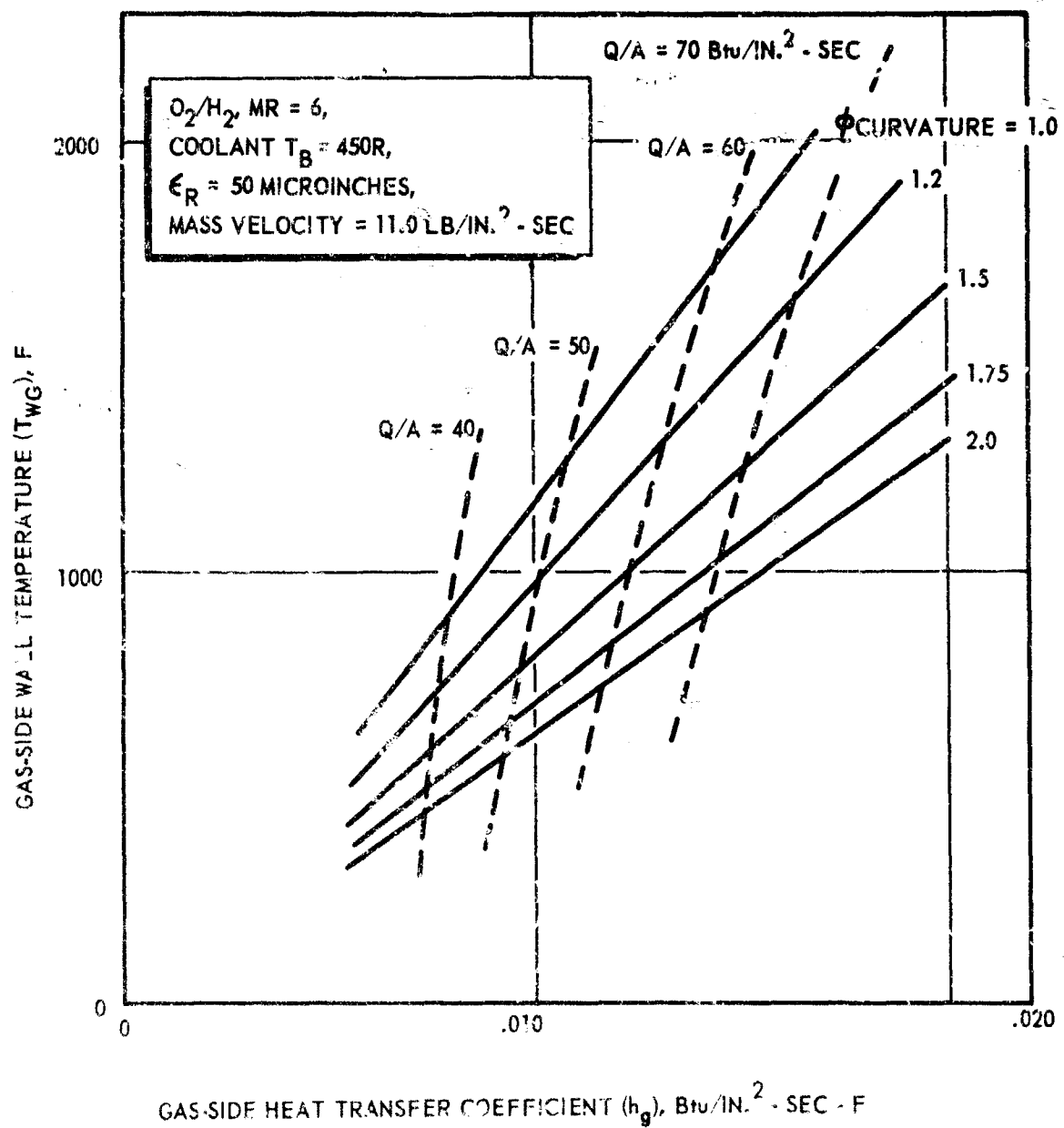


Figure 65. Cooling Limit Results for OFHC Copper

CONFIDENTIAL

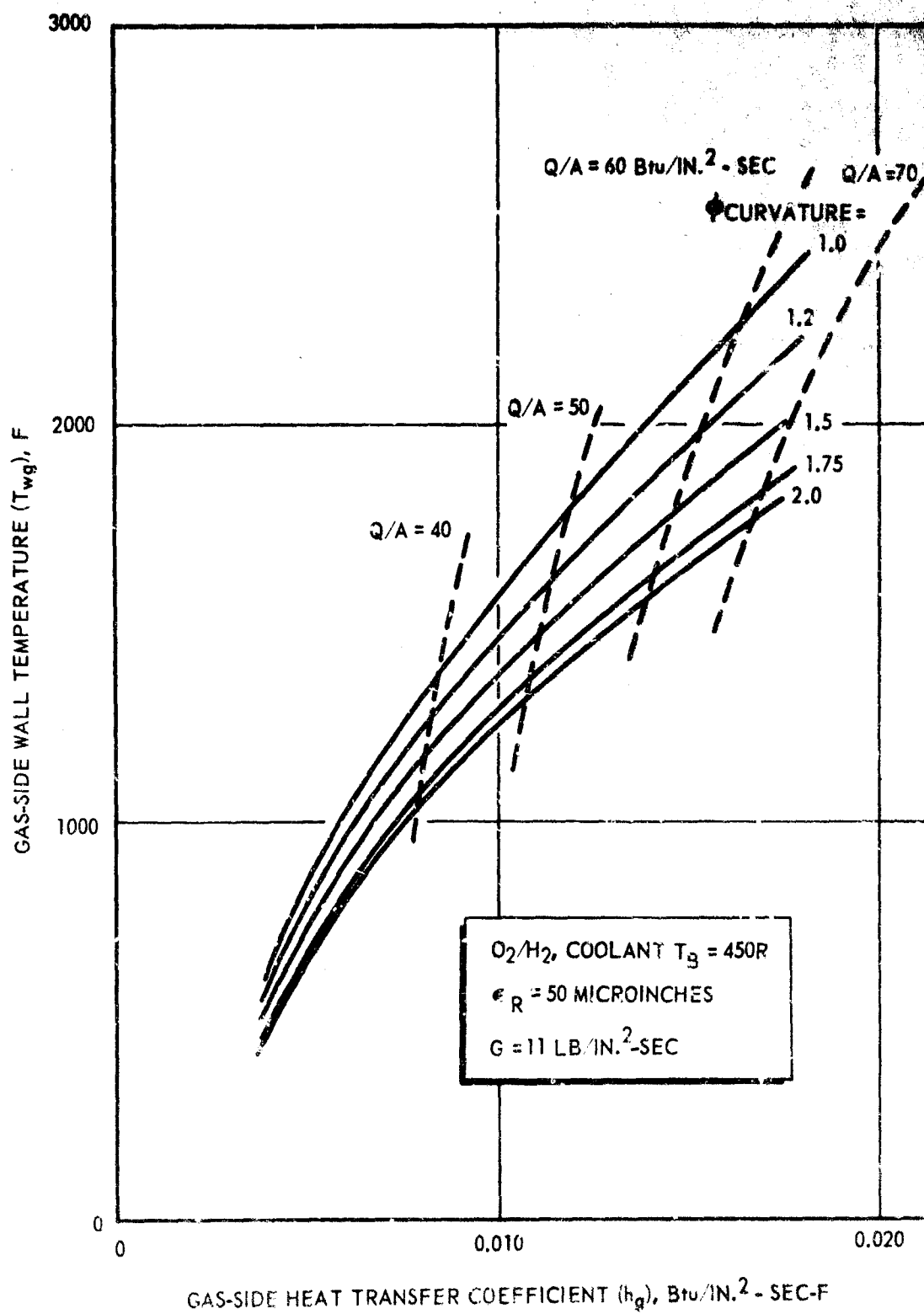


Figure 66. Cooling Limits for Nickel 200

CONFIDENTIAL

a curvature factor of at least 1.75. It is noted that nickel 270, due to its somewhat higher conductivity, would operate at lower wall temperature.

(C) Copper conduction capability using the annealing temperature of about 900F is 40 and 67 Btu/in.²-sec for the range in curvature examined. Thus, copper can also handle the anticipated throat heat fluxes.

(C) The temperatures indicated are typical of what would be expected in the outer body throat region. The inner body will operate at lower wall temperatures because of the more desirable hydrogen coolant temperature existing in the inner body throat region (200 to 250R).

(4) Thrust Chamber Materials Investigation

(U) To utilize all available Rocketdyne experience, a survey was made of all regeneratively cooled production thrust chambers to study their life-limiting processes. Particular note was made of the J-2 liquid oxygen-hydrogen thrust chamber life history. This survey led to a summary of thrust chamber life-limiting processes as given below:

Axial Tube Splits Cause Rapid Failure

Hydraulic pressure spikes can burst tubes.

Hydraulic pressure can burst tubes if steady stress at high temperature causes creep.

Either of the above failure modes are aggravated by oxidation-erosion which thins the tube wall.

Transverse Tube Microcracks Cause Gradual Degradation

Cyclic thermal strains can cause plastic flow which eventually results in transverse tube microcracks.

These microcracks are not self-propagating and are closed during steady-state operation.

(U) A materials evaluation and selection effort was then planned to provide the critical data needed to select a long-life, high-performance, fabricable tube material.

The logic flow diagram for the material selection program is shown in figure 67.

CONFIDENTIAL

CONFIDENTIAL

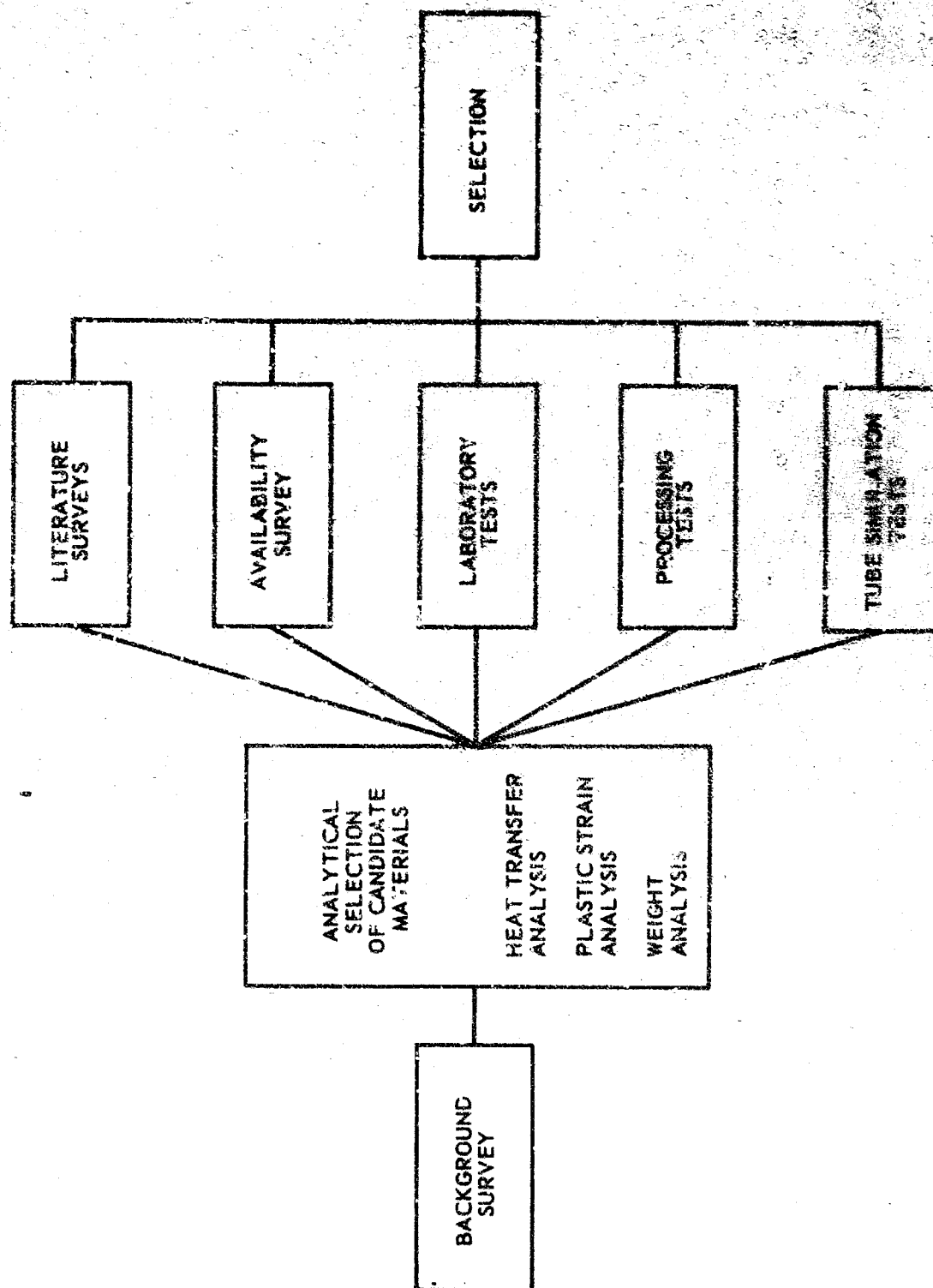


Figure 67. Material Selection Program

CONFIDENTIAL

CONFIDENTIAL

(U) To select a group of candidate tube materials, an effort was made to utilize basic analytical techniques to screen a broad range of materials. A heat transfer analysis; plastic strain analysis; analytically predicted fatigue diagram; and weight analysis were used to select a group of candidate materials.

(U) The candidate materials thus selected were then the subject of preliminary studies in processing, availability, and cost. As a result of these preliminary studies, a further screening of the original candidates was made. The original candidate materials which survived the preliminary screening are shown in Table 19.

(U) The first quarterly progress report described the results of the material property literature survey. Derivation of the plastic strain analysis was also given, and is summarized in Fig. 68.

(U) In the second quarter, the oxidation-erosion studies, diffusion layers and coatings studies, braze and heat treat process studies, as well as the fatigue screening tests, and ductility screening tests were completed. The creep screening tests and surface protection screening tests were removed from the materials selection program because the results of the initial studies indicated they would be premature and perhaps unnecessary. Some tube simulation fatigue tests have been accomplished.

(U) A separately funded tube-tapering feasibility program was also completed and the results were made available for the material selection program. The materials evaluated in this program were type 347 stainless steel, nickel 200, nickel 270, and OFHC copper. These materials were experimentally tapered to ADP tube dimensions and tolerances. Inspection of the finished tubes yielded an initial estimate of tube tapering confidence with regard to process time, tolerance control, lubricant contamination, and the effect of inclusions in the material.

(U) No major difficulties which prevented the successful collection of adequate data, were experienced although the tube simulation fatigue test facility experienced some high-power-level-run problems. This prevented the collection of tube-tester fatigue data on nickel and copper tubes in the second quarter.

(U) The oxidation-erosion studies revealed that from strictly thermodynamic considerations, copper and nickel should not oxidize in a water vapor environment.

CONFIDENTIAL

TABLE 19

CANDIDATE MATERIALS FOR THRUST CHAMBER USAGE

Original Candidates, Selected by Analysis

Nickel	200
	270
	TD
Copper	OFEC
	Boron Deoxidized
	Beryllium Alloy 10
	Zirconium Alloy
	Chromium Alloy
Stainless Steel	347

Screened Candidates, Evaluated by Tests

Nickel	200
	270
Copper	OFEC

Additional Candidates for Long-Range Application, Evaluated by Tests

Copper	Boron Deoxidized
	Beryllium Alloy 10

CONFIDENTIAL

MATHEMATICAL RELATIONSHIPS

$$\text{Axial Plastic Strain, } \epsilon_{P_{\text{axial}}} = \alpha \left[\left(\frac{Q}{K} t \right) \left(\frac{\nu}{1-\nu} \right) + T_{wg} - T_B \right] - \frac{\sigma_y}{E}$$

$$\text{Tangential Plastic Strain, } \epsilon_{P_{\text{tang}}} = \alpha \left(\frac{Q}{K} t \right) - \frac{\sigma_y}{E}$$

$$\text{Effective Plastic Strain, } \epsilon_{P_{\text{effective}}} = \frac{2}{\sqrt{3}} \sqrt{\epsilon_{P_{\text{tang}}}^2 + \epsilon_{P_{\text{tang}}} \epsilon_{P_{\text{axial}}} + \epsilon_{P_{\text{axial}}}^2}$$

$$\text{Cyclic Plastic Strain } \Delta \epsilon_P = 2 \epsilon_{P_{\text{effective}}}$$

$$\text{Appearance of microcracks } N_f = \frac{k \sqrt{C}}{\sqrt{\Delta \epsilon_P}}$$

Where $\frac{Q}{K}$ = Heat flux, K = thermal conductivity, T_{wg} = Gas Wall Temperature,

T_B = Coolant bulk temperature, ν = Poisson's ratio, σ_y = yield stress

E = Elastic modulus, C = experimentally determined, temperature

Dependent number k = experimentally determined exponent

N_f = No. of engine starts before numerous tube cracks appear.

Figure 68. Plastic Strain Analysis.

CONFIDENTIAL

CONFIDENTIAL

(U) With excess hydrogen in the water vapor, copper and possibly nickel should not oxidize, even under the flow conditions characteristic of ADP thrust chambers. It seems probable then, that the oxidation-erosion problem, if it appears, centers around such practical considerations as nonuniform mixture ratio distribution, and adverse perturbations in tube temperature. These factors can only be determined by tests, and are characteristic of injector design, start sequence, throttling range, and other system-controlled effects.

(U) The diffusion layers and coatings studies were intended to reveal those state-of-the-art processes which might be applied to nickel or copper tubes to enhance their oxidation-erosion resistance. Two different approaches were explored. Studies indicated that braze alloy wetting may increase the oxidation resistance of nickel and copper since these alloys are essentially composed of noble metals. A concurrent literature review revealed the existence of several state-of-the-art intermetallic diffusion processes which would be applicable to nickel and possibly copper. Diffusions of aluminum appear particularly attractive because such diffusions reputedly have ductilities close to that of the base metal. Other diffusion systems in current use employ chromium and aluminum-chromium combinations. All diffusion coatings would adversely affect thermal conductivity to some degree. The significance of this degradation could only be determined by heat transfer tests and analyses.

(U) As a result of the oxidation-erosion and diffusion layers and coatings studies, a decision was made to eliminate the surface protection screening tests until a firm requirement was established by hot-firing tests.

(U) The mechanical property and ductility tests were simple tensile tests on rod and ADP tube specimens, both in the annealed condition, and were also processed in a way similar to an ADP furnace brazed tube. Tests were conducted at room temperature in air and also at elevated temperature in an argon environment. The results of these tests are shown in Table 20. Some significant findings from these tests were the excessive low yield stress of nickel 270 and the effects of grain size on the tube materials' apparent tensile properties. The grain structure of nickel 200 and 270, OFHC copper, and beryllium copper No. 10 prior to brazing and postbrazing is shown in figure 69 through 72. All except the Cu-Pe No. 10 are circular specimens.

It is not apparent from published data nor from the fatigue results reported here that large grains have a deleterious effect upon life. However, where the grain boundaries extend completely across the tube wall as shown (figure 69 through 72) for nickel 270 and OFHC copper, mechanical behavior becomes erratic and intergranular penetration of contaminants becomes more hazardous.

CONFIDENTIAL

CONFIDENTIAL

TABLE 20

MECHANICAL PROPERTY TESTS: SUMMARY OF RESULTS

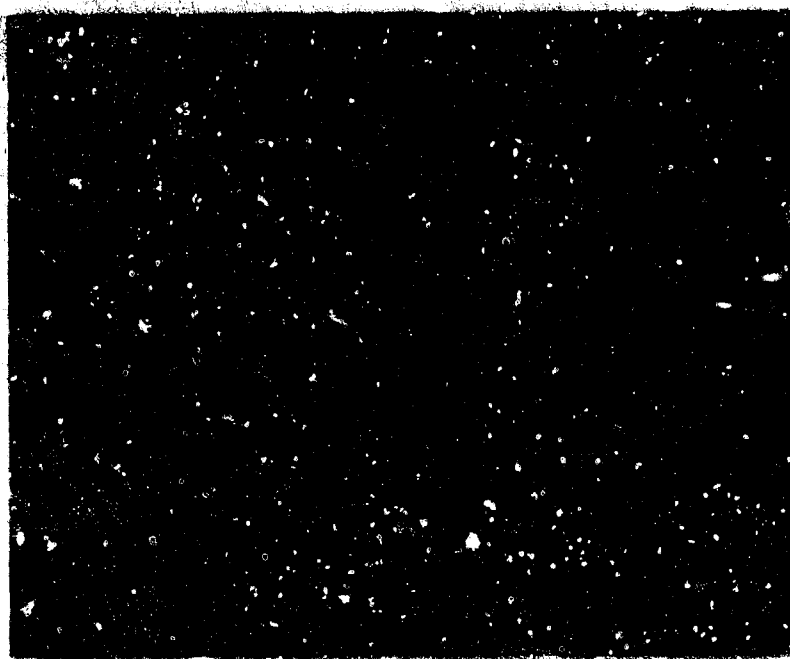
Bar Stock Tensile Properties							
Material	Condition	Test Temperature, °F	0.2 Percent Yield Strength, psi	0.5 Percent Yield Strength, psi	Ultimate Strength, psi	Elongation (1-Inch Gage Length), percent	Reduction of Area, percent
Ni 200	Annealed	*	21,700	29,500	67,600	47.5	85.4
Ni 200	Brazed	*	20,300	23,700	57,900	41.0	64.0
Ni 200	Annealed	1400	6,500	7,200	13,400	92.0	99.1
Ni 200	Brazed	1400	6,100	7,200	14,200	78.0	96.0
Ni 270	Annealed	*	21,700	24,400	50,800	66.3	88.5
Ni 270	Brazed	*	14,600	16,500	46,100	31.5	35.9
Ni 270	Annealed	1400	3,000	3,600	6,200	75.5	99.9
Ni 270	Brazed	1400	-	-	7,350	53.0	80.3
OFEC	Annealed	*	10,300	11,900	30,000	50.0	80.1
OFEC	Brazed	*	8,300	9,400	24,900	41.0	76.3

Tubing Tensile Properties								
Material	Condition	Test Temperature, °F	0.2 Percent Yield Strength, psi	0.5 Percent Yield Strength, psi	Ultimate Strength, psi	Elongation (1-Inch Gage Length), percent	Uniform Reduction of Area, percent	Local Reduction of Area, percent
Ni 200	Annealed	*	20,500	22,700	73,700	39.0	46.2	95.0
Ni 200	Brazed	*	9,500	11,200	50,900	28.2	27.8	95.0
Ni 200	Annealed	1400	-	-	18,200	89.0	79.9	95.0
Ni 200	Brazed	1400	7,100	7,900	12,100	15.4	18.9	18.9
Ni 270	Brazed	*	4,500	6,200	37,900	25.0	29.6	95.0
Ni 270	Brazed	1400	4,500	4,800	8,600	25.4	19.4	50 to 99
Ni 270	Binder Brazed Without Vacuum	1400	5,700	5,900	9,500	24.0	33.4	90 to 99
Ni 270	Binder Brazed With Vacuum	1400	4,400	5,000	9,100	23.6	37.9	99.0
OFEC	Annealed	*	6,100	7,400	32,730	-	-	-
OFEC	Brazed	*	4,500	5,600	26,200	18.6	24.0	99.0

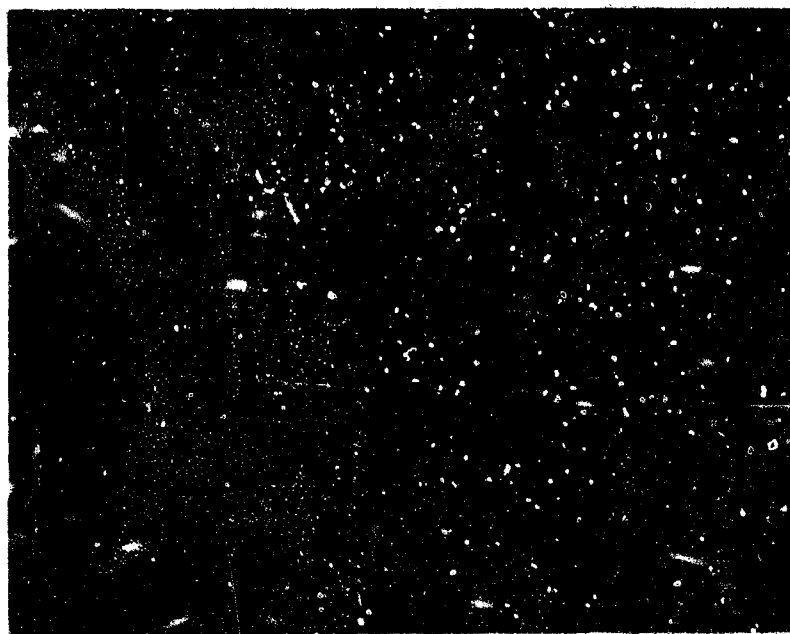
*Room Temperature

CONFIDENTIAL

CONFIDENTIAL



(b) OFHC Copper After Simulated
Brase Cycle

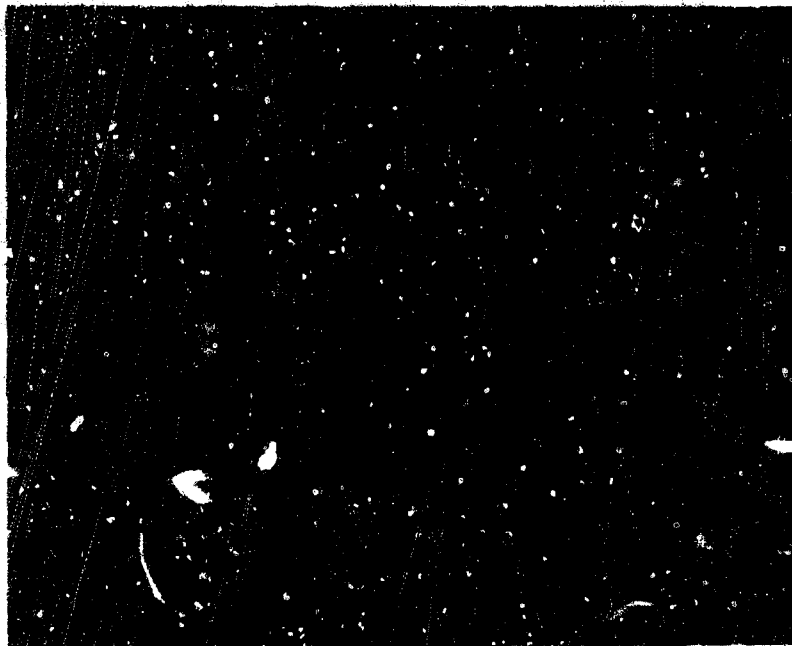


(a) OFHC Copper Annealed

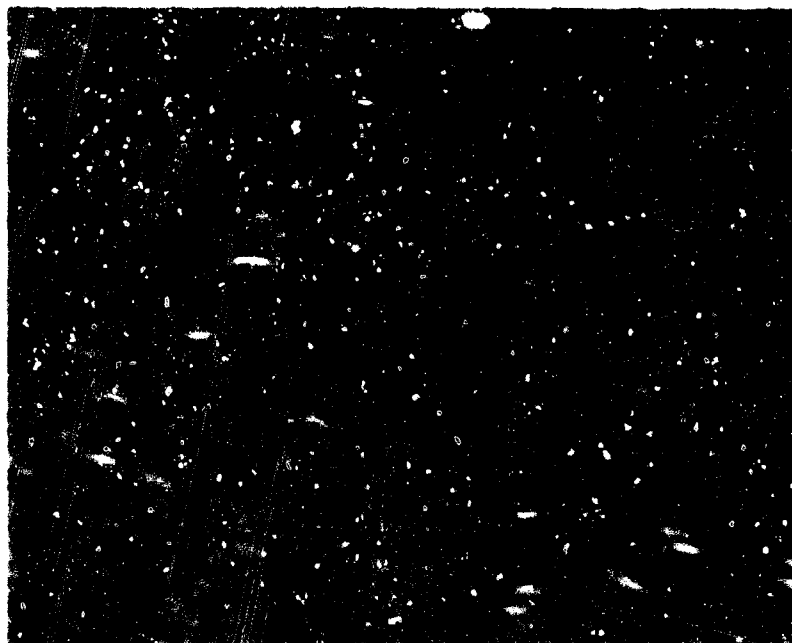
Figure 69. Comparison of OFHC Copper Tube Grain Size in the
Annealed Condition and After Simulated AHP
Brase Cycle

CONFIDENTIAL

CONFIDENTIAL



(b) After Brazing

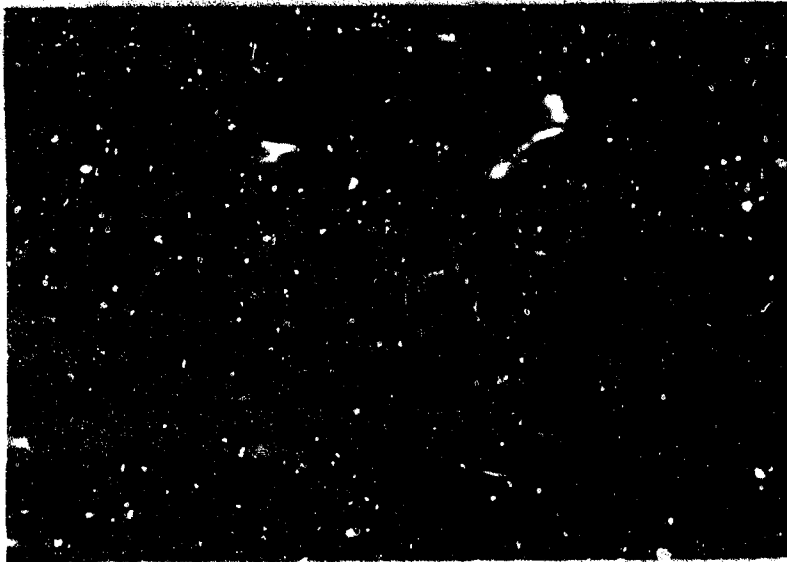


(a) Prior to Brazing

Figure 70. Comparison of Beryllium-Copper Grain Size Prior to Brazing and After Brazing

CONFIDENTIAL

CONFIDENTIAL



(b) Nickel 270 After Simulated
Brazing Cycle



(a) Nickel 270 Annealed
After Simulated ADP Furnace Brazing Cycle

Figure 71. Comparison of Nickel 270 Tube Grain Size in the Annealed Condition and
After Simulated ADP Furnace Brazing Cycle

CONFIDENTIAL

CONFIDENTIAL



(b) Nickel 200 After Simulated
Braze Cycle



(a) Nickel 200 Annealed

Figure 72. Comparison of Nickel 200 Tube Grain Size in the Annealed Condition and
After Simulated ADP Furnace Braze Cycle

CONFIDENTIAL

CONFIDENTIAL

(U) As a result of these tests and posttest metallographic analyses, further investigations of the effects of grain size on the mechanical properties and fatigue life of nickel 200 in the furnace brazed condition were conducted.

(U) The braze process and contamination studies and tests were intended to define initially proposed furnace step braze cycles for each candidate tube material. These initially proposed braze cycles were then applied to test specimens to determine the alloy wetting and flow characteristics, and to determine any tendencies for the braze alloys to induce tube alloying or intergranular penetration. The results of these tests are shown in Tables 21 and 22. The results of these tests indicate that while nickel 200 and 270 apparently may be successfully furnace brazed with current technology, brazing of the OFHC and beryllium copper is limited by tendencies of the common braze alloys to dissolve part of the base metal.

(U) The mechanical strain at elevated temperature fatigue tests were designed to simulate the strain cycle experienced by a thrust chamber during the start and shutdown sequence. These tests were run at constant elevated temperatures, and utilized rod specimens which were axially strained. Materials in the annealed and furnace brazed condition were tested. The plastic strain analysis described previously was used to predict the equivalent axial strains which each material would experience as a thrust chamber throat tube. These tests were run at temperatures which represented the maximum predicted tube gas wall temperature for each material. Tests were also run at a reduced temperature known to represent a condition of minimum ductility for each material. All tests were run in an argon environment. Table 23 shows a summary of the test conditions.

(U) A record of each load-strain cycle was continuously printed out by automatic equipment. Typical load strain cycles recorded in these tests are shown in figure 73. The unsymmetrical curve developed after a large number of cycles represents the load-deflection behavior of the progressing fatigue crack alternately stressed in tension and compression. As the crack grows, the tensile load-carrying ability decreases as strain remains constant, thus providing a convenient technique for recording crack progression.

(U) While it is customary in tests of this nature to report the number of cycles to complete fracture, a more meaningful technique was used which gave a measure of the development of internal fatigue damage, as well as the conventional cyclic life. This was obtained by plotting the ratio of maximum cyclic tension -- compression loads in the specimen vs the number of test cycles. These load values were obtained from the load-strain hysteresis loops, as shown in figure 73. Groups

CONFIDENTIAL

TABLE 21

BRAZING FEASIBILITY TESTS, NICKEL 200,

Tubing Material	Braze Filler Metal	Braze Temperature, F	Braze Atmosphere	Vis- Wet
Nickel 200 and Nickel 270	90%Ag-10%Pd (RB0170-062)	1975	Hydrogen	G
	82%Au-18%Ni (RB0170-064)	1800	Hydrogen	G
	90%Ag-5%Pd-4% Cu-1%Ni (RB0170-105)	1800	Hydrogen	G
	72%Ag-28%Cu (AWS, BAg-8)	1500	Argon*	G
	60%Ag-30%Cu-10%Sn (Handy and Harman Braze 603)	1350	Argon*	G
	61.5%Ag-24%Cu- 14.5%In (Handy and Harman Braze 615)	1350	Argon*	G
Beryllium Copper	62%Cu-35%Au-3%Ni (RB0170-065)	1900	Hydrogen	G
	50%Au-50%Cu (Handy and Harman Premabraz 402)	1800	Hydrogen*	G
	72%Ag-28%Cu (AWS, BAg-8)	1500	Argon*	G
	60%Ag-30%Cu-10%Sn (Handy and Harman Braze 603)	1350	Argon*	G
	61.5%Ag-24%Cu -14.5%In (Handy and Harman Braze 615)	1350	Argon*	G

*Flux applied to specimens

TABLE 21

TS, NICKEL 200, 270, AND BERYLLIUM COPPER

Braze Atmosphere	Visual Examination		Microstructure Examination	
			Alloying, inch	Intergranular Penetration, inch
	Wetting	Flow		
Hydrogen	Good	Good	< 0.001	< 0.001
Hydrogen	Good	Good	< 0.0015	< 0.001
Hydrogen	Good	Good	< 0.001	< 0.001
Argon*	Good	Fair	< 0.001	< 0.001
Argon*	Good	Fair	< 0.001	< 0.001
Argon*	Good	Fair	< 0.001	< 0.001
Hydrogen*	Good	Good	Grain Boundary Melting	
Hydrogen*	Good	Good	0.006	< 0.001
Argon*	Good	Fair	0.003	< 0.001
Argon*	Good	Fair	0.004	< 0.001
Argon*	Good	Fair	0.005	< 0.001

CONFIDENTIAL

This page is intentionally left blank

CONFIDENTIAL

CONFIDENTIAL

TABLE 22

BRAZING FEASIBILITY TESTS

Tubing Material	Braze Filler Metal	Braze Temperature, F	Braze Atmosphere	Vi
				We
OFHC Copper	62%Cu-35%Au-3%Ni (RB0170-065)	1900	Hydrogen	
	50%Au-50%Cu (Handy and Harman Premabraz 402)	1800	Hydrogen	
	72%Ag-28%Cu (AWS, BAg-8)	1500	Argon*	
	60%Ag-30%Cu-10%Sn (Handy and Harman Braze 603)	1350	Argon*	
	61.5%Ag-24%Cu -14.5%In (Handy and Harman Braze 615)	1350	Argon*	

*Flux applied to specimens

TABLE 22

FEASIBILITY TESTS, OFHC COPPER

Braze Atmosphere	Visual Examination		Microstructure Examination	
			Alloying, inch	Intergranular Penetration, inch
	Wetting	Flow		
Hydrogen	Good	Good	0.0056	< 0.001
Hydrogen	Good	Good	< 0.001	< 0.001
Argon*	Good	Fair	0.002	< 0.001
Argon*	Good	Fair	0.0015	< 0.001
Argon*	Good	Fair	0.002	< 0.001

CONFIDENTIAL

This page is intentionally left blank

CONFIDENTIAL

CONFIDENTIAL

TABLE 23

MECHANICAL STRAIN AT ELEVATED TEMPERATURE FATIGUE TESTS, SUMMARY OF TEST CONDITIONS

Material	Condition	Cyclic Strain, in./in.	Test Temperature, F	No. of Specimens
Type 347 Stainless Steel	Annealed, 1975 F	0.0360	1650	2
Nickel 200	Annealed, 1350 F	0.0257	1400	2
Nickel 200	Annealed, 1350 F	0.0257	1100	2
Nickel 200	ADP Step Braze Cycle, 1975 F	0.0257	1400	1
Nickel 200	ADP Step Braze Cycle, 1975 F	0.0257	1100	1
Nickel 270	ADP Step Braze Cycle, 1975 F	0.0257	1400	2
Nickel 270	ADP Step Braze Cycle, 1975 F	0.0257	1100	2
OFHC Copper	Annealed, 900 F	0.0134	750	2
OFHC Copper	Annealed, 900 F	0.0134	500	2
OFHC Copper	ADP Step Braze Cycle, 1900 F	0.0134	750	1
OFHC Copper	ADP Step Braze Cycle, 1900 F	0.0134	500	1
Beryllium Copper Alloy 10	ADP Step Braze Cycle, 1800 F	0.0098	750	1
Beryllium Copper Alloy 10	ADP Step Braze Cycle, 1800 F	0.0098	500	1
Beryllium Copper Alloy 10	Heat Treat to Optimum Properties	0.0098	750	2
Beryllium Copper Alloy 10	Heat Treat to Optimum Properties	0.0098	500	2

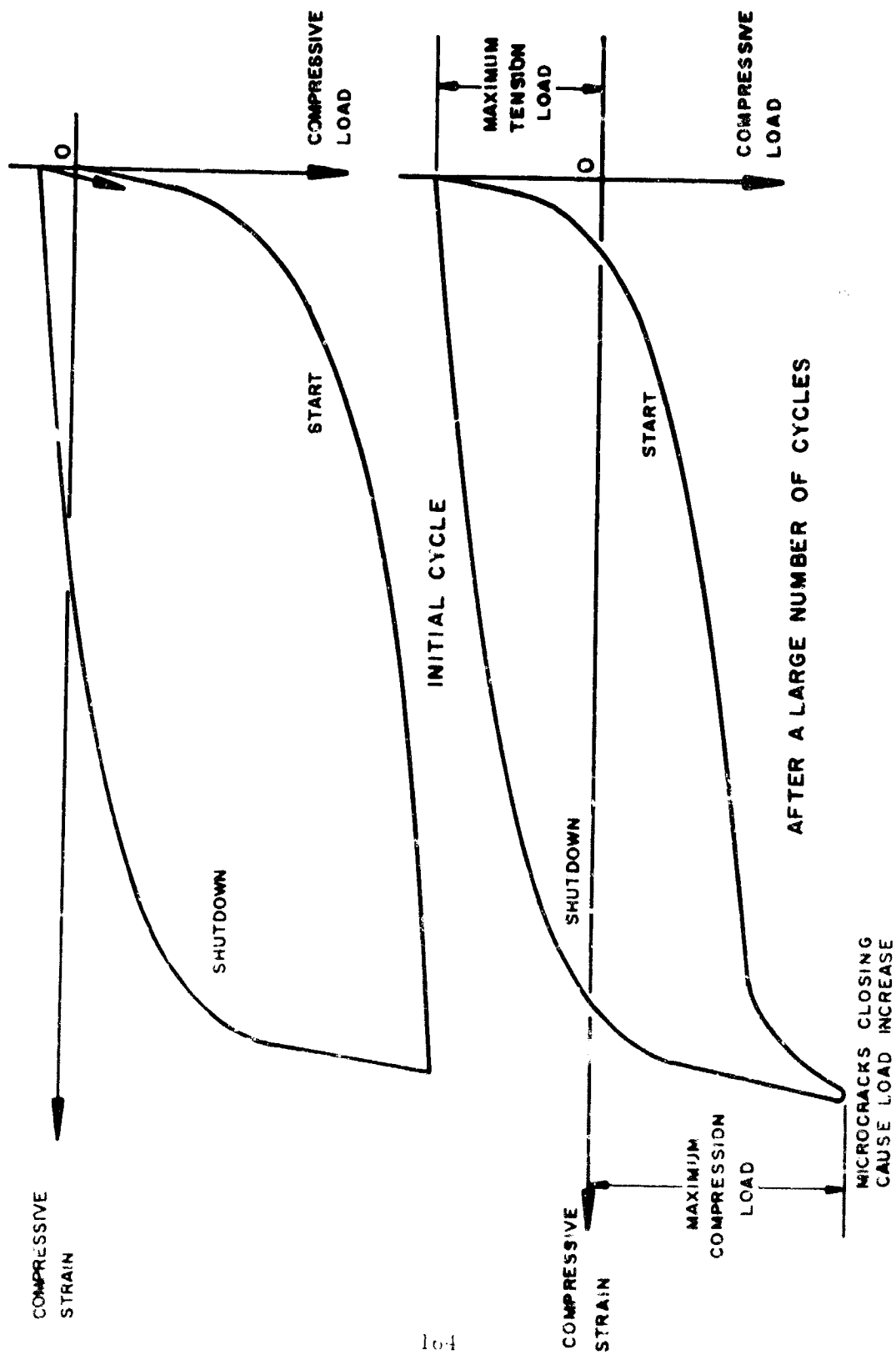


Figure 73. Axial Load, Strain Cycle for a Thrust Chamber Tube

CONFIDENTIAL

of curves for each common material and process condition were then drawn for each specimen run at various test temperatures.

(U) Figure 74 shows two such curves for furnace brazed nickel 200. Since the thermally induced strain in a thrust chamber tube actually occurs over a range of temperatures, an average temperature fatigue curve has been estimated. The arithmetic average used was felt to be conservative for this case.

(U) The average curves for each material, both in the annealed and processed condition plotted together for comparison purposes, are shown in figure 75. These curves are useful in comparing materials, as well as for estimating the number of start sequences required to cause transverse through-cracks in a thrust chamber tube.

(U) The tube simulation fatigue tests were initiated in the second quarter. A typical formed tube and completed tube specimen is shown in figure 76. An instrumented tube specimen installed in the tube tester prior to installation of the pressure chamber is shown in figure 77. A spring-loaded chromel/alumel thermocouple located on the tube crown (center of specimen) is used for the programmed cycling control. Other instrumentation shown includes voltage pickups and electrically insulated thermocouples at the ends of the heated specimen. Similar instrumentation is employed on the diametrically opposed tube crown.

(U) Several tube tester specimens were thermally cycled to failure. These include three 347 CRES tubes and one Hastelloy-X tube, all of 0.010-inch wall thickness. These materials were tested prior to nickel and copper because of material availability. Also, the analytical model was initially based on data obtained from J-2 thrust chamber tests and other sources. Most experimental data available were on stainless steel. Cyclic fatigue data obtained agree with the analytical technique and data used for predicting the fatigue life of ADP tubular chambers. One OFHC copper and two nickel 200 specimens were fabricated. Testing of these specimens is scheduled for the next quarter.

(U) The test results of the stainless-steel and Hastelloy-X tube specimens are summarized in Table 24. The coolant-side operating conditions, hydrogen flowrate, and bulk temperature (ambient), were maintained constant for all tests. Each cycle was programmed for 27 seconds duration which consisted of a 6-second hold at elevated temperature, a 5-second ramp, a 5-second decay, and an 11-second hold at ambient temperature.

CONFIDENTIAL

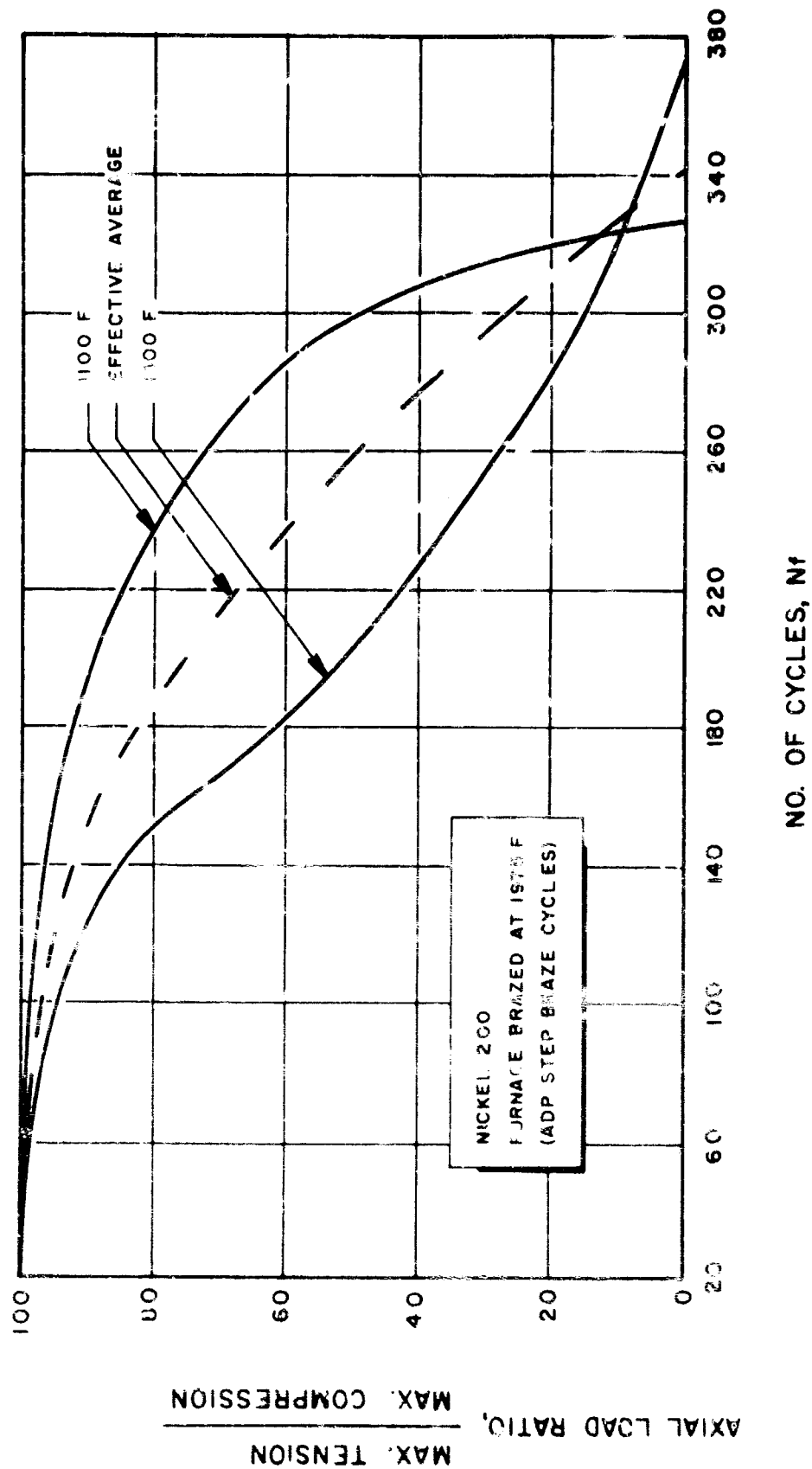


Figure 24. Mechanical Strain at Elevated Temperatures, Test Results on Braze Nickel 200

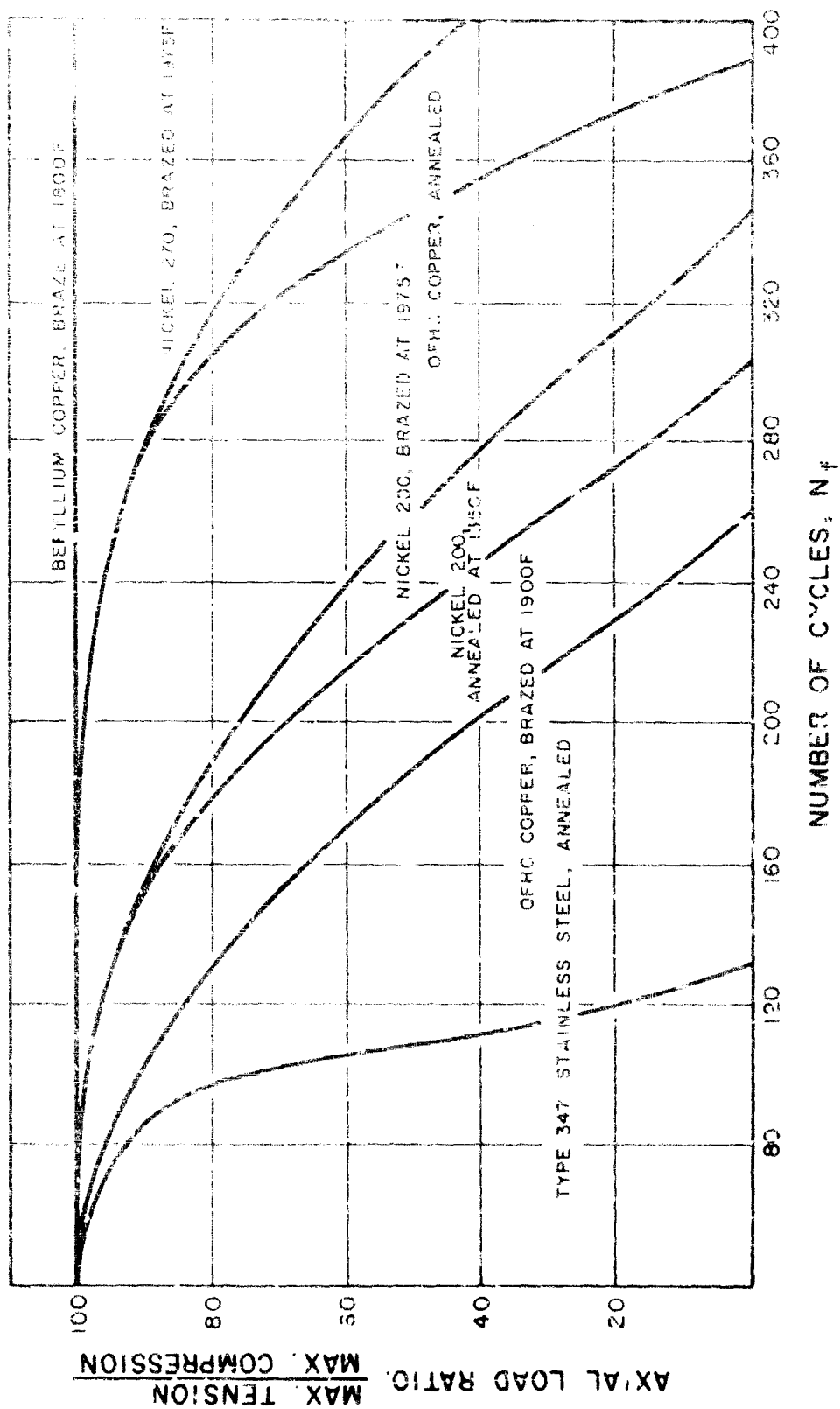
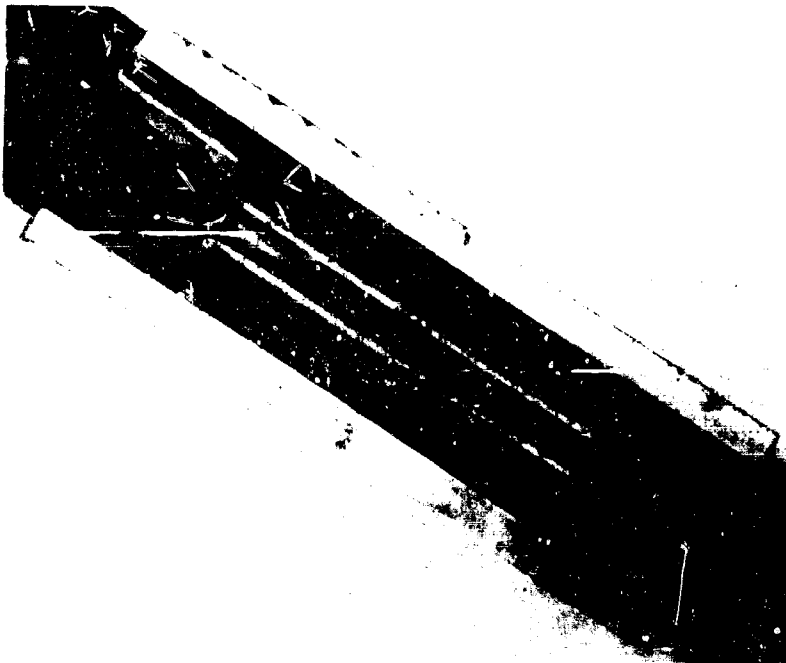


Figure 75. Mechanical Strain at Elevated Temperatures, Test Results of Candidate Materials



(a)

LX



(b)

Figure 76. Typical Tube Tester Thermal Fatigue Crack
(347 CRES Specimen After 500 Cycles at
70 to 1100 F)

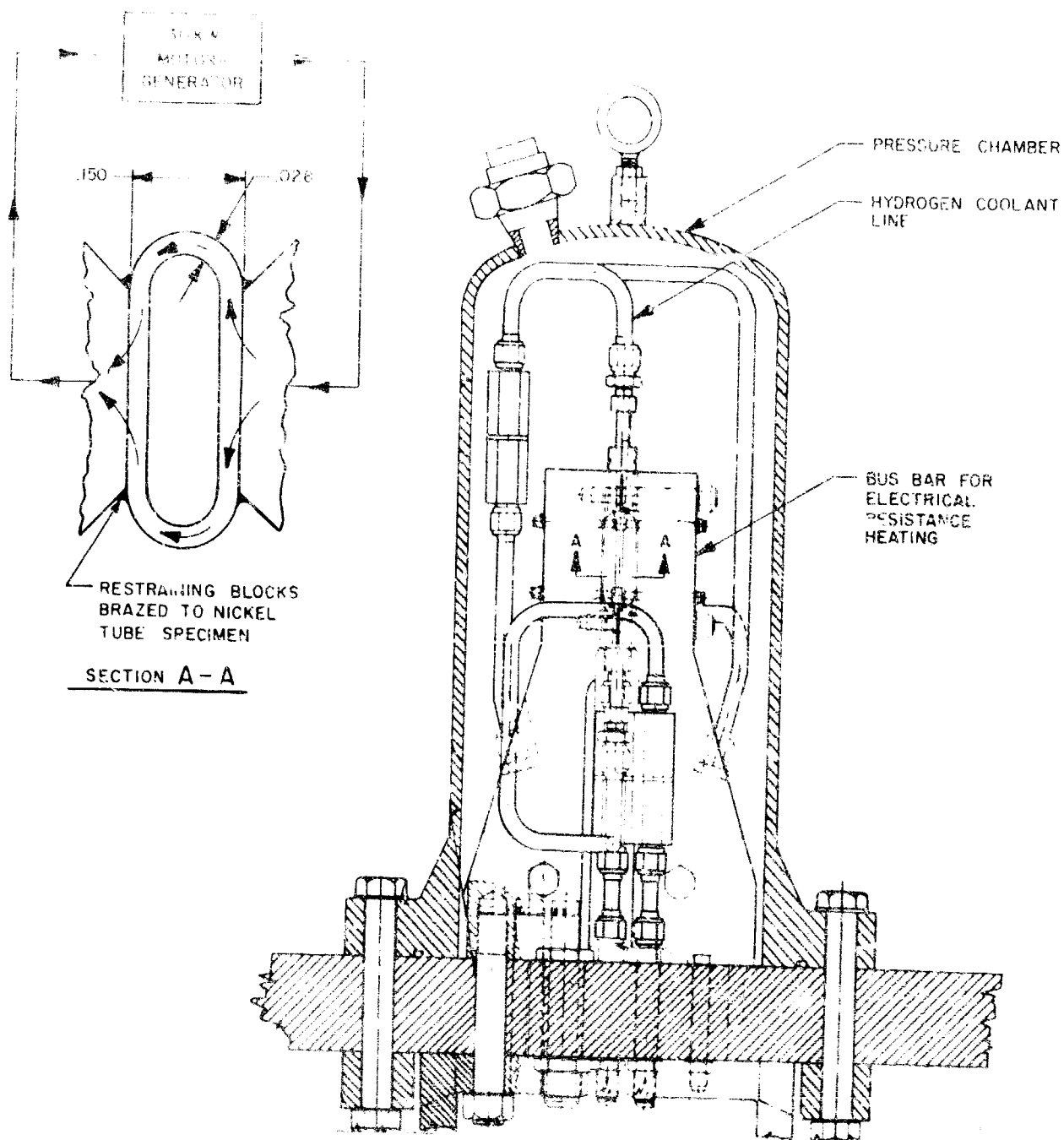


Figure 77. Thrust Chamber Tube Tester (High Pressure)

TABLE 24

HASTELLOY-X VS STAINLESS STEEL TEST RESULTS

Specimen Tested	Maximum Wall Temperature, F	Heat Flux Btu/in. ² -sec	ΔT Wall	Predicted N_f Cycles	Test N_f Cycles	Calculated $\Delta \epsilon_p$
347 CRES	1100	13.1	220	270	270	0.0243
347 CRES	1600	15.9	236	68	64	0.0392
347 CRES	2050	19.9	278	--	9	0.0550
Hastelloy-X	1600	17.8	260	--	21	0.0310

* Cyclic plastic strain based on test operating conditions.

CONFIDENTIAL

(U) One test was run at 1100F wall temperature, this being the highest temperature at which cyclic fatigue data were available on stainless steel. Although this steel specimen tested at 1100F incurred thermal fatigue cracks at 270 cycles, testing was resumed to 300 cycles. Cracks were detected by both a rise in tube external (bell jar) pressure and by infrared TV coverage. Testing beyond initiation of fatigue cracks simulated thrust chamber operation with transverse tube cracks. Figure 76 depicts tube failures photographed after 300 cycles.

(U) Another stainless steel specimen was targeted for 1600F, which is the anticipated operating gas-side tube-wall temperature for stainless-steel tubes in the ADP thrust chamber; the 2050F test provides data on the reduction in cyclic fatigue life at extremely high wall temperatures.

(U) Even though stainless steel will not be considered for the demonstrator module tubes, these results are significant in providing an experimental check on the method of prediction of cyclic fatigue life analytically from material properties determined in the laboratory. Additionally, these tube tester results on stainless steel are correlated with actual hot-line life of stainless-steel tubes used on the J-2 thrust chamber, to calibrate the analysis further.

(U) The agreement of the tube tester type 347 stainless-steel test results with the life characteristics used to predict the life for the ADP chamber is reflected in Table 24. Based on these results, it is believed that the analytical model can be used with confidence in predicting the thermal fatigue life of the candidate thrust chamber materials. This will be verified with continuing testing of nickel and OFHC copper specimens.

(U) To select a tube material for the demonstrator segment thrust chamber, a criteria list was developed as an aid. The criteria were taken from life, performance, and fabrication considerations. Each tube material was then evaluated by these criteria, as determined from the results of the Materials Selection Program, from previous experience, from published literature, and from the results of the hot-firing tests.

(U) A comparison of the demonstrator segment thrust chamber tube materials, as determined by these criteria, is given in Table 25. It was concluded that nickel 200 offered the best combination of necessary features for this application. This material was therefore selected, in combination with a process cycle which produced the best obtainable properties.

CONFIDENTIAL

TABLE 25

FACTORS AFFECTING SELECTION OF 20K-SEGMENT TUBE MATERIAL

(Based on State-of-the-Art Fabrication Technology and ADP
Operating Conditions)

Material Criterion	Type 347 Stainless Steel	Nickel 200	Nickel 270	OFHC Copper
Strength to Withstand Hydraulic Stress	Good	Good	Poor	Good
Thermal Stress Fatigue Resistance	Poor	Good	Poor	Fair
Metallurgical Stability	Excellent	Good	Poor	Poor
Oxidation-Erosion Resistance	Good	Good	Good	Good
System Compatibility	Excellent	Good	Good	Fair
Comparative Coolant Pressure Drop	1.0	0.85	0.75	0.95
Comparative Weight	1.0	1.05	1.05	1.20
Up-rating Capability	Poor	Fair	Fair	Good
Drawing, Tapering, and Forming Confidence	Good	Excellent	Excellent	Good
Brazing Confidence	Excellent	Good	Good	Poor
Availability	Good	Good	Good	Good
Total Cost	Low	Low	Low	Low

CONFIDENTIAL

(U) A similar comparison was made of the long-range candidate materials (Table 26). It was seen that the beryllium copper alloy No. 10 material offered a large increase in thermal fatigue resistance, especially in the fully heat-treated condition. This is due to the fact that no plastic strain is induced in this condition. Its practical thrust chamber use, however, awaits the development of suitable manufacturing processes.

c. Problem Areas and Solutions

No particular problem areas have been encountered on this effort to date.

d. Testing

(1) Test Results

Results of laboratory and simulator experiments were discussed in the Progress During Report Period section. There were no hot-fire test results.

(2) Test Facilities and Procedures

(C) Program Test Plan for 2.5K Tube-Wall Chamber. A test plan has been written for the 2.5K tube-wall chambers. The primary objective of this test program is to evaluate regenerative-cooling capability of each tube material to chamber pressures of 1500 psia.

(C) A tentative test schedule for each chamber is shown in Table 27. All tests will be run at a chamber mixture ratio of 5.0, because this approximates the maximum heat fluxes. Test duration will be 5 seconds to ensure steady-state instrument readings. Hardware instrumentation will include heat transfer and performance measurements. Direct hot-gas, wall-temperature measurements will be attempted using braze alloy spots on the tube surface and also by using small thermocouples brazed to the tube surface. Coolant measurements will include flowrate and inlet and outlet temperatures and pressures. For performance, thrust, chamber pressure, injection flowrates, and hydrogen injection, temperature will be measured.

(U) Tube Instrumentation. The two techniques investigated to obtain gas-side, tube-wall temperatures were: (1) installation of micro-miniature thermocouples, and (2) application of braze alloy deposits on tube-wall surfaces. Braze alloy deposits will be selectively employed on the 2.5K chambers.

CONFIDENTIAL

TABLE 26

FACTORS AFFECTING SELECTION OF LONG-RANGE TUBE MATERIALS
(Based on Current Knowledge and ADP Operating Conditions)

Material Criterion	Boron Deoxidized Copper	Beryllium Copper Partial Heat Treat	Beryllium Copper Full Heat Treat
Strength to Withstand Hydraulic Stress	Good	Excellent	Excellent
Thermal Stress Fatigue Resistance	Good	Excellent	Unlimited
Metallurgical Stability	Good	Excellent	Excellent
Oxidation-Erosion Resistance	Fair	Good	Excellent
System Compatibility	Fair	Good	Good
Comparative Coolant Pressure Drop	0.95	0.95	0.95
Comparative Weight	1.20	1.05	1.05
Upgrading Capability	Good	Excellent	Excellent
Drawing, Tapering, and Forming Confidence	Good	Unknown	Unknown
Brazing Confidence	Poor	Poor	Poor
Availability	Fair	Good	Good
Total Cost	Low	Moderate	Moderate

CONFIDENTIAL

TABLE 27

TENTATIVE TEST SCHEDULE FOR EACH CHAMBER

Test No.	Chamber Pressure, psi	Mixture Ratio (Coolant), o/f	Mixture Ratio (Chamber), o/f	Duration, seconds
1	300	5	5	5
2	300	6	↑	↑
3	600	5	↑	↑
4	600	6	↑	↑
5	900	5	↑	↑
6	900	6	↑	↑
7	1100	4	↑	↑
8	1100	5	↑	↑
9	1100	6	↑	↑
10	1300	4	↑	↑
11	1300	5	↑	↑
12	1300	6	↑	↑
13	1500	4	↑	↑
14	1500	5	↑	↑
15	1500	6	↓	↓
16	1500	7	5	5

CONFIDENTIAL

(U) The evaluation of braze alloy remelt temperatures and their application were completed and reported last quarter. These temperature indicators will be applied post-furnace brazing of the assembly. This is necessary because the furnace braze alloy melting temperature is higher than that of applicable temperature indicators. Braze alloy deposits will be used in accessible (divergent region) areas only.

(U) Micro-miniature thermocouple installations using high-temperature (1900F) braze were unsuccessful. This high-temperature application was necessary because the thermocouples must be installed prior to furnace brazing the tubular chamber assembly. The installations resulted in gas-side tube surface discontinuities which were not acceptable for the operating conditions of the ADP thrust chamber.

e. Summary of Planned Effort for Next Report Period

(U) Fabrication of a 2.5K copper chamber segment and a nickel chamber segment will be completed and testing initiated shortly thereafter. The thrust chamber materials investigation will be directed toward the derivation and programming of an extensive tube stress analysis program. More rigorous analytical techniques will be developed which take into account the complete stress and strain history of a thrust chamber tube during a typical mission cycle.

CONFIDENTIAL

3. THRUST CHAMBER NOZZLE DEMONSTRATION

One of the major objectives of the fabrication and test task of the current program is to demonstrate performance capability of the aerospike thrust chamber. Full-scale, 250K thrust chambers duplicating the combustion and nozzle expansion features of the demonstrator module thrust chamber are being used for performance demonstration. One solid-wall 250K chamber is being fabricated for the following purposes:

1. Verify injector integrity and compatibility before exposing tube wall chamber
2. Evaluate hypergolic and hot-gas ignition
3. Rate the injector-combustor stability by pulse gun as well as operational test
4. Provide an alternative means of evaluating combustor and nozzle performance
5. Evaluate tapoff gases and demonstrate feasibility of tapoff source of turbine power on the aerospike chamber

Two 250K tube-wall chambers are being fabricated to provide long-duration capability for performance measurements. These chambers will be operated with varying degrees of base bleed and in a diffuser for simulating altitude conditions.

Injector and combustor features duplicate those presently being designed into the demonstrator module chamber.

a. Status

(U) All forgings for the inner bodies have been received. The first forging (to be used on the solid-wall chamber) has been rough machined and the OFHC copper surfacing has been completed. The final finish machining for contour is progressing (figure 78). The welding of the second inner body ring forgings to the conical assembly for the first tube-wall inner body is being completed.

(U) The outer film-cooled solid-wall body (figure 79) has the film coolant ring (figure 80) welded in place and the welding of the OFHC copper on the surface is in progress. The ring forging for the first tube-wall outer body has been received and rough machining has been completed. The propellant feed holes are now being drilled.

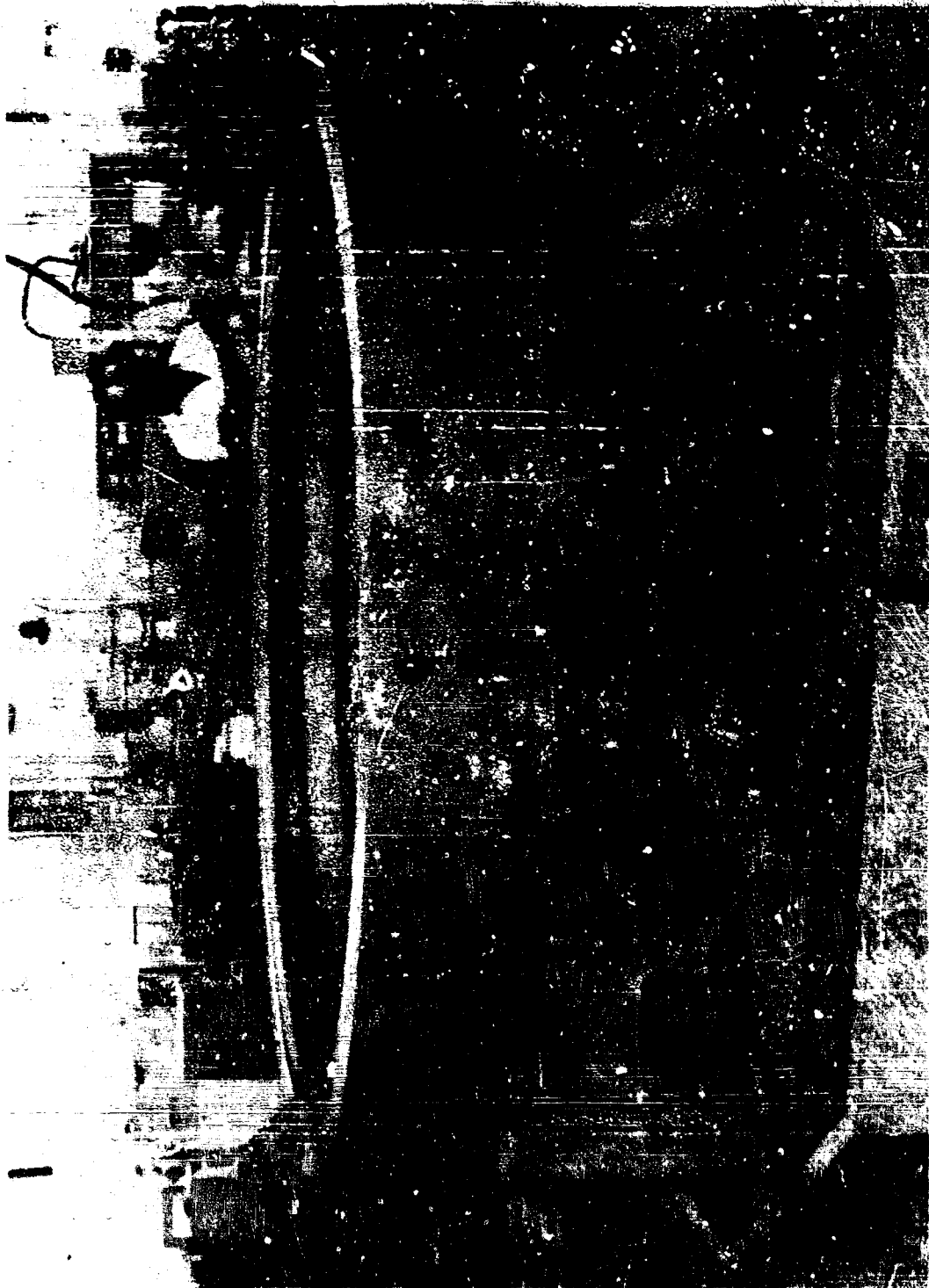
CONFIDENTIAL



Figure 78. ADP Inner Solid Wall Nozzle No. 1

CONFIDENTIAL

CONFIDENTIAL



1X732-8/16/66-515

Figure 79. ADP Outer Solid Wall No. 1

CONFIDENTIAL

CONFIDENTIAL



LXA2-7/21/66-CID

Figure 80. Solid Wall Inner Film Coolant Ring

CONFIDENTIAL

CONFIDENTIAL

(U) The pilot runs with the tube forming dies have been completed. The tubes for the brazing test specimen are currently being formed (figure 81). The flow test unit (figure 82) for calibrating the tubes has been completed and initial checkouts accomplished with satisfactory results.

(U) The first injector assembly has been machined and all of the propellant feed holes have been drilled. Currently, the oxidizer and fuel manifolds are being welded in place (figure 83). The second unit has been rough machined and the propellant feed holes are being drilled. Detail fabrication of the oxidizer and fuel manifolds is progressing. The baffles for the first unit are at the electroform supplier for the depositing of copper on the face of the baffle.

b. Progress During the Report Period

(1) 250K Solid-Wall Thrust Chamber

(C) The final solid-wall chamber design (figure 84 and 85) is composed of two major units: the outer body of the combustion chamber and expansion shroud, and an inner body and expansion nozzle. Radial and axial positioning of the inner and outer body are maintained by attachment to the injector. Thermal and pressure loads are transmitted through shear lips on the interface at the attach bolt circle. Thrust loads are transmitted through the inner chamber body, utilizing an eight-point thrust mounting structure (figure 86). A thrust duration of approximately 0.7 second at full thrust is made possible through the utilization of film cooling and copper-lined throat. The inner and outer body are presently 20 percent completed. Both bodies have the coolant manifolds and inlets finish machined and film coolant orifice rings welded in place. Presently, the copper weld for the throat region is in work. Upon completion of welding, the inner contour and balance of the chamber will be finish machined.

(U) The inner and outer combustor body finalized design (figure 84 and 85) incorporates film coolant rings located 1.5 inches above the throat. The coolant flows through orifices in the ring which are directed toward the converging wall of the throat, providing a boundary layer of coolant along the surfaces of the throat and nozzle. To improve the life capability of the chamber further, the throat is lined with 0.75-inch thick, high thermal conductivity copper which provides a margin of safety during operation and also the potential of brief operation without coolant.

(U) The injector used with the solid-wall chamber assembly is identical to that planned for the tube-wall assemblies except, since there is no circulation of fuel in the injector crossover passages during solid-wall

CONFIDENTIAL

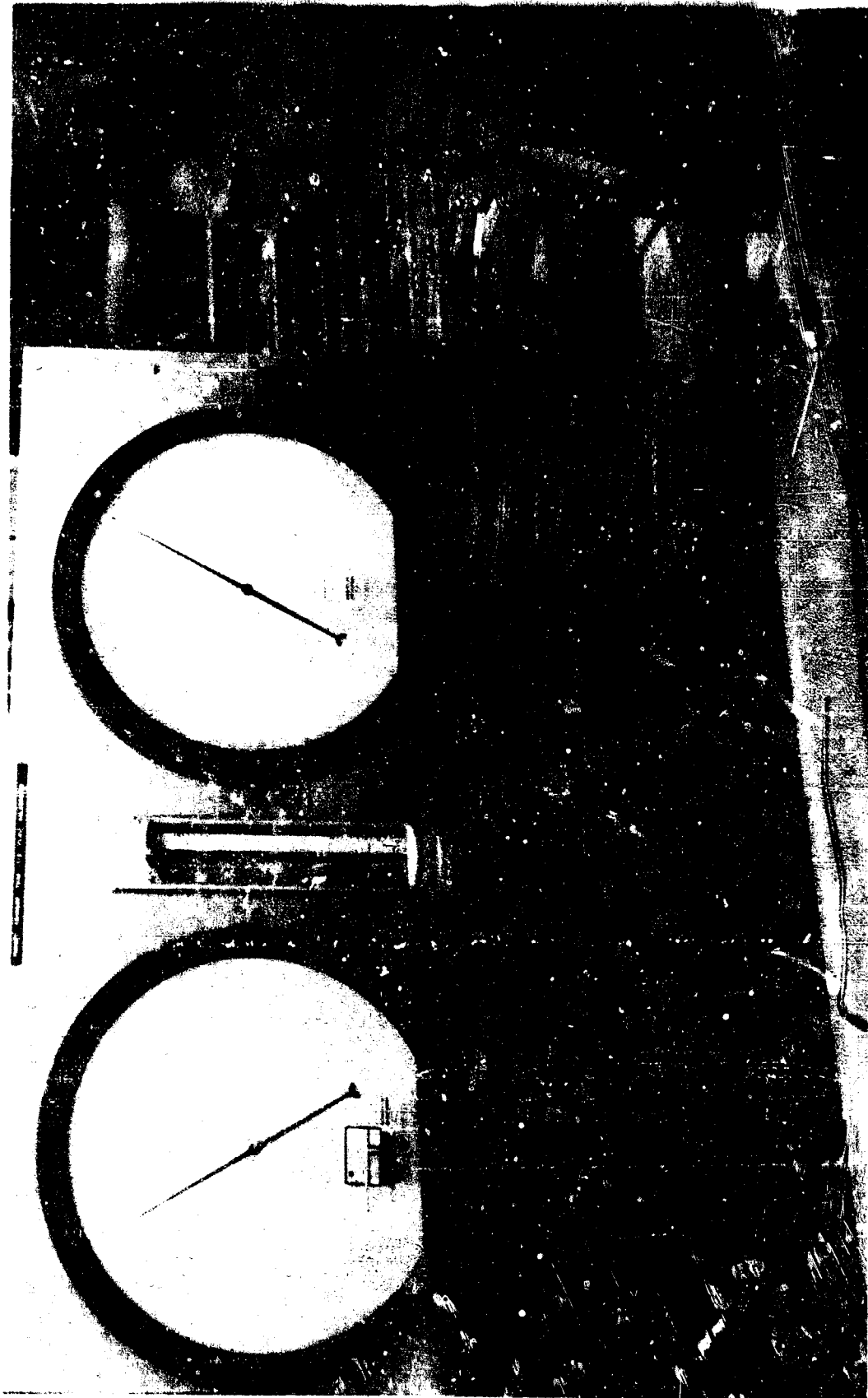


11E31-9/8/66-C1

Figure 81. Inner and Outer Thrust Chamber Tubes

CONFIDENTIAL

CONFIDENTIAL



LXE42-8/26/66-CLK

Figure 32. ADP Thrust Chamber Tube Calibration Console

CONFIDENTIAL

CONFIDENTIAL



DX32-8/16/66-CIB

Figure 83. ADP Injector No. 1

CONFIDENTIAL

CONFIDENTIAL

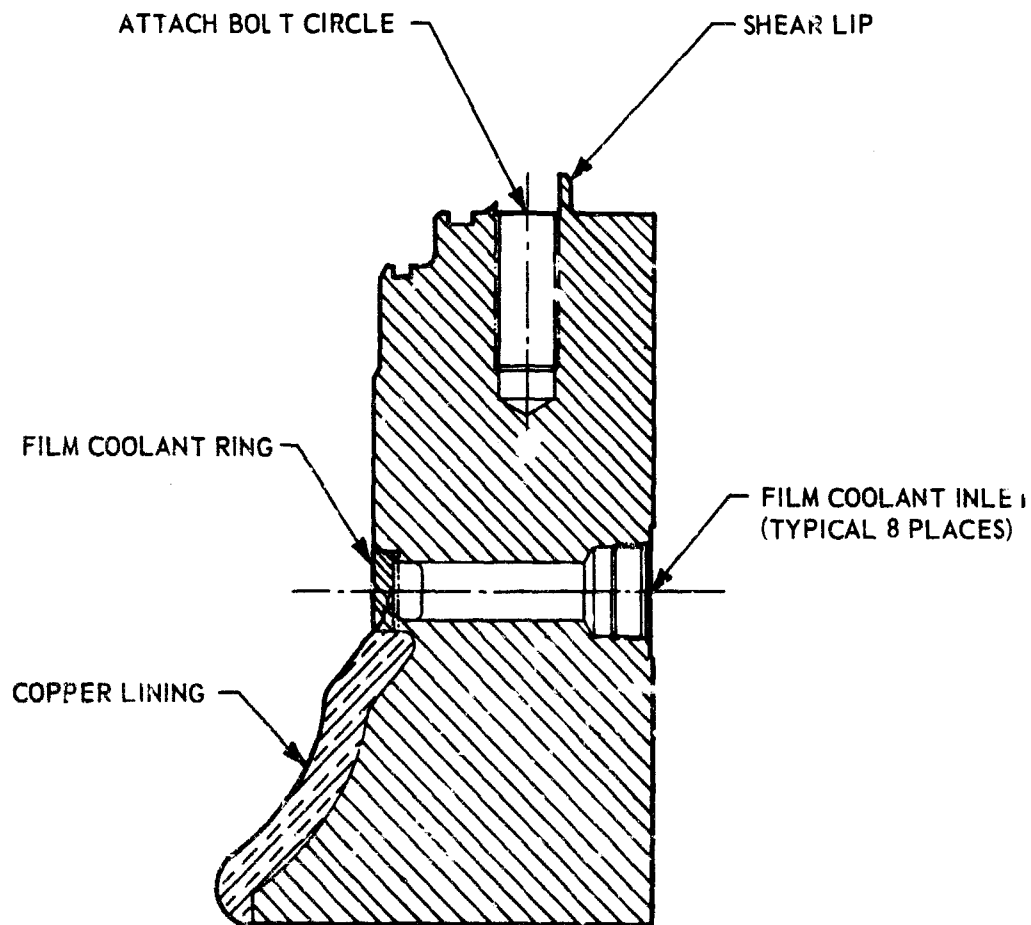


Figure 84. 250K Solid Wall Thrust Chamber Outer Body Assembly

CONFIDENTIAL

CONFIDENTIAL

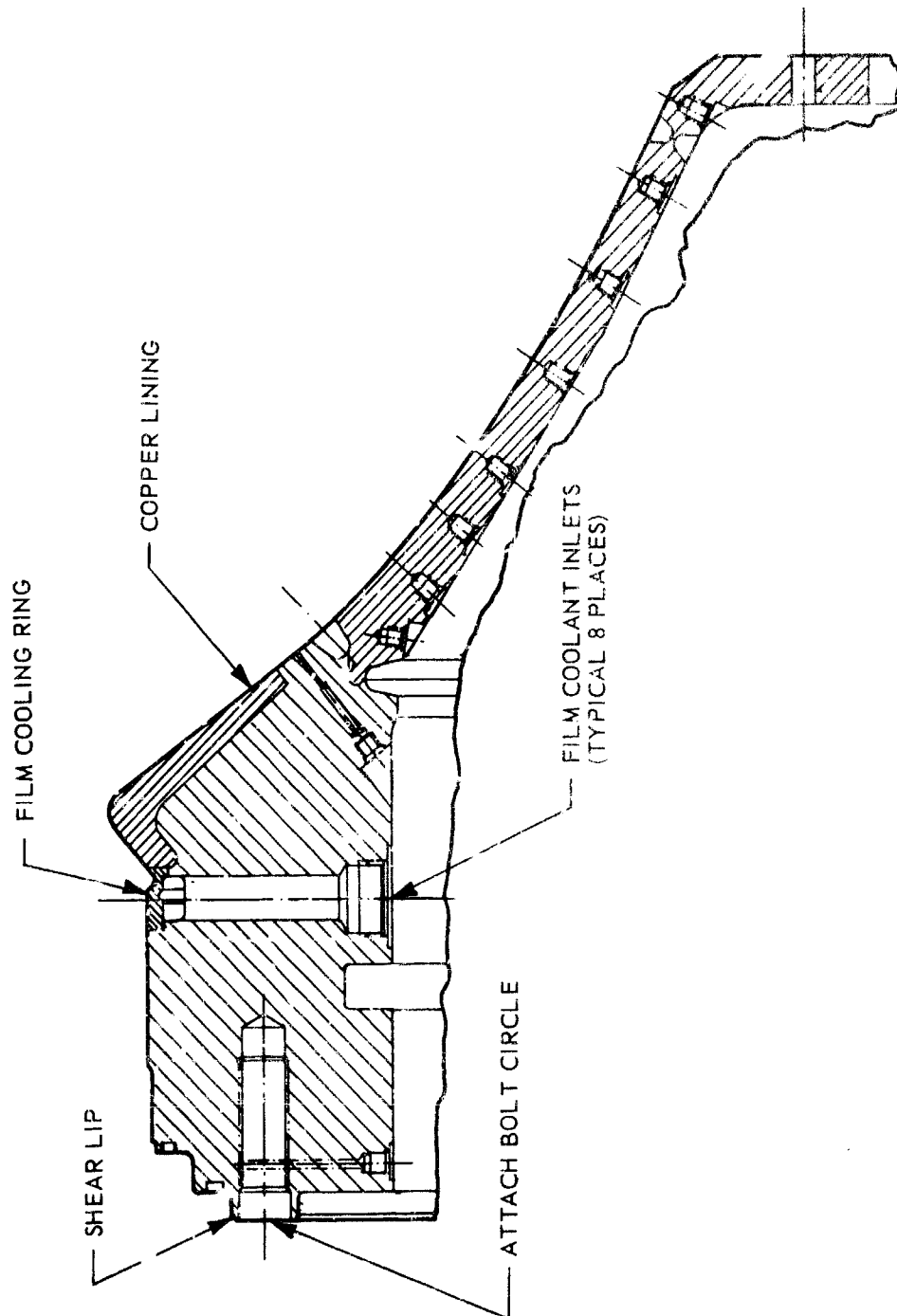
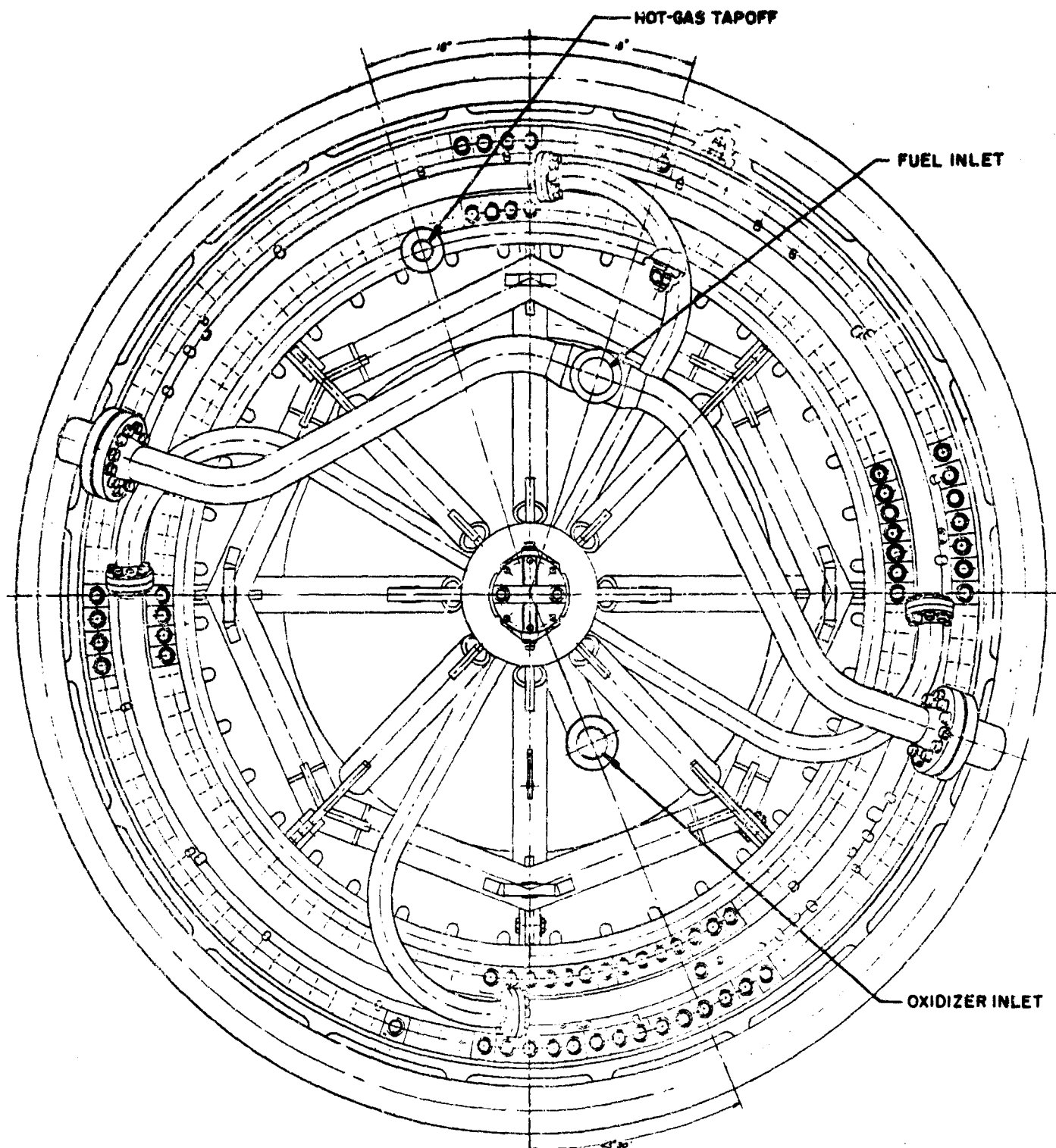


Figure 35. 250K Solid Wall Thrust Chamber Inner Body Assembly

CONFIDENTIAL

CONFIDENTIAL



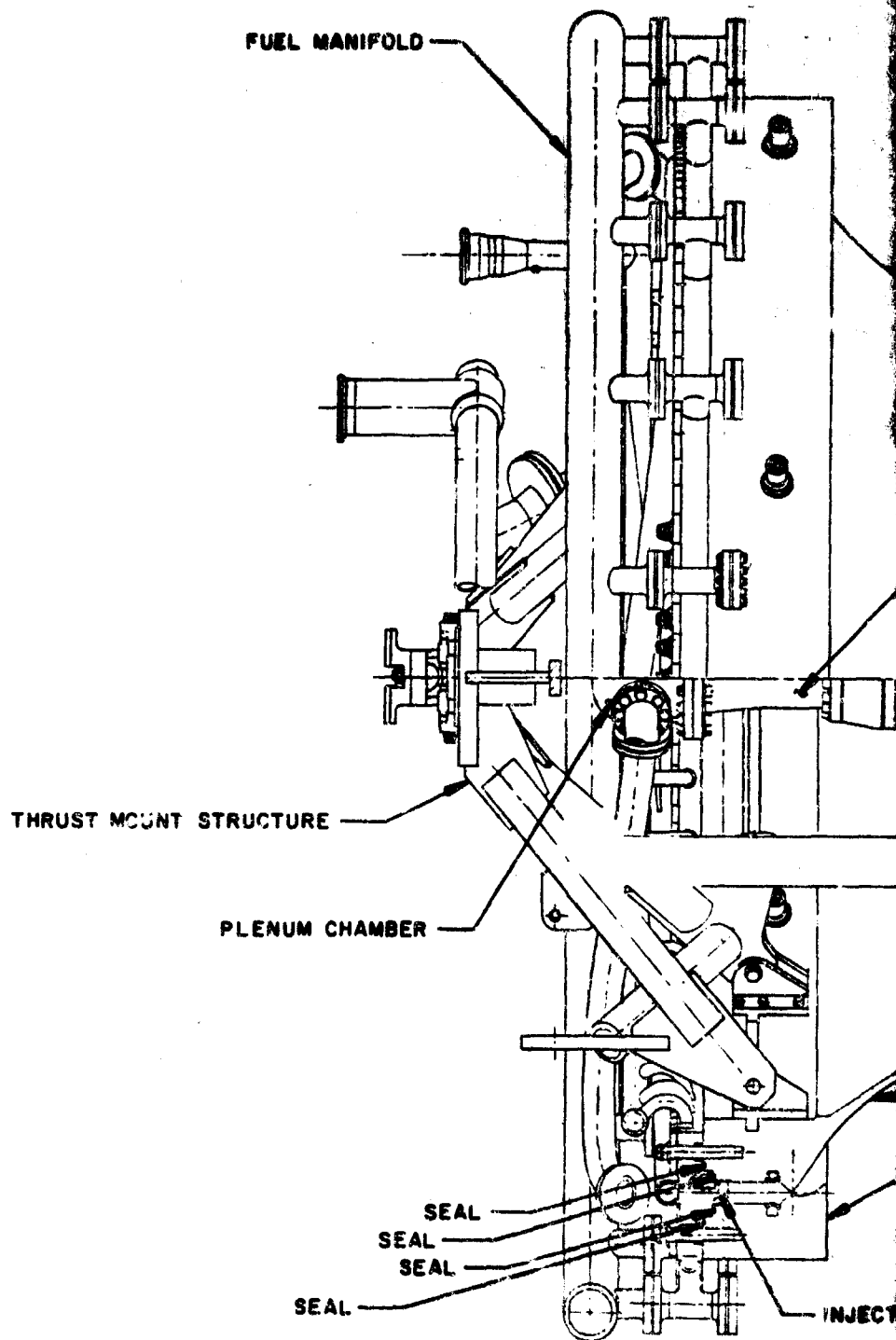


Figure 86. 250
Th

2

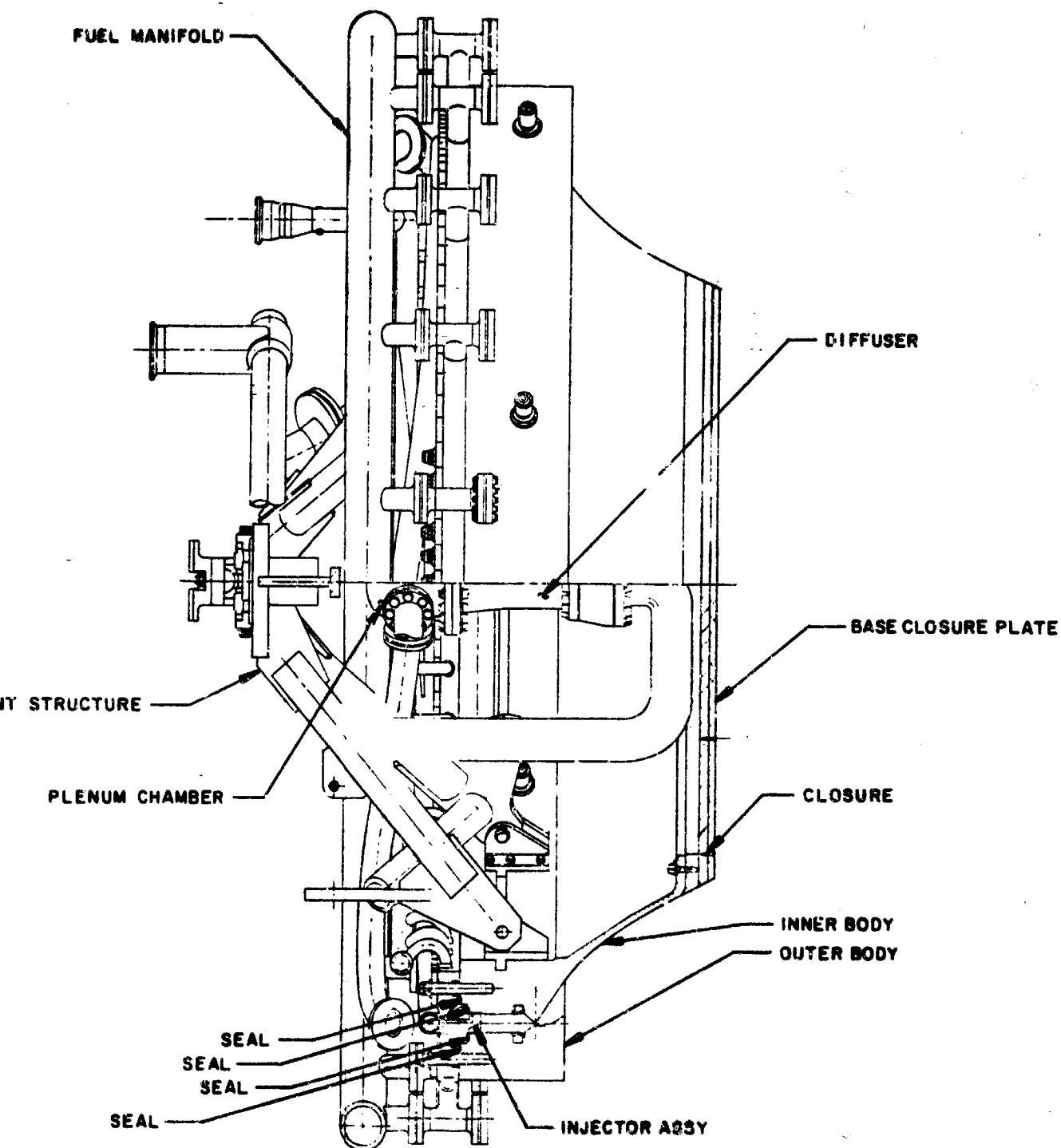


Figure 86. 250K Film Cooled Solid Wall Thrust Chamber

CONFIDENTIAL

This page is intentionally left blank

CONFIDENTIAL

CONFIDENTIAL

chamber testing, two pressurizing ports will be directed into the manifold in this area to maintain an inert gas pressure greater than the chamber across the seals between the injector and chamber bodies.

(C) The oxidizer is directed from the facility supply source through a line into the diffuser and the plenum chamber which then distributes the oxidizer through four tangential inlets in the manifold. Here, it is fed directly to the injector passageways leading to the oxidizer injection orifices. The fuel also is directed from the facility through a supply line. From the distribution manifold, the fuel is fed through 20 inlets around the periphery of the injector fuel inlet manifold which feeds the injector orifices and baffles. Naflex seals are utilized for sealing all flanged connections in the fuel and oxidizer systems. A base closure plate is attached at the nozzle end. The entire thrust chamber is provided with extensive instrumentation boss attachments.

(C) Stability Testing Provisions. The instrumentation and stability provisions for the solid-wall engine were finalized this quarter. Stability testing will be accomplished by pulse guns in three adjacent compartments located 1 inch below the injector face. The pulse guns were chosen for their ability to provide a directional burst of energy in the region most likely to induce instability. Located on the outer wall of the thrust chamber (figure 87), the guns are easily serviced and insensitive to thermal detonation, allowing the chamber to be "pulsed" at any time during mainstage.

(U) The gun (figure 88) is designed to accept either a 300 H & H (rifle) or a 38 special (pistol) cartridge. The shell can utilize various powder loadings, and when utilized with burst diaphragms of 7500, 10,000, and 20,000 psig, provides varying values of over pressure.

(U) High-frequency pressure transducers provide data during stability runs for evaluation of over pressure and damping characteristics. The transducer ports (Photocon type) also may be adapted to streak photography windows.

(U) During the chamber run, an electrical squib is detonated and drives the firing pin into a standard rifle or pistol primer which ignites the powder. The burst diaphragm prevents the gas charge from escaping into the chamber until the full charge is developed.

(2) 250K Tube-Wall Thrust Chamber

The structural and mechanical design of the 250K tube-wall chamber were described in the previous quarterly. During this quarter,

CONFIDENTIAL

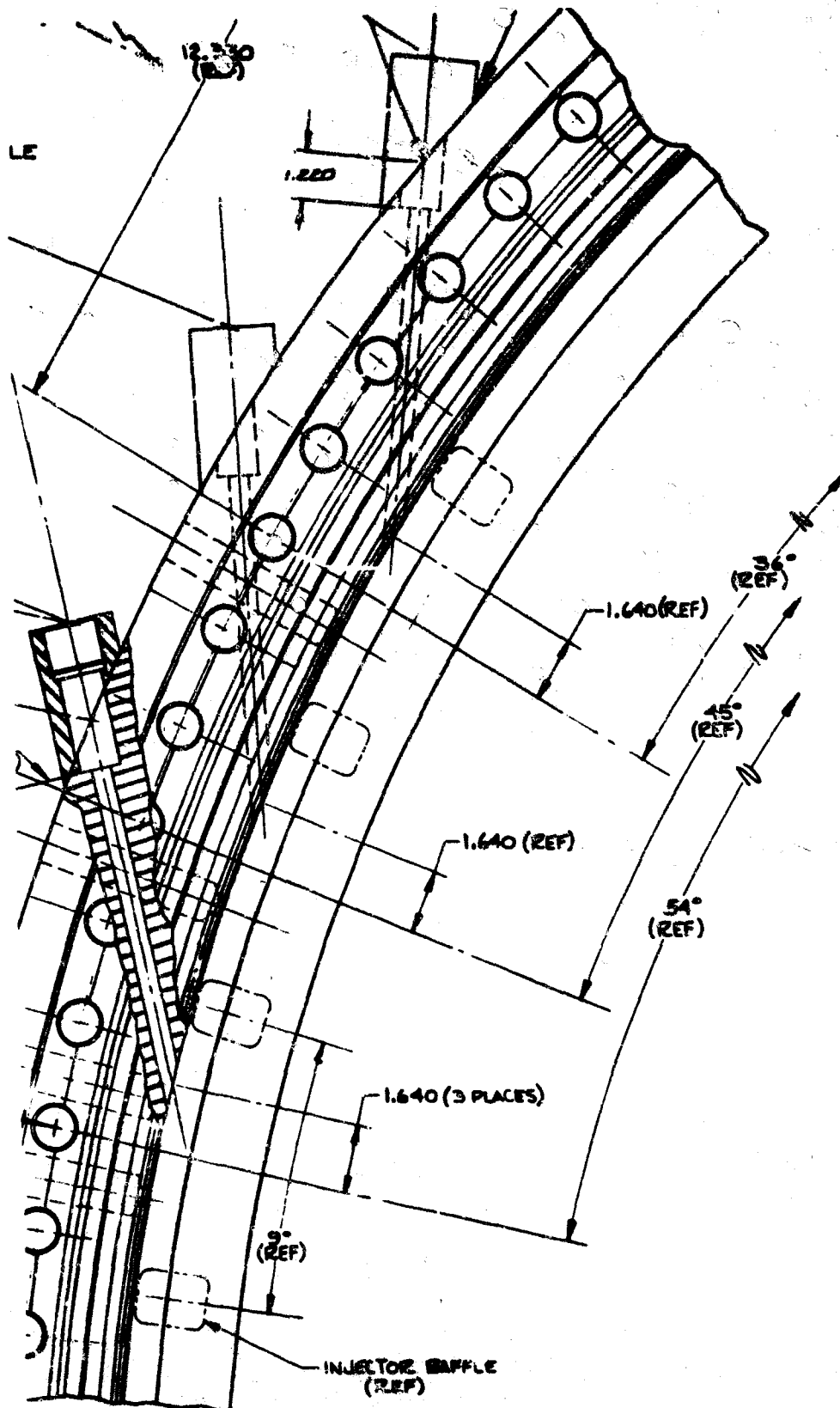


Figure 87. Chamber Locations of Pulse Gun Ports

CONFIDENTIAL

CONFIDENTIAL

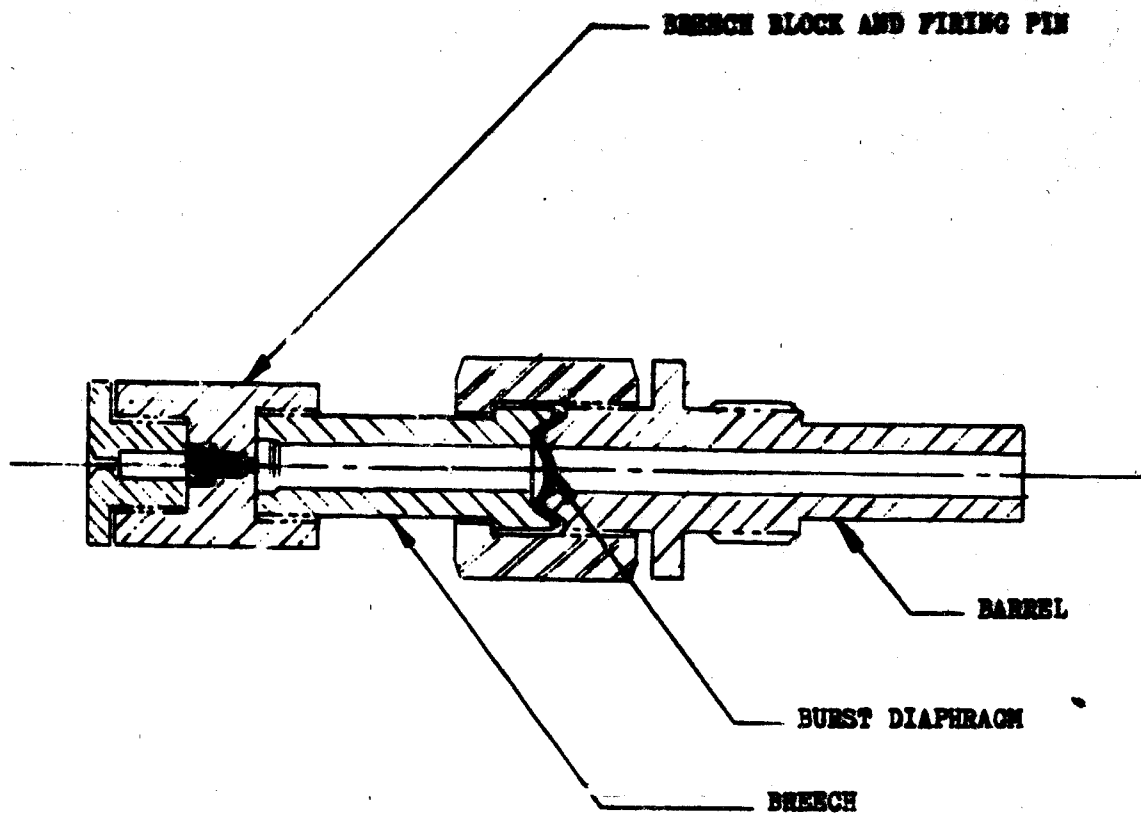


Figure 88. Pulse Gun

CONFIDENTIAL

CONFIDENTIAL

major design effort on this chamber was completed. Instrumentation requirements were determined and provisions for (1) temperature sensors, (2) static, high-frequency, and pressure pickups, and (3) other instruments were incorporated into the design.

(C) Nozzle. Continuity of the final aerodynamic spike nozzle contour design for the inner wall beyond the end of the regeneratively cooled section is obtained by the use of a solid-wall, uncooled nozzle extension. The extension begins 16.00 inches downstream of the throat, terminating 37.03 inches from the throat plane. The minimum wall thicknesses at various axial stations were defined during this quarter. Thermal and stress analyses were based on a backwall temperature of 100F and a hot-gas surface temperature of 2250F.

(U) The cone is fabricated of rolled and welded 304L CRES plate with welded flanges at either end. Instrumentation ports for pressure taps are provided at various axial locations for verification of nozzle pressure profile. The material order was released during this report period.

(U) Manifolding. The design and analysis of a balanced fuel distribution system has been completed in this report period. A constant area manifold with a maximum flow variation of less than 1.0 percent at the rated flow conditions has been selected for the fuel inlet to the inner wall tubes utilizing two inlets. Equal distribution from the inlets to the manifold is achieved through the use of tees incorporating flow splitters and directional vanes, as shown in figure 89. Fuel flow from a single facility interface to the fuel manifold is accomplished through the use of a symmetrical "Y" duct assembly using spacer Naflex seals at the manifold inlets.

(C) Finalization of the fuel circuit from the aft end of the outer wall tube to the injector fuel manifold tee also effected during this report period. Fuel flow from the tubes is evenly discharged to a collector manifold which is incorporated in the outer wall structure (figure 90). Fuel flow from the manifold is then carried by 20 equally spaced fuel transfer ducts to the injector inlet tees. That portion of the fuel which is bypassed returns to the facility via the fuel distribution manifold which is used for the inlet on the solid-wall, film-cooled thrust chamber. The fuel system schematic is shown in figure 91.

(U) Base Closure. Design of the base closure and secondary flow gas generator system for the tubular chamber inner wall assembly has been completed during this report period.

CONFIDENTIAL

CONFIDENTIAL

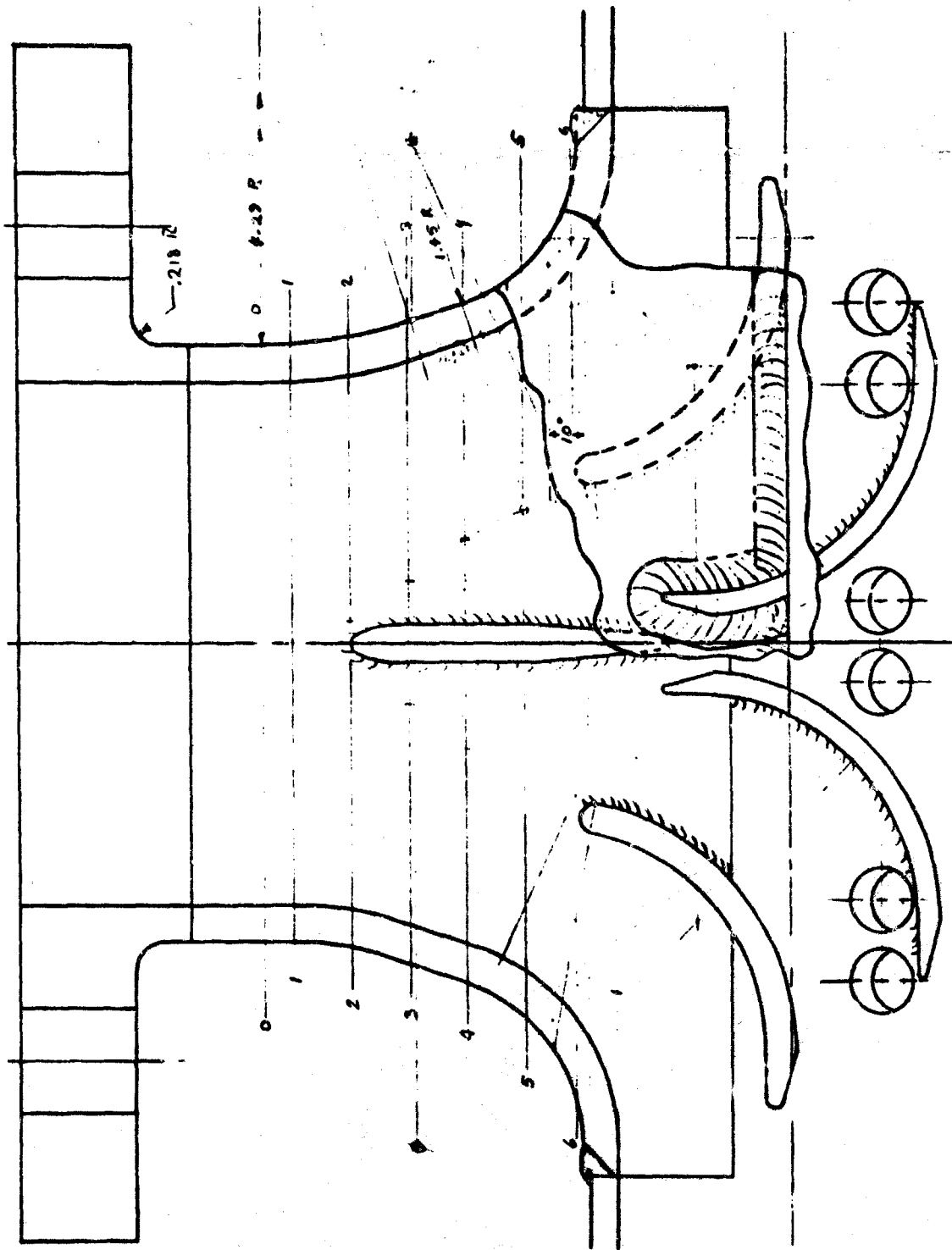


Figure 89. Fuel Manifold Inlet Tee

CONFIDENTIAL

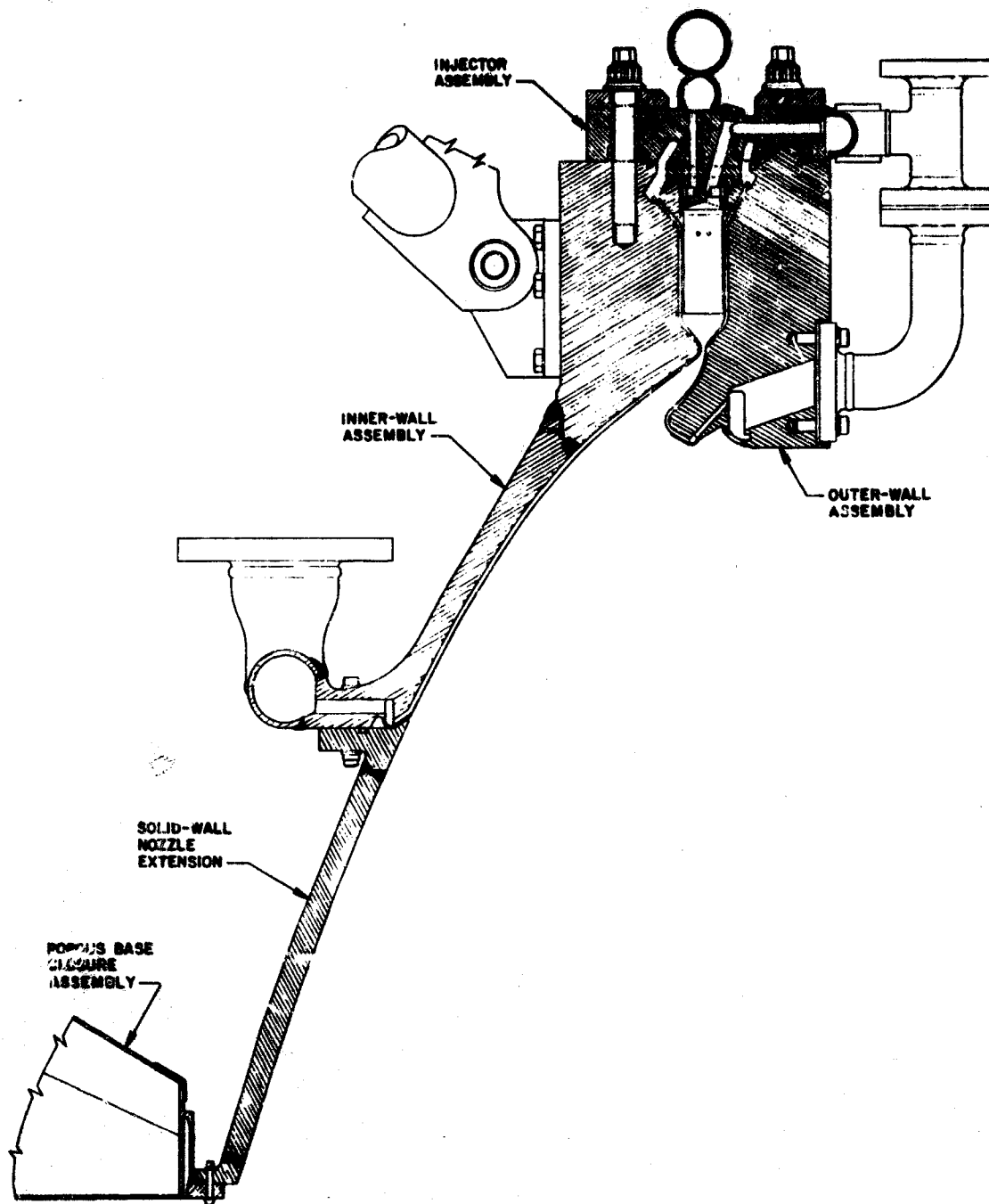


Figure 90. ADP 250K Thrust Chamber Tube-Wall Assembly

CONFIDENTIAL

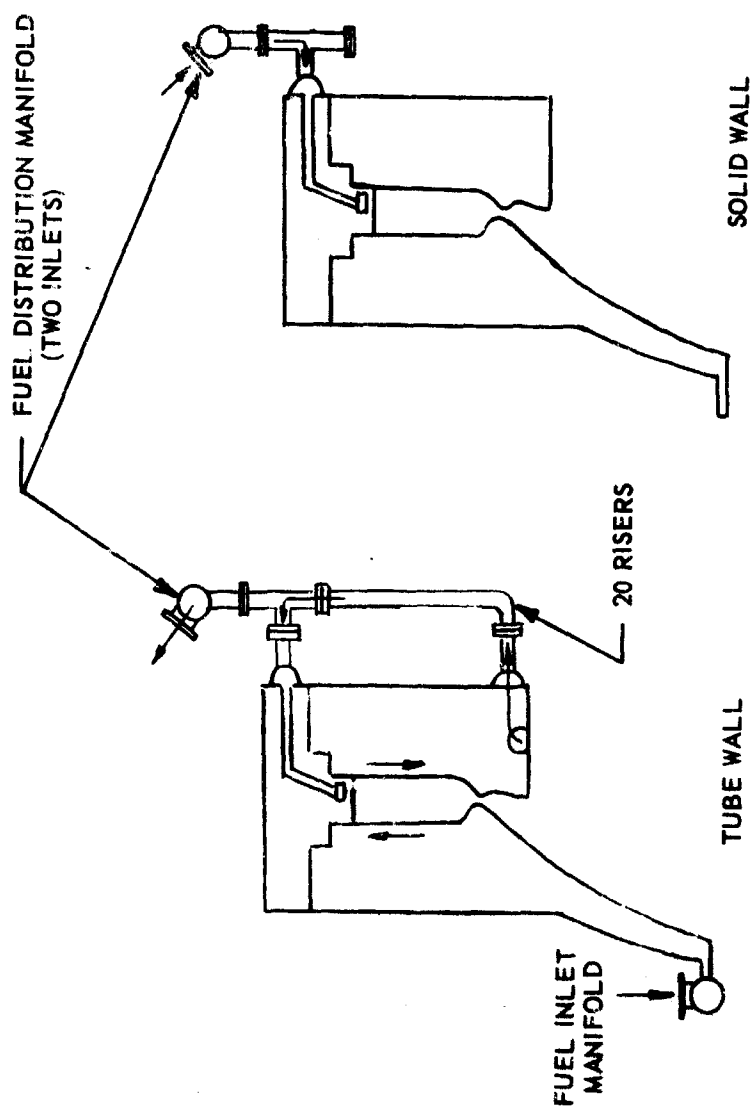


Figure 91. Hydrogen Flow Circuit

CONFIDENTIAL

CONFIDENTIAL

(U) The centerbody is a welded assembly of 347 CRES. Its geometry is that of an oblique cone truncated at its forward end parallel to its base. The base closure is a prepunched flat metal sheet (a perforated plate), welded to the centerbody cone. An omega joint, having an external flange, encircles and is welded to the OD of the base closure. The base closure is bolted to the nozzle at the base flange. A Viton-A O-ring provides sealing between the centerbody and the nozzle. The omega joint absorbs thermal deflections between the centerbody and nozzle. The centerbody functions as a closeout to the engine nozzle and transmits backpressure thrust in the base region to the engine structure.

(C) A J-2 gas generator (P/N 308360) provides secondary gas flow to the center body. Gas generator provisions include the gas generator valve assembly, two bleed valves on the gas generator valve assembly, a "T" adapter that incorporates a hot-gas bypass port, and a boss for GN_2 purge. The gas generator capability has been increased from 8 lb/sec (approximately) to 11 lb/sec (approximately) at 1200F and 800 psia P. The gas generator can be throttled to 4 lb/sec (approximately). A lower secondary flowrate can be achieved through use of a bypass.

(U) The gas generator bolts to the forward flange of the centerbody, and Naflex groove seals are used to seal joints between gas generator, bypass assembly, and the centerbody. Gas generator gas flows into a tubular well inside the centerbody. The tube is welded to the centerbody at the inlet flange and extends aft to near the base of the centerbody. Orifice holes perforate the walls of the tube over most of its length. The holes control and diffuse the gas flow into the plenum chamber. To allow for reducing the orificing area, provision is made for bolting a close-fitting concentric sleeve, of selected length, to the end of the tubular well. A plate bolted to the centerbody base plate provides access to the sleeve and tubular well.

(U) Release for fabrication of the base closure assembly will be effected during the next report period.

(3) 250K Experimental Injector

(C) The injector design is basically a one-piece, stainless-steel annular welded assembly consisting of the injector body, the fuel, the LOX, and the hot-gas manifold system. The operation of the injector was described in the first quarterly. During this quarter, design of the baffles, selection of the first injector strip configuration, and definition of the hot-gas and hypergolic ignition systems have been emphasized.

CONFIDENTIAL

(C) Hot-Gas Ignition and Tapoff Circuit. The hot-gas system is an integral part of the injector assembly. It consists of a uniform cross section toroid located inboard and forward of the inner injector flange. Forty transfer lines welded to the inner injector flange connect the manifold to passages in the injector body, support the manifold, and provide for thermal deflection. Each passage in the injector body, from the transfer line to the baffle at the injector face, is lined with insulating sleeves to reduce heat transfer into the body in areas adjacent to cryogenic passages. The baffles have one common passage and four ports, two per side, that open into the combustion chamber. Ignition flows in from the manifold to the combustion chamber; hot-gas tapoff gases flow from the combustion chamber to the manifold.

(C) Baffles. Two OFHC electroformed baffle designs are released, one design with hot-gas tapoff ports and one without ports. Each design has a 347 CRES core with an electroformed OFHC copper jacket. The jacket has passages for regenerative fuel coolant flow. Twenty-nine CRES cores have been machined and sent for electroforming.

(U) One furnace-brazed baffle design has been released. The furnace-brazed design consists of an OFHC copper jacket, drilled, formed, and furnace brazed to a 347 CRES core. This design has provision for hot-gas ports.

(C) Injector Strips. The machined strip design (backup for the coined design) has been released. The design pattern is a basic triplet pattern, described in a later section of this report.

(C) Ignition Systems. For the solid-wall chamber, provision is made for both hypergolic (chlorine-trifluoride) and hot-gas ignition (fuel-rich gases). The hot-gas ignition is being evaluated in an in-house program. The results of this program show that satisfactory ignition can be achieved with nominal mixture ratio of 1:1 hot gases if the thrust chamber mixture ratio is above the theoretical limit of 1:1. The hypergolic system is described in detail here.

(C) A study was made of existing ClF_3 systems, and an analysis was made of four manifold designs. The design selected (see First Quarterly Progress Report), with some modification, was found to best suit the engine from a volume and ignition delay standpoint.

(C) Each of the 40 combustion compartments contains one igniter tube. The tube, which passes through the fuel manifold and terminates at a recessed position 0.125 inch behind the face of the fuel strip, is formed on the outlet end and indexed such that the ClF_3 forms a fan which sprays parallel to the chamber walls. This fan direction prevents the ClF_3 from impinging on the walls of the chamber (figure 92).

CONFIDENTIAL

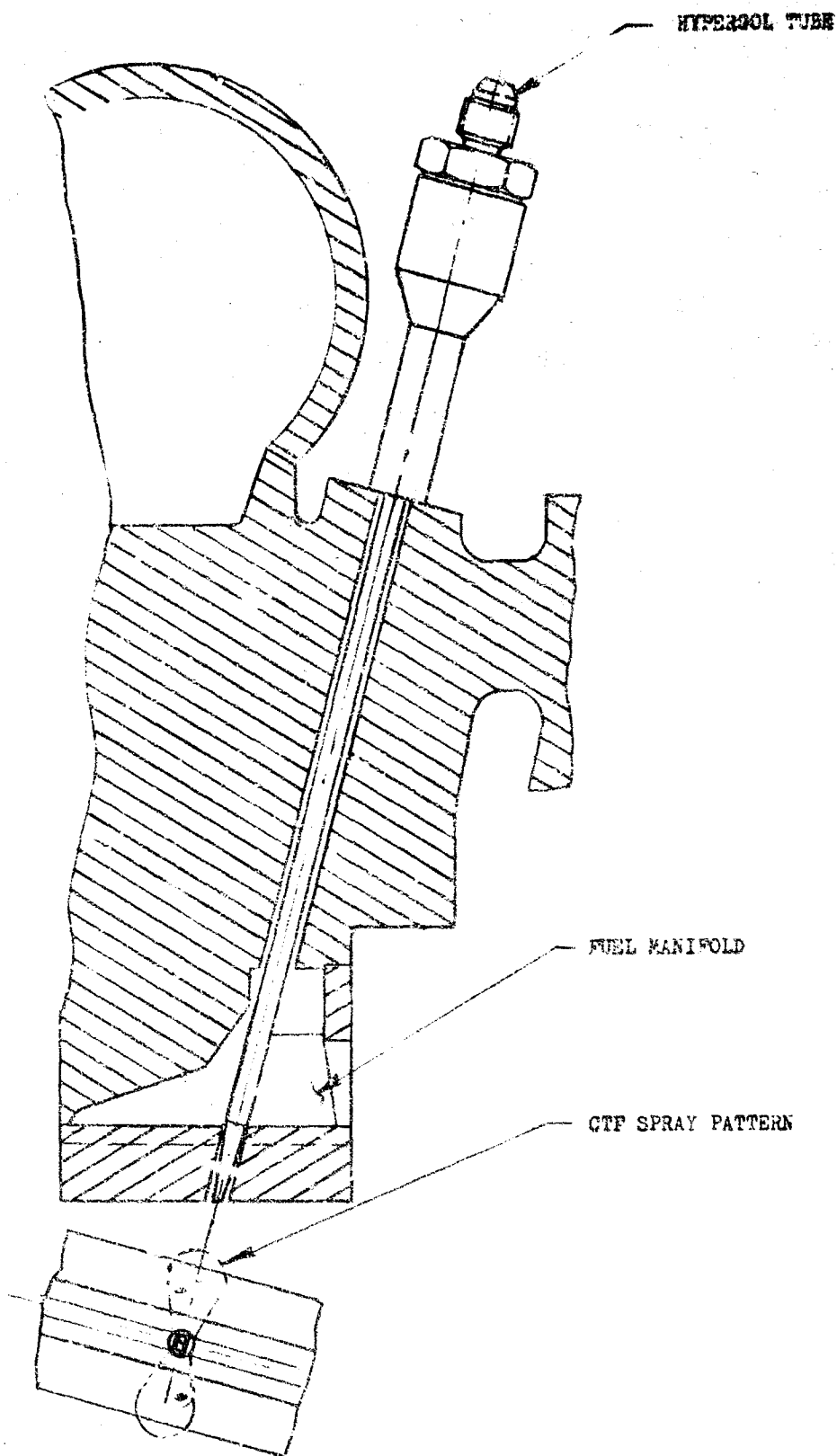


Figure 92. Hypergol Tube

CONFIDENTIAL

CONFIDENTIAL

(C) The manifold consists of five major welded components. A typical quadrant (figure 93) consists of (1) a welded assembly containing ten feed tubes, two secondary plenums, and a splitter tube, and (2) a transfer tube which is part of a second welded assembly, consisting of four transfer tubes, one primary plenum, and a supply tube.

(U) The ClF_3 system is pressurized by GOX tapped off from the high-pressure LOX system. Following expulsion of the ClF_3 , the manifold continues to flow LOX, providing a purge condition, sustained ignition, and cooling for the tube at the injector face.

(C) Tapoff Manifold. The hot-gas tapoff manifold assembly consists of a toroidal collector ring of constant area cross section, one outlet riser to facility ducting, a separate interconnect tube for each of the 40 combustion chamber compartments, and AND bosses for temperature and pressure taps. All material is 347 CRES except the flanged outlet to facility ducting. The flange is a Graylock weld-neck flange (316 CRES).

(U) Interconnect tubes are welded to the tapoff ports on the ID of the injector flanges. Flow into and out of the manifold is at 90 degrees to the flow in the collector ring.

(C) Oxidizer Manifold Studies. The oxidizer manifold development effort for the ADP thrust chamber is being carried out and reported under NASA Contract NAS8-20349. The manifold evaluation is identical to the LOX manifold being fabricated for the 250K injector. The unit is shown in figure 94 undergoing full-flow tests.

(U) 250K Thrust Structure. The design of the 250K thrust mount assembly has been finalized and the stress analysis completed (figure 86) in this report period.

(U) The final design consists of eight equally spaced struts radiating out and aft from a center gimbal mounting plate (designed to accept a standard J-2 gimbal bearing) to vertical gussets which attach to mounting brackets via pinned clevis joints. The mounting brackets contain a close tolerance shear tang which mates with a groove on the inside diameter of the inner wall of the thrust chamber. The brackets are attached to the chamber wall with bolts.

(U) Additional struts, two from alternate vertical gussets, connect at a point above the intermediate gusset to provide stabilizer attach points at a height above the thrust chamber to meet facility requirements. Extension of the vertical gussets at the gimbal mounting plate provide attach points for primary load cell calibration.

CONFIDENTIAL

CONFIDENTIAL

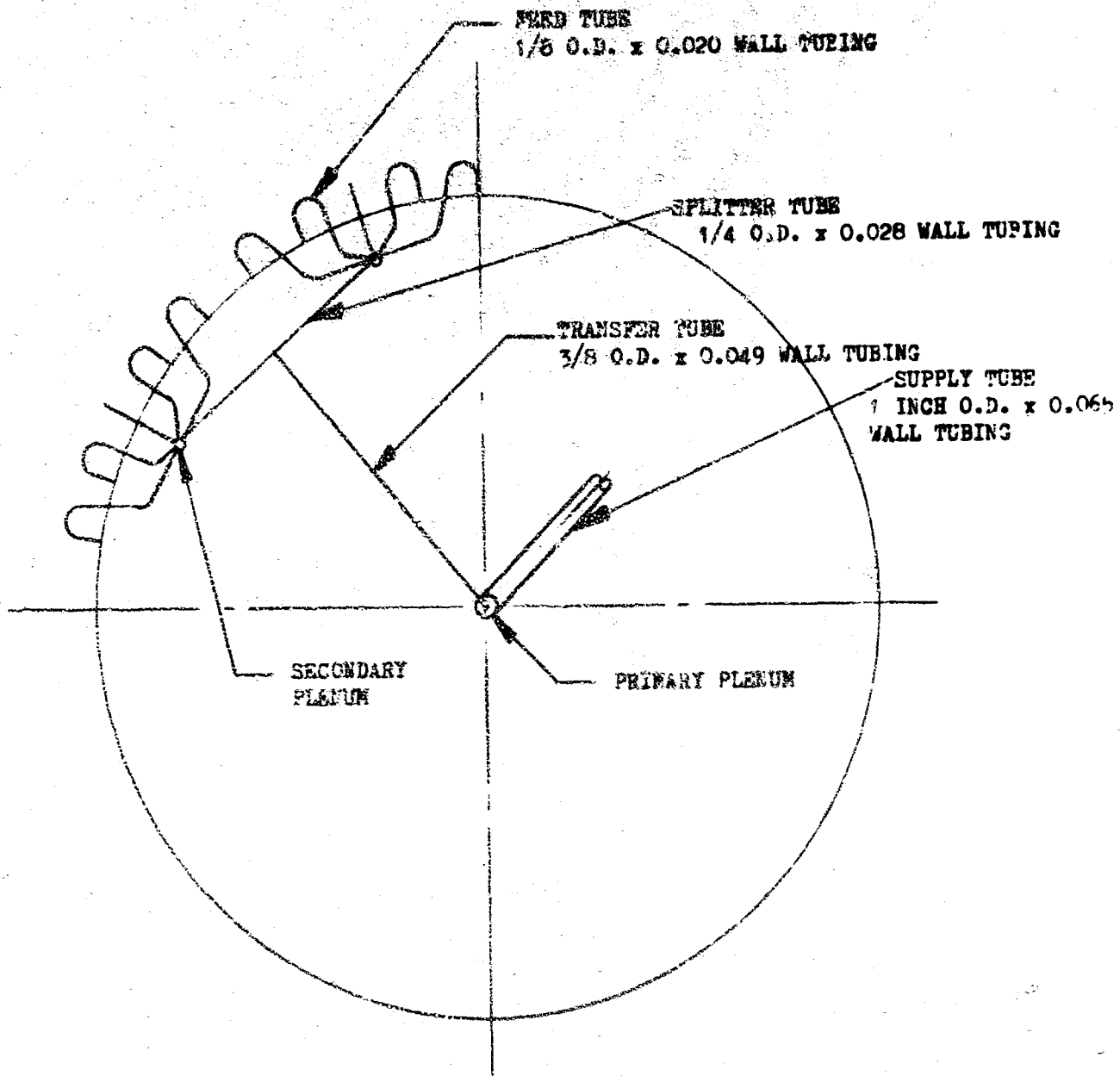


Figure 93. Hypergol Manifold

CONFIDENTIAL

CONFIDENTIAL



Figure 94. LOX Manifold Flow and Distribution Tests

CONFIDENTIAL

CONFIDENTIAL

(U) The assembly will be a welded fabrication of 4340 steel plate and 4135 steel tubing heat treated to the required strength level.

c. Problem Areas and Solutions -- Manufacturing

(U) During this report period, three manufacturing problems were satisfactorily resolved. The boring of the horizontal feed holes in the injector assemblies was accomplished by adapting the Quackenbush drilling units by building jigs to mount the units to the injector body itself.

Problems encountered in forming of the tube assemblies were resolved by adapting the tube forming dies to another press and applying 30,000 psi during the forming operation.

The successful broaching of a test specimen during the reporting period demonstrated that the proposed method had resolved the problem of forming the grooves in the injector body assembly.

d. Testing

(i) Test Facilities

(U) Facility Feed System Dynamics. A mathematical model including oxidizer facility feedlines, thrust chamber feed systems, and combustion chamber dynamics was formulated for the analysis of chug modes of instability should they occur on 250K testing. Since the gaseous hydrogen has negligible dynamics in the range of frequencies where chug might occur, the facility fuel feed system was excluded from consideration.

(U) The complete chug model was developed in three steps: (1) the oxidizer facility lines were modeled and resonant frequencies determined, (2) the thrust chamber oxidizer manifold, feed legs, and injection passages were added to obtain the total oxidizer feed system response, and (3) the combustion process was added together with a hydrogen flow description through the injector. A block diagram representation of the total chug model is shown in figure 95.

(U) The facility oxidizer feed system at NFL-D2 consists of 48 inches of 8-inch-diameter line, 47' inches of 6-inch-diameter line and two facility Annin valves.

CONFIDENTIAL

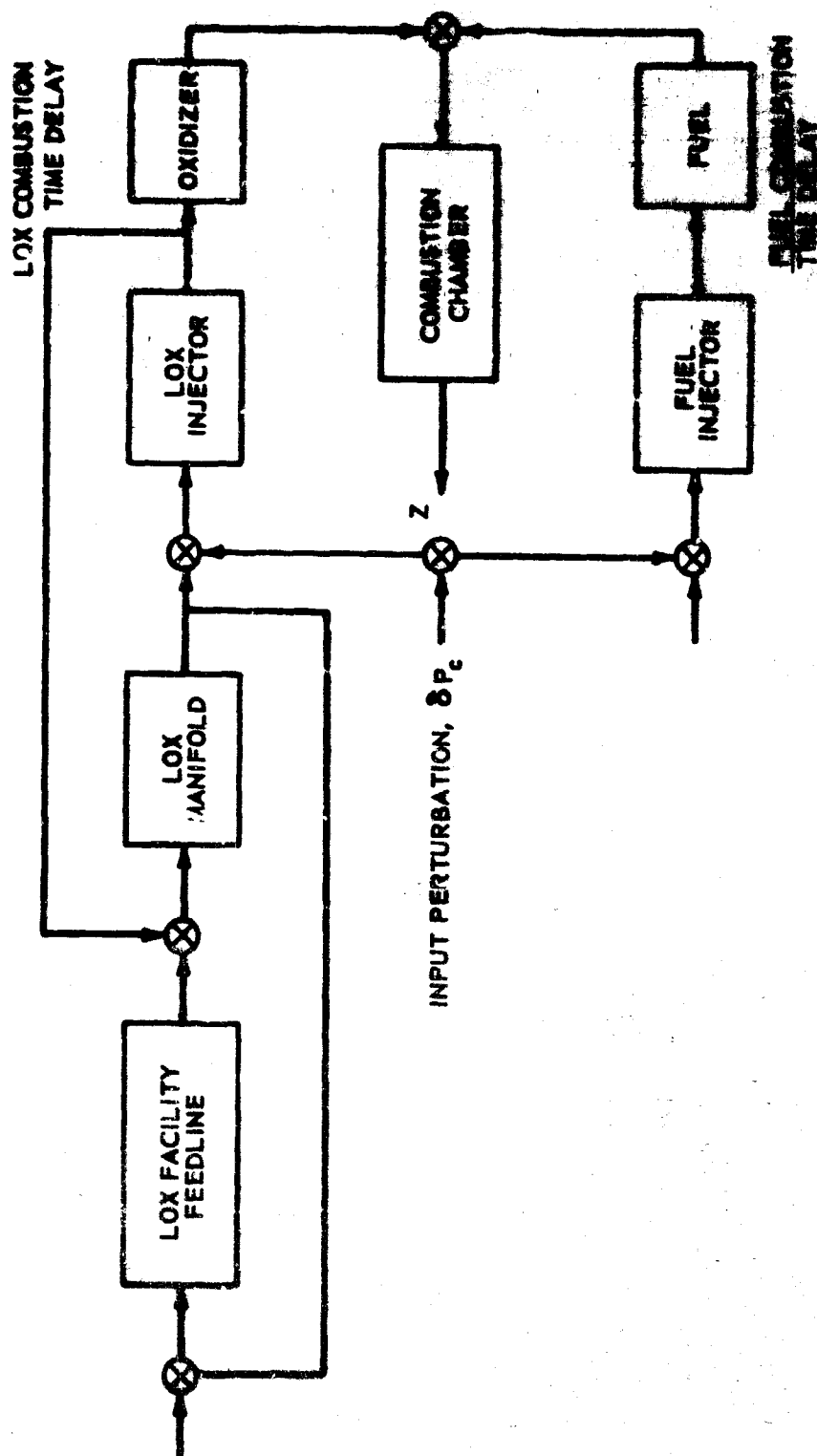


Figure 95. Block Diagram Representation of the ADF "Chug" Model 1

CONFIDENTIAL

CONFIDENTIAL

(U) The dynamic behavior of the facility line was determined using a digital computer frequency response routine when pressure perturbation was introduced at the downstream end of the line. The pressure and flowrate ratios along the line to the input perturbation, presented in terms of both magnitude and phase as functions of frequency, are indicative of the line dynamics.

(U) A nominal oxidizer flowrate of 475 lb/sec, corresponding to a thrust level of 250K, was first evaluated. Both pressures and flowrates within the facility line exhibited resonances at 40, 80, 120, and 750 cps with the highest peak gain at 80 cps.

(U) The oxidizer facility line description was then modified to include the assumed length of line necessary to connect the existing facility feed system to the thrust chamber oxidizer inlet flange. Each flowrate condition was re-run without any attendant change in resonant frequency or gain magnitudes.

(U) The oxidizer feed system description was extended to include the thrust chamber assembly. The plenum and diffuser sections were treated as a single volume and represented by a lumped description of the compliance. The four feed legs were assumed to act as parallel flow paths and, as such, were represented by a single, one-dimensional wave equation for a line of the equivalent cross-sectional area and length. A lumped compliance description of the torus manifold also was employed. An equivalent work representative of the injector resulted in lumped values of inertance and resistance for the feed passages.

(U) The describing equations for the thrust chamber LOX feed system were coupled to the previously derived facility line representation. Again, the digital frequency response routine was used to determine the dynamic behavior of the total oxidizer system. In this instance, the input perturbation was introduced to chamber pressure. At the nominal 250K LOX flowrate, resonant peaks in torus manifold pressure were observed at 160 and 360 cps. Facility line pressures also reflected a peak at 240 cps. Significantly, pressure response upstream of the four legs indicated that frequencies above 500 cps were not transmitted and the feedline was essentially decoupled from the chamber at high frequencies.

(U) Completion of an ADP thrust chamber "chug" model required the addition of the hydrogen injector dynamics and the chamber gas-side dynamics to the LOX feed system description. Again, because of the presence of gaseous hydrogen prior to injection into the chamber, fuel injection pressure was assumed to be constant. A linear equation was used to describe fuel injector flowrate.

CONFIDENTIAL

(U) The combustion process was analytically represented by time-delayed injector flowrates. The time constants for the delays were determined by considering the flight time-to-impingement at injection velocities plus a time interval for gas generation to occur. The total delay represented approximately the time required for each propellant stream to travel twice the impingement distance at injection velocity.

(U) Fuel and combustion dynamics were then coupled to the description of the oxidizer feed system to compute the "chug" model. The block diagram of the chug model is illustrated in figure 95. A chamber pressure perturbation was introduced again and the digital frequency response routine employed to determine dynamic behavior. For the case of the computed model, however, the frequency response provides more information than merely to identify resonances within the model components. By considering the model open loop (i. e., not permitting chamber pressure to feed back to the feed system), the Bode stability criterion may be employed to determine if chug will be encountered. Stated briefly, the Bode criterion requires that for a sinusoidal input, the open loop gain, $Z/\Delta P_c$, must be less than unity at the point of 180 degree phase shift for the system to be stable.

(U) The two ADP performance extremes (50K and 250K) were evaluated using the chug model. At 250K, the $Z/\Delta P_c$ phase ratio never reaches 180 degree shift although gain is greater than unity at several frequencies. The thrust chamber should, therefore, not experience a chug mode at 250K thrust.

(U) For the 50K performance level, 180 degree phase shift does occur at 240 to 250 cps, indicating that at the lower thrust level a chug mode may be experienced and facility decoupling provisions may be necessary. The developed model also will be of use to the selection of any necessary facility revisions.

(U) Instrumentation Box Identification System. A system to identify all instrumentation taps on the 250K chamber has been devised so that the taps are fully described by the tap number. No cross reference is necessary to determine tap location, fluid media, or tap type. The system is described in Appendix D. The total chamber instrumentation provisions are listed in Table 28.

CONFIDENTIAL

e. Summary of Planned Effort for Next Report Period

(U) During the next reporting period, the electroformed baffles for the first two injectors will be received from the electroforming source. Only one set (40 each) will have hot gas tapoff ports. The copper injector strips will be machined and the orifice holes drilled to support brazing of injector units No. 1 and No. 2.

(U) The first injector is scheduled for completion (through calibration) 11 November 1966. This unit will be assembled with the inner and outer solid-wall bodies thrust mount, base closure, and associated manifolding and ducting, and the total assembly will be ready for delivery to the test facility on 18 November 1966.

TABLE 28

250K CHAMBER INSTRUMENTATION PROVISIONS

Tap Location	Number of Taps		
	Static Pressure	Dynamic	
Common (SWTC and TWTC)			
Injector-Chamber Pressure	6		
Fuel Injection Manifold	5	5	4
LOX Manifold	12	10	7
LOX Line	4	5	3
Hot-Gas Tapoff	1		8
ASI	4		2
SOLID WALL CHAMBER			
Combustion Chamber	7	7	4
Nozzle Profile	19		5
Base Closure	5		3
Fuel Inlet Manifold			2
TUBE-WALL CHAMBER			
Fuel Inlet Manifold	7	3	2
Fuel Up-tube Manifold	2		2

CONFIDENTIAL

TABLE 28

250K CHAMBER INSTRUMENTATION PROVISIONS (Concluded)

Tap Location	Number of Taps		
	Static Pressure	Dynamic	Temperature
TUBE-WALL CHAMBER (cont)			
Fuel Down-tube Inlet Manifold	4	2	4
Fuel Down-tube Outlet Manifold	4	4	4
Fuel Transfer Tubes	4	4	4
Center Body Plenum	9		2
Uncooled Nozzle Extension	4		
Gas Generator	4		1

(U) The forming and calibration of the tubes for the inner and outer tube wall body assemblies of Unit No. 1 will be completed. These tubes will be stacked into the bodies and the brazing of the units will be in process.

(U) A complete testing program plan for the solid-wall chamber will be prepared early in the next quarter. This plan will include test by test description objectives, instrumentation requirements, and starting and shutdown procedures.

CONFIDENTIAL

4. SEGMENT STRUCTURAL EVALUATION

(U) The 20K segment chamber is being designed, manufactured, and tested to provide advanced structural and fabrication data for a lightweight demonstrator module chamber design. Complete structural simulation of a 360-degree annular combustion chamber cannot be obtained with a model chamber segment. The ability of the structure to maintain throat dimensions throughout the operating range and with repeated firings will be simulated very closely. Also, construction of the demonstrator module structural members and regenerative cooling of all structural parts will be closely simulated. The effects of differences between the 20K segment and demonstrator module will be analytically determined and used to interpret the test results.

a. Status

(U) The design requirement specification for the 20K demonstrator module chamber segment was completed and issued.

(U) Salient design features presently established for the 20K demonstrator module chamber segment are:

1. A straight chamber length including three combustion zone compartments, the center compartment duplicating a compartment of the demonstrator module chamber
2. Internal tie bolts housed within the combustion zone baffles
3. A symmetrical combustion chamber, convergent nozzle, throat and expansion nozzle with a divergent half-angle of 15 degrees to an area ratio of 3.5
4. A machined titanium backup structure adhesively bonded to the regeneratively cooled tube bundle
5. Temperature, structural, and high-frequency pressure instrumentation

(U) The design of the 20K demonstrator module segment has progressed to the final layout stage for both the injector and chamber assembly.

b. Progress During the Report Period

(C) Design analyses involving structural concept, material, coolant circuitry and fabrication technique for a lightweight demonstrator

CONFIDENTIAL

module chamber (see Demonstrator Module section) has precipitated several major design criteria for the 20K segment chamber. The structure is composed of machined titanium adhesively bonded to the regeneratively cooled tube bundle.

(U) An internal structural configuration utilizing equally spaced structural baffles, each containing two bolts, will carry loads across the chamber.

(C) Nickel 200 was selected as the material for the regeneratively cooled chamber tubes because of its "life" properties at the predicted hot-firing conditions. Tooling for the fabrication of the 20K segment tubes will be common with that used on the 2.5K segment program. A series circuit similar to that of the demonstrator module was selected to cool the "inner" body, structural baffle, and "outer" body, respectively.

c. Problem Areas and Solutions

(U) The initial results of a demonstrator module chamber design study involving the two prime internal structural arrangements, i.e., a single row of 80 support struts and 40 separate combustion baffles vs 40 structural baffles each containing 2 bolts, indicated the 80-strut concept to be appreciably lighter than the 40-structural baffle concept. Based on this input, the 20K demonstrator module segment chamber design was initiated. Subsequent refinement of this configuration eliminated the apparent weight advantage of the 80-strut configuration. A reappraisal of the two structural configurations resulted in the 20K design being changed to the concept of baffles with internal bolts. This has resulted in a schedule slippage; however, the orders for long lead items have been placed and this task can be brought back on schedule by an accelerated design effort.

d. Summary of Planned Effort for Next Report Period

(U) Effort during the next report period will be directed toward the following goals:

1. Release of the tube design for fabrication
2. Completion of the final chamber layout preparatory to a critical design review
3. Detailing and release of all long-lead chamber body components for fabrication
4. Completion of injector assembly layout and release of the body for fabrication
5. Release of a preliminary hot-firing test requirements memo

CONFIDENTIAL

This page is intentionally left blank

CONFIDENTIAL

CONFIDENTIAL

SECTION IV

(C) CONCLUSIONS AND RECOMMENDATIONS

1. Experience of over 100 tests has shown that the 2.5K solid-wall, cooled segment provides an effective and low-cost means of evaluating aerospike thrust chamber injectors.
2. 2.5K segment test results have shown that the triplet injector pattern selected for the 250K injector is stable over the operating range throttled to 20 percent rated thrust and 5 to 7:1 mixture ratio. These tests showed further that injector durability and chamber wall heat transfer are satisfactory for 250K experimental tests.
3. Performance testing of the triplet injector pattern in the 2.5K segment has shown that this injector delivers a combustion (η) efficiency greater than that necessary to meet the overall specific impulse requirements for the engine over the operating range.
4. From analytical studies, laboratory materials fatigue tests, brazing tests, tube tester simulation tests, and general hot-fire experience, it is concluded that Nickel 200 is superior to stainless steel and pure (OFHC) copper as an ADP demonstrator module thrust chamber tube material. However, beryllium-copper shows great long-range promise as a superior material to nickel when available in tube form. Hot-firing evaluation in the exact ADP aerospike configuration is needed to confirm this and provide information on limits. Stainless steel will not meet the life requirements of the ADP.
5. From dynamic and static models and design studies, it is concluded that throttling and mixture control of the aerospike engine can best be accomplished by two hot-gas throttle valves in the turbine supply. Simplicity and reliability, dynamic response, static balance effects on the system and other components, performance, and weight were heavy considerations in this conclusion. The aerospike engine will operate satisfactorily as a demonstrator engine with either open loop or closed loop modes of control to these valves.
6. A design study was made of three fuel turbopump arrangements to meet the ADP aerospike flow and head requirements. The conclusion is that a two-stage centrifugal pump best

CONFIDENTIAL

CONFIDENTIAL

meets requirements for a demonstrator engine, with the Phase II demonstration to be conducted in mid 1969. Development cost and performance margin were important factors in reaching this conclusion.

7. From design study of lightweight thrust chamber structures, it was concluded that a machined titanium backup structure adhesively bonded to the brazed cooling jacket-manifold assembly is the best design for the demonstrator module thrust chamber with the Phase II demonstration to be conducted in mid 1969. The major tradeoff in this selection was between (1) weight and (2) development costs, schedule, and confidence.

CONFIDENTIAL

CONFIDENTIAL

REFERENCES

1. R-6499, Investigation of Cooling Problems at High Chamber Pressures, Final Report, Rocketdyne, a Division of North American Aviation, Inc., Canoga Park, California, May 1965.

CONFIDENTIAL

CONFIDENTIAL

This page is intentionally left blank

CONFIDENTIAL

APPENDIX A

DETERMINATION AND VALUE OF INFLUENCE COEFFICIENTS USED IN THRUST CHAMBER DATA REDUCTION

(U) Thrust chamber performance efficiency is calculated relative to theoretical thermodynamic shifting propellant performance. The theoretical performance is calculated subject to seven assumptions:

1. Thermodynamic equilibrium is reached in the combustion chamber after adiabatic reaction.
2. Expansion through the nozzle is isentropic.
3. Products of combustion behave as ideal gases.
4. The expansion process involves the one-dimensional flow of inviscid gases.
5. Gas velocity at the nozzle entrance is zero.
6. Propellants are chemically pure.
7. Initial temperature for the oxidizer is the boiling point at 1 atmosphere pressure and for the fuel is room temperature (70 F).

(U) Since the real thrust chamber does not operate under such idealized conditions, the real thrust chamber data cannot be directly compared with theoretical thermodynamic performance. Therefore, it follows that either the test data must be adjusted to the same reference base as the theoretical values or the theoretical calculations must be made so that the effect of finite contraction ratio, friction, heat transfer, nozzle throat area change due to thermal effects, nozzle divergence, and deviation from one-dimensional flow are properly taken into account. The former procedure is used in the reduction of ADP thrust chamber test data.

STAGNATION PRESSURE LOSS

(U) Measured static pressure is adjusted for stagnation pressure loss by application of a function dependent on contraction ratio, specific heat ratio, and nozzle entrance Mach number.

$$\eta (P_0) = F (k, A_c/A_t, M) = 0.9953 \quad (1)$$

FRICITION

(U) A boundary-layer analysis is used to obtain the skin friction coefficient from which the frictional drag force is computed. The integral momentum boundary-layer equation, in conjunction with a Rocketdyne skin friction correlation (Ref. 1), was used to evaluate the frictional drag. The friction influence coefficient is given by:

$$\eta_f = F (\theta, \delta, M_\infty, U, u, \mu, k, T_R) \quad (2)$$

$$\eta_f = 1.0135 \quad (3)$$

(U) The dependence of η_f on chamber pressure and mixture ratio is shown in figure A-1.

HEAT TRANSFER

(U) In a water-cooled thrust chamber, the heat transferred to the coolant water is lost and not available for conversion to directed velocity. This heat loss results in a reduction of combustion gas temperature and, consequently, the delivered performance is less than the ideal thermodynamic performance. The influence of heat loss on performance was calculated by using a modified theoretical thermodynamic propellant performance program that accounts for heat transfer in the energy balance. A heat flux profile typical of the experimentally determined heat flux profile was employed. The performance calculations with heat loss are made incrementally so that the effect of spatially distributed heat transfer on the flow field properties is calculated and, thereby, the effect of heat loss on performance is calculated. These heat loss influence coefficients are:

$$\eta_{H.L.} (c^*) = F (Q/A, \dot{w}, T_c, T_t, H_c, H_t) \quad (4)$$

$$\bar{\eta}_{H.L.} (c^*) = 1.0078 \quad (5)$$

and

$$\eta_{H.L.} (F) = F (Q/A, \dot{w}, T_c, T_e, H_c, H_e) \quad (6)$$

$$\bar{\eta}_{H.L.} (F) = 1.0095 \quad (7)$$

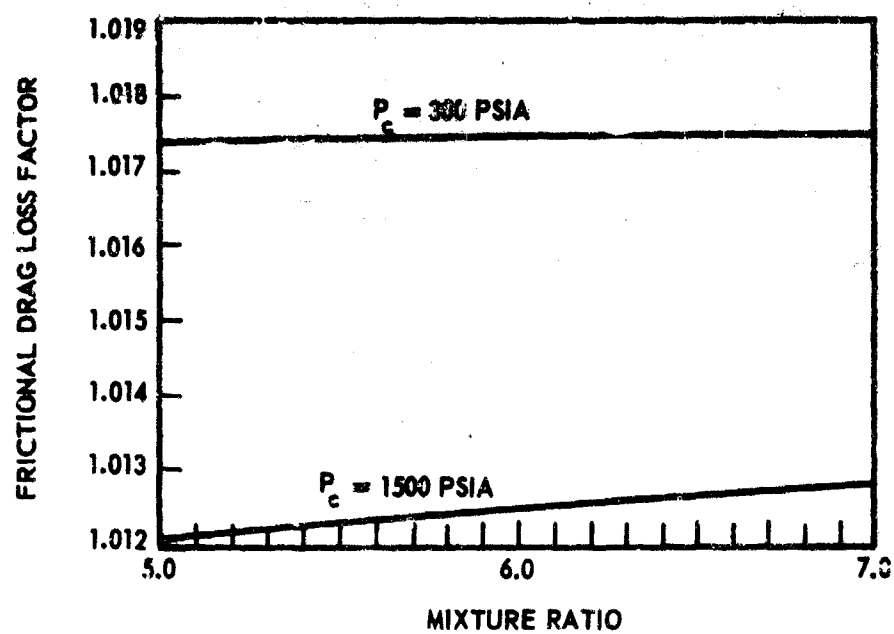


Figure A-1. Influence Coefficient to Account for Effect of Frictional Drag on Thrust

CONFIDENTIAL

(U) The variation of $H.L. (c^*)$ and $H.L. (F)$ with respect to chamber pressure and mixture ratio is shown in figure A-2 and A-3.

NOZZLE THROAT AREA CHANGE

(U) Nozzle throat area during a test is different from the nozzle throat area before or after a test. During a test, there are pressure loads acting on the internal nozzle surface upon which thermal effects due to the increased wall temperature (as the result of heat flux) are superimposed. In the 2.5K ADP water-cooled thrust chamber, the hardware is sufficiently massive so that the effect of internal pressure loads is negligibly small compared to the thermal effects. Due to the heat flux, the nozzle throat area is less than in the cool pretest condition. The influence coefficient for nozzle throat area change due to thermal effects is:

$$\eta_{TH} (A_t) = F (\nu_p, \nu_e, \epsilon, \sigma, E, \epsilon_{TH}) \quad (8)$$

$$\bar{\eta}_{TH} (A_t) = 0.9830 \quad (9)$$

(U) The value given in Eq. 9 is based on past experience and will be replaced as soon as the analysis of thermal effects on throat area is completed.

NOZZLE DIVERGENCE

(U) Nozzle divergence losses were evaluated by comparing two-dimensional axisymmetric thrust coefficient with the ideal one-dimensional nozzle thrust coefficient. The two-dimensional nozzle thrust coefficient was computed by a method of characteristics analysis which utilizes variable flow field properties and the internal contour of the nozzle used on the thrust chamber. It is clear that

$$\Delta C_F = C_F (1-D) - C_F (2-D) \quad (10)$$

and

$$\Delta C_F = \Delta F \quad (11)$$

so that

$$\bar{\eta}_{DIV} = 1.0110 \quad (12)$$

CONFIDENTIAL

CONFIDENTIAL

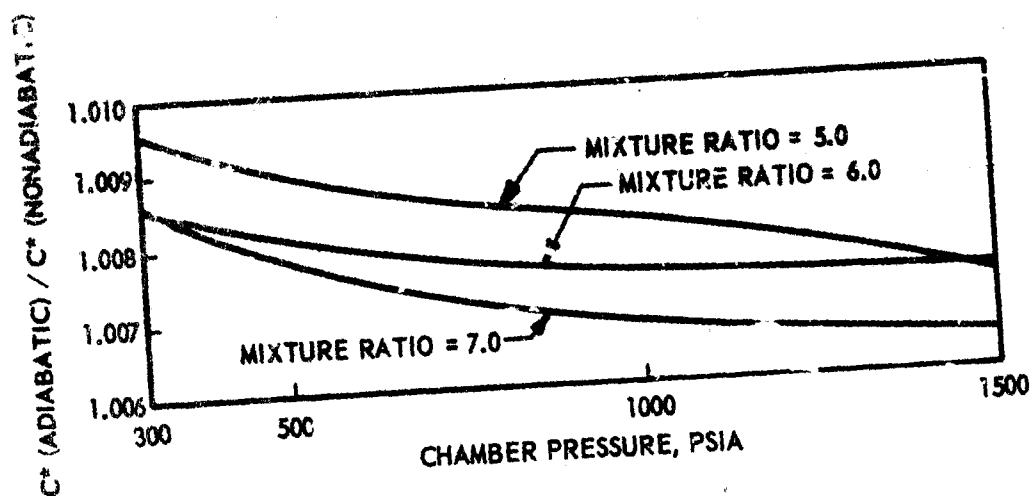


Figure A-2. Influence Coefficient for Variation in Characteristic Velocity due to Heat Loss

CONFIDENTIAL

CONFIDENTIAL

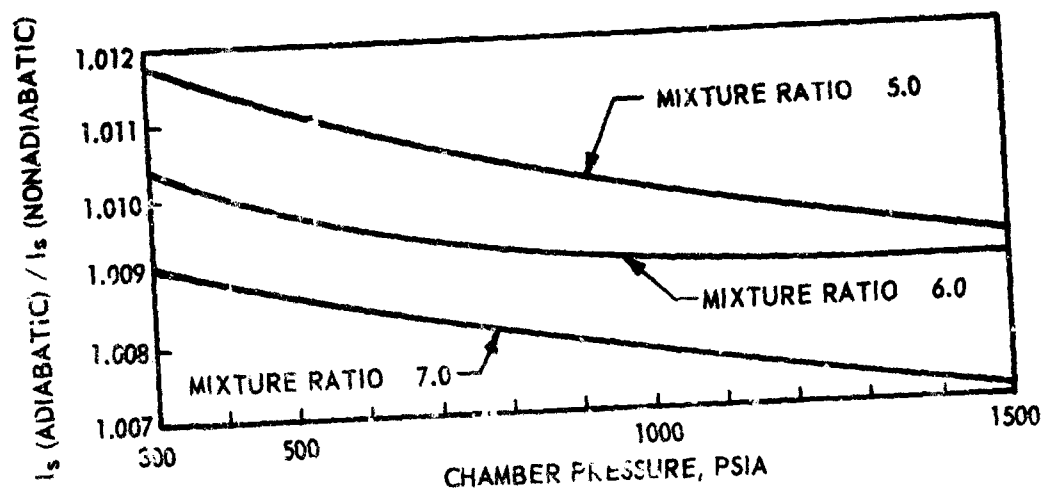


Figure A-3. Influence Coefficient for Variation in Specific Impulse Due to Heat Loss

CONFIDENTIAL

CONFIDENTIAL

(U) Nozzle divergence loss dependence on chamber pressure and mixture ratio is shown in figure A-4.

NON ONE-DIMENSIONAL FLOW

(U) In the linearized theory of transonic flow, the mass flow crossing the throat section is always found to be less than the critical flow corresponding to one-dimensional conditions. The ratio of the two-dimensional mass flow to the one-dimensional mass flow is the nozzle discharge coefficient. The nozzle discharge influence coefficient is:

$$\eta_{CD} = F(k, R_t, R_c) \quad (13)$$

$$\eta_{CD} = 0.997$$

(U) These influence coefficients and the resultant average value for the influence coefficient are summarized in Table A-1.

TABLE A-1
INFLUENCE COEFFICIENT SUMMARY

PHYSICAL EFFECT	INFLUENCE ON EXPERIMENTAL	
	Characteristic Velocity	Specific Impulse
Heat Loss	1.0078	1.0095
Friction		1.0135
Nozzle Divergence		1.0110
Nozzle Discharge Coefficient	0.9970	
Throat Shrinkage	0.9830*	
Stagnation Pressure Loss	0.9953	
Resultant Value	0.9831	1.0344

* Tentative Value

CONFIDENTIAL

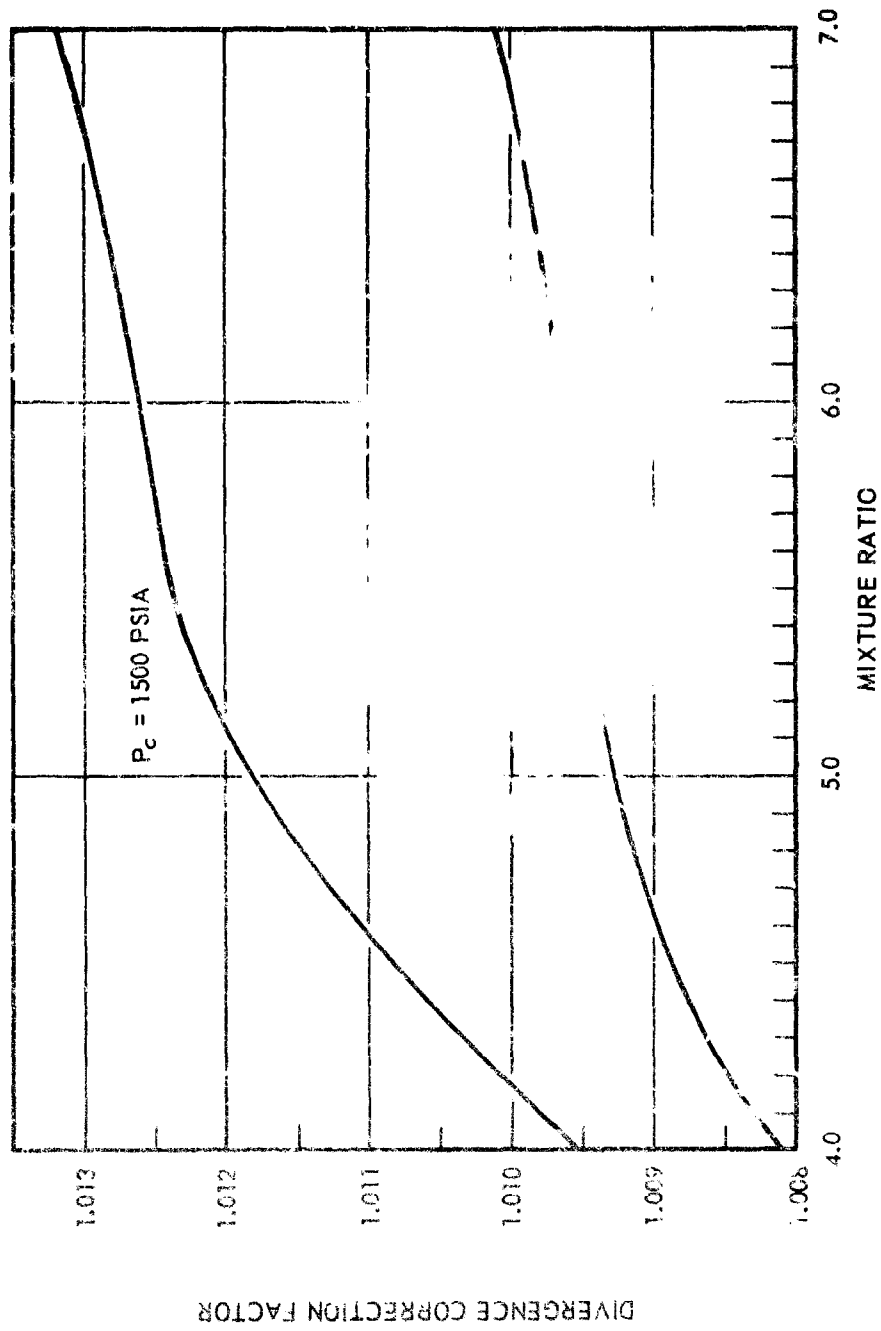


Figure A-4 Divergence Correction for 2500-Pound-Thrust ADP Thrust Chamber

CONFIDENTIAL

CONFIDENTIAL

APPENDIX B

HEAT TRANSFER DATA REDUCTION FOR WATER-COOLED SEGMENTS

(U) The heat transfer data output includes the water flowrate and overall bulk temperature rise for each transverse water/coolant passage. The water flowrates are measured with a turbine flowmeter and the bulk temperature rises are obtained with chromel-alumel thermopiles installed to measure the inlet and outlet temperature difference directly.

(U) The heat transfer rate into each water passage is given in terms of the water flowrate, the water specific heat ($C_p = 1 \text{ Btu/lbm-F}$), and the water bulk temperature rise by:

$$q = \dot{w} C_p \Delta T_B \quad (B-1)$$

(U) The average chamber heat flux in the region of the coolant passage is obtained by associating a one-dimensional gas-side heat transfer area with each passage and dividing the heat transfer rate into the passage by the appropriate area:

$$q/A = \frac{\dot{m} C_p \Delta T_B}{A} \quad (B-2)$$

(U) An average gas-side heat transfer coefficient is obtained for each passage using the relation:

$$h_g = \frac{q/A}{(T_{aw} - T_{wc}) - \frac{x}{k} q/A} \quad (B-3)$$

(U) The coolant side wall temperature is taken to be 30 F above the saturation temperature of the coolant. The use of this value assumes the coolant side to be in the nucleate boiling regime. The water velocities utilized with this chamber are sometimes high enough, particularly for the low chamber pressure runs, to suppress nucleate boiling. In this case, the assumed coolant side wall temperature will be in error. This simplifying assumption can result in up to 7 percent error in the calculated gas-side film coefficient in the low heat flux regions of the chamber.

CONFIDENTIAL

(U) The actual combustion temperature is obtained from the ideal combustion temperature corresponding to 100 percent combustion efficiency by:

$$T_c = T_{c \text{ ideal}} \eta_C^{*2} \quad (\text{B-4})$$

(U) The adiabatic wall temperature used in Eq. 3 is obtained from the actual combustion temperature by the relation:

$$T_{aw} = T_c \frac{1 + \sqrt{\frac{PR}{2} \frac{\gamma - 1}{2} M_\infty^2}}{1 + \frac{\gamma - 1}{2} M_\infty^2} \quad (\text{B-5})$$

(U) The difference between T_{aw} and T_c is negligible in the combustor where the Mach number is low, and reaches a maximum of about 2 percent near the nozzle exit.

(U) Although the coolant passage geometry is highly two-dimensional, a one-dimensional relation (Eq. 3) will yield correct heat transfer coefficients if the proper value of the wall thickness or "reach" x is used. In reducing these data, the arithmetic average between the maximum and minimum "reaches" for each passage is used in Eq. 3. It is estimated that this introduces up to 3 percent error in the calculated gas-side film coefficient.

(U) During short-duration tests (3 to 5 seconds), the high heat sink capacity of the copper block in the region behind the coolant passages prevents the chamber from entirely reaching steady-state operation. As a result, a slight amount of heat leaks past the coolant passage into the copper backup structure. The amount of leakage depends on the coolant passage spacing and the local heat flux. For the small spacings and high heat transfer rates of the ADP segment, a two-dimensional analysis of the amount of heat leakage should be less than 1 percent in the throat region and less than 3 percent in the lower heat flux regions of the combustion zone.

Local average Stanton numbers:

$$N_{ST} = \frac{h}{\rho_\infty V_\infty} \quad (\text{B-6})$$

and both length and hydraulic diameter Reynolds numbers are computed to provide further correlation of the data. Frozen expansion gas product specific heat and viscosity values corresponding to ideal

CONFIDENTIAL

chamber conditions are used. A 3 percent change in the characteristic velocity efficiency results in only a 1 percent change in the combustion product specific heat.

In addition, the heat transfer data correlating parameter

$$N_{ST} \times (N_{PR})^{2/3} \quad (B-7)$$

is computed. Through the modified Reynold's analogy

$$N_{ST} \times (N_{PR})^{2/3} = C_F/2 \quad (B-8)$$

for flow over a flat plate, this parameter is equal to the local skin friction coefficient divided by two and, hence, provides a direct indication of local boundary-layer development.

CONFIDENTIAL

This page is intentionally left blank

CONFIDENTIAL

CONFIDENTIAL

APPENDIX C

HOT GAS TAPOFF CALCULATIONS

(U) Since the pressure ratio across the gas tapoff orifice was always greater than two, flow through the orifice was sonic and the flowrate could be determined by use of the following expression:

$$\dot{w} = C_D P A \frac{k \left(\frac{2}{k+1} \right)^{(k+1)/(k-1)}}{RT} g M \quad (1)$$

where \dot{w} = flowrate
 C_D = discharge coefficient (1.0)
 P = pressure upstream of orifice
 A = orifice area
 k = specific heat ratio
 M = molecular weight
 R = universal gas constant
 T = temperature
 \dot{w}_O = gas tapoff oxidizer flowrate
 \dot{w}_f = gas tapoff fuel flowrate
 \dot{w} = total gas tapoff flowrate
 MR = gas tapoff mixture ratio

(U) For a fuel-rich gas, the adiabatic combustion temperature is a unique function of the mixture ratio. The relationship between combustion temperature and mixture ratio for the oxygen-hydrogen system is presented in figure C-1. No difficulty is experienced in using these data over a wide range of tapoff pressures because, at low mixture ratios, combustion temperature is nearly independent of the system pressure. Specific heat ratio was taken from figure C-1, and average molecular weight was then obtained from figure C-2, for the mixture ratio determined from figure C-1, using the measured tapoff temperature. These values were used in Eq. 1 to calculate total tapoff flowrate. This flowrate was decomposed into oxidizer and fuel flowrate by use of the expressions:

CONFIDENTIAL

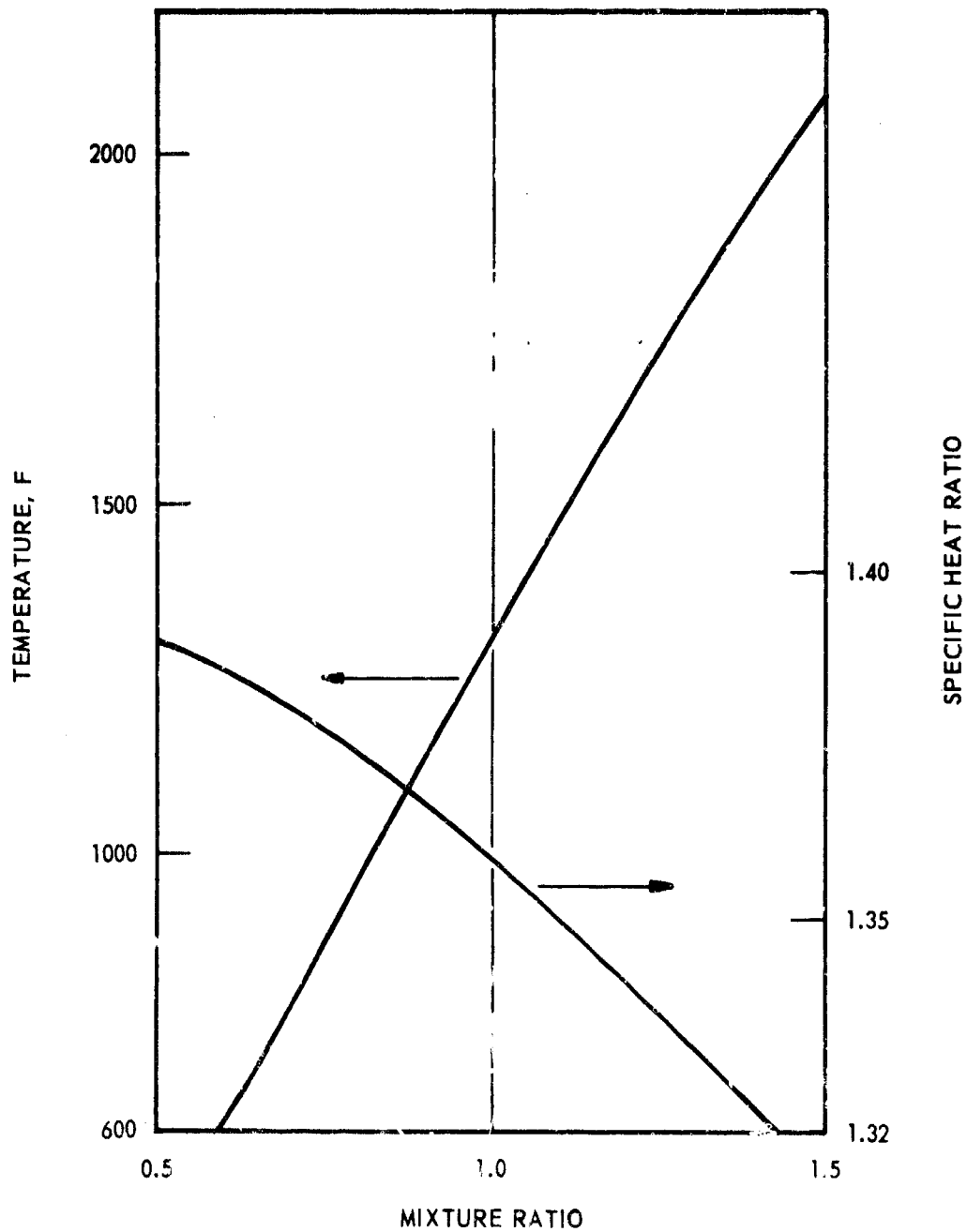


Figure C-1. Combustion Temperature for LOX/LH₂ at a Chamber Pressure of 600 psia

CONFIDENTIAL

CONFIDENTIAL

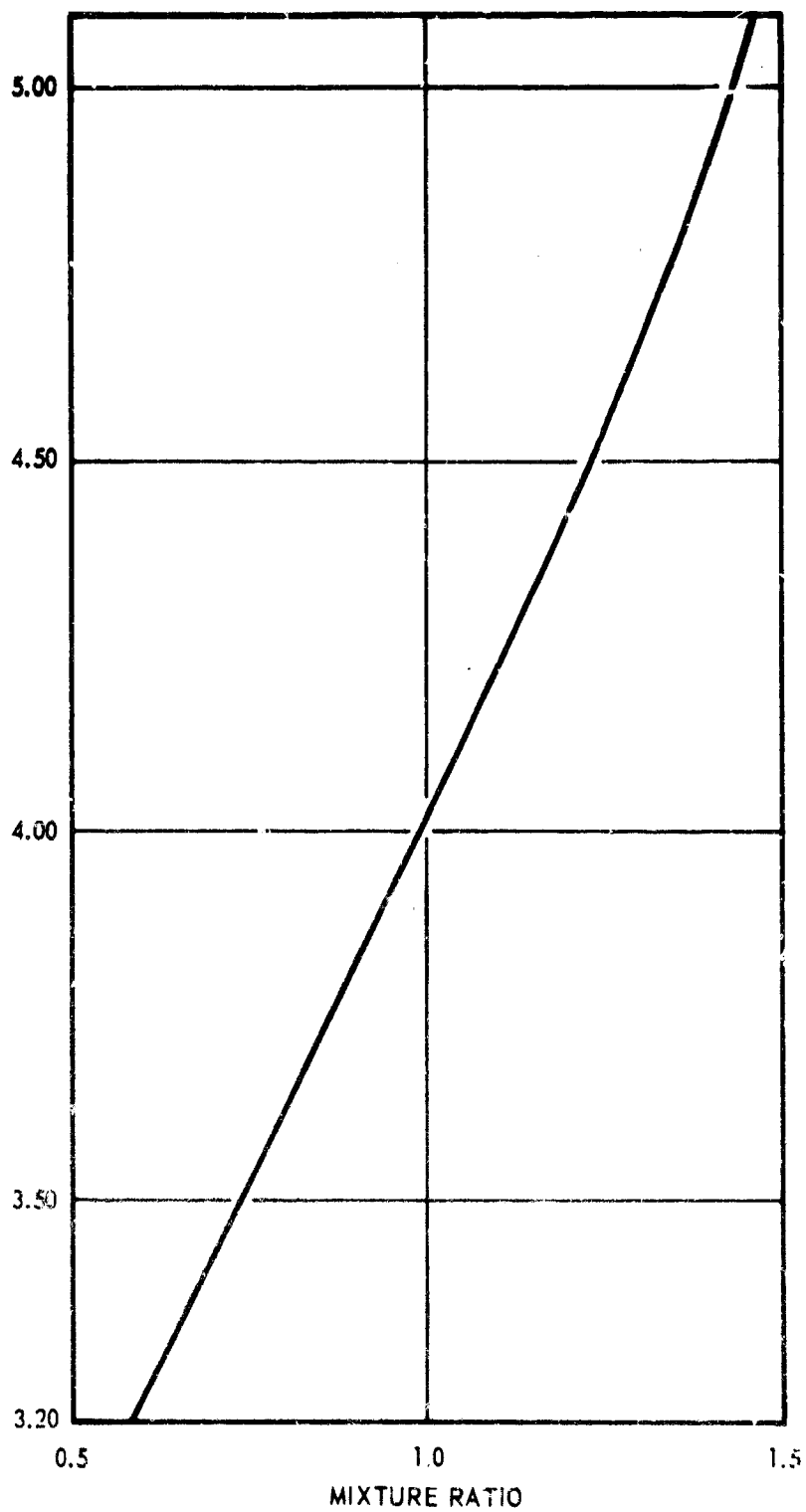


Figure C-2. Combustion Products Molecular Weight for LOX/LH₂ at a Pressure of 600 psia

CONFIDENTIAL

CONFIDENTIAL

$$\dot{w}_o = \frac{MR}{MR + 1} \dot{w} \quad (2)$$

and

$$\dot{w}_f = \dot{w} - \dot{w}_o \quad (3)$$

CONFIDENTIAL

CONFIDENTIAL

APPENDIX D

INSTRUMENTATION BOX IDENTIFICATION SYSTEM

(U) A system to identify all instrumentation taps on the 250K chamber has been devised so that the taps are fully described by the tap number. No cross reference is necessary to determine tap location, fluid media, or tap type.

(U) The aerospike chamber is divided into zones for instrumentation identification purposes. The zones are numbered starting at the inlet and progressing along the flow path of the particular media (figure D-1).

(U) Angular location is defined in degrees clockwise of an index point looking from forward to aft along the axial center line of the chamber. The reference point for all 250K aerospike chambers is defined as the 12:00 o'clock position of the chamber when installed on test stand D-2 at NFL.

(U) The tap identification system is illustrated with the following example:

A	E
B	F
C	
D	G
C G 3 i	-136.5 P -3.3

where:

A. Major Component

C = thrust chamber

G = gas generator

L = line

I = igniter

B. Fluid Media

O = oxidizer

F = fuel

G = combustion gas

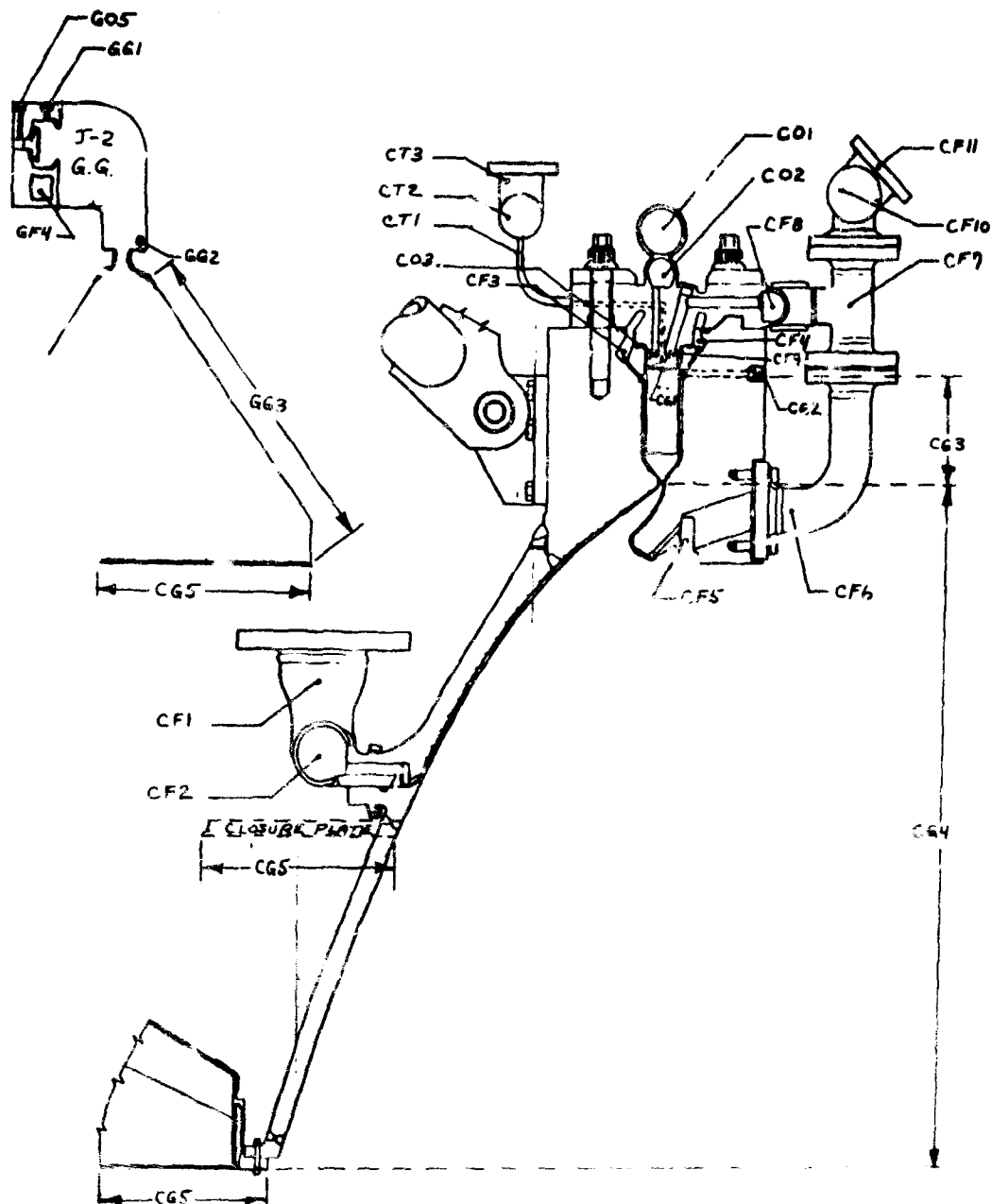


Figure D-1. ADP Solid-Wall and Tubular Thrust Chamber Boss Nomenclature

CONFIDENTIAL

N = inert gas
T = tapoff gas
I = igniter fluid
Z = other

C. Chamber Zone

D. Minor Component (used only where additional clarification is required)

i = inner body
o = outer body
d = dome

E. Angular Location in Degrees from Reference Point

F. Type of Boss

P = static pressure
T = temperature
D = dynamic pressure
A = accelerometer
B = bomb boss or pulse gun
S = seal vent
C = solid-state flowmeter or pressure
- = purge (no letter designation)

G. Axial Distance referenced from Injector Face or Radial Distance referenced from Chamber Centerline (whichever is applicable)

Tap identifications are called out on all chamber drawings and are stamped or etched at each location.